Geomicrobiological investigation of amorphous organic matter in fossil anoxic sediments and comparison with recent bacterial analogs

Pacton, Muriel

UNIVERSITE DE GENEVE
Département de géologie et de paléontologie

FACULTE DES SCIENCES
Professeur G.E. Gorin

UNIVERSITE PARIS-SUD
UMR-CNRS 8148

FACULTE DES SCIENCES
Docteur N. Fiet

Geomicrobiological Investigation of Amorphous Organic Matter in Fossil Anoxic Sediments and Comparison with Recent Bacterial Analogs

THESE

Présentée à la Faculté des sciences de l'Université de Genève pour obtenir le grade de Docteur ès sciences, mention Sciences de la Terre

par

Muriel PACTON

de

Saint Michel sur Orge (France)

Thèse No 3919

GENEVE
Atelier de production de la Section de physique
2008

ABSTRACT

Organic-rich rocks deposited under anoxic marine conditions form a large proportion of petroleum source rocks. Therefore, their organic content has been extensively studied, particularly the microscopically-amorphous organic matter (AOM), which is by far the dominant constituent in these rocks. No structure can be identified at this scale of observation. In blue-light microscopy, when AOM exhibits fluorescence and is associated with high hydrogen indices (obtained from Rock-Eval pyrolysis), it is commonly interpreted as being of phytoplanktonic and/or bacterial origin. The debate on the origin of organic-rich marine sediments still concentrates on the "productivity versus preservation" controversy. The notion of organic matter (OM) preservation is still unclear, whereas processes of OM degradation involving bacteria as the major agent have been defined, based essentially on organic geochemistry. Organic matter accumulation and preservation depend on specific processes in the water column and within the sediments. Only a small part of the degradation products from common biomacromolecules (e.g. proteins and polysaccharides) escape complete destruction through condensation processes. Other preservation pathways exist according to the component biological nature and depositional environment. Although many geologists have used organic biomarkers to evaluate the dominant source of OM (terrestrial plants, algae…), there remain many uncertainties about the different types and real origin of AOM constituents. Consequently, it is still a matter of debate whether organic geochemistry really gives a representative picture of the chemical nature of AOM.

None of the known preservation pathways refers to an important bacterial product, the extracellular polymeric substances (EPS), undetectable with standard geochemical analyses. Most bacteria in the natural environment live on surfaces as slime-encased biofilm communities constituted of EPS. Extracellular polymeric substances are a generic term referring to a high-molecular-weight polymer that is composed of sugar residues, excreted outside the cell by a micro-organism into the surrounding environment.

This research presents a study of fossil AOM in some well-studied depositional environments at different scales of observation: 1) the deep-water Miocene Monterey Formation of the Naples Beach section (California); 2) the Upper Jurassic bituminous shales at Orbagnoux (France) deposited in a shallow back-reef environment; 3) three Lower Cretaceous black shales refer to oceanic anoxic events (OAEs) in Central Italy, i.e., the Selli (OAE1a), Urbino and 113 levels (OAE1b).

In order to characterize the relationship between bacterial contribution to OM formation and preservation pathways, recent bacterial analogs have been considered: sulphuroxidizing bacteria, cyanobacterial biofilm and hypersaline microbial mats.

Amorphous organic matter was extracted palynologically from the laminites before being studied using the following microscopical tools: Scanning Electron Microscopy (SEM) which illustrates the AOM surface down to micrometer-scale; Atomic Force Microscopy (AFM) which permits the observation of AOM surface with a resolution down to 10 nanometers; Transmission Electron Microscopy (TEM) on ultrathin section which reveals the texture of AOM constituents with a resolution between one micrometer and 10 nanometers. A geochemical approach has also been used including Rock-Eval pyrolysis, FTIR spectroscopy and isotope analysis. Then, DNA extraction has also been performed in the Urbino level.

Potential artefacts that might result from acid attack during sample prepation have been evaluated by comparing recent bacteria with similar bacteria that underwent acid treatment. This chemical attack does not affect AOM morphology and chemical nature, except for EPS and some chemical bonds. Contrary to previous observations, the microscopic data show that fossil AOM is structured at a nanometer-scale. The bacterial presence is microscopically well identified by filaments and cocci. The morphology of EPS appears either closely associated with AOM microstructure or only locally present. Comparisons with recent bacterial analogs imply that EPS play an important protective role in

OM preservation. At the nanoscale, “nanoballs” constitute a large part of AOM when a strong microbial activity is observed in anoxic samples, i.e., in the Kimmeridgian laminites and Urbino level. They are interpreted as nanobacteria and indicative of a low level of OM degradation. This sheds new light on OM preservation pathways and emphasizes the role of bacterial activity, i.e., EPS, in the sorptive preservation pathway. Ultralaminae, so far known as remnants of microalgal cell walls, are in fact also bacterial cell walls and thylakoids. The latter provide a new paleogeographical tool and restrict water depth to the water into which sunlight penetrates sufficiently to influence the growth of plants and animals called the photic zone. The microscopical and geochemical data indicate that the studied OAEs are derived from photosynthetic microbial mats (shallow-water deposits), which contradicts previous studies. The identification of fossil bacterial DNA in the Urbino level points to exceptional OM preservation conditions and to proteobacteria as dominant microorganisms in the formation of this OAE deposit.

This study illustrates the importance of combining optical and chemical analyses when investigating AOM. So far, bacteria have often been considered as agents of OM degradation. Results presented here point to the contrary and highlight that bacterial activity could be more of a preservation than a degradation agent in OM fossilization.

This research was financed by the Swiss National Fundation (grants n° 2000.68091 and 2000.112320, Prof. Georges Gorin).

RESUME

L'étude de la matière organique sédimentaire (MOS) se base sur les palynomorphes, utilisés pour la biostratigraphie ou encore comme indicateurs paléoenvironnementaux (marin, lacustre ou terrestre), mais également une fraction non figurée appelée matière organique amorphe (MOA). Cette dernière est un constituant essentiel des roches-mères et a été longuement investiguée par les pétroliers. Elle est majoritairement présente dans des sédiments anoxiques, mais plus récemment a été découverte dans les systèmes d'upwelling. Classiquement, elle est déterminée par microscopie optique associée à la fluorescence bleue et par géochimie organique qui permet la détermination des composés organiques solubles. Son origine reste cependant très controversée. Lorsqu'elle est fortement fluorescente associée à des hauts indices d'hydrogène (données de pyrolyse Rock-Eval), elle est définie comme étant phytoplanctonique et/ou bacterienne. Les seules structures visibles sont les ultralaminae en microscopie éléctronique à transmission (MET), qui sont les témoins des restes de parois algaires et, de ce fait, implique la préservation sélective comme processus important pour la préservation de la MO durant sa transformation dans la colonne d'eau et dans les sédiments. La transformation de la MO s'effectue par des réactions d'oxydo-réduction mais également sous l'action de différentes bactéries dépendant du milieu. Leur contribution est largement reconnue mais leur action et l'empreinte qu'elles laissent dans le fossile sont encore mal comprises.

Le but de ce travail est d'établir la signification paléoenvironmentale de la MOA à partir d'environnements bien documentés avec une approche microscopique et géochimique. Trois sites ont été considérés, à savoir, la Formation Monterey en Californie datée du Miocène (section de Naples Beach), les laminites d'Orbagnoux dans le Jura français datées du Kimméridgien et enfin trois niveaux en Italie Centrale appartenant aux événements océaniques anoxiques du Crétacé inférieur comprenant le niveau Selli (OAE1a) et les niveaux Urbino et 113 (OAE1b). La MO fossile est comparée aux analogues microbiens proposés d'après la littérature. Ainsi des bactéries sulfuroxydantes et un biofilm cyanobactérien sont respectivement comparés aux échantillons de la Formation Monterey et d'Orbagnoux. La contribution des bactéries lors de la formation des OAE's étant peu connue, deux tapis microbiens actuels ont été considérés. En effet, les communautés vivant selon une distribution verticale confèrent au tapis un fonctionnement comparable à un microenvironnement regroupant les horizons oxiques et anoxiques.

Les échantillons actuels et fossiles ont subi les mêmes analyses et par conséquent le même traitement chimique afin d'isoler la MO de la fraction minérale. Cette première étape a permis d'évaluer les artéfacts possibles dans la MO fossile. Il en résulte que ce traitement a une faible incidence sur l'observation future et ne contrarie donc pas l'interprétation de structures organiques. Les outils microscopiques utilisés comprennent le microscope optique, associé avec la fluorescence bleue, le microscope électronique à balayage, le microscope électronique à transmission (associé à des coupes ultraminces) et le microscope à force atomique. La pyrolyse Rock-Eval, les isotopes et enfin la spectroscopie infra-rouge ont été utilisées pour caractériser géochimiquement la MO fossile. L'extraction d'ADN a été possible sur le niveau Urbino, traduisant des conditions de préservations hors du commun. L'analyse en lames minces et par DRX a permis de cibler précisément l'environnement de dépôt.

Cette investigation géomicrobiologique met en évidence de nouvelles perspectiques sur la formation de la MOA. En effet, contrairement aux études précédentes, il apparaît que la MOA est nanostructurée, en particulier par les sécrétions des bactéries, appelées EPS. Ces polysaccharides, hautement hydratés, conditionnent la structuration de la MO et la protègent des réactions de dégradation. Ainsi leur action est semblable à celle des argiles et regroupée sous le terme de préservation par adsorption. Les ultralaminae sont plus précisément composés de parois bactériennes et de thylakoides (membranes servant à la réalisation de la photosynthèse), en plus des parois algaires. Les thylakoides sont donc un nouvel outil paléogéographique qui implique un paléoenvironnement restreint à la zone photique. Par conséquent, les niveaux d'OAEs étudiés ici seraient en fait des dépôts de faible profondeur correspondant à des tapis microbiens photosynthétiques et non des dépôts de grande profondeur.

L'investigation de la MO à l'échelle nanométrique met en évidence l'existence de nanoboules, assimilables à des nannobactéries, qui traduisent un état peu avancé dans la diagenèse.

En conclusion, cette nouvelle approche géomicrobiologique par comparaison microscopique et géochimique a mis en évidence le rôle complexe de l'activité bactérienne dans la transformation de la MO. Les bactéries apparaissent comme des agents de préservation alors qu'elles n'étaient considérées jusqu'àlors que comme des vecteurs de destruction de la MO.

REMERCIEMENTS

Je remercie très chaleureusement tout d'abord le Professeur Georges Gorin pour m'avoir permis de vivre cette aventure à la fois scientifique et humaine. Je lui suis profondément reconnaissante pour sa confiance, ses grandes connaissances sur la matière organique et son esprit critique qui ont largement contribués à la qualité de ce travail. Je le remercie également de ses nombreuses heures passées à corriger les manuscrits malgré un emploi du temps très chargé.
Je remercie également le Dr. Nicolas Fiet pour m'avoir donné la chance de faire cette thèse, tous les moyens qu'il a mis en œuvre afin de facilité les échanges inter-disciplinaires et bien sûr, pour son soutien et son inconditionnel optimisme malgré la distance.
Je tiens à remercier vivement Daniel Ariztégui pour ses conseils avisés, le temps qu'il m'a accordé malgré un emploi du temps surchargé, les précieux contacts qu'il m'a donné et enfin ses encouragements malgré la difficulté.
Je remercie le Dr. Cris Vasconcelos pour son accueil, son aide précieuse et de m'avoir initiée à la géomicrobiologie et de son soutien sans faille.
Je tiens à exprimer toute ma reconnaissance au Dr. Richard Tyson pour avoir accepté de juger cette thèse, toutes les corrections qu'il m'a suggérées à caractère scientifique notamment sur la matière organique sensu stricto mais aussi sur la qualité de l'anglais.

Je tiens à remercier ceux qui ont contribué à la réalisation de résultats probants de cette thèse :

- François Gischig pour la réalisation des lames minces et du dispositif ingénieux qui a permis l'extraction d'ADN fossile (Genève);
- Rosanna Martini pour les images MEB (Genève);
- Fabio Caponni pour la stérilisation du matériel (Genève) ;
- Danielle Jaillard et Jéril Degrouard pour m'avoir formée et permis d'être autonome sur l'ultramicrotomie et l'utilisation du MET ainsi que les nombreuses discussions très enrichissantes sans qui deux publications n'auraient pas été possibles (Centre Commun de Microscopie Electronique, Orsay). Je les remercie également pour leur grande disponibilité et leur bonne humeur ;
- Philippe Pradel pour sa patience et son professionnalisme lors des nombreuses heures passés à l'AFM et les échantillons passés aux DRX (Orsay) ;
- Olivier Dufaure pour les préparations des échantillons préalables aux DRX, malgré des échantillons un peu réfractaires (Orsay) ;
- Rémy Pichon pour m'avoir formée sur la spectrométrie infra-rouge (Orsay) ;
- Marc Massot pour les datations ^{14}C (Orsay) ;
- L'équipe de génétique et biologie moléculaire de Mickael Dubow qui a été la seule à croire à la préservation de l'ADN fossile malgré le scepticisme de la communauté scientifique et un grand merci tout particulier à Eric Prestel, qui malgré ses obligations, a investi beaucoup de temps dans la réalisation de cette thématique avec brio.
- Sandra Levay pour dénicher les articles introuvables et sa grande disponibilité (Genève) ;
- Et enfin Gilbert Overney pour l'aspect technique, présent dans les moments les plus critiques (Genève).

Je remercie très chaleureusement ma collègue et amie Karine Plée pour son enthousiasme, les discussions scientifiques qui m'ont beaucoup apportées et bien sûr son soutien immuable à Genève, en congrès et en excursion, sans oublier le snorkelling.
Je remercie également tous les doctorants et les diplômants avec qui j'ai eu beaucoup de plaisir à discuter et partir en camps de terrain. Je remercie également Jacques Metzger et Rosanna Martini pour les TPs mémorables passés ensembles.

Enfin je tiens à remercier du plus profond de mon cœur mes proches et plus particulièrement mes parents pour leur soutien inconditionnel, leur bienveillance vis à vis de mes animaux, et leur contribution à cette thèse (merci papa pour le support AFM !); également Christophe pour son écoute attentive sans oublier Ukira.

TABLE OF CONTENTS

LIST OF FIGURES

LIST OF TABLES

1. INTRODUCTION AND AIMS OF STUDY

The study of sedimentary organic matter (SOM) greatly contributes to paleoenvironmental reconstructions in sedimentary basins. Besides continental vegetal fragments, structured constituents include palynomorphs (e.g., spores, pollen, dinoflagellates, etc.), which are studied by palynology and are used as biostratigraphic and paleoecological indicators. The group referred to as "amorphous organic matter" (AOM) is the most problematic in terms of palaeogeographical interpretation, particularly when trying to determine its origin. It is defined as structureless at the scale of light microscopy, and includes phytoplankton- or bacterially-derived AOM, higher plant resins and amorphous products from the diagenesis of macrophyte tissues (Tyson, 1995). It is often difficult to interpret AOM in transmitted natural light (Batten, 1983; Combaz, 1980; Masran and Pocock, 1981; Misra, 1991; Pocock, 1982; Venkatachala, 1981, 1984). It is necessary to resort to other observation methods, such as fluorescence, scanning or transmission electron microscopy (Batten, 1996; Tyson, 1995; Venkatachala, 1984) or simple etching techniques (Tribovillard, 1998). Organic geochemistry (biomarkers) is another technique, though quite time-consuming. The resort to quick evaluation techniques like Rock-Eval pyrolysis to interpret AOM as continental or marine may also be misleading. Consequently, a multidisciplinary investigation of AOM at the interface between geology and biology is recommended. The development of geomicrobiology has shown the contribution of microbes and bacteria to the formation of sedimentary rocks and SOM, particularly AOM (Folk and Lynch, 2001; Noffke et al. 2001; Oschmann 2000; Tribovillard 1998).

This research will attempt to better characterize AOM in some fossil anoxic environments and compare it with present-day environments and bacteria. The following, well-known anoxic palaeofacies have been investigated:

i) The organic-rich, deep-water sediments of the **Miocene Monterey Formation in California** (e.g. Isaacs & Rüllköter, 2001).
ii) The **Upper Jurassic bituminous shales at Orbagnoux in the French Jura** (Mongenot et al., 1997; Mongenot et al., 1999; Tribovillard et al., 1999; Tribovillard et al,. 2000).
iii) Black Shales belonging to Oceanic Anoxic Events (OAEs) in the **Lower Cretaceous of the Marche-Umbria Basin in Central Italy,** including the **Selli (OAE1a), Urbino** and **113** levels, the latter being equivalent to the OAE1b and deposited in an upper bathyal environment (Cecca et al., 1995; Coccioni et al., 1992; Tornaghi et al., 1989).

The objectives of this work are (Fig. 1-1):

- to characterize AOM extracted by standard palynological techniques (see Steffen and Gorin, 1993) in some well-interpreted anoxic palaeoenvironments by using optical and geochemical techniques. The microscopical methods used to study AOM are the following: standard microscopy in natural and blue-light fluorescence, scanning electron microscopy (SEM), atomic force microscopy (AFM) and transmission electron microscopy (TEM). These tools give a general overview of the AOM organization, structure and nature. The geochemical methods include Rock-Eval pyrolysis, organic geochemistry, molecular biology and stable C isotopes.
- to compare this fossil AOM with some present-day analogs exposed to acid treatment: a culture of microbial mats from Brazil and Tunisia by comparison to Orbagnoux, a culture of sulphur-oxidizing bacteria such as *Beggiatoa* (Strohl et al. 1978, Jorgensen et al. 1999, Grabovitch et al. 2001, Muβmann et al. 2003) as analogue for the Monterey Formation, and finally recent continental sediments (peat bog and caldera lake) in order to evaluate the degradation precursor stages.
- to understand the qualitative and quantitative role of the inorganic matrix in the SOM preservation using chemical analyses: XRD (X-ray diffraction) and FTIR spectroscopy (Fourier Transformed Infra-Red).

- Few samples have been analyzed with a lot of methods rather than classic number of samples for a Ph.D. with only few methods. This choice does not lead to statistical analyses.

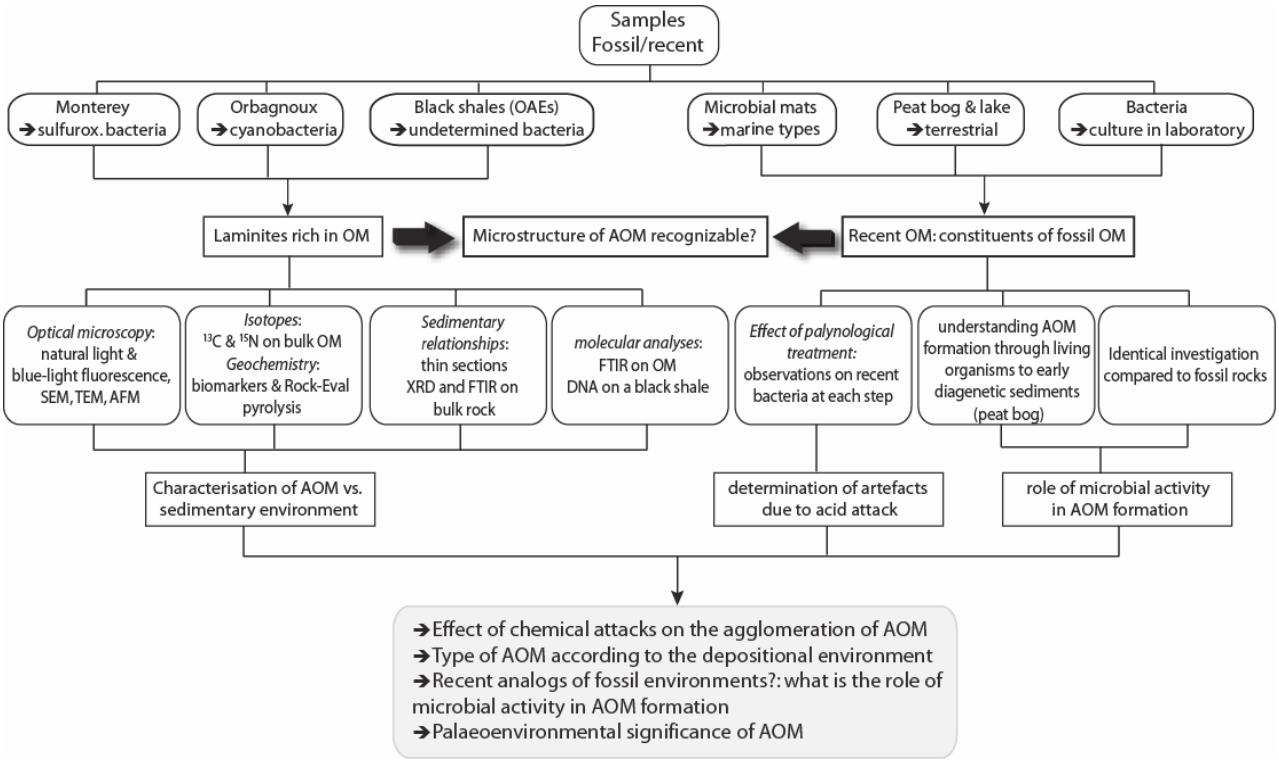

Figure 1-1: aims of study

2. SEDIMENTARY ORGANIC MATTER AND GEOMICROBIOLOGY:

STATE OF THE ART

2.1. Sedimentary organic matter

2.1.1. PRODUCTION OF ORGANIC MATTER

2.1.1.1. Primary productivity

The primary productivity refers to the transformation of chemical or solar energy into biomass. Most primary production occurs through photosynthesis, whereby green plants convert solar energy, carbon dioxide, and water to glucose and eventually to plant tissues. In addition, some bacteria in the deep sea can convert chemical energy to biomass through chemosynthesis.
Primary production in seas and oceans is initially enhanced by unicellular algae (phytoplankton), through fixation of CO_2 or HCO_3^-. These include diatoms, dinoflagellates and coccolithophores. The growth is controlled by the availability of nutrients, especially nitrogen and phosphorus and light, as well as by grazing of herbivores.

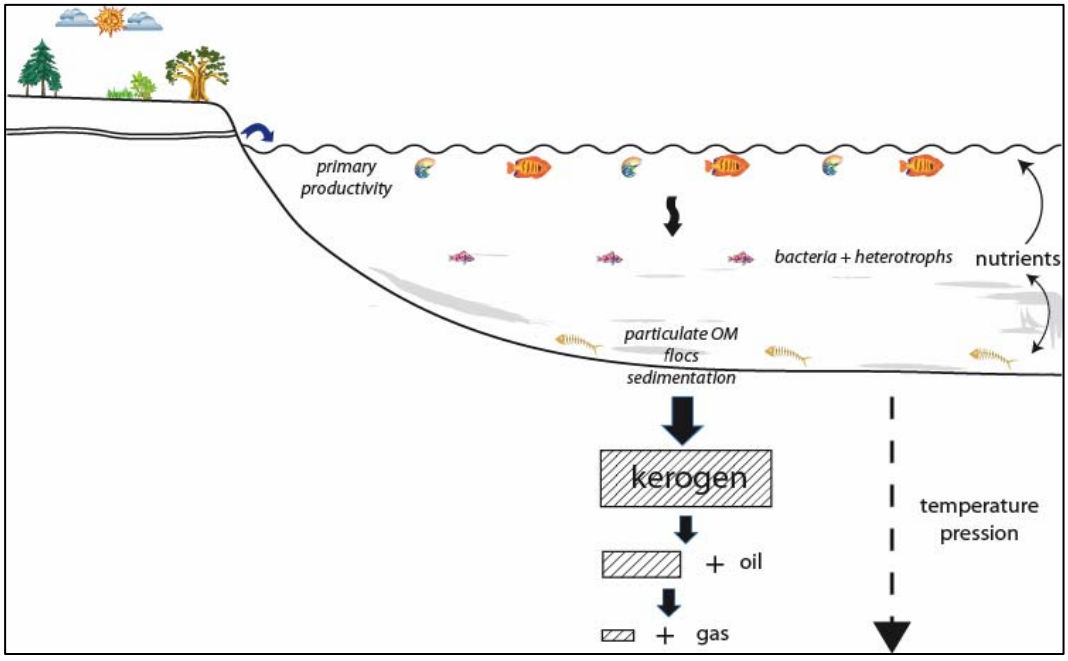

Figure 2-1 : OM cycle in marine sediments

2.1.1.2. Biological composition of sedimentary organic matter

Organic matter encountered in marine sediments has two origins: an autochthonous source essentially in the photic zone and an allochthonous one (rivers and wind). It is derived from primary and secondary resources. Primary resources include carbohydrates (such as sugars, starch, and cellulose), lignin, protein and other compounds such as nucleic acids, resins, etc. Secondary resources comprise cellulose, chitin, peptidoglycan and melanin. All these compounds have specific properties in the development of living organisms. Proteins have a structural role in the cells and act as organic matrix in the mineralization of shells. Carbohydrates, including sugars and their polymers, are energy sources and form the supporting tissues of some plants. Cellulose and chitin are the most widespread polysaccharides in the nature. Lipids comprise pigments, hormones and phospholipids of cellular membranes. They are used as energy sources or have protective functions. Lipids encompass molecules insoluble in water but soluble in apolar solvent and are produced by living organisms. The composition of the biomass varies according to the organism. Lignin is a polymer of phenols, and a major constituent of vegetal tissues responsible for their rigidity.

2.1.1.3. Degradation processes

The degradation of OM occurs in the water column, at the sediment-water interface and within the sediment (Fig. 2-1). In the upper part of the water column, most of primary productivity is consumed by zooplankton and bacteria. Part of the OM is remineralized to CO_2, H_2O, NH_4^+ and serves as a nutrient supply for phytoplankton. The other part is formed of particulate or dissolved OM. Many factors occur, such as sedimentation rate, nature of sediments, bottom water conditions (oxic versus anoxic) and microorganisms (transport: physical, chemical and biological phenomenon).
The organic carbon production in the water column depends on the following factors:
- oxygen depletion in bottom waters or in sediment;
- adsorption of certain compounds to mineral particles;
- preservation of organic compounds as shell constituents;
- changes in the rate of SOM deposition;
- high input of terrigenous organic compounds, which are more stable than the organic matter;
- dominant supply of clay sediments within which oxygenation of pore water is restricted.

Biological molecules undergo modifications which result in various components (amino acids, lipids, polysaccharides…). The degree of decomposition depends upon the substrate. For example, the depolymerization of starch and cellulose through fungi and bacteria is easy. On the contrary, the decomposition of lignin requires many enzymes. It depends on the chemical nature of molecules. Lipids are made of hydrocarbon skeletons and have few reactive sites. Therefore, they are not easily biodegradable. Lignin has a 3-dimensional structure that results in a great chemical stability. Similarly to lipids, lignin is also weakly biodegradable. There are two products of decomposition: i) Simple molecules, resulting from the complete decomposition of OM: CO_2, CH_4, NH_3, H_2S, H_2O, etc.; ii) molecules resulting from the selective decomposition of biological precursors: amino acids, peptides, simple sugars, polycarbohydrates, fatty acids, lipids, phenols, acid phenols, lignin, etc.
Decomposition is initiated through mechanical processes (laceration of tissues by rain, hail, wind, hydrodynamic movements), chemical (oxygen, pH, light), or biochemical agents (enzymes, bacteria, fungi, burrowing organisms).

Organic matter undergoes changes in composition with increasing burial depth and temperature. The three steps in the transformation of OM to hydrocarbons are called diagenesis, catagenesis, and metagenesis. Hydrocarbons exist as gaseous, liquid, and solid phases, depending on temperature, pressure, burial time, and chemical composition.

2.1.1.4. Diagenesis

Early OM transformations are marked by the partial change from biopolymers synthetized by living organisms to geopolymers through fractionation, partial destruction and rearrangement of the building stones of the macromolecules (Tissot and Welte, 1984). Biochemical degradation is controlled by bacteria, actinomycetes, fungi and algae. Five processes are considered:

- oxic degradation occurring in the upper part of the water column;
- fermentation is an anaerobic process by which bacteria, instead of using molecular oxygen (respiration), use oxidized forms of OM, particularly carbohydrates (Tissot and Welte, 1978);
- nitrate reduction.

Sulfate reduction and methanogenesis are two terminal anaerobic bioremineralization pathways that convert low-molecular-weight products of other bacterial processes (degradation of polymers, fermentation) to CO_2 and methane:

- sulphate reduction: Sulfate-reducing bacteria are physiologically and phylogenetically highly diverse (Castro et al., 2000; Widdel and Bak, 1992). They oxidize a wide variety of low-molecular-weight compounds (short-chain fatty acids, alcohols, alkanes, aromatic compounds, acetate) to CO_2. In marine sediments, the range of sulfate-reducing bacteria is limited by sulfate availability.
- methanogenesis: When sulfate is depleted, methanogenic archaea become the dominant anaerobic microbial population. Autotrophic methanogens utilize hydrogen as energy source for the reduction of CO_2 to methane; specialized genera of methanogens are also capable of inter- and intramolecular disproportionation of C_1 and C_2 carbon compounds (methanol, methylamines, acetate) to methane and CO_2 (Boone et al. 1993). Where methane and sulfate coexist (e.g., at the interface of sulfate-reducing and methanogenic sediment layers, or at marine methane seeps and vents), sulfate-dependent anaerobic methane oxidation takes place; methane of biogenic origin is oxidized to CO_2 with sulfate as the terminal electron acceptor (Valentine and Reeburgh, 2000). As proposed originally on the basis of biogeochemical field data and thermodynamic considerations (Hoehler et al. 1994), anaerobic methane oxidation is carried out by syntrophic consortia of methanotrophic archaea and sulfate-reducing bacteria, in which the sulfate-reducing partner catalyzes the electron transfer from methane to sulfate and assimilates a portion of the methane oxidation products (Boetius et al., 2000; Orphan et al., 2001b).

2.1.2. CLASSIFICATION OF SEDIMENTARY ORGANIC MATTER

2.1.2.1. Organic constituents in microscopy

Organic constituents in microscopy are divided in several group (for details, see Tyson, 1995) and especially AOM which belongs to the Amorphous Group (Fig. 2-2). In this chapter, only AOM is described.

<table>
<tr><th colspan="2">ORIGIN</th><th>GROUP</th><th colspan="2">CONSTITUENT</th></tr>
<tr><td rowspan="8">CONTINENTAL (allochthonous)</td><td rowspan="4">higher plant debris</td><td rowspan="4">phytoclasts</td><td rowspan="2">opaque</td><td>equidimens.</td></tr>
<tr><td>lath-shaped</td></tr>
<tr><td colspan="2">semi-opaque</td></tr>
<tr><td colspan="2">translucent</td></tr>
<tr><td colspan="2">cuticles</td></tr>
<tr><td rowspan="2">pollen & spores</td><td rowspan="2">sporomorphs</td><td colspan="2">bisaccates</td></tr>
<tr><td colspan="2">non-saccates</td></tr>
<tr><td colspan="2">freshwater algae</td><td colspan="2">Pediastrum
Botryococcus</td></tr>
<tr><td rowspan="3">MARINE (autochthonous)</td><td>degraded plant debris</td><td rowspan="2">amorphous organic matter (AOM)</td><td colspan="2" rowspan="2">non fluorescent AOM
fluorescent AOM</td></tr>
<tr><td>degraded phytoplankton</td></tr>
<tr><td colspan="2">marine phytoplankton</td><td colspan="2">dinocysts & acritarchs</td></tr>
<tr><td colspan="2">foraminifera</td><td colspan="2">other marine algae</td></tr>
<tr><td colspan="2">foraminifera</td><td colspan="2">foraminiferal test linings</td></tr>
</table>

Figure 2-2: Classification of organic constituents in the marine realm; modified after Steffen and Gorin (1993).

The Amorphous Group contains resin and amber, amorphous terrestrial "humic" materials and the amorphous organic matter (AOM). According to Tyson (1995), AOM consists of all particulate organic components that appear structureless at the scale of light microscopy. It includes phytoplankton or bacterially-derived amorphous organic matter, higher plant resins, and amorphous products of the diagenesis of macrophyte tissues. The amorphous material commonly acts as a matrix for a diversity of structured inclusions.
Palynologists use the term amorphous in a purely descriptive sense that is not meant to imply a precise physico-chemical condition that applies at all possible scales of observation.
Several classifications have been established based on optical characteristics. They are purely descriptive or related to OM origin:

- Terrestrially-derived OM

The gelified type, defined by Combaz (1980), is characterized by homogeneous, compact, and brown to black colour with sharp edges. Masran and Pocock (1981) noted that terrestrially-derived AOM is darker (dark-yellow to amber) than algal-derived AOM. In aerobic conditions, AOM appears as brown orange colour with a granular texture (Pocock 1982). According to Venkatachala (1981, 1984), biodegraded terrestrial OM is characterized by semi-AOM associated with fungal and bacterial remains at the beginning of degradation. At a later stage, it is transformed into a "finely divided AOM" with no visible structure. Optically it appears as yellow to amber-coloured, botryoidal and granular masses. It displays a strong association with bacteria and is preferentially formed in low-energy reducing environments. The bacterial activity transforms terrestrially-derived OM to a hydrogen-richer OM, thereby enhancing its hydrocarbon source potential.
Batten (1983, 1996) observed that terrestrially-derived AOM comprising biodegraded cellular remains tends to be more fibrous, membranous or spongy. Moreover, the gelified OM is defined as homogenous particles formed during degradation of plant tissues.

- Marine-derived OM

Masran and Pocock (1981) defined green-yellow AOM under aerobic conditions. AOM produced by biodegraded marine plants is green-yellow under aerobic conditions, whereas it appears grey black and rich in organo-pyrite under reducing conditions.
Pocock (1982) established that the marine-sourced AOM is green-yellow in colour and its texture fluffy. Moreover, grey AOM of marine origin is produced under reducing conditions. The semi-AOM material is described as an intermediate stage between structured OM and completely biodegraded OM.

Wood and Gorin (1998) noted that AOM derived from marine phytoplankton or bacteria, is fluffy, yellow and light-brown to brown.
Venkatachala (1981) distinguished biodegraded aqueous OM marked by its dark-brown to greenish yellow, granular (spongy under SEM) aspect. This type is mostly composed of algal remains, and appears flaky when derived from filamentous algae. Moreover, it may also be composed of phytoplankton generally associated with grey AOM in a reducing environment or with granular greenish yellow AOM in a partially oxidizing environment.
According to Batten (1983, 1996), AOM of aquatic origin is largely derived from algal material with microbial mats possibly involved. It appears as more granular or flaky, although it may be partly filamentous when relatively unaltered.

- AOM of undistinguished source

Combaz (1980) defined three types of AOM independently of its origin:
The grumose-type particles vary in size and have a light-brown to yellow colour increasing with thickness. The granular type differs from the grumose type through numerous inclusions within the particles. The powdery brownish to yellowish subcolloidal type is assumed to be an artefact during sample preparation or contamination by drilling mud. The dark-coloured pellicular type has been moulded to carbonate crystals and displays their imprint.
Venkatachala (1981) defined AOM sensu stricto as having a yellowish brown or orange colour. It is produced in an aerobic environment with a limited supply of oxygen. This type can be further subdivided into flaky, granular, spongy and granular types. Bacterially degraded OM also yield yellowish to green-brown AOM.
Whitaker (1984) considered that the laminar pale and coarse orange types in AOM are mainly derived from bacterial biomass. In blue-light fluorescence, they appear as dull or brighter yellow fragments.
Boussafir and Lallier-Vergès (1997) associated AOM to OM preservation processes: diffuse AOM is attributed to selective preservation, whereas homogenous AOM is assumed to result from natural vulcanization.
Mongenot et al. (1997) distinguished a dominant orange with an intense yellow-green fluorescence and a minor dark, non-fluorescing one. This strongly fluorescent AOM is thought to be typical of the vulcanization pathway.
Pellaton (2003) established three types of AOM. Dark-brown AOM is usually flaky, granular, thick and displays sharp or blurred edges. Internal structures may be visible. It is fluorescent or non-fluorescent and may contain fluorescent inclusions. Light-brown AOM is very similar to dark-brown AOM except that it is thin. The distinction is based on their colour in transmitted light microscopy. Fine AOM is usually rounded, very thin with blurred edges, fluffy and may contain pyrite. It may be fluorescent or non-fluorescent and may contain fluorescent inclusions.

The blue-light fluorescence gives more information about AOM origin. For immature samples, fluorescence is not just an indicator of organic matter source, but also of the degree of chemical preservation (Tyson et al., 2005). The level of fluorescence exhibited by the matrix of AOM particles is generally constant within any one sample (except for cuttings), and reflects the general redox status of the depositional environment (Gregory et al., 1991; Tribovillard et al., 1991; Tyson, 1984). Polymerization, aromatization and condensation during maturation result in a decrease in fluorescence intensity, which shifts towards the red (i.e. green $\rightarrow$ yellow $\rightarrow$ orange $\rightarrow$ brown) and progressively declines in intensity (Tyson, 1995).
According to (Bertrand et al., 1986), algal structure fluoresces more strongly than that of mainly aromatic woody structures. Tyson (1995) considers non fluorescent AOM in marine sediments as terrestrially-derived or strongly degraded plankton-derived OM. The fluorescence of AOM of algal/bacterial origin characterizes low energy, stagnant and oxygen-depleted paleoenvironments (Bujak et al., 1977; Staplin, 1969; Tyson, 1987). Marine AOM is fluorescent to non-fluorescent, whereas terrestrial AOM is non-fluorescent.

- technical limitations in the determination of AOM

The isolation of kerogen by heavy liquid could lead to a potentially selective and significant loss of specific organic components (Powell et al., 1982). AOM is often intimately associated with very fine

clay mineral material and its true abundance may only be apparent in fluorescence observations. As noted by Tyson (1995), much of what has been called amorphous or structureless organic matter is actually degraded phytoclast material that just lacks definitive and specific biological structure. The apparently sulfurized, nanoscopically amorphous orange variety of AOM seen in some iron-limited organic-rich shales (Boussafir et al., 1995) may be more homogeneous, and also exhibits a more fluorescent matrix (Tribovillard et al., 2001). The appearance of plankton- or bacterially-derived AOM varies most significantly with its preservation state: with "degradation it becomes increasingly more dull and heterogeneous when viewed under fluorescence, often more greyish in colour rather than yellow, orange, or brown, matte rather than lustrous, of lower relief…and less cohesive and less resistant to palynological oxidation treatment" (Tyson, 1989, 1995). Although transmitted light observation can prove the physical survival of plankton- or bacterially-derived AOM, fluorescence observations are essential for establishing the degree of chemical preservation of its originally oil-prone composition.

2.1.2.2. Geochemical classification

Based on Rock-Eval pyrolysis data (see chapter 3.1.5.3), OM can be classified into three types on a HI-Tmax diagram (Espitalié et al., 1985a, 1985b and 1986; Fig. 2-3):

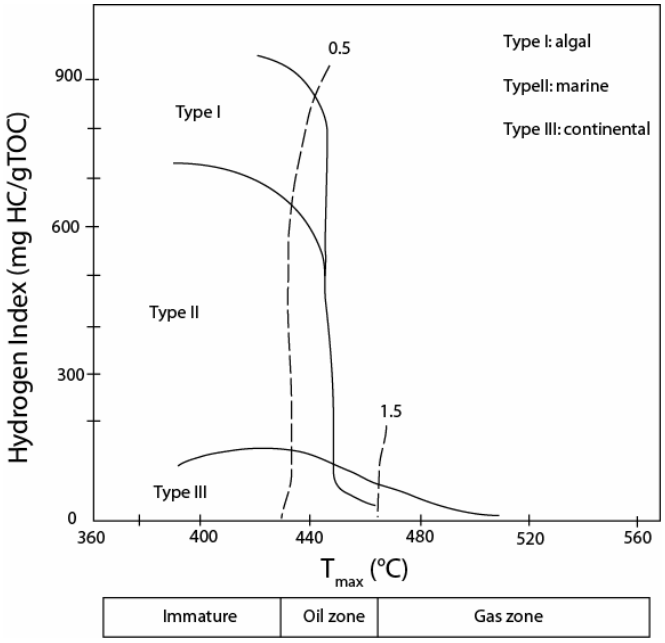

Figure 2-3 : Classification of OM types based on Hydrogen Index and Temperature. Modified from Espitalié et al. (1986).

Type I: Its standard was originally defined as the Eocene lacustrine oil shale of the Green River Formation, USA (Durand and Monin, 1980), and was consequently considered to be of lacustrine origin with a high initial H/C and a very low O/C ratio (Tissot and Welte, 1984). It is better defined as algal matter including *Botryococcus*, *Tasmanites*, *Pediastrum*…than lacustrine OM. It contains a significant contribution from lipid material, especially long-chain aliphatic. These lipids are predominantly derived from alginite, and particularly algaenan, although amorphous bacterial matter may also have a contribution. It contains low amounts of aromatic units and heteroatoms (Killops and Killops, 2006).
Type II: it is usually related to marine sediments where autochthonous OM has been deposited in a reducing environment (Tissot and Welte, 1984). Organic matter is derived from a mixture of phytoplankton, zooplankton and bacteria. It shows a relatively high H/C ratio and low O/C ratio. The type example is the Toarcian black shale of the Paris Basin. Aliphatic structures are important and

comprise abundant chains, mostly of moderate length (up to C_{25}) and ring systems. Type II kerogen can potentially be formed in any environment, but in marine settings its major source is the mixture of autochthonous OM from phytoplankton (and possibly also zooplankton and bacteria) together with an allochthonous contribution of higher plant material.
Type III: it is derived essentially from continental plants, it contains much identifiable vegetal debris (Tissot and Welte, 1984). It has a low initial H/C ratio and a high initial O/C ratio. The type example is the deltaic Cretaceous facies of the Douala Basin in Cameroon. Only minor amounts of aliphatic groups are present, dominated by methyl and other short chains, and often bound to oxygen-containing groups. A few long alkyl chains are present originating from cuticular coatings. This is essentially formed from vascular plants and contains much identifiable plant debris, so vitrinite macerals predominate.

2.1.3. PRESERVATION PROCESSES OF SEDIMENTARY ORGANIC MATTER (SOM)

Differential preservation of OM depends firstly on its components. The resistance of organic compounds to chemical degradation and decay varies according to their nature. Plant cell walls (composed primarily of the polysaccharide polymer cellulose) are far more likely to escape decomposition than internal membranes and organelles, which are rich in protein, lipids and sugar. Secondary compounds, such as those impregnating or covering cell wall, can also be resistant to decomposition; examples include lignin, waxes, cutin, sporopollenin and the resting cysts of some marine algae.
The preservation of OM, leading to the formation of oil source rocks and oil shales, is related to different mechanisms directly associated with the environment. For a long time, it has been thought that kerogens were formed according to the degradation-recondensation pathway from a chemical point of view (Tissot & Welte, 1984). Only a small part of the degradation products of common biomacromolecules (i.e. proteins and polysaccharides) escape complete destruction in sediments owing to condensation reactions. On the other hand, these random condensations lead to the formation of the complex macromolecular structure of kerogens. Other ways of preservation must be added according to the biological nature of components and the depositional environments such as the selective preservation and the natural vulcanization (also called sulphurization).
Differentiation of kerogens originating from these pathways can be made with morphological and geochemical studies.

Degradation-recondensation

The degradation-recondensation pathway leads to OM which does not retain any of the morphological features of the source organisms: it appears as aggregates devoid of a well-defined shape and as a heterogeneous, diffuse, sometimes granular, material. This model is based on a diagenetic fragmentation of the biomacromolecules of the OM. Monomers are transformed by re-organization into a group of humic substances which, as a whole, further evolve into geopolymers as a result of polycondensation (Tissot and Welte, 1984).

2.1.3.1. Selective preservation

This pathway is based on the production by some living organisms, especially microalgae, of insoluble biomacromolecules highly resistant to chemical and microbial degradation. These biomacromolecules are not affected by drastic basic and acid hydrolyses and also show an extreme resistance to microbial attacks. These biomacromolecules commonly occur in the cell walls or protective envelopes of a

number of organisms, including higher plants (cutans and suberans), microalgae (algaenans), cyanobacteria, and bacteria (bacterans) (Largeau, 1995).
Insoluble and non-hydrolyzable macromolecular structures present in protective envelopes of a number of extant organisms resist chemical and biochemical degradation (Derenne et al., 1991; Goth et al., 1988; Largeau et al., 1990; Tegelaar et al., 1989). The high preservation potential of such molecules promotes their selective preservation, thus their enrichment in the sediments, whereas polysaccharides and polypeptides, i.e, the most abundant biomolecules present in biomass, are readily degraded during deposition or diagenetic processes.
Very thin lamellar structures are distinguished from AOM in TEM: the ultralaminae, typically originating from the selective preservation of the very thin resistant cell walls that occur in numerous species of microalgae. Most fossil ultralaminae are 10 to 30 nm thick and associated into small bundles. Raynaud et al. (1989) were the first to propose an origin: they could correspond either to cellular membranes issued from phytoplankton which are strengthened by rigidifying agents (hopanetrols and sterols), or to cell walls composed of insoluble acid-resistant biopolymers. Comparisons have been made with lacustrine algae. Indeed, they exhibit morphological features closely related to those of the algaenans isolated from two extant Chlorophyceae (green microalgae) with thin resistant outer walls (Largeau et al., 1990a). Algaenans are non hydrolysable macromolecules occurring in the outer wall of numerous microalgae, especially chlorophyceae (de Leeuw and Largeau, 1991; Tegelaar et al., 1989). Furthermore, major differences in morphological features can be noted. In sharp contrast, extensive fragmentations and/or distorsions of thin outer walls occur during algaenan isolation and, as a result, the isolated resistant materials closely resemble fossil ultralaminae (Largeau et al., 1991a).

Organic matter is characterized by low TOC in the case of a very low content in orange AOM, the presence of ultralaminar structures associated to brown AOM in relation to resistant cell walls of green microalgae and the presence of “lignaceous” debris in the black AOM (Boussafir and Lallier-Verges, 1997).

2.1.3.2. Vulcanization

Natural vulcanization is an intermolecular incorporation of inorganic sulphur species into low-molecular-weight functionalized lipids and carbohydrates resulting in the formation of high-molecular-weight SOM. Two primary classes of reactions for sulphur incorporation have been cited: the intramolecular incorporation of sulphur, which leads to low-molecular-weight cyclic sulphur compounds such as thianes, thiolanes, and thiophenes, and intermolecular sulphur incorporation which binds organic compounds into macromolecular material through (poly)sulfide linkages (Adam et al., 1993; Kohnen et al., 1991; Sinninghé Damsté et al., 1989; Sinninghé Damsté et al., 1988).
This process is very important inasmuch as it protects lipidic, hydrogen-rich, organic matter from bacterial degradation and can promote or, at least, enhance petroleum source-rock formation marked by the involvement of non-polar macromolecules. They could be related to algal or bacterial precursors which essentially exist in living organisms as mono- or polyunsaturated species or are easily transformed into such species by diagenetic processes (e.g. steroids). It appears that the alkenes or polyenes become selectively trapped into a macromolecular network by reactions with inorganic sulphur species produced by bacteria (Adam et al., 1993). Natural vulcanization could have been enhanced by the lack of reactive iron (Tribovillard et al., 1994). In the absence of any iron sulfide, Fe was a limiting factor for pyrite formation and HS^--H_2S could react with lipidic organic matter and form organic sulphur compounds.
Kerogens appear as homogeneous, gel-like, amorphous materials in TEM (Mongenot et al., 1997).

2.1.3.3. Sorptive protection

The mechanism of sorptive protection pathway involves a protective role by minerals. This hypothesis was supported by correlations between TOC and surface areas of mineral grains in various coastal

sediments (Bergamaschi et al., 1997; Keil et al., 1994a; Keil et al., 1994b; Mayer, 1994a, b; Mayer et al., 1988). Such correlations were ascribed to a monolayer adsorption of organic compounds onto minerals. In addition to a physical protection from biodegradation (the small size of the pores excludes hydrolytic enzymes), OM adsorption onto pores should favour subsequent condensation reactions by concentrating the reactants (Collins et al., 1995). As observed by Salmon et al. (2000), adsorption on the mineral phase possibly played a role; however, the alternation of OM and clay nanolayers suggests a physical protection mechanism. In soils, part of the sorbed OM seems to be located in small pores that are inaccessible for microorganisms (Kaiser and Guggenberger, 2003).

2.1.3.4. Oxidative reticulation

The oxidative reticulation occurs during diagenesis under relatively oxic conditions showed by intense bioturbation and well developed benthic fauna. This consists of lipid cross-linking via oxygen incorporation (Riboulleau et al., 2001).

2.1.4. BIOMARKERS

Sedimentary organic matter deposited in different environments can be characterized by specific chemical components, which can be related to specific organisms and can provide paleoenvironmental information. The latter, called biological markers or biomarkers (Eglinton and Calvin, 1967; Eglinton et al., 1964), are molecular fossils, meaning that these compounds originated from formerly living organisms. They occur in sediments, rocks and crude oils and show little or no change in structure from their parent organic molecules in living organisms. The study of these molecular distributions can give a wide range of information, such as changes in OM input (bacteria, phytoplankton, higher plants) and processes (Eh, pH). Indeed, biomarkers give access to paleoenvironmental conditions and OM thermal evolution. Biomarkers have been widely applied to marine settings as proxies for organic matter inputs (Brassell and Farrimond, 1986; Kenig et al., 1995; Pancost et al., 1998; Werne et al., 2000).
Biomarkers are complex organic compounds made of C, H and other elements. Information is based on carbon skeleton, type and position of functional groups, isotopis content (i.e., ^{13}C and ^{14}C).
Commonly used biomarkers are branched or normal alkanes, acyclic isoprenoid alkanes, terpanoid compounds and steranes, and also their unsaturated equivalents. Lipids can provide valuable information about the bacterial contribution to the total SOM. Phospholipids constitute the bilayer of the cell wall and are the major lipids of bacterial cell membranes.
Three characteristics distinguish biomarkers from many other organic compounds (Peters and Moldowan, 1993):

- Biomarkers have structures composed of repeating subunits, indicating that their precursors were components in living organisms
- Each parent biomarker is common in certain organisms
- The principal identifying structural characteristics of the biomarkers are chemically stable during sedimentation and early burial.

The aliphatic content of SOM is generally higher than that of coal, reflecting the input of highly aliphatic planktonic and microbial lipids to the original SOM (Killops and Killops, 2005). Highly aliphatic macromolecules have also been identified in the cell walls of cyanobacteria and may make an important contribution to amorphous kerogen (Chalansonnet et al., 1998). Algae can also contribute aromatic material to kerogen.

2.1.5. ISOTOPIC SIGNATURE OF OM

Stable isotope analysis is a powerful tool to attempt the reconstruction of modern metabolic pathways, ancient environments and correlate rocks from different sources.
Most elements of biological interest (carbon, hydrogen, nitrogen, oxygen and sulfur) have two or more stable isotopes, with the lightest of these present in much greater abundance than the others. The heavy isotopes of these elements are incredibly useful as biological tracers, most notably carbon, nitrogen and sulfur, as they are abundant in the Earth, the atmosphere and living things. Each has a heavy isotope (^{13}C, ^{15}N and ^{34}S) with a natural abundance of ~1% or less and a light isotope (^{12}C, ^{14}N and ^{32}S) that makes up most or all of the remainder.
Studies examining stable isotopes measure the fractionation of isotopes, usually reported as delta, a value given in parts per thousand or per mil (‰). Delta values are not absolute isotope abundances but differences between sample readings and a natural abundance standard, different for each element, which is considered delta = zero.
Used standards :

- carbon - Vienna PeeDee Belemnite (VPDB) from South Carolina, USA
- nitrogen - atmospheric air
- hydrogen and oxygen - standard mean ocean water value (SMOW)
- sulfur - Canyon Diablo meteorite.

Delta values change based on physical and biological fractionation. Light isotopes will separate from heavier isotopes for many different reasons:

- organic processes - biochemical processes, such as photosynthesis and bacterial reduction, usually prefer lighter isotopes because lighter isotopes generally have weaker bonds, which are preferentially broken by the mediating microorganisms. Thus, the resulting biomass is enriched in the lighter isotope compared to the heavier isotope
- physical processes such as evaporation and diffusion separate the lighter isotopes from the heavier, as the lighter ones will preferentially evaporate or diffuse first.

2.2. Geomicrobiology

2.2.1. INTRODUCTION TO GEOMICROBIOLOGY

2.2.1.1. Definition

Microorganisms are generally able to carry out their life processes of growth, generation, and reproduction independently from other cells, either of the same kind or of a different kind. A single cell is an entity isolated from other cells by a cell membrane (and perhaps a cell wall) and containing a variety of chemicals and subcellular structures. All cells are made up of four macromolecules: proteins, nucleic acids, lipids and polysaccharides. It is through the cell membrane that nutrients and other substances needed by the cell enter. Within a cell, and bounded by the cytoplasmic membrane, is a complex mixture of substances and structures called the cytoplasm. A cell wall gives structural strength to a cell. The cell wall is relatively permeable and located outside the membrane; it is a much stronger layer than the membrane itself.
Two structural types of cells can be differentiated: the *prokaryote* and the *eukaryote* (Fig. 2-4). Eukaryotic cells are generally larger and structurally more complex than prokaryotic cells, having exclusively membrane-bound internal structures called organelles. These include the nucleus, mitochondria, and chloroplasts (in photosynthetic cells). Eukaryotic microorganisms include algae, fungi and protozoa. In contrast to eukaryotic cells, prokaryotic cells have a simpler internal structure, lacking membrane-enclosed organelles. Prokaryotes consist of the **Bacteria** and the **Archea**. In general, microbial cells are small, about 1-5µm long and 1 µm wide.

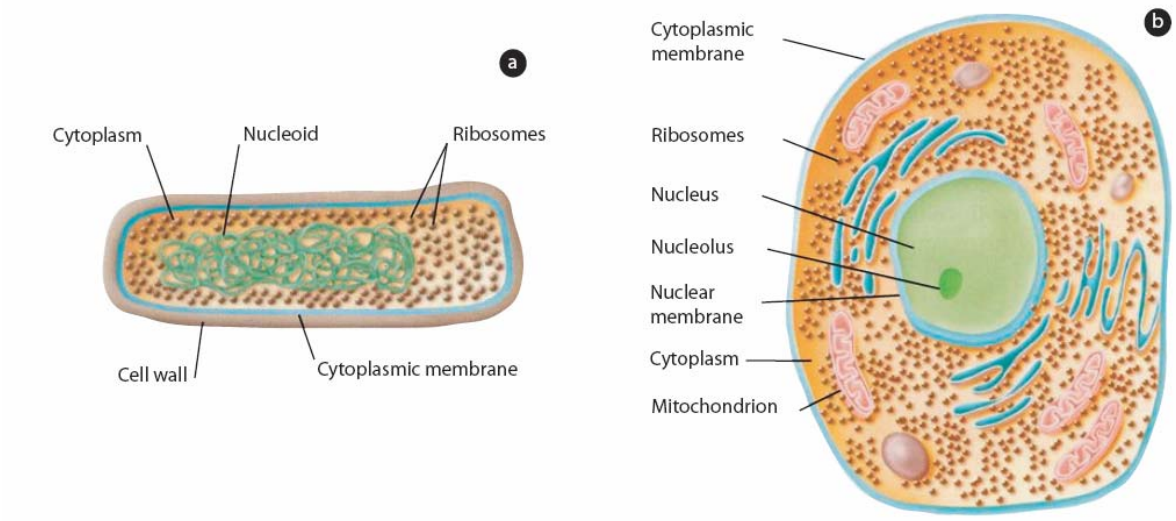

Figure 2-4: Schematic representation of prokaryotic(a) and eukaryotic (b) cell; from Madigan et al., 2003

From comparative ribosomal RNA sequences three phylogenetically distinct lineages of cells have been identified (Fig. 2-5); two of these lineages contain only prokaryotes, whereas the third one is composed of eukaryotes. The lineages, referred to as evolutionary domains, are called the **Bacteria**, **Archea** and **Eukarya**. These domains are thought to have diverged from a common ancestral organism early in the history of life on Earth. It seems quite likely that a structure like that of the cell wall has developed several times in the course of evolution. All archaebacteria, eubacteria and cyanobacteria (or blue-green algae) have complex walls with an energetically rather costly biosynthesis. Neither in composition nor in biosynthesis do they have any common ground with the cell walls of plants.

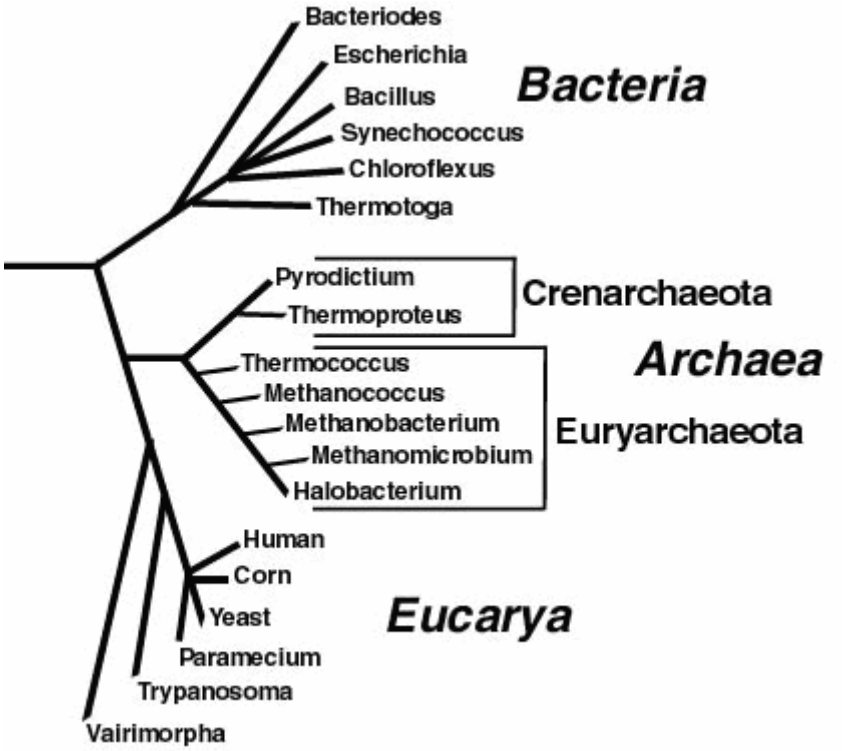

Figure 2-5 : The pylogenetic tree, based on 16S/18S rRNA sequence comparisons (Konhauser 2007)

2.2.1.2. Physiology of microorganisms

Energy required for cell growth can be obtained in three ways: organic chemicals, inorganic chemicals, or light.
Energy is obtained by oxidizing the compounds and is conserved in the cell as the high-energy compound called ATP. Microorganisms extract energy from the compound in the presence of oxygen (aerobes) or in the absence of oxygen (anaerobes). Organisms that obtain energy from organic compounds are called **chemoorganotrophs**, from inorganic compounds called **chemolithotrophs**, and from light called **phototrophs**. All cells require carbon as a major nutrient. Microbial cells are either **heterotrophic**, requiring one or more organic compounds as their carbon source, or **autotrophic**, where CO_2 is the source of cell carbon.

2.2.2. BACTERIA: GENERALITIES

2.2.2.1. Cell morphology

Three shapes have been commonly accepted to describe most bacteria (Madigan et al., 2003): coccus (spherical or ovoid), rod (cylindrical), and spirilla (forming spiral-shaped patterns). Unusual shapes allow recognition of typical bacteria such as spirochete, tightly coiled bacteria, or filamentous bacteria, which form long, thin cells or chains of cells.

2.2.2.2. Cell membrane and cell walls

The cytoplasmic membrane is a thin structure that completely surrounds the cell. Only about 8 nm thick, this vital structure is the barrier separating the inside of the cell (cytoplasm) from its environment. This is also a highly selective barrier, enabling a cell to concentrate specific metabolites and excrete waste materials. Chemically, it is a phospholipid bilayer.
There are considerable pressures inside a bacterial cell, so bacteria need to withstand them with cell walls. Bacteria are classified in two classes based on the composition of their cell wall (Fig. 2-6; Madigan et al., 2003). The cell wall of *Gram-positive* is composed of several layers of peptidoglycan with a thickness ranging from 15 to 80 nm. The cell wall of *Gram-negative* is high in lipid content and low in peptidoglycan content. It is composed of two unique regions which surround the 6 to 15 nm thick outer plasma membrane: the periplasmic space and the lipopolysaccharide layer (LPS). The periplasmic space separates the outer membrane from the unique peptidoglycan layer (2-7 nm). The The Gram-negative cell wall is similar to a cytoplasmic membrane, typically only a few layers thick and generally much thinner than Gram-positive types.

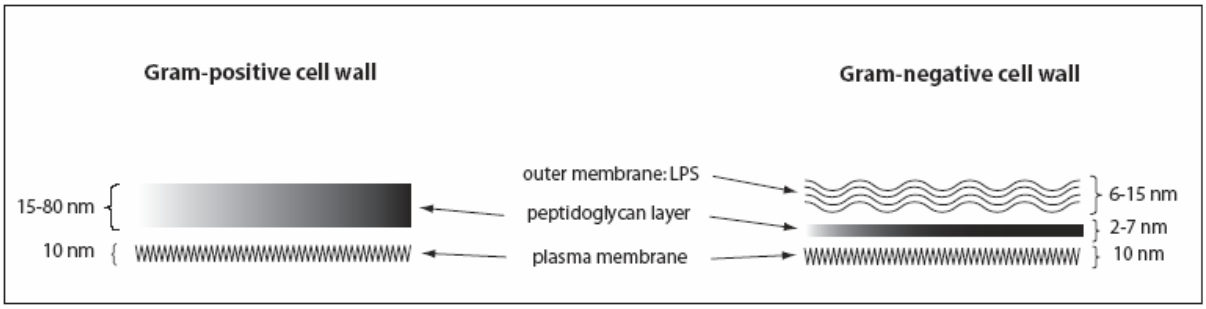

Figure 2-6 : schematic representation of Gram-negative and Gram-positive cell walls; LPS: lipopolysaccharide.

2.2.2.3. Proteobacteria : generalities

The extreme diversity of energy-generating mechanisms is a unique biochemical characteristic of the Proteobacteria: some are chemoorganotrophs (e.g., *Escherichia coli*), others are chemolithotrophs (e.g., the sulfur-oxidizing bacteria such as the thiobacilli and the ammonia-oxidizing bacteria such as *Nitrosomonas*) or phototrophs (e.g., the purple colored *Chromatium*, *Rhodospirillum* and many others). Concerning their relationship towards oxygen, the Proteobacteria include strictly aerobic and anaerobic species as well as facultative aerobes and microaerophiles. Denitrifiers are reported among the "Alphaproteobacteria," "Betaproteobacteria," "Gammaproteobacteria," and the "Epsilonproteobacteria." The importance of the proteobacterial cell is highlighted not only as the donor of the mitochondria (Falah and Gupta, 1994; Margulis, 1993), but also as one of the fusion partners (the other being a archaeal cell) giving rise to the ancestral eukaryotic cell (Gupta, 2000) for an extensive list of references). Phototrophic bacteria occur only in the "Alphaproteobacteria," "Betaproteobacteria" and "Gammaproteobacteria"; these anoxygenic phototrophic purple bacteria can be subdivided into the purple sulfur (PS; e.g., *Chromatium* and *Ectothiorhodospira*) and purple nonsulfur (PNS) bacteria (e.g., *Rhodospirillum*). All known PS bacteria belong to the "Gammaproteobacteria" and use H_2S or S° as sole electron donor. The PNS bacteria occur among the "Alphaproteobacteria" and "Betaproteobacteria." A great number of phototrophic Proteobacteria are versatile and can easily switch from a phototrophic to a heterotrophic lifestyle in the absence of light.

The β-proteobacteria are identified in various freshwater and terrestrial habitats, whereas they are rarely found in marine environments (Nold and Zwart, 1998). They contain some purple nonsulfur phototrophs, various chemolithotrophs, some methylotrophs, a great number of chemoorganotrophs and some nitrogen-fixing bacteria.

The “acidovorans” group has at present the status of the family Comamonadaceae, a phylogenetically coherent but physiologically heterogeneous group of prokaryotes encompassing genera such as *Acidovorax*, *Comamonas*, *Delftia*, *Hydrogenophaga*, *Variovorax*, *Xylophilus*, *Rhodoferax*, *Roseateles*, *Rubrivivax*, *Leptothrix* and *Sphaerotilus*.

2.2.3. ALGAE: GENERALITIES

Algae encompass several groups of living organisms that capture light energy through photosynthesis, converting inorganic substances into simple sugars using the captured energy (Madigan et al., 2003). Algae have been traditionally regarded as simple plants, and some are closely related to the higher plants. Others appear to represent different protist groups, alongside other organisms that are traditionally considered more animal-like (that is, Protozoa). Thus algae do not represent a single evolutionary direction or line, but a level of organization that may have developed several times in the early history of life on Earth.
All algae have photosynthetic machinery ultimately derived from the cyanobacteria, and so produce oxygen as a by-product of photosynthesis, unlike non-cyanobacterial photosynthetic bacteria.
Algae can endure dryness and other conditions in symbiosis with fungi.

Algae show considerable diversity in the structure and chemistry of their cell walls. Algal cells may be naked or may be covered by complete, rigid cell walls, incomplete cell walls, or a serie of plates, strips or inorganic and sometimes organic scales. In general, cell walls comprise two components, an amorphous component which forms the matrix and in which the fibrillar or second component is embedded. The fibrillar component forms the rigid skeleton of the cell wall, and is commonly cellulose. The amorphous components are mainly polysaccharides.

2.2.3.1. Prokaryotic algae: cyanobacteria

Traditionally the cyanobacteria have been included among the algae, referred to as the cyanophytes or blue-green algae, (the term "algae" refers to any aquatic organisms capable of photosynthesis), though some recent treatises on algae specifically exclude them. Cyanobacteria are some of the oldest organisms to appear in the fossil record, dating back to about 3.8 billion years (Precambrian). Ancient cyanobacteria likely produced much of the oxygen in the Earth's atmosphere.
Cyanobacteria can be unicellular, colonial, or filamentous. They have a prokariotic cell structure typical of bacteria and conduct photosynthesis directly within the cytoplasm, rather than in specialized organelles. Some filamentous blue-green algae have specialized cells, termed heterocysts, in which nitrogen fixation occurs.

2.2.3.2. Eukaryotic algae

All other algae are eukaryotes and conduct photosynthesis within membrane-bound structures (organelles) called chloroplasts.
Forms of algae:
Most of the simpler algae are unicellular flagellates or amoeboids, but colonial and non-motile forms have developed independently among several of the groups.

2.2.4. BIOFILMS AND EXOPOLYMER SUBSTANCES

Most bacteria in their natural environment live on surfaces as slime-encased, biofilm communities. In contrast to their planktonic counterparts, sessile bacterial populations are significantly more resistant (by several orders of magnitude) to environmental stresses such as harmful chemicals, antibiotics and predation (for a review see Sutherland et al., 2001). Biofilms are a collection of microorganisms surrounded by the slime they secrete, attached to either an inert or living surface.
Whereas biofilms are the dominant growth form of bacteria in nature, little is known about the biological factors that allow growth as biofilms. The ability of individual bacteria to grow slowly and survive starvation stresses, express a variety of biofilm-activated genes. Organisms within a biofilm community perform many metabolic activities as a group through a phenomenon known as quorum-sensing. Bacteria in nature, including those within biofilms, live as mixed populations.
Prigent-Combaret et al. (1999) showed that bacteria within biofilms encounter higher-osmolarity conditions, greater oxygen limitation, and higher cell density than in the liquid phase. With so many genes involved, it is perhaps not surprising that biofilm formation is regarded as a process in permanent evolution. Nevertheless, their observation is not very easy because of their highly hydrated nature. Destructive analysis can eliminate critical information on the spatial distribution, interrelationships, and structure of these constituents.

2.2.4.1. Glossary

Biofilms: Microorganisms grow on surfaces enclosed in biofilms. These are microcolonies of bacterial cells attached to a surface and encased in adhesive polysaccharides excreted by the cells. Biofilms trap nutrients for growth of the microbial population and help prevent detachment of cells on surfaces present in flowing systems. Cell-to-cell communication is critical in the development and maintenance of a biofilm (Madigan et al., 2003).

exopolysaccharide or **EPS :** Generic term referring to a high-molecular-weight polymer which is composed of sugar residues, but is excreted outside the cell by a micro-organism into the surrounding environment. It is synonymous of *exopolysaccharide*, *exocellular polymer*, *extracellular polymer*, *exopolymer*. This term does not distinguish between bound polymer (capsule) and polymer excreted into the surrounding environment. In biofilms, EPS may refer to the polymers that extend between cells, forming a matrix and anchoring the cells to each other and to the substratum (Madigan et al., 2003).

Glycocalyx: extracellular polymeric material produced by some bacteria. This term initially applied to the polysaccharide matrix excreted by epithelial cells forming a coating on the surface of epithelial tissue. It is also called slime layer, EPS, or matrix polymer (Madigan et al., 2003).

Capsule: A well organized bacterial glycocalyx that is firmly attached to the bacterial cell wall. It protects bacteria from host defenses (Madigan et al., 2003).

Slime layer: Slime layers are a diffuse mat of polymer fibers surrounding cells which appear unattached to a single cell. Slime layers protect cells from drying, serve to trap nutrients, or may bind cells together (Madigan et al., 2003).

Heterotrophic bacteria are crucial to transformation and remineralization of organic carbon, nitrogen and other nutrients throughout oceans (Azam, 1998; Azam et al., 1993). When bacteria and microalgae are associated with surfaces (e.g., sediment particles of intertidal sandflats, plant surfaces) they secrete a matrix of mucilaginous extracellular polymers (EPS) to form a “microbial biofilm”

2.2.4.2. Exopolymeric substances

a) Exopolymeric substances and biofilms

Past researchers assumed that biofilm bacteria behaved much like solitary, free-floating microorganisms (Jorand et al., 1998). While it is true that biofilm bacteria have exactly the same genetic makeup as their free-roving cousins, their biochemistry is very different because they switch to using a different set of genes.
In general, EPS are considered to be largely composed of microbial polysaccharides. However, other EPS may also be associated with biofilm systems, e.g., proteins, nucleic acids, and polymeric lipophilic compounds. Thus, the chemical composition varies widely (Jorand et al., 1998).
The chemical composition has several effects on biofilm formation in different ways (for a review see Sutherland, 2001). Apparent variations in composition of the mixtures are the result of differential synthesis of the component polymers. It is also quite possible that within extensive biofilms, different subpopulations might have miscellaneous micro-environments leading to production of different mixtures of polysaccharides. The proportions of different EPS in mixed biofilms do not necessarily reflect the proportions of the cells present, nor do the EPS contribute equally to the structure and properties of the resulting biofilms. Many of these polysaccharides are relatively soluble, and because of their large molecular mass, yield highly viscous aqueous solutions. A few will form weak gels, which dissolve in excess solvent, thus sloughing off the exposed surface of biofilms. Changes may occur when ions are present. The EPS contribute directly to the properties of biofilms in that they normally permit considerable amounts of water to be bound (Sutherland, 2001).
Polymer gels are networks of molecules interconnected by chemical or physical crosslinks. These interactions give polymer gels a unique set of physical properties (Verdugo, 1994). Polymer molecules may assemble to form “tangled networks” or “covalently crosslinked networks” stabilized by Ca ion bonds. Electron probe microanalyses reveal that microgels resulting from DOM polymer assembly are generally rich in Ca, and low in Mg and P (Chin et al., 1998). Tanaka's theory of gel-swelling suggests that the degree of crosslinking changes as a result of Ca sequestration (Tokita and Tanaka, 1991). The polymer gel acts as a Donan trap, similar to an ion-exchange resin, and concentrates cations with various degrees of specificity depending on how the network is assembled (Chin et al., 1998).

The genetic code for the biofilm construction is a known phenomenon: extractive studies have often indicated that a considerable fraction of the biofilm EPS is DNA. Thus, scanning transmission X-ray microscopy (STXM) and confocal laser scanning microscopy (CLSM) imaging both provide support for the contention that nucleic acids exist extracellularly and may have a structural role in biofilms (Lawrence et al., 2003). Recent work using DNase enzymes indicated that extracellular DNA might have a structural role in biofilm formation and stability (Whitchurch et al., 2002). Sauer (2003) demonstrated the protein responsible for the formation of biofilm in *Escherichia Coli*. Among the genes that showed increased expression in biofilms were three involved in adhesion and autoaggregation, several encoding structural proteins. One protein known to play a key role in biofilm formation is RpoS, the σ^S subunit of RNA polymerase in *E. Coli*. It governs the expression of many genes induced during the stationary phase of growth and is considered to be the master regulator of the general stress response in *E. Coli*. A large number of proteins were found to be differentially produced during the different stages of biofilm development; several proteins were differentially expressed after one day of biofilm growth and the protein-expression pattern showed maximum change compared with the expression pattern in planktonic cells in mature biofilm cells.

There are different stages in biofilm development (Fig. 2-7; Sauer et al., 2003). At stage 1, bacterial cells attach reversibly to the surface. Then, at stage 2, the cells attach irreversibly, a step mediated by EPS, and the cells lose their flagella-driven motility. At stage 3, the first maturation phase is reached, as indicated by early development of biofilm architecture. The second maturation phase is reached at stage 4 with fully mature biofilms, as indicated by the complex biofilm architecture. At the dispersion stage (5), single motile cells (dark) disperse from the microcolonies. Although development of biofilm

is related to the specific bacteria, there are different ways for microorganisms to secrete EPS depending on their environment (Voloshin and Kaprelyants, 2004).

.

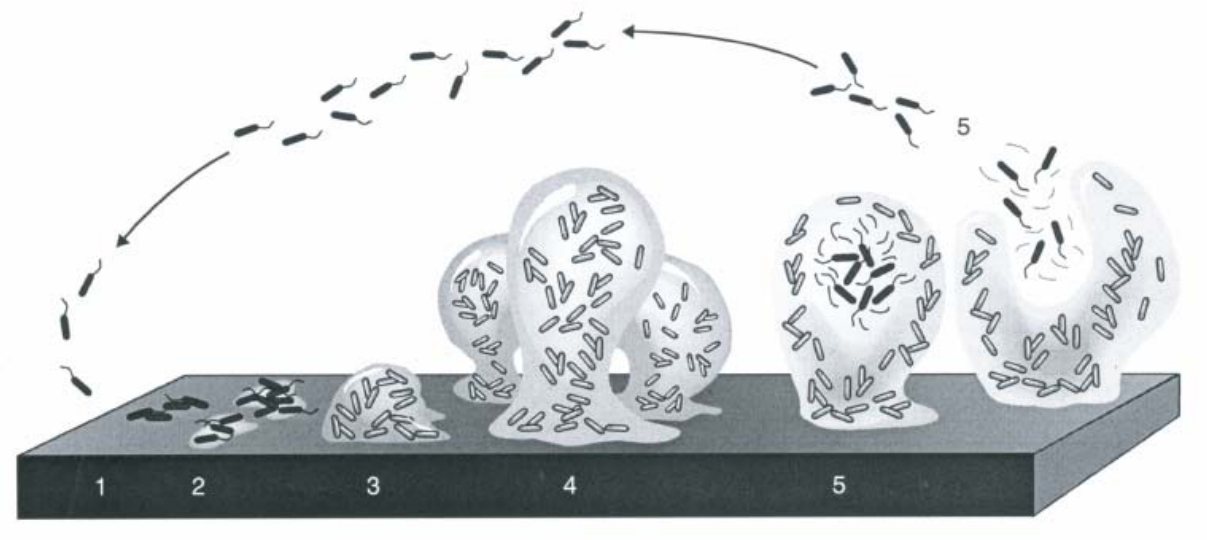

Figure 2-7: the five different stages of bacterial biofilm development (after Sauer, 2003)

Extracellular polymeric substances bind and concentrate a range of metal ions, metalloids and molecules. Many metal ions, such as Cd^{2+}, Cu^{2+}, Cr^{3+}, Pb^{2+}, etc., are efficiently chelated by EPS. The strength of the binding affinity in the complex will depend largely on ion size/charge ratios, and a number of other factors, such as EPS composition, physical gel state, pH, and ionic salinity.

Microbial exopolysaccharides contain a range of ester-linked groups and pyruvate ketals (Lindberg, 1990; Sutherland, 1990). Phosphate groups may also contribute to the binding capacity of EPS. Their occurrence in bacterial EPS is relatively common (Sutherland, 1990).

b) Morphology and architecture

In the past, it was assumed that biofilms contained disorderly clumps of bacteria located in no particular structure or pattern. New techniques to magnify biofilms without destroying the gel-like structures have enabled researchers to discover the complex structure of biofilms as if viewing a city from a satellite. Within this slime, they can form complex communities with intricate architecture featuring columns, water channels, and mushroom-like towers. Some microcolonies are simple conical structures, while others are mushroom-shaped. Water currents (arrows) flow in channels between the colonies carrying nutrients and waste (Costerton et al., 1995).
Generally, the morphologies of biofilms that occur in aquatic systems are mushroom-like (Costerton et al., 1994) with stalked EPS-encapsulated cells growing from the substratum and channels for fluid flow around and through the stalks. This well-characterized structure of aquatic biofilms is now understood to facilitate cell-cell communication. In the absence of fluid flow, however, such as in soil systems, in food, or on plant leaf surfaces, biofilms may appear as patchy films or dense microcolonies. These biofilms are unsaturated, i.e., they grow in an environment that is only transiently wet (Auerbach et al., 2000).
In most cases, the base of the biofilm is a bed of dense, opaque slime 5 to 10 micrometers thick. It is a sticky mix of polysacharides, other polymeric substances and water, all produced by the bacteria. Soaring 100 to 200 micrometers upwards are colonies of bacteria shaped like mushrooms or cones. Above “street level” comes more slime, this time of a more watery makeup and variable consistency with a network of channels through which water, bacterial garbage, nutrients, enzymes, metabolites and oxygen travel.

The EPS will also contribute to the mechanical stability of the biofilms (Mayer et al., 1999), enabling them to withstand considerable shear forces. In some polymers, the interaction with ions may yield relatively rigid gels which are less readily deformed by shear, thus producing a much more stable biofilm. Mayer *et al*. (1999) suggested that biofilms might indeed represent gel-like structures, but these may be very weak and consequently may be readily destroyed by shear or dissolution of the polysaccharides.

Exopolymeric substances have recently been subdivided into three subtypes: linear, branched and cyclic (Starkey et al., 2004). In some cases, depending on the microbial species and environment, the glycocalyx has been described as forming polymeric strands that wrap around the surface, or strands that interact with one another to form helical duplexes (Mayer et al., 1999). The glycocalyx consists of a highly hydrated polyanionic matrix (>90 % water) surrounding the bacterial cell and can be composed of hundreds to thousands of monomeric EPS units. The composition and degree of substitution of these EPS subunits may vary widely, and cells may make multiple forms. The glycocalyx may be involved in mediating bacterial adhesion, and the attachment of bacteria to form biofilms can actually increase EPS production in sessile cells (Erlandsen et al., 2004).

2.2.4.3. Consequences of sample preparation on EPS study

Exopolymer substances are highly hydrated structures, so that their observation is quite difficult and requires the use of fixers to preserve spatial distribution. However, the common method in electronic microscopy, i.e., air-drying and glutaraldehyde fixation preserves the polysaccharide biofilm, but the bacteria are distorted or collapsed. It is the same for TEM, as demonstrated by Erlandsen et al. (2004). Ultrastructural detection of the glycocalyx has been difficult because of its high polysaccharide content, which does not interact with the common postfixation stain osmium. Therefore, the glycocalyx scatters few electrons and is relatively indistinguishable in conventionally processed samples for TEM.
For nearly three decades, cationic probes such as alcian blue and ruthenium red have been used to increase the electron density of the glycocalyx for TEM analysis of a wide variety of microbes and more recently, lysine has been used to improve preservation of the glycocalyx (Fassel and Edmiston, 1999). The use of cationic dyes to protect the glycocalyx from collapse during dehydration/critical point drying and of low-voltage SEM has several distinct advantages over TEM.
The use of confocal laser scanning microscopy (CLSM) leads to a more complex knowledge about EPS. CLSM allows non-destructive optical sectioning of biofilms. Combined with multiple staining, multichannel flow cells, time lapse imaging and digital image processing, confocal microscopy offers a powerful suite of techniques for the elucidation of the development of architecture in biofilms and its influence on biofilm structure and function (Palmer and Sternberg, 1999).

2.2.4.4. Degradation and preservation in sediments

The degradation of EPS is shown by Decho et al. (2005), where natural EPS may be rapidly transformed post-secretion by heterotrophic degradation, specifically by sulphate-reducing bacteria, to a more-refractory remnant polymer that is relatively slow to accumulate in marine stromatolites.
However, nutrients in water are not a vital factor for the development of biofilms but only a limiting agent. As for example, Rogers et al. (1998) argue for the “mineral” nutrients. Microorganisms are known to extract P from cryptocrystalline Fe phosphates and Al phosphates, and from some crystalline phosphate minerals as well (Ehrlich, 1996). The plagioclase and Ontario microcline specimens are almost completely barren of colonizing microorganisms, and are devoid of any evidence of chemical weathering. The surfaces have little evidence of biological material such as glycocalyx, and they are generally smooth and unaltered. The oligoclase specimens have a few attached rod-shaped microorganisms, but no evidence of biofilm development. They hypothesize that the P in specific feldspars is released due to microbially produced acidity and chelating ligands in the vicinity of

attached microorganisms. The P in feldspars is apparently available, but only at surface-exposed apatite inclusions, so microorganisms benefit from the wide-scale weathering of feldspar and the progressive exposure in new apatite. The release of a limiting nutrient resulting from the silicate weathering promotes microbial growth, which in turn increases mineral weathering.
Researchers are studying the chemicals (called sigma factors) which signal bacteria to change their biochemistry to life in a biofilm (Costerton, 1995). If they can discover a "reverse sigma factor" which would change biofilm bacteria into planktonic free-floaters, it might be possible to dissolve biofilms by "sending the equivalent of an evacuation signal" (Coghlan, 1996).
Lithified bacterial biofilms associated with fossilized soft tissues of animal and vegetal macrofossils are well known in the fossil record (Dunn et al., 1997; Franzen, 1994; Liebig, 1998; Martill, 1987; Martill and Wilby, 1994). A study of fossils in the Eocene Messel Formation (Germany) revealed that the preservation of some soft tissues is due to their replacement by bacterial biofilms (Wuttke, 1983). After death, organic constituents of bacterial cells undergo diagenetic processes resulting in the production of bacterial biomarkers such as bacteriohopanes (Peters and Moldowan, 1993). Typical features exhibiting a smooth, sometimes fibrillar or ropy texture in Oligocene deposits resemble those of a marine biofilm (Toporski et al., 2002). Another example is given by Arp et al. (1998) from microbialites in alkaline salt lakes, where detrital particles such as quartz and feldspar grains, allochthonous carbonate crystals, partly calcified pellets, and arthropod remains, are bound within the biofilm. Early shrinkage of the EPS results in a spatial accumulation of seed crystals forming layers or patches separated from the accumulated detrital components. The filamentous mat is subsequently transformed into an organic mucus within which structures are poorly defined. The mucus substances serve as a Ca^{2+} buffer, preventing mineral precipitation at first, an effect that protects microorganisms and their microenvironments. Nucleation and precipitation does not start until the buffer capacity is overcome. Polysaccharides are generally very hydrophilic because of their polar OH-groups.

2.2.5. MICROBIAL MATS

The adherent bacteria produce microcolonies that initially develop into biofilms composed of only one bacterial type. Given time, and a sufficient supply of energy, undisturbed biofilms thicken into mats, with new species joining the fray to form a complex community of interrelated species (Konhauser, 2007).
Mat development is permitted in areas where grazing macrofauna is rare or absent. These include subtidal marine environments, intermittently exposed intertidal marine environments, hypersaline lakes, hydrothermal springs and lakes or marine basins with anoxic bottom waters.
In general, mat development occurs with a limited vertical extension and only a few millimeters in thickness. However, under more favourable conditions, they become more stable structures with grow rates of the order of 1 mm per year, balanced by biomass decomposition in the bottom layers (Fenchel, 2002).
A mat is a vertically stratified ecosystem where microorganisms with different metabolisms and growth requirements live in community (Fig. 2-8). Cyanobacteria, diatoms and other microalgae are dominant in the early stages of biofilm formation. The mats become slowly enriched in a variety of organic compounds due to the overproduction of carbon during photosynthesis and lysis of the primary producers. These compounds are degraded by fermentative and heterotrophic bacteria. Aerobic heterotrophs are functionally important as their activity leads to O_2 depletion, whereas sulfate-reducing bacteria provide H_2S for later colonizing representatives of the colourless and purple sulfur bacteria. Once a mat is fully developed, its architecture includes an array of irregular, three-dimensional cell aggregates separated by a canal system that acts as a conduit for fluid flow between all parts of the mat. A mat is governed by complex pathways in which primary production of organic carbon and nitrogen fixation by phototrophy and chemoautotrophy in the upper mat are balanced by heterotrophic decomposition below (Konhauser, 2007). This phenomenon can be observed using microelectrodes, which measure oxygen and sulfide in extremely fine intervals, about 100 µm or less.

Oxygen and sulfide measurements are often taken together because gradients of both form in many microbial environments as a result of photosynthesis and sulfate reduction, respectively. Near the zone where O_2 and H_2S begin to mix, intense activity by phototrophic and chemolithotrophic sulfur bacteria lead to consumption of both to the limits of detection of the microelectrodes (Madigan et al., 2003).

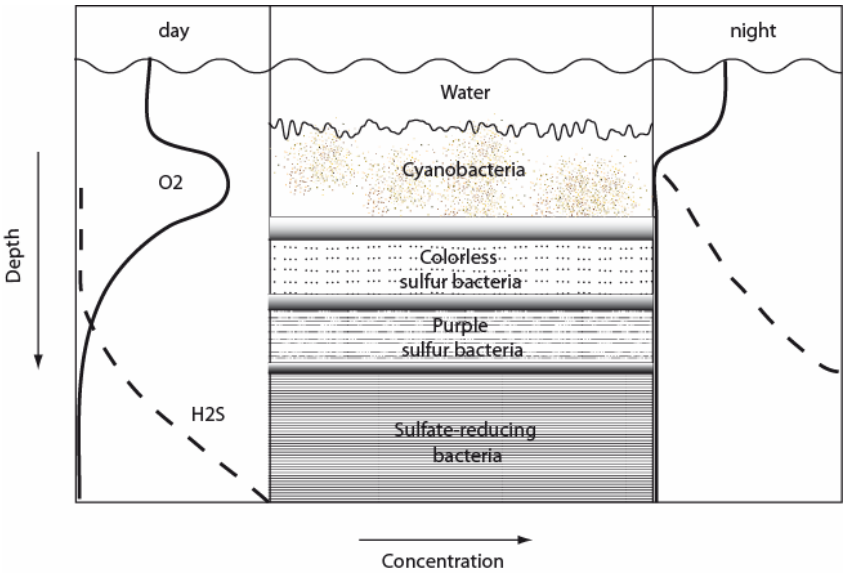

Figure 2-8 : schematic representation of a photosynthetic microbial mat; modified from Konhauser (2007).

2.2.6. ANCIENT DNA

Ancient DNA makes it possible to go back in time and understand more precisely palaeoenvironmental conditions. DNA sequences from ancient fossils have great potential for studies of phylogeny, biogeography and molecular evolution (Soltis et al., 1995).
Theoretical considerations and empirical studies suggest maximal DNA survival of 50 thousand (Kyr) to 1 million (Ma) years (Austin et al., 1997a; Austin et al., 1997b; Hofreiter et al., 2001; Lindahl, 1993; Pääbo et al., 2004; Pääbo and Wilson, 1991; Poinar et al., 1996; Smith et al., 2001; Willerslev and Cooper, 2005; Willerslev et al., 2004a; Willerslev et al., 2004b). However, several studies show the preservation of ancient DNA from plants, animals and microbes in soft tissues, minerals and sediments (Cano and Borucki, 1995; Cano et al., 1993; Cano et al., 1992a; Cano et al., 1992b; DeSalle, 1994; DeSalle et al., 1993; DeSalle et al., 1992; Fish et al., 2002; Golenberg et al., 1990; Kennedy et al., 1994; Kim et al., 2004; Lambert et al., 1998; Morita, 2000; Poinar et al., 1993; Soltis et al., 1992; Vreeland and Rosenzweig, 2002; Vreeland et al., 2000; Woodward et al., 1994). Although the viability of these results is hotly contested, the processes of DNA preservation remain unclear.
It is the environmental conditions of preservation ranther than the age of cell that determines the rate of genomic degradation (Willerslev and Cooper, 2005). The question is in which conditions environmental parameters can slow down the rate of spontaneous chemical decay of DNA? Predicting long-term DNA survival remains problematic, in part because the rates of DNA degradation under various environmental conditions are poorly understood (Nicholson et al., 2000). The post-mortem DNA decay is normally governed by endogenous nucleases. Rapid dessiccation, low temperature or high salt concentrations, nucleases can themselves become destroyed or inactivated before all nucleic acids are reduced to mononucleotides (Hofreiter et al., 2001). Hydrated DNA at moderate temperatures degrades to short fragments on a time scale of thousands of years. However, high ionic strenght, partial dehydration, and anoxia can slow the degeneration process (Lindahl, 1993) making it possible in theory for DNA to survive for much longer periods if preserved under certain conditions. The interactions of bacteria with minerals, such as clay, silica, calcite and sulfides, may shield DNA from enzymatic or oxic degradation (Inagaki et al., 2005).

The most important problem of ancient DNA viability is the contamination: laboratory-based and sample-based contamination (Hebsgaard et al., 2005).

2.2.7. NANOSTRUCTURES: A BIOLOGICAL ORIGIN?

"Nanoballs" (20-200 nm) have been found in carbonates in the 1990's. These nanoballs, closely associated to mineral precipitations, are encountered in various environments ranging from rocks to living organisms, i.e., seawater, terrigenous and carbonate rocks, and as pathogenic calcifications within living organisms. This is the beginning of the controversy between geologists and biologists, the latter arguing that these nanostructures are too small to be biologically viable. Indeed, nannobacterial cells would be too small to be viable, because they could not accommodate genetic machinery, enzymes and protein-synthesizing ribosomes. However, stressed bacteria can reduce considerably their volume, while basic cell functions are still maintained. Their viability is shown by a positive response to nucleic fluorochrom, although extraction of DNA is still impossible. Therefore, their mode of multiplication remains obscure. Some artefacts are encountered in nature where precipitates may resemble those grown from sterile solution. Moreover, several authors consider nannobacteria as technical artefacts produced by acid etching or gold coating (used in SEM preparations). Nevertheless, there are cases where artefacts can be excluded: nannobacteria can be observed in nature in low proportions without using etching or in SEM preparations using a short coating time.

The role of nanoballs in mineral precipitation is unclear, but their action is proven. Sceptical scientists argue that they could be artefacts of inorganic origin or organic molecules, but they cannot explain why nannobacteria can be cultured in a medium and why they respond positively to DNA probes. These cells would be responsible for the initiation of mineralization followed by abiotic precipitation. Their cell wall seems to have a halo of Ca^{2+}, which can create a locally oversaturated microenvironment and trigger crystallization within or around the bacterial body. 16S rDNA sequencing has tentatively assigned nannobacteria to the α-2subgroup of proteobacteria.

The fact that it has not been possible so far to extract any DNA sequence from nanoballs does not prove that nannobacteria do not exist.

3. METHODS

3.1. Techniques

Few samples have been analyzed using various microscopical and geochemical methods. Some of them were time-consuming so that is the reason why few samples have been considered in this Ph.D. They were summerized in A1.

3.1.1. PALYNOLOGY

Palynology is primarily the study of organic microfossils such as pollen, spores, marine organisms (dinoflagellates, acritarchs), etc. Moreover, this method also permits the study of amorphous organic matter in microscopy. There are three main techniques for the optical study of OM: microscopy in transmitted light (palynological method), in reflected light (petrography of coals and bitumen) and in fluorescence (indicative of the biochemical nature of OM and its degree of diagenesis).
A chemical attack is used to separate organic matter and dissolve minerals so that only the insoluble fraction is preserved, which is called kerogen (Durand and Nicaise, 1980). The use of different acids (HCl, HF) destroys respectively carbonates and silicates and a separation with dense liquid allows the elimination of the remaining mineral fraction. At the end, there remains only organic material with often framboidal pyrite. To determinate the effect of this acid treatment, we compare with well-known present-day material.
Palynofacies slides have been prepared with a standard preparation technique using HCL, HF and heavy liquid separation (Steffen and Gorin, 1993).

3.1.2. EFFECT OF ACID TREATMENT

Acid attack on bulk rock minerals is rarely complete for various reasons (Durand and Nicaise, 1980):
- All the minerals cannot be dissolved (e.g. iron sulfide)
- During HF attack, there is frequently neoformation of complex fluorides
- The minerals are protected from chemical attack by OM.

Acids especially HCl, and to a lesser extent HF, have a hydrolyzing effect on the OM in sediments. The less degraded the OM the stronger the effect. However, measurements made at the Institut Français du Pétrole (IFP) indicate that for ancient sediments the carbon loss due to hydrolysis during the preparation of the kerogen is generally low. Methods of investigation such as elemental analysis, FTIR, dark field electron microscopy and thermogravimetry do not show any important modifications.
In the case of recent material, a large part of the organic residue after the acid attack probably consists of the organic fraction which is not contemporary with sedimentation (reworked products) which are more resistant.
Moreover, no change in the isotopic signatures ($\delta^{13}C$ and $\delta^{15}N$) was apparent; with FTIR before the treatment the 1040 cm-1 band, commonly assigned to carbohydrates, was completely masked by the presence of silica (Rumpel et al., 2006).
As demonstrated by Rumpel et al. (2006), purification of SOM using HF is based on the breakdown of Si–O bonds, leading to the solubilisation of minerals. If small organic molecules are adsorbed to these minerals, they may be dissolved and lost during the treatment. Changes following HF treatment may include hydrolysis of organic compounds and melanoidin formation through recondensation of proteins and polysaccharides. Loss of OM upon HF treatment is most probably due to loss of water

soluble compounds as well as hydrolysis of some macromolecular constituents of SOM, like labile proteinaceous and polysaccharide components (Skjemstad et al., 1994).

3.1.3. OPTICAL OBSERVATIONS

3.1.3.1. Optical Microscopy

The optical microscope remains the fundamental tool for organic vs. mineral phase identification in thin sections and palynological slides. Two sources of light can be used:

1) natural light

Organic matter in palynological slides is composed of different structured elements and amorphous organic matter. They have been observed at a magnification of 10, 25 and 40 using a Leitz Diaplan microscope.

2) blue light fluorescence

The same palynological slides are subsequently studied in immersion oil using a 450-490 nm excitation filter (dichroic mirror DM500 and barrier filter AFC 0515) and at a magnification of 25 and 40 (Leitz Diaplan).

Fluorescence is the capacity of molecules to decay to lower levels by emitting radiation when they are excited to high energy. The blue UV radiation (400-490 nm) is commonly used because of its low penetrative power. It gives a better three-dimensional representation of the surface relief and fine morphology of palynomorphs. Fluorescence is not produced by the general hydrogen-rich nature of kerogens, but by particular compounds, called fluorophors and chromophors. They are defined as functional groups in a molecule which will absorb energy at a specific wavelength and re-emit it at a different (but equally specific) wavelength. Examples include the carotenoids of sporinite, the isoprenoids of alginite and resinite, the phenols of cutinite, and others aromatic structures (Tyson, 1995). However, fluorescence is apparently enhanced when these fluorophors are dispersed throughout an aliphatic medium (Robert, 1988). It is an excellent means to detect the presence of small, translucent palynomorphs or palynomorphs shrouded by AOM (McPhilemy, 1988). Fluorescence properties can be affected by preservation state as well as organic matter source (Tyson, 1984).

Counting of AOM, total phytoclasts and total palynomorphs has been carried out for each sample (300 counts per sample). Samples have been selected for their high AOM content. Blue-light fluorescence is an indicator of OM source and also an indicator of the degree of chemical preservation. The fluorescence scale has been estimated after Tyson (1995). FS1 refers to non-fluorescent OM (matrix and palynomorphs), FS2 is attributed to fluorescent palynomorphs but non-fluorescent matrix, FS3-5 characterized a progressive increase of fluorescent intensity of the AOM matrix and FS6 indicates a strong and homogeneous fluorescence of the AOM matrix. The fluorescence scale index (FSI) has been calculated (FSI = FS * %AOM/100).

3.1.3.2. Scanning Electron Microscope

The scanning electron microscope (SEM) is an instrument producing high resolution images of a sample surface. There are different possibilities to create an image with a characteristic three-dimensional quality. The microscope used in this study is a Jeol JSM 6400 model located at the University of Geneva (Switzerland).

- Principles applied to OM study

To image structure and distribution of organic matter, mode of secondary electrons (low energy <50 eV) is selected. Due to their low energy, these electrons must originate within a few tenths of a nanometer from the surface. The electrons are detected by a scintillator-photomultiplier device and the resulting signal used to modulate the intensity of a CRT that is rastered in conjunction with the raster-scanned primary beam. Because secondary electrons come from the near surface region, the brightness

of the signal depends on the surface area that is exposed to the primary beam. This surface area is relatively small for a flat surface, but increases for steep surfaces. Thus steep surface and edges (cliffs) tend to be brighter than flat surfaces resulting in images with good three-dimensional contrast. Using this technique, resolutions of the order of 5 nm are possible.

The spatial resolution of the SEM depends on the size of the electron spot which in turn depends on the magnetic electron-optical system which produces the scanning beam. The resolution is also limited by the size of the interaction volume, or the extent of material which interacts with the electron beam. The SEM has compensating advantages, though, including the ability to image a comparatively large area of the specimen; the ability to image bulk materials (not just thin films or foils); and the variety of analytical modes available for measuring the composition and nature of the specimen.

◆ Preparation of samples

1) rocks and kerogen

Rocks are only broken whereas kerogens are dried in a dessicator, then, they are deposited on a carbon film with a brush. The metallization with gold lasts for 120 seconds.

2) biological sample: critical point drying

Biological samples are hydrated, so we need to replace water by a fixator to preserve the entire structure (cytoskeleton):

• glutaraldehyde (2.5%) for 12h
• rinse with sodium cacodylate for 20 min
• successive rinses with ethanol at progressive concentrations (30, 50, 70, 90, 100% x 2) for 10 min each time
• successive rinses with amyl acetate at progressive concentrations (30, 50, 75, 100% x 2) up to 100% for 10 min each time
• critical point drying

The sample is metallized immediately after being taken out of the critical point drying machine.

3.1.3.3. Transmission Electron Microscope

◆ Principles

Transmission electron microscopy (TEM) is an imaging technique whereby a beam of electrons is focused onto a specimen, thereby causing an enlarged version which can be detected by a CCD camera. The transmission electron microscope (TEM) operates on the same basic principles as the light microscope but uses electrons instead of light. TEMs use electrons as a «light source» and their much lower wavelength make it possible to get a resolution a thousand times better than with a light microscope. The resolution is up to a few angströms. However, the maximum resolution that one can image is determined by the wavelength of the photons that are being used to probe the sample; nothing smaller than the wavelength being used can be resolved.
The image can be studied directly by the operator or photographed with a camera. TEM used for this study is a Phillips CM100 model located at the University of Paris-Sud (CCME).

◆ constraints of the method

The specimens must be very thin and able to withstand the high vacuum present inside the instrument. For biological specimens, the maximum specimen thickness is roughly 1 micrometre. To withstand the instrument vacuum, biological specimens like bacteria are typically fixed using a negative staining material such as uranyl acetate. When ultrathin sections are performed, it is necessary to do a compromise between the size of the studied area and the mechanical compression. A very small section close to a square-form is ideal. It is very difficult to select a part of the sample at this scale.

◆ Preparation of samples

Many materials require an extensive sample preparation to produce a sample thin enough to be electron transparent, and changes in the structure may occur during this process. Also the observation

field view is relatively small, so that the region analysed may not be characteristic of the whole sample. Also there is a potential risk that the sample may be damaged by the electron beam, particularly in the case of biological material.

1) sections in embedded material

Biological tissues contain large quantities of water. The water must be replaced by resin to withstand vacuum. To avoid disruption as a result of water loss, the tissue has to be preserved with different fixatives (i.e. glutaraldehyde). The latter cross-links molecules with each other and trap them together as stable structures. The tissue is then dehydrated in alcohol or acetone. After that, the sample can be embedded in plastic which polymerizes into a solid hard plastic block for 72 hours at 120°C. The block is cut into thin sections by a diamond knife using an instrument called an ultramicrotome (fig. 3-1). Each section is only 70-90 nm thick. Thin sections are recovered and deposited on a copper grid and stained with heavy metals (uranyl acetate). The slice of tissue can now be studied under the electron beam. Thin sections (70 nm) were obtained using a Leica ultramicrotome located at the University of Paris-Sud (CCME).

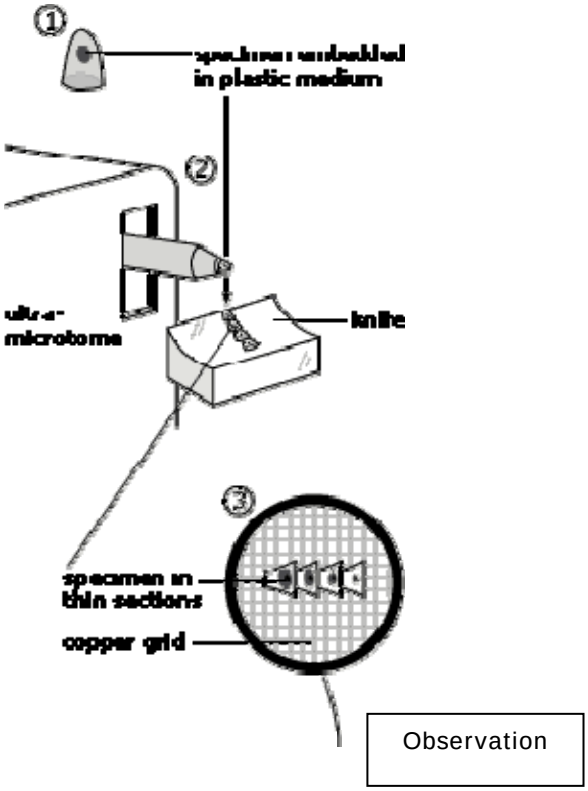

Figure 3-1 : principle of ultrathin sections, after Nobel Web AB (2007).

2) negative staining of isolated material

The isolated material (which can be a solution with bacteria or a solution with isolated molecules) is spread on a support grid coated with plastic (Fig. 3-2). A solution of heavy metal salt is added. The metal salt solution does not bind to the material but forms a "shadow" around it on the grid. The specimen will appear as a negative picture when viewing it in the TEM.

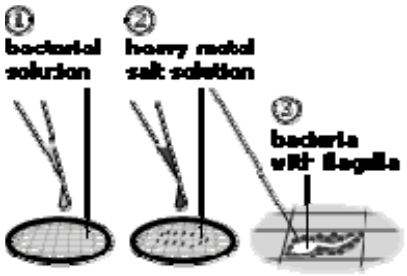

Figure 3-2 : *deposition of isolated sample, after Nobel Web AB (2007).*

3.1.3.4. Atomic Force Microscope

The atomic force microscope (AFM) is a very powerful microscope where images have a resolution down to nanometer-scale. This apparatus is equipped with a cantilever with a sharp tip at its end, typically composed of silicon or silicon nitride with nanometer-scale tip sizes (Fig. 3-3). The tip is brought into close proximity of a sample surface. The force between the tip and the sample leads to a deflection of the cantilever according to Hooke's law (elasticity states that if a force is applied to an elastic spring or prismatic rod, its extension is linearly proportional to its tensile stress and modulus of elasticity), where the spring constant of the cantilever is known.

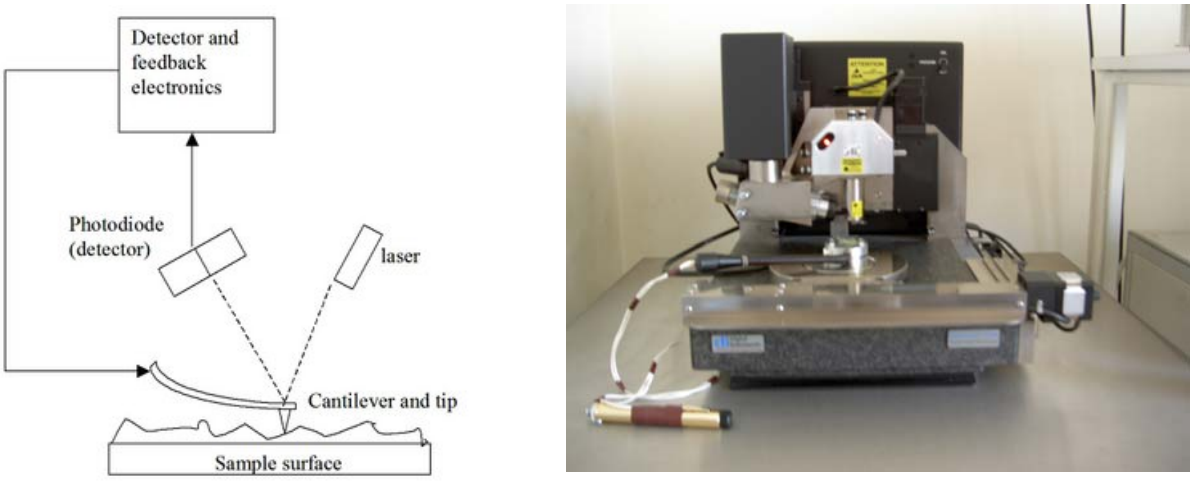

Figure 3-3: Principles of atomic force microscope.

Typically, the deflection is measured using a laser spot reflected from the top of the cantilever into an array of photodiodes. However a laser detection system can be expensive and bulky; an alternative method in determining cantilever deflection is by using piezoresistive AFM probes. These probes are fabricated with piezoresistive elements. Using a Wheatstone bridge, strain in the AFM probe due to deflection can be measured, but this method is not as sensitive as the laser deflection method.
If the tip were scanned at constant height, there would be a risk that the tip would collide with the surface, causing damage. Hence, in most cases a feedback mechanism is employed to adjust the tip-to-sample distance to keep the force between the tip and the sample constant. The resulting map of $s(x,y)$ represents the topography of the sample.
Several modes of operation have been developed for the AFM. The primary modes of operation are contact mode, non-contact mode, and dynamic contact mode. In the **non-contact mode** used in this study, the cantilever is externally oscillated by a piezometer (ability of certain crystals to generate a voltage in response to applied mechanical stress) at or close to its resonance frequency. The oscillation gets modified by the tip-sample interaction forces; these changes in oscillation with respect to the

external reference oscillation provide information about the sample's characteristics. Because most samples develop a liquid meniscus layer, keeping the probe tip close enough to the sample for the inter-atomic forces to become detectable while preventing the tip from sticking to the surface presents a major hurdle for non-contact mode in ambient conditions. Schemes for non-contact and dynamic contact mode operation include frequency modulation and the more common amplitude modulation. In frequency modulation, changes in the oscillation frequency provide information about a sample's characteristics. In amplitude modulation (better known as intermittent contact or tapping mode), changes in the oscillation amplitude yield topographic information about the sample. Additionally, changes in the phase of oscillation under tapping mode can be used to discriminate between different types of materials on the surface.
The AFM provides a true three-dimensional surface profile. Additionally, samples viewed by an AFM do not require any special treatment that would actually destroy the sample and prevent its reuse. While an electron microscope needs an expensive vacuum environment for proper operation, most AFM modes can work perfectly well in an ambient or even liquid environment. The main problem is the preparation of the sample, which must be placed on the support without sellotape or solvent to keep a natural topography. Organic samples in this study have undergone ultrasounds (30s), then were deposited on a TEM grid, previously UV-ionized for 12 hours. The grid is attached to a glass slide to standardize general height of the sample (Fig. 3-4). AFM observations were conducted using a Digital Instruments (Veeco) Nanoscope III Dimension 3100 housed at the Laboratory of Geology (Paris-Sud University), at room temperature and air.

Figure 3-4: *support for sample in atomic force microscope.*

There are major differences in the acquisition of images with the AFM, compared to the electron microscope. The electron microscope can show an area of the order of some squared millimetres and a field depth in the order of millimetres. The AFM can only show a maximum height of the order of micrometres and a maximum area of about 100 by 100 micrometres. Additionally, the AFM cannot scan images as fast as an electron microscope. It may take several minutes for a typical region to be scanned with the AFM, whereas an electron microscope is capable of scanning at near real-time (although at relatively low quality).

3.1.4. ISOTOPIC ANALYSIS

3.1.4.1. Stable isotopes

Samples were analyzed for carbon and nitrogen isotope composition ($\delta^{13}C$ and $\delta^{15}N$) by flash combustion on an elemental analyzer (Carlo Erba 1108 EA) connected to an isotope ratio mass spectrometer (ThermoFischer/Finnigan MAT Delta S) that was operated in the continuous helium flow

via a Conflo II split interface (EA-IRMS). The $\delta^{1\square}C$ and $\delta^{15}N$ values are reported relative to V-PDB and atmospheric nitrogen in air-N_2 (AIR), respectively. The reproducibility, assessed by replicate analyses of laboratory standards was better than 0.1 ‰ (1 s) for both $\delta^{13}C$ and $\delta^{15}N$ values. The accuracy of the analyses is checked periodically by analyses of international reference materials. Because inorganic carbon is effectively removed from the solid samples in the pretreatment, the carbon analyzed is referred to as organic carbon (C_{org}) in this study. Analyses have been carried out at the stable isotope laboratory (University of Lausanne).

3.1.5. CHEMICAL, GEOCHEMICAL AND BIOCHEMICAL ANALYSIS

3.1.5.1. X-Ray Diffraction

X-ray diffraction is a common method used to identify the nature and structure of crystallized products. It is based on the periodic arrangement of atoms in tridimentional reticular plane. An incident X-ray beam on a pair of parallel planes P1 and P2, separated by an interplanar spacing d are related to Bragg's low: $\mathbf{k\lambda = 2d \sin\theta}$
where k is a constant, λ, the source wavelength and θ, angle of the two parallel incident rays 1 and 2.

Powder or Debye-Scherrer method is the most commonly used when material can be reduced down to a fine powder (about 0.01 mm). The first hypothesis is that among all small crystals (theoretically non-oriented), the number would be sufficient to have crystalline faces according to 2θ angle of Bragg.
Mineralogy determinations were performed on a Philips PW 1729 diffractometer with CuKα radiation and Ni filter, under 40 kV and an intensity of 25 mA at the University of Paris-Sud.
For bulk rocks, samples were just crushed and put on a special glass slide. For the clay fraction, additional treatments are required: for organic-rich samples, the first step is the destruction of OM by hydrogen peroxide in a heating sand bath. Then the protocol of Holtzapffel (1985) was used. Samples are washed with distilled water, and then, under agitation, are decarbonated with chlorhydric acid (N/5). Successive decantation/washing cycles with distilled water lead to the defloculation of clay material and the neutralization. After homogenization and decantation (time calculated from Stokes' law), the first two centimeters are taken with a pipette:

Stokes' law: $V = C * d^2$

V = downfall speed

d = particle diameter

C = Stockes' constant depending on the difference of density between particle and liquid, liquid viscosity, and gravity acceleration.

After centrifugation (3500 tr/min, 40 min), the bottom part is recovered and put on a scraped slide.
Three preparations have been realized for each sample. One is untreated and air dried; the second is placed in a saturated ethylene-glycol solution (inducing the swelling of smectite) and the third is heated at 490°C for 2 hours. This treatment leads to the characterization of hydrated minerals or kaolinite with the preservation of chlorite.

3.1.5.2. Fourier Transform Infrared Spectroscopy

- Principles (Dekker, 1988; Silverstein et al., 1991; Silverstein and Webster, 1996)

Fourier Transform Infrared Spectroscopy (FTIR) is a tool for identifying types of chemical bonds in a molecule by producing an infrared absorption spectrum. It can be utilized to quantify some

components of an unknown mixture. FTIR can be used to identify chemicals from spills, paints, polymers, coatings, drugs, and contaminants. FTIR is perhaps the most powerful tool for identifying types of chemical bonds (functional groups).
By interpreting the infrared absorption spectrum, the chemical bonds in a molecule can be determined. FTIR spectra of pure compounds are generally so unique that they are like a molecular "fingerprint". Whereas organic compounds have very rich and detailed spectra, inorganic compounds are usually much simpler. For most common samples, the spectrum of an unknown constituent can be identified by comparison with a library of known compounds.
Because the strength of the absorption is proportional to the concentration, FTIR can be used for some quantitative analyses. Usually these are rather simple types of tests in the concentration range of a few ppm up to the percent level.
Molecular bonds vibrate at various frequencies depending on the elements and the type of bonds. For any given bond, there are several specific frequencies at which it can vibrate. According to quantum mechanics, these frequencies correspond to the ground state (lowest frequency) and several excited states (higher frequencies). One way to cause the frequency of a molecular vibration to increase is to excite the bond by having it absorb light energy. For any given transition between two states, the light energy (determined by the wavelength) must exactly equal the difference in energy between the two states (usually ground state (E_0) and the first excited state (E_1)).

All spectra were recorded at 4 cm^{-1} resolution with 64 scans (measurement time > 4 min) with a strong Norton–Beer apodization on a Perkin-Elmer Model 1600 Fourier transform infrared spectrometer (University of Paris-Sud), in the wave number range 4000 to 450 cm^{-1}. The spectrometer was equipped with a diffuse reflectance accessory which permits DRIFT measurements with high sensitivity on powders. All spectra were corrected by the Kubelka–Munk function. The system was purged and maintained permanently under nitrogen to reduce atmospheric CO_2 and H_2O absorption. Before a spectrum was run, the height of the sample cup was adjusted by using the alignment routine provided by Perkin-Elmer (energy equal or higher than 5%), to optimize the signal. A background spectrum was measured for pure KBr. Sample spectra were automatically rated against background to minimize CO_2 and H_2O bands. Correlation coefficients between two spectra of the same samples were about 99%.

- Preparation of samples

Samples for FTIR can be prepared in a number of ways. Solid samples can be milled with potassium bromide (KBr) to form a very fine powder. This powder is then compressed into a thin pellet which can be analyzed. KBr is also transparent in the IR.

3.1.5.3. Rock-Eval pyrolysis

Rock-Eval pyrolysis (Espitalié et al., 1985a, 1985b, 1986; Espitalié et al., 1977) is used to identify the type and maturity of organic matter and to detect petroleum potential in sediments. This method consists of a programmed temperature heating (in a pyrolysis oven) in an inert atmosphere (helium) of a small sample (~100 mg) in order to quantitatively and selectively determine (1) the free hydrocarbons contained in the sample and (2) the hydrocarbon- and oxygen-containing compounds (CO_2) that are volatilized during the cracking of the unextractable organic matter in the sample (kerogen).
The pyrolysis oven temperature program is as follows: for 3 min, the oven is kept isothermally at 300°C and the free hydrocarbons are volatilized and measured as the S_1 peak (detected by FID). The temperature is then increased from 300° to 550°C (at a rate of 25°C/min). This is the phase of volatilization of the very heavy hydrocarbon compounds (>C_{40}) as well as the cracking of nonvolatile organic matter. The hydrocarbons released from this thermal cracking are measured as the S_2 peak (by FID). The temperature at which S_2 reaches its maximum depends on the nature and maturity of the kerogen and is called T_{max}. The CO_2 issued from kerogen cracking is trapped in the 300°-390°C range. The trap is heated, and CO_2 is released and detected on a TCD during the cooling of the pyrolysis oven

(S_3 peak). A Rock-Eval 6® apparatus (Vinci Technologies) was used for qualitative and quantitative analyses of the organic matter (University of Paris VI).

The type and maturity of organic matter in petroleum source rocks can be characterized from Rock Eval pyrolysis data (tab. 3-1).

Rock-Eval parameters	
parameters	Geochemical meaning
S_1	amount of free hydrocarbons (gas and oil) in the sample (in milligrams of hydrocarbon per gram of rock). If S_1 >1 mg/g, it may be indicative of an oil show. S_1 normally increases with depth. Contamination of samples by drilling fluids and mud can give an abnormally high value for S_1.
S_2	amount of hydrocarbons generated through thermal cracking of nonvolatile organic matter. S_2 is an indication of the quantity of hydrocarbons that the rock has the potential of producing should burial and maturation continue until complete generation. This parameter normally decreases with burial depths >1 km.
S_3	amount of CO_2 (in milligrams CO_2 per gram of rock) produced during pyrolysis of kerogen. S_3 is an indication of the amount of oxygen in the kerogen and is used to calculate the oxygen index (see below). Contamination of the samples should be suspected if abnormally high S_3 values are obtained. High concentrations of carbonates that break down at lower temperatures than 390°C will also cause higher S_3 values than expected.
T_{max}	temperature at which the maximum release of hydrocarbons from cracking of kerogen occurs during pyrolysis (top of S_2 peak). T_{max} is an indication of the stage of maturation of the organic matter.
TOC	RE II apparatus can also be used to determine the TOC of the sample by oxidizing (in an oxidation oven kept at 600°C) the organic matter remaining in the sample after pyrolysis (residual organic carbon). The TOC is then determined by adding the residual organic carbon detected to the pyrolyzed organic carbon, which in turn is measured from the hydrocarbon compounds issuing from pyrolysis.
HI	hydrogen index (HI = [100 x S_2]/TOC). HI is a parameter used to characterize the origin of organic matter. Marine organisms and algae, in general, are composed of lipid- and protein-rich organic matter, where the ratio of H to C is higher than in the carbohydrate-rich constituents of land plants. HI typically ranges from ~100 to 600 in geological samples.
OI	oxygen index (OI = [100 x S_3]/TOC). OI is a parameter that correlates with the ratio of O to C, which is high for polysacharride-rich remains of land plants and inert organic material (residual organic matter) encountered as background in marine sediments. OI values range from near 0 to ~150.
PI	production index (PI = S_1/[S_1 + S_2]). PI is used to characterize the evolution level of the organic matter.
PC	pyrolyzable carbon (PC = 0.083 x [S_1 + S_2]). PC corresponds to carbon content of hydrocarbons volatilized and pyrolyzed during the analysis.

Table 3-1: *meaning of geochemical Rock-Eval parameters*

The results permit the identification of OM type and its maturation (Fig. 3-5; Espitalié et al., 1977). They can be estimated by: (1) the value of HI and OI and (2) T_{max} range. T_{max} = 400°-430°C represents immature OM; T_{max} = 435°-450°C represents mature OM or the oil zone; T_{max} > 450°C represents the overmature, gas-prone zone.

This method requires no specific preparation of samples, the bulk rock just needs to be crushed into a very fine powder. The TOC should be comprise between 0.5 and 1% for best results.

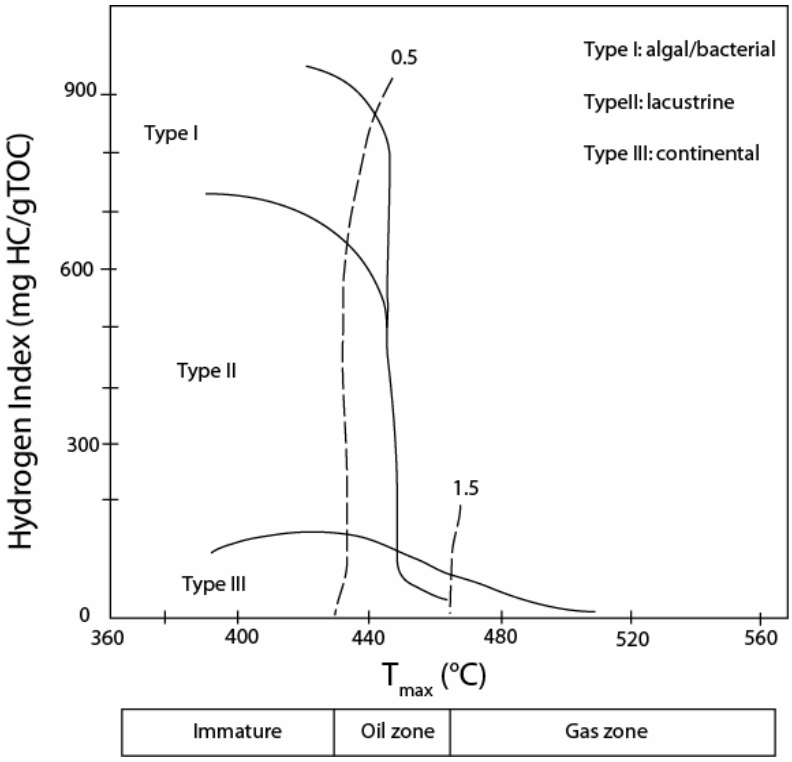

Figure 3-5 : Classification of OM types based on Hydrogen Index and Temperature. Modified from Espitalié et al. (1986).

3.1.6. DNA SEQUENCING

Since 1950, the DNA molecule has been commonly used to identify living organisms. Nevertheless, extracting and sequencing ancient DNA has proved difficult and controversial. This investigation has been perfomed in the Urbino level through sequencing of 16S DNA at the Institute of Genetics and Microbiology under the supervision of Dr. Michael Dubow and Eric Prestel (University Paris-Sud).

Brief reminders of structure and replication of DNA

The *deoxyribonucleic acid* or *deoxyribose nucleic acid* (**DNA)** is a nucleic acid that contains the genetic instructions specifying the biological development of all cellular forms of life. Each vine-like molecule is a strand of DNA: a chemically linked chain of nucleotides, each of which consists of a sugar, a phosphate and one of five kinds of nucleobases ("bases"). In many species, only a small fraction of the total sequence of the genome appears to encode protein.

Steps of replication:

- A portion of the double helix is unwound by a helicase.
- A molecule of a DNA polymerase binds to one strand of the DNA and begins moving along it in the 3' to 5' direction, using it as a template for assembling a leading strand of nucleotides and reforming a double helix. In eukaryotes, this molecule is called DNA polymerase delta (δ).
- Because DNA synthesis can only occur 5' to 3', a molecule of a second type of DNA polymerase (epsilon, ε, in eukaryotes) binds to the other template strand as the double helix opens. This molecule must synthesize discontinuous segments of polynucleotides (called Okazaki fragments). Another enzyme, DNA ligase I then stitches these together into the lagging strand.

1) solubilization of DNA

Emulsifying agents are used to dissolve lipidic compounds associated to proteases to digest proteins.

2) precipitation of DNA

DNA is purified by phenol extraction, then, it is concentrated by ethanol precipitation.

3) agarose gel electrophoresis

This is a common method to control the presence of chromosomic DNA. This method separates macromolecules-either nucleic acids or proteins-on the basis of size, electric charge, and other physical properties. Because of its negatively-charged phosphate groups, DNA migrates toward the positive electrode (anode) when a direct current is applied. The smaller the fragment, the farther it migrates in the gel.

4) amplification of this DNA: PCR

The purpose of a PCR (Polymerase Chain Reaction; Fig.3-6) is to make a huge number of copies of a gene. This is necessary to have enough starting template for sequencing.

The cycling reactions :

There are three major steps in a PCR, which are repeated for 30 or 40 cycles. This is done on an automated cycler, which can heat and cool the tubes with the reaction mixture in a very short time.

1) Denaturation at 94°C

During the denaturation, the double strand melts open to single stranded DNA, all enzymatic reactions stop (for example : the extension from a previous cycle).

2) Annealing at 54°C

The primers are jiggling around, because of the Brownian motion. Ionic bonds are constantly formed and broken between the single stranded primer and the single stranded template. The more stable bonds last a little bit longer (primers that fit exactly) and on that little piece of double stranded DNA (template and primer), the polymerase can attach itself and starts copying the template. Once there are a few bases built, the ionic bond is so strong between the template and the primer that it does not break anymore.

3) extension at 72°C

This is the ideal working temperature for the polymerase. The primers, where there are a few bases built, already have a stronger ionic attraction to the template than the forces breaking these attractions. Primers which are on positions with no exact match, get loose again (because of the higher temperature) and do not give an extension of the fragment.

The bases (complementary to the template) are coupled to the primer on the 3' side (the polymerase adds dNTP's from 5' to 3', reading the template from 3' to 5' side, bases are added complementarily to the template)

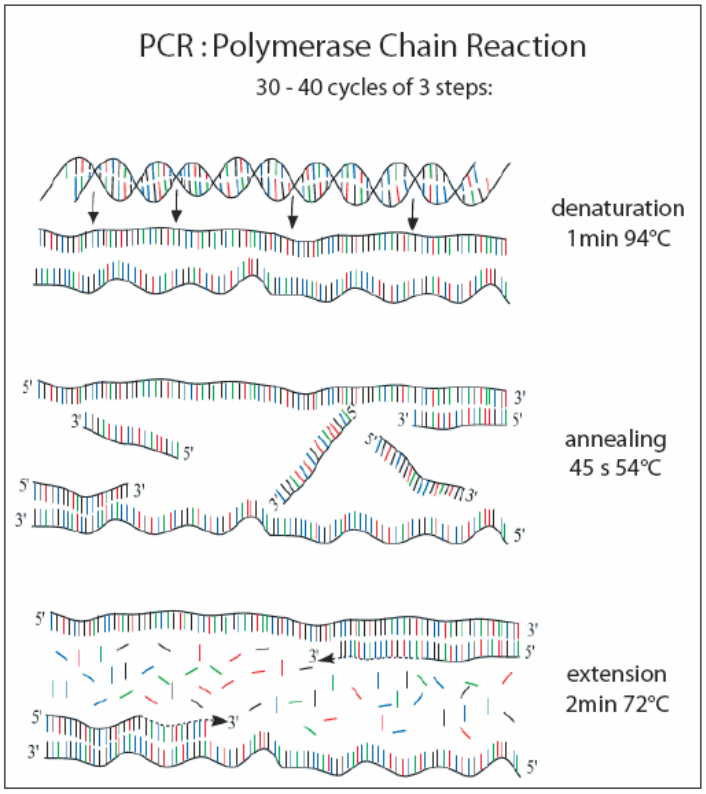

Figure 3-6: The different steps in Polymerase Chain Reaction.

Because both strands are copied during PCR, there is an exponential increase (Fig. 3-7) of the number of copies of the gene. If there is only one copy of the wanted gene before the cycling starts, , there will be two copies after one cycle, four copies after two cycles, eight copies after three cycles and so on.

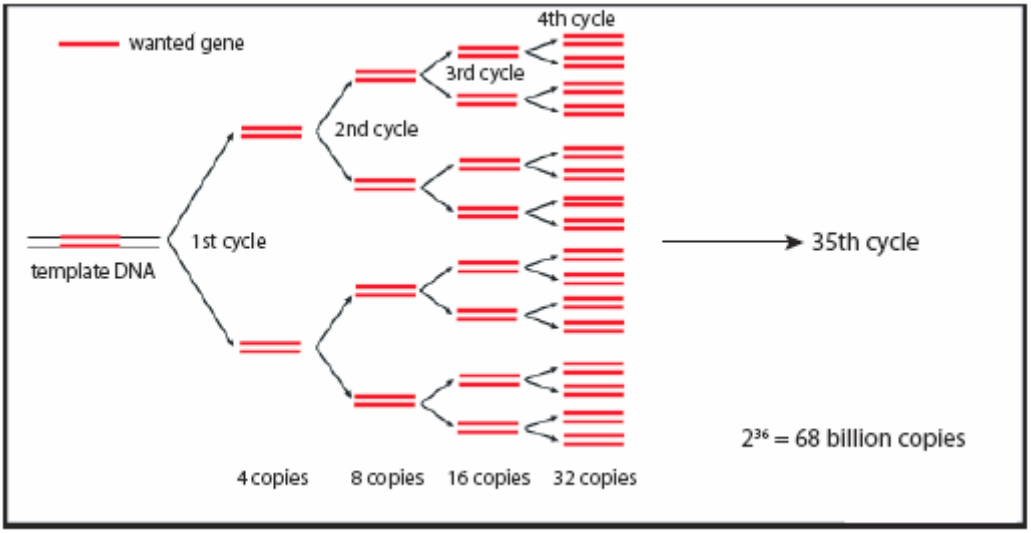

Figure 3-7: The exponential amplification of the gene in PCR.

5) insert in a plasmid

Definition: Plasmids are (typically) circular double-stranded DNA molecules that are separate from the chromosomal DNA (Fig. 3-8). They usually occur in bacteria, sometimes in eukaryotic organisms. Their size varies from 1 to over 400 kilobase pairs (kbp). There may be only one copy for large plasmids, to hundreds of copies of the same plasmid present in a single cell.

Figure 3-8: *Schematic drawing of a bacterium with plasmids enclosed. (1) Chromosomal DNA. (2) Plasmids.*

Functions: Genes on plasmids with high numbers of copies are usually expressed at high levels. In nature, these genes often encode proteins (e.g., enzymes) that protect the bacterium from one or more antibiotics. Plasmids enter the bacterial cell with relative ease. Every plasmid contains at least one DNA sequence that serves as an *origin of replication* or *ori* (a starting point for DNA replication), which enables the plasmid DNA to be duplicated independently from the chromosomal DNA.

Interest: Initially, the gene to be replicated is inserted in a plasmid. These plasmids contain, in addition to the inserted gene, one or more genes capable of providing antibiotic resistance to the bacterium that harbors them. Plasmids are deliberately introduced into bacteria in the laboratory transforming the cell with the incoming genes.
The plasmid carrying genes for antibiotic resistance, and a DNA strand, which contains the gene of interest, are both cut with the same restriction endonuclease. The plasmid is opened up and the gene is freed from its parent DNA strand. The opened plasmid and the freed gene are mixed with DNA ligase,

which covalently links the two into a molecule of recombinant DNA (Fig. 3-9). In every case, the recombinant DNA must be taken up by the cell in a form which can be replicated and expressed. This is achieved by incorporating the DNA in a vector (plasmid).

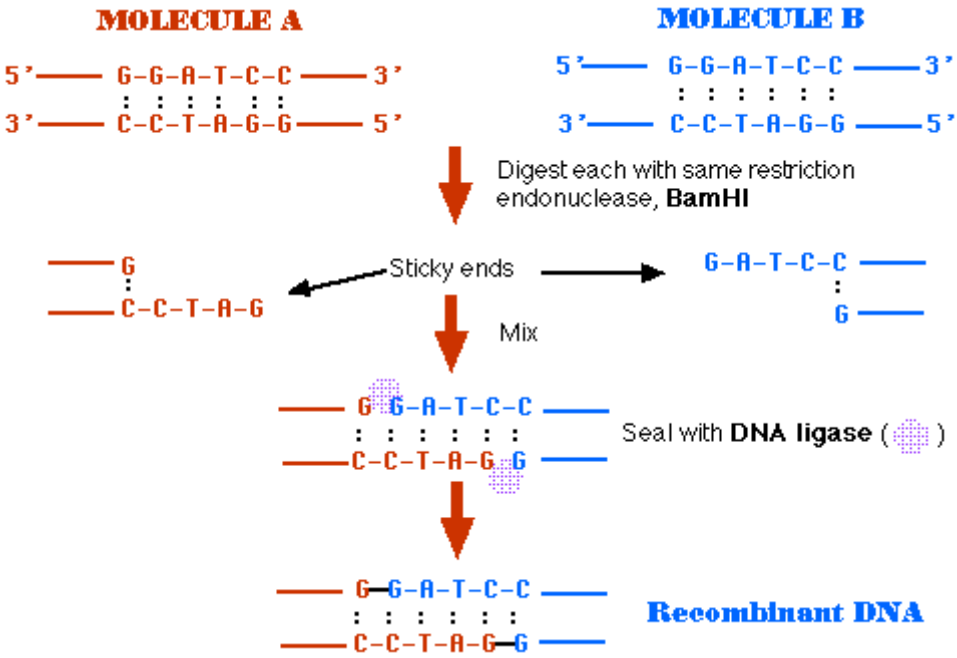

Figure 3-9: *Overview of recombinant DNA*

6) plasmid placed in competent cells: transformation - cloning

The plasmids are subsequently inserted into bacteria (competent *E. coli*) by a process called *transformation*, which are then cultured on specific antibiotic (using agar plates). Bacteria, which took up one or more copies of the plasmid, express (make protein from) the gene that confers antibiotic resistance. This is typically a protein which can break down any antibiotics that would otherwise kill the cell. As a result, only the bacteria with antibiotic resistance can survive, those containing the genes to be replicated. The antibiotic will, however, kill those bacteria that did not receive a plasmid, because they have no antibiotic resistance genes. In this way, the antibiotic acts as a filter selecting out only the modified bacteria. Now these bacteria can be grown in large amounts, harvested and lysed to isolate the plasmid of interest. Each colony represents a clone of transformed cells.

Plasmids + copies of the DNA fragment produce quantities of recombinant DNA.

This recombinant DNA stew is allowed to transform a bacterial culture, which is then exposed to antibiotics. All the cells except those which have been encoded by the plasmid DNA recombinant are killed, leaving a cell culture containing the desired recombinant DNA.

DNA cloning allows a copy of any specific part of a DNA (or RNA) sequence to be selected among many others and produced in an unlimited amount.

It is possible for several different types of plasmids to coexist in a single cell, e.g., seven different plasmids have been found in *E. coli*. On the other hand, related plasmids are often 'incompatible', resulting in the loss of one of them from the cell line. Therefore, plasmids can be assigned into *incompatibility groups*, depending on their ability to coexist in a single cell. These incompatibility groupings are due to the regulation of vital plasmid functions.

7) Purification of recombinant DNA

After the cloning, bacteria are picked and resuspended before undergoing a PCR. Then, a control with gel electrophoresis is necessary to make sure that recombinant DNA is present (Fig. 3-10). The ladder is a mixture of fragments with known size to compare with the PCR fragments.

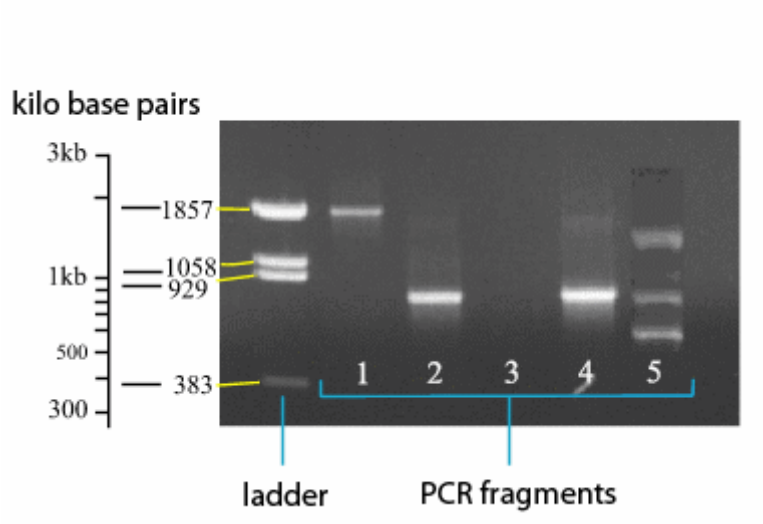

Figure 3-10: *Verification of the PCR product on gel.*

8) retrieval of DNA for sequencing

4. GEOLOGICAL AND BIOLOGICAL SETTINGS OF STUDIED SAMPLES

4.1. Fossil anoxic environments

4.1.1. THE MIOCENE MONTEREY FORMATION OF THE NAPLES BEACH SECTION

4.1.1.1. Geology and palaeoenvironment

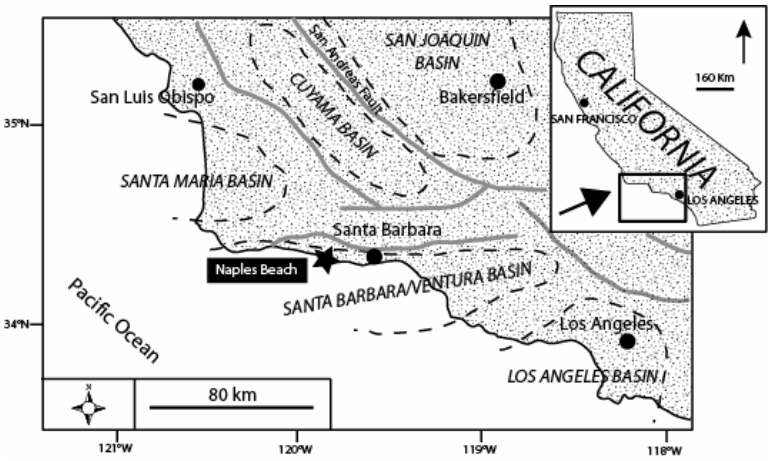

Figure 4-1 : location of the Naples Beach section (California).

The studied section is located at Naples Beach near Santa Barbara, California (Fig. 4-1). Black shales of Miocene age have been sampled. Climate in the Miocene was governed by a general cooling trend which is called the Monterey hypothesis (Vincent and Burger, 1985). Simultaneously, in the Late Oligocene to Early Miocene, plate tectonic reorganization takes place in a generally extensional context. The Monterey Formation is the result of sedimentation in a series of rapidly subsiding, sediment-starved basins (Ingle, 1981; Pisciotto and Garrison, 1981). This formation is characterized by various facies classified by Isaacs (2001) into two units: the Phosphatic Shale Member and the Siliceous Shale Member (Fig. 4-2). The upper siliceous facies is dominated by diatomaceous shales, diatomites, and/or their burial-diagenetic equivalents (porcelanites, cherts). This facies has been attributed both to an increased primary production of biogenic silica in response to climatic deterioration and intensified oceanic circulation and to a continued tectonic subsidence and consequent trapping of clastic sediments in nearshore shelf and basin areas (Isaacs and Rullkötter, 2001). Predominantly laminated fabrics, high organic-carbon contents, and scarcity of macrobenthic body fossils in the siliceous facies have been related to deposition in anoxic silled basins and in shelf, slope, and bank-top environments that intersected oceanic oxygen minimum zone (OMZ) (Pisciotto and Garrison, 1981).
The Monterey Formation is an important hydrocarbon source rock, owing to both deposition in high productivity regimes and enhanced OM preservation associated with oxygen-deficient waters.

Oxygenation events recorded by all bioturbated bed types represent periods of reduced potential for OM preservation and, possibly, decreased OM production (Ozalas et al., 1994).

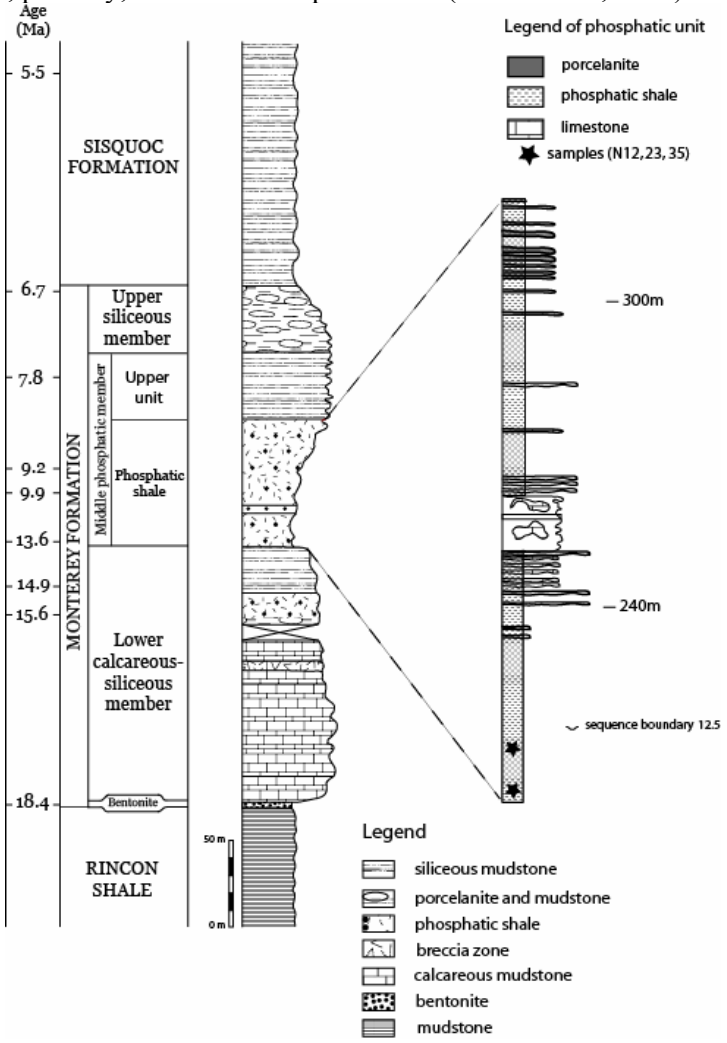

Figure 4-2 : Stratigraphical column of the Monterey Formation of the Naples Beach section; modified after Isaacs (2001.)Location of studied samples.

4.1.1.2. Origin and nature of OM

Organic matter in the Monterey Formation has a kerogen composition situated between Rock-Eval types II and III. Indeed, Naples Beach material typically displays an HI of less than 400 mg HC/g TOC and often of less of than 350 mg HC/g TOC (Katz and Royle, 2001).
Samples are dominated by AOM with minor alginate and traces of terrestrial macerals (inertinite and vitrinite). Monterey alginite is composed of platy particles of 5-50 µm, whereas AOM is an accumulation of small 0.1-1 µm fluffy, structureless aggregates (Stankiewicz et al., 1996).
Katz and Royle (2001) suggests that this apparent kerogen composition could be a reflection of:
- the presence of both terrestrial and marine components in the kerogen
- poor preservation of marine OM
- or the combined effect of a low thermal maturity level and an abundance of heteroatoms, which reduced the effective relative hydrocarbon yield.

When considering the relation between OM and its environment of deposition, (Föllmi et al., 2005) suggest that the accumulation rates calculated are not related to the quantity of OM accumulated from primary production but rather to the balance between the quantity of OM received by gravity-flow deposition from shallower areas and the quantity of OM lost by winnowing, erosion, and removal to

deeper areas. This implies that the generally high TOC values of up to 22wt% are the result of excellent preservation conditions, which overruled the negative effects on OM preservation resulting from sediment accumulation dynamics.

The Monterey kerogen has been well studied by organic geochemistry. The products from kerogen hydrolysis include mono- and dicarboxylic acids with straight chain, isoprenoid and extended hopanoid carbon skeletons, as well as α-hydroxy fatty acids, *n*-alkanols, *n*-alkan-2-ones, 6,10-dimethylundecan-2-one, 6,10,14-trimethylpentadecan-2-one, hopanoid ketoacids, saturated C_{28}-C_{30} steroid acids and unsaturated steroid alcohols (Ahmed et al., 2001; Hold et al., 1998). Ether and sulphur bond cleavage releases phytane, acyclic and cyclic biphytanes, 5β and 5α steranes (C_{27}-C_{29}), and a predominance of even numbered *n*-alkanes (Höld et al, 1998). Sulfur-bond cleavage additionally releases a highly branched isoprenoid alkane and a C_{35} hopanoid (Hold et al., 1998; Schouten et al., 1995). The low relative abundances of diasteranes probably result from the low levels of thermal maturity (Hughes et al., 1985) and/or low clay mineral content (Sieskind et al., 1979). The relative importance of the C_{29} steranes does not necessary reflect a significant amount of terrestrial organic matter (Volkman, 1986). It is more likely that the C_{29} steranes were derived from algal sources. Thus the relative abundance of C_{29} steranes would be consistent with diatoms having been the primary source for the organic matter in the Monterey Formation.
The most abundant component is 28,30-*dinor*-hopane. It is thought to be derived from chemotrophic bacteria, either sulphate reducers (Katz and Elrod, 1983; Williams, 1984) or hydrogen sulphide oxidizers, which exist at the anoxic-oxic interface (Schoell et al., 1992). This compound seems to indicate at least intermittent anoxic conditions at or very near the sediment-water interface. The variability in the 28,30-*dinor*-hopane/17α-hopane ratio implies that the level of bacterial activity has varied (Katz and Royle, 2001).
Schoell et al. (1992) compared a crude oil from California with sediments from the Monterey Formation. They concluded that the limited distribution of hopanoids in plants suggests that prokaryotes are the most important source for these triterpenoids in marine sediments. In the Californian crude oil a multitude of prokaryotic organisms, including methylotrophic bacteria, are possible sources for the C_{29} and C_{30} hopane. However, the isotopic similarity of these hopanes with the C_{27} sterane from algal primary producers suggests that the bacterial community which synthesized these hopanes was either autotrophic planktonic cyanobacteria or heterotrophic bacteria involved in the degradation of planktonic organic matter in the water column.
Photoautotrophic cyanobacteria use dissolved CO_2 as their carbon source. Therefore, their polycyclic lipids should be isotopically similar to steranes derived from autotrophic algae living in a similar or the same environment (Schoell et al., 1992).
Early diagenetic formation of organic sulphur compounds results from reaction of reduced sulphur (e.g., H_2S, polysulfides, or elemental sulphur) with lipid functional groups, such as double bonds (Sinninghé Damsté et al., 1990).
Pristane and phytane in the free lipid and sulphur-bound fractions are of similar origins and are derived from algae and/or archeabacteria ; the lack of isotopic signatures indicative of methanotrophs in these and other marine-derived organic assemblages could possibly reflect fundamental differences of methane recycling in sulphate-containing (e.g. marine) as opposed to sulphate-deficient (e.g. lacustrine) (Schoell et al., 1992).

4.1.1.3. Evidence of fossilized bacteria

The presence of fossil bacteria has been proven by remnants of bacterial cell walls which are supposed to be sulphur-oxidizing bacteria of the family Beggiatoceae (Williams, 1984; Williams and Reimers, 1983). The authors conclude that the organically-bound texture of these Miocene rocks resembles that of the sediments bound by sulphur-oxidizing bacteria in modern deep-water cores. In the Monterey Formation, zones which contain diagenetic phosphate also contain abundant organic mats, which in many cases appear to have confined or controlled growth of the phosphatic nodules and laminae.

These mats, which mimic shallow-water stromatolites, are bound by a network of colourless filamentous sulphur-oxidizing bacteria of the family Beggiatoceae (Williams and Reimers 1983). Like shallow-water cyanobacterial mats (Krumbein, 1983), sulphur-oxidizing bacterial mats contain a microbial community associated with the filamentous framework. Textures similar to those of modern bacterially-bound sediments of offshore Peru are preserved in laminated-mat diatomites of the Monterey Formation.
Beggiatoaceae species fix isotopically light nitrogen as part of their metabolic processes if other nitrogenous nutrients such as NO_3^- and NH_4^+ are depleted (Nelson et al., 1982). Mat-laminated zones in the Monterey Formation are characterized by isotopically light nitrogen, which is driven during diagenesis to slightly heavier values (Williams and Reimers 1983).
The ^{13}C depletion in bis*nor*-hopane (BNH) requires biosynthesis by an organism that utilizes ^{13}C depleted substrates. Sulfur-oxidizing bacteria could be a source of ^{13}C-depleted hopanes in marine systems, similarly to ammonia-oxidizing bacteria in lacustrine systems (Freeman et al., 1990). Sulfur-oxidizing bacteria may have flourished at the interface of H_2S-rich sediments with overlying suboxic waters or at an anoxic/oxic interface in the water column or sediments. In both cases, ^{13}C-depleted CO_2 is available from either the sediment or the anoxic water body. Katz and Elrod (1983) proposed that BNH could be related to bacteria, such as *Thioploca* spp., which forms the fossilized bacterial mats in the Monterey Formation. However, McCaffrey et al. (1989) found that *Thioploca* spp. does not synthesize hopanes and that its biomass ($\delta^{13}C$ of -21,8‰) is not depleted in ^{13}C compared to primary carbon from autotrophs. These two arguments speak against *Thioploca* as a source organism of BNH in Monterey organic matter. *Beggiatoa* is from the same family as *Thioploca*, i.e., Beggiatoaceae.
Ammonia, CO_2 and ^{13}C-depleted methane from remineralized organic matter are generally available to chemolithoautotrophic bacteria inhabiting the sediment-water interface between anoxic sediments and suboxic/oxic bottom waters. Paull et al.,0 (1992) argue against *Beggiatoa*, because $\delta^{13}C$ and $\delta^{15}N$ values are not consistent with those of Monterey organic matter. Schimmelmann et al. (2001) note that methylotrophy utilizing D- and ^{13}C-depleted biogenic methane generated by methanogenic bacteria within anoxic sediments cannot produce fossil organic matter with isotopic compositions matching that of organic matter from the Monterey Formation (Alperin et al., 1992).

4.1.1.4. The role of modern bacterial mats: comparison with Miocene sediments

Dead filaments are quickly decomposed, leaving only as fossil remnants of filaments, and more commonly, the protective mucilaginous sheaths that house them (Williams and Reimers, 1983).
The Santa Barbara Basin, Gulf of California, and coastal upwelling region off Peru and Chile are all considered as modern analogs for the Miocene Monterey Formation (Donegan and Schrader, 1981; Pisciotto and Garrison, 1981; Soutar et al., 1981).
Sulfur-oxidizing bacteria live in waters much deeper that those where algae and photosynthetic bacteria thrive. Most studies suggest that they are chemoheterotrophs, utilizing organic carbon in the sediments as a source of cell carbon (Strohl et al., 1981).
The simultaneous occurrence of phosphate and mat-laminated sediments may be coincidental, because the preferred environment for both appears to be the boundaries of OMZ. Alternatively, mats may form a barrier to the diffusion of dissolved organic phosphate from the sediments back to the water column (Williams, 1984). Consequently, a good analogue to the Miocene rocks is the Peru margin which is characterized by a region of upwelling with a great productivity. Organic matter in the Monterey Formation accumulated under dysoxic-anoxic conditions with little or no terrestrial input, as indicated by the presence of laminated sediments as well as low-oxygen benthic foraminifera assemblages, the consistently low pristane/phytane ratios and the relatively high sulphur content of the organic matter.

4.1.2. KIMMERIDGIAN BITUMINOUS LAMINITES

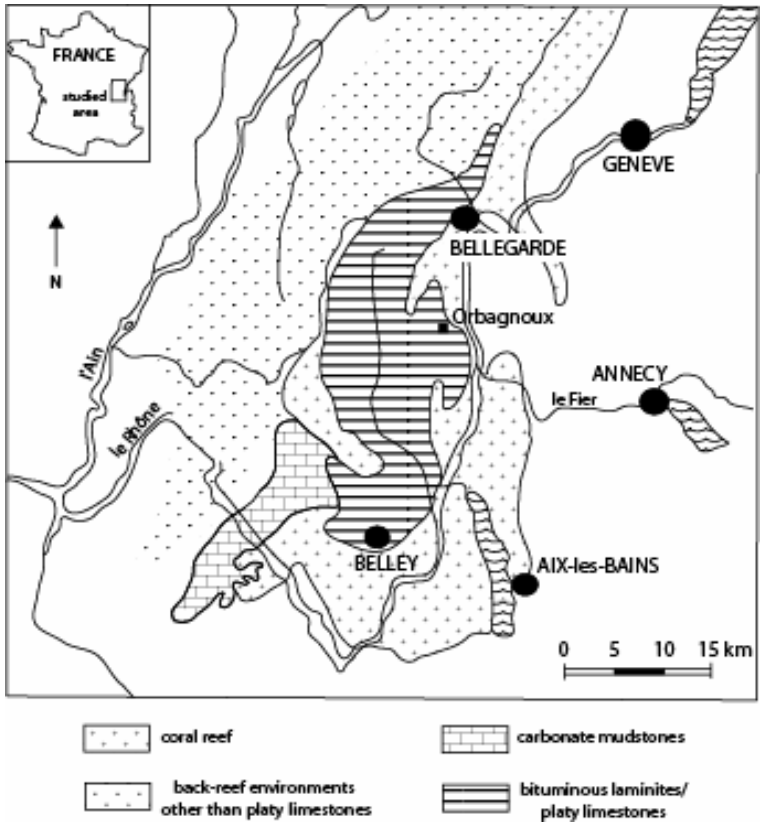

Figure 4-3 : palaeoenvironmental reconstruction of the French Jura in Kimmeridgian times; modified after Bernier (1984).

4.1.2.1. Palaeogeography

The studied outcrop is located near Orbagnoux in the French Jura (Fig. 4-3). During the Late Jurassic, the area of the Tethys was a carbonate platform, which underwent a shallowing-up trend from pelagic to paralic deposition (Bernier, 1984). During this relative sea-level fall, a barrier reef developed and produced an isolated shallow lagoon. Many authors (Bernier, 1984; Bernier and Courtinat, 1979; Bernier et al., 1991; Courtinat, 1989; Gorin et al., 1989; Gubler and Louis, 1956; Mongenot et al., 1997; Riche, 1904; Tribovillard, 1998; Tribovillard et al., 1994; Tribovillard et al., 1991; Tribovillard et al., 1992) have concluded that the organic-rich facies was deposited as a result of various parameters, e.g., enhanced phytoplankton production in a very quiet depositional environment, the presence of cyanobacterial activity, which developed biofilms at the sediment surface and a pronounced scarcity of reactive iron that allowed the early vulcanization of organic matter.
This paleolagoon is characterized by three lithological units (Tribovillard et al., 1999):

- unit 1: Neritic limestones called "calcaires de Tabalcon" are a result of a relative sea-level fall and platform progradation.
- unit 2: laminated sediments deposited in a lagoonal environment leading to the development of stromatolites and OM accumulation.
- unit 3: the depositional environment deepened temporarily, which led to the deposition of platy limestones, the "calcaires en plaquettes"

The laminated sediments, especially the dark parallel laminae, are the subject of this study.

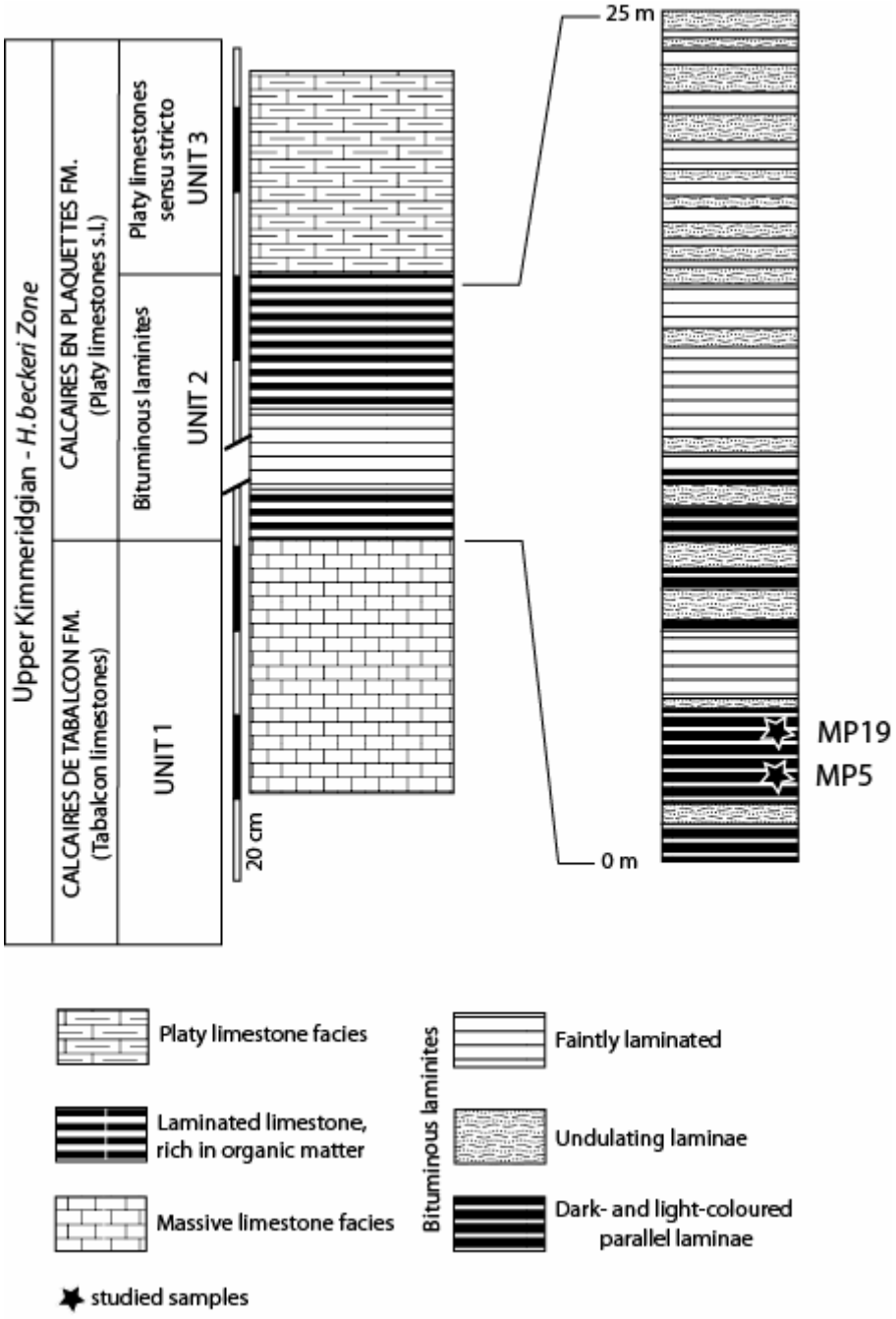

Figure 4-4 : Stratigraphical column of the Kimmeridgian laminites and location of studied samples; modified after Tribovillard et al. (1999).

4.1.2.2. Laminites

The bituminous laminites comprise five calcareous facies (Mongenot et al., 1997): four are OM-rich with a TOC ranging between 2 and 8.6%, massive limestones include dark-coloured, parallel laminae and light- or dark-coloured, undulating laminae. The carbonaceous matrix is exclusively constituted of coccoliths. The fifth (organic-poor) facies is characterized by light-coloured undulating laminae, related to cyanobacterial mat development. Organic matter in all these facies shows high hydrogen indices (from 780 to 960 mg HC/g TOC), indicative of type I OM (Gorin et al., 1989). Organic matter is essentially amorphous, of the grumelose type (Bernier and Courtinat, 1979).

Palaeoenvironmental observations suggested that the demise of the bituminous laminites may have been caused by a simple event: a moderate increase in the hydrodynamic energy of the local depositional environment at Orbagnoux. This local rise in energy may have originated from various mechanisms, including change in lagoon morphology or a decrease in the protection offered by the reef barrier, as a result of either relative sea-level rise or a decline in the coral reef (Tribovillard et al., 1999).
Geochemical analyses and palynofacies indicate that AOM in this interval results from bacterial reworking of marine phytoplankton, i.e., leiospheres and dinoflagellates (Gorin et al., 1989). The steranes distribution shows the predominance of the biologically-derived 20R-α(H),14α(H),17α(H).

♦ *parallel laminae*

These are made of alternating, submillimeter, lighter or darker coloured laminae. Various macro- and microfossils are present, including ammonites, benthic foraminifera and ostracods. The light-coloured laminae are composed exclusively of coccospheres and coccoliths. The dark-coloured laminae contain fewer coccoliths and coccospheres, embedded within a matrix of structureless, gel-like, organic matter. The organic laminae build an anastomosing mesh-like network. The palynological residue of 30 studied samples is composed of at least 95% of gel-like OM which appears nanoscopically amorphous when observed by TEM (Mongenot et al., 1997).
High S-contents occur in organic constituents and in the OM network, and the main sulphur species are thiophenes (Sarret et al., 2002). The kerogen appears to be composed of two types of units with different chemical structures and source organisms (Hopfgartner et al., 1990; Mongenot et al., 1999). The dominant type corresponds to macromolecular units based on intermolecularly sulphur-linked, normal C_{14} to C_{24} hydrocarbon chains with a marked odd-even predominance and a sharp maximum at C_{18}. These chains exhibit a high degree of cross-linking via (poly)sulphide bridges. They probably originate from cyanobacterial lipids, especially *n*-alcohols. The second type is based on longer, normal, hydrocarbon chains, up to C_{31}, and characterized by a lower degree of cross-linking. They could derive from algal lipids, likely sourced from the coccolithophorid *C. margereli*, whose mineral remains form the bulk of the rock matrix. This OM was most likely derived from planktonic algae (Tribovillard et al., 1992; Mongenot et al., 1997, 1999).
Based on geochemical data, the amorphous texture of the OM strongly suggests a negligible role of the selective preservation pathway (Mongenot et al., 1997). On the contrary, a major role was played by the lipid vulcanization pathway according to geochemical studies, which indicate that the lipids were mostly of algal origin. Moreover, the macromolecular compounds formed by S-incorporation into lipids are capable of surviving early diagenesis but also strongly oxic, post-depositional conditions probably induced by emersion (Mongenot et al., 1997; Mongenot et al., 2000).
As a consequence, the parallel laminated facies seems to derive mostly from settling mechanisms: periods of flourishing coccolithophorids led to the accumulation of lighter coloured laminae, consisting exclusively of coccoliths. These periods alternated with episodes of organic matter accumulation derived from planktonic algae (Tribovillard et al., 1992; Mongenot et al., 1997, 1999).

♦ *undulating laminae*

This facies comprises irregularly undulating, alternating light- or dark-coloured, laminae, subparallel to bedding. The thickness of these laminae is the same as those in the parallel laminated facies. Thin-section observations show an alternation of dark laminae, consisting of bundles of very thin seams, and light-coloured, thicker, carbonate laminae, occasionally containing abundant peloids. These peloids are interpreted as being of cyanobacterial origin (Tribovillard, 1998).
As concluded previously by Tribovillard et al. (1992), the biolaminations must have resulted from self-burial processes, i.e. mat-by-mat overgrowth related to ecological changes possibly affecting water salinity, light intensity and temperature in the absence of particle settling (Gerdes et al., 1991). The common presence of oxygen-demanding planktonic and benthonic organisms supports the

conclusion that the water column must have remained continuously oxic, whereas the underlying sediments were constantly characterized by anoxic porewaters. The sharp chemical interface was probably caused by the presence of cyanobacterial biofilms acting as a barrier between the two contrasting environments. Moreover, the simultaneous occurrence of abundant organic matter and reducing conditions favoured intense sulphate reduction. Hence, large amounts of sulphides were released and trapped within the sediment below the cyanobacterial barrier leading to the vulcanization process. Mongenot et al. (2000) suggest that lower OM contents are due to the extensive mineralization of mat biomass before sulfurization.

4.1.2.3. Palaeoenvironmental setting

Molecular biomarkers typical of anoxigenic photosynthetic bacteria (isorenieratene derivatives, Pancost et al., 1998) occur both in the parallel laminae and the undulating ones (that is, associated with in situ growth and detrital laminae). The presence of such molecules is generally interpreted as indicating anoxic conditions in the water column, since these bacteria are strictly anaerobic and need to be in the photic zone. However, at Orbagnoux, the frequent occurrence — and sometimes abundance — of oxygen-demanding, planktonic, nektonic and benthic organisms within the parallel laminae facies, proves the presence of at least episodically oxygenated waters. According to Tribovillard et al. (2000), the comparison between Orbagnoux and a recent analogue (Kopara Lake) indicates the occurence of cyanobacteria at surface and anoxigenic photosynthetic bacteria below the surface. Additionally, the palaeolagoon pools would have occupied small places, separated by larger carbonate zones, without laminated and OM-rich facies, but with platy limestone facies (Tribovillard et al., 2000).
The bituminous laminites would result from the alternation of periods of grossly laminated sediment — or palaeokopara — in situ growth (undulating laminae sequences) and periods of particle settling in a quiet environment (parallel laminae sequences). The latter contain many fossils (even ammonites) and their main carbonate contributors are coccoliths. They correspond to periods during which the Orbagnoux palaeolagoon was experiencing more open-marine conditions: for instance, increased water depth could have caused decreased illumination of the bottom and, consequently, decreased cyanobacterial growth. During such a time, sedimentation would have been fed by settling coccoliths and coccospheres, as well as organic-walled (phyto-) plankton (Tribovillard et al., 2000).

4.1.3. CRETACEOUS BLACK SHALES

4.1.3.1. Oceanic Anoxic Event (OAE) concept

The Middle Cretaceous is generally referred to as a greenhouse period characterized by exceptionally warm climates (Hallam, 1985; Wilson and Norris, 2001), a weak meridional temperature gradient (Huber et al., 1995) and high levels of atmospheric carbon dioxide (Berner, 1994; Freeman and Hayes, 1992). During this period, specific periods (approximately 50 ka to 1 Ma long) of enhanced OM deposition took place in marine environments, which are called oceanic anoxic events (OAEs) (Arthur et al., 1990; Schlanger and Jenkyns, 1976).
There were two OAEs during the Middle Cretaceous: a long-lasting event spanning the Barremian-Albian interval (OAE1) and a Cenomanian-Turonian short event (OAE2). Among all the OAEs, three are certainly global in nature, whereas other OAEs (OAE1b, OAE1c, and OAE1d) have only regional significance. This is partially due to the submarine volcanic activity which affected the climate and the physico-chemical structure of the oceans (Jenkyns, 1999; Kerr, 1998; Larson, 1991a, b; Larson and Erba, 1999; Leckie et al., 2002). Usually, calcareous nannofossils and foraminifera are abundant below and above black shales representing OAE1a and OAE2, associated with a dominance of radiolarians and organic-walled microorganisms.
These events are often associated with periods of dramatic climatic change and biotic turnover, and each apparently represents the sequestration of vast quantities of organic carbon into the geosphere (Jenkyns, 1999, 2003).
Enhanced preservation of OM during the OAEs probably resulted from global expansion of the OMZ. This hypothesis is supported by the chamber elongation of Early Cretaceous planktonic foraminifera recently interpreted as an adaptive response to oxygen depletion in the upper water column (Aguado et al., 1999; Bellanca et al., 2002; BouDagher-Fadel et al., 1997; Cobianchi et al., 1999; Coccioni and Luciani, 2004, 2005; Luciani et al., 2001; Magniez-Jannin, 1998; Premoli Silva et al., 1999).
Whereas the cause(s) of these events is widely debated, most authors acknowledge a complicated interplay between global warmth, increased surface water productivity and/or deep-water stagnation. Despite the uncertainties, all authors agree that the OAEs were associated with major steps in climate evolution because the burial of the excess of organic carbon must have had an influence on global temperatures by drawing down CO_2.

4.1.3.2. The Aptian OAE1a

♦ Llithological description

The lower Aptian OAE1a belongs to the *Deshayesites deshayesi* ammonite zone, *Globigerinelloides blowi* foraminiferal zone and *Chiastozygus litterarius* nannofossil zone (Baudin et al., 1998). The Selli Level, defined by Coccioni et al. (1987), is a prominent horizon at the transition between the Maiolica and Marne a Fucoidi pelagic formations in the Umbria-Marche Basin. In the type area the Livello Selli is subdivided in two parts: a lower "green interval" which gradually passes into an upper "black interval" (Fig. 4-5). According to Baudin et al. (1998), the green interval ranges from 0.28 to 1.9 m in thickness and consists of bioturbated to laminated grey to olive-grey mudstones alternating with cm-thick, radiolarian-rich layers. The black interval ranges from 0.5 to 1.1 m in thickness and consists mainly of laminated, moderate brown to brownish-black and dark-grey to black shales containing cm-thick, radiolarian-rich layers. Pyritic nodules are frequent in this interval. *Leupoldinids* and *Nassellaria* dominate respectively planktonic foraminiferal and radiolarian assemblages (Premoli Silva and Sliter, 1999). The Selli level is characterized by an uneven distribution of the hedbergellids and globigerinelloidids and a contemporary diversification within the "clavate" group (Premoli Silva

and Sliter, 1999). Bioturbation and organic linings of foraminifera are the only indications of benthic life (Galeotti, 1998). Fish remains (scales and vertebrae) are also common.
There are rapid changes in $\delta^{13}C$ values indicating a perturbation of the carbon cycle (Arthur et al., 1990; Jenkyns, 1995).

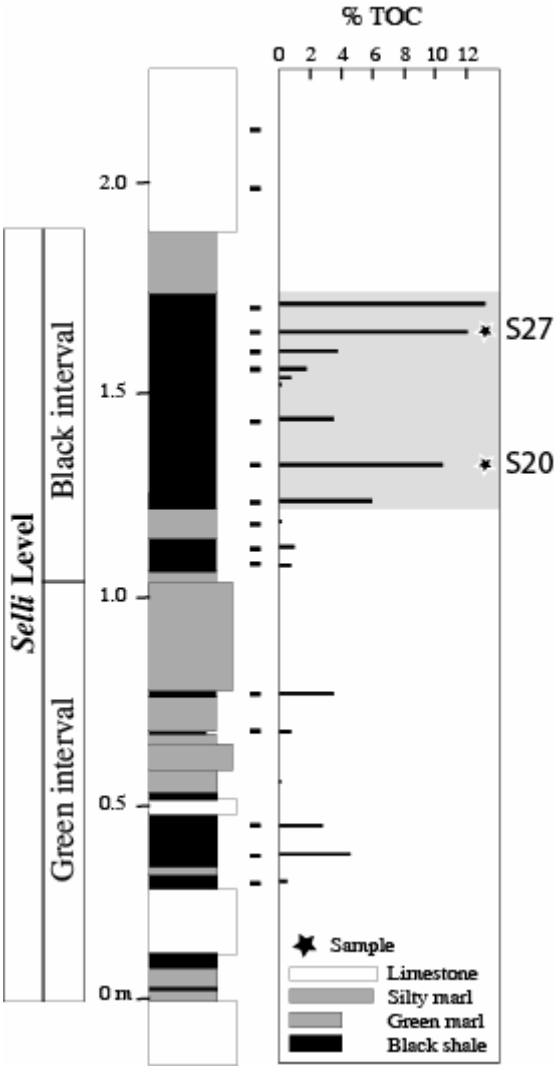

Figure 4-5 : stratigraphical column of the Selli Level at Gorgo a Cerbara and location of studied samples, after Fiet (1998).

♦ *organic matter*

The organic-rich layers of the Selli Level contain predominantly marine OM (Erbacher, 1994; Pratt and King, 1986). The AOM in the Cismon section (Italy) is characterized by a weak fluorescence and by remnants of woody or cuticular structures (Hochuli et al., 1999). Heimhofer et al. (2006) characterize SOM in the Vocotian Basin (SE France) as moderate to strong UV fluorescence of the amorphous fraction and the palynomorphs. The non-fluorescent AOM is interpreted as a more degraded stage of an originally homogeneous fraction. Three types of phytoclasts have been differentiated: membranes comprise single layered plant tissue including recognizable cuticular debris of terrestrial origin and altered plant fragments of uncertain origin. The other two types, woody debris of brown colour and opaque particles consisting of oxidized or charred wood and other plant debris, represent the most degradation-resistant part of the assemblages. Weakened fluorescence of the palynomorphs and AOM must be attributed to a different degree of alteration.

According to Coccioni et al. (1989), the greenish-grey mudstones and radiolarian-rich layers of the Selli Level usually show trace fossils referable to *Planolites* and *Chondrites*.
Oxic degradation can also be inferred from the relatively weak fluorescence of palynomorphs, especially of the dinoflagellate cysts (Hochuli et al., 1999). Evidence of ocean fertility and primary production during the deposition of the Early Aptian Selli black shales is supported by the relatively high accumulation rates of C_{org} inferred from the sedimentation rates provided by Herbert (1992) of ~0.2gC/cm^2/k.y.

♦ *isotopes*

The negative trend of $\delta^{18}O$ measured in the carbonate-rich horizons and the low $\delta^{18}O$ values measured in the Selli unit support the evidence of warming (increase of 5°C) of the surface ocean water and decreased salinity levels due to enhanced continental runoff (Hochuli et al., 1999).
The negative spike at the base of the $\delta^{13}C$ excursion, documented for OAE1a, is interpreted as reflecting a massive methane release inducing global warming (Beerling et al., 2002).

♦ *Biomarkers*

The biomarker Pristane/Phytane ratio (>2) shows a distinct oxic influence in the depositional environment (Hochuli et al., 1999).
Pancost et al. (2004) documented the occurrence of specific biomarkers (e.g. maleimides and high molecular weight porphyrins) in Central Italy (Selli Level). These biomarkers are diagnostic for green sulphur bacteria and indicate short-lived periods of euxinic conditions (i.e., a water column containing free H_2S) reaching the photic zone during formation of the OAE1a.
The extractable hydrocarbons in OM of the Vocontian Basin, are dominated primarily by short-chain *n*-alkanes, acyclic isoprenoids and abundant steroidal and hopanoid hydrocarbons (Heimhofer et al., 2004). Peak maxima are represented by pristane and phytane, followed by short-chain *n*-alkanes (*n*-C_{15} to *n*-C_{19}) and steranes (C_{27} and C_{29}). On the contrary, long-chain *n*-alkanes (*n*-C_{27} to *n*-C_{33}) with a relatively low odd-over-even predominance (OEP) of 1.4–1.7, are only a minor constituent. A significant algal contribution is suggested from the high abundance of short-chain *n*-alkanes (Farrimond et al., 1990; Gelpi et al., 1970) and of steroidal components (Volkman, 1986). Furthermore, high quantities of phytane point to a phytoplanktonic source (Didyk et al., 1978; Kohnen et al., 1992). Bacterial contributions are recorded through the high abundance of hopanes (Rohmer et al., 1992). There is no evidence for an important cyanobacterial contribution in the studied interval.

♦ *Palaeoclimatology*

A phase of carbonate platform demise has been documented from the northern Tethys margin as well as from circum-Atlantic regions (Weissert et al., 1998), which slightly predates the OAE 1a. According to Larson and Erba (1999), the Middle-Cretaceous period of global warmth was triggered by extensive submarine volcanic activity including increased spreading rates along mid-ocean ridges and the formation of extensive oceanic plateaus. The latter are termed "Large Igneous Provinces" in relation with the emplacement of the giant Ontong Java and Manihiki Plateaus, and construction of the Nova Canton. The accompanying volcanic degassing may have resulted in exceptionally high atmospheric carbon dioxide levels and related Mid-Cretaceous greenhouse warming (Arthur et al., 1985).
Based on geochemical evidence (Brass et al., 1982) and general ocean circulation model experiments (Barron and Peterson, 1990; Bice et al., 1997), deepwater circulation in the mid-Cretaceous ocean was predominantly controlled by the formation of warm and saline waters in low-latitude shelf areas. These unusual palaeoceanographic conditions favoured the formation of thinly laminated, organic-rich

black shales in hemipelagic and pelagic environments, which reflect deposition under dysoxic–anoxic bottom water conditions.
Two hypotheses have been proposed for this deposition, i.e., enrichment in organic carbon:

i) The first model is based on reduced oceanic circulation, coincident with reduced productivity. Indeed, the decline in oxygen-rich deep water production prevents the aerobic degradation of OM within the water column and at the sediment–water interface, resulting in its accumulation at the seafloor and in sediments (Arthur et al., 1990; Bralower and Thierstein, 1984; Erbacher et al., 2001; Schlanger and Jenkyns, 1976; Tyson, 1995).
ii) The second model is a high-productivity one requiring efficient circulation and nutrient recycling. This causes increased oxygen deficiency within the water column and hence, increased OM preservation under dysoxic to anoxic bottom waters. The important role of enhanced oceanic palaeoproductivity to account for the increase in OM burial during the middle-Cretaceous OAEs has been emphasized by various authors (Arthur et al., 1987; Erba, 1994, 2004; Jenkyns, 1999; Pedersen and Calvert, 1990; Premoli Silva et al., 1999; Weissert et al., 1998).

Recently, it has become evident that depositional conditions of such organic accumulations are more complex and require other parameters than only anoxia and productivity.
Other parameters must be taken into account. Sea-level fluctuations have been suggested by various authors to play a key role in the formation of black shales in hemipelagic and pelagic settings (Bréhéret, 1994; Erbacher et al., 1996; Strasser et al., 2001). According to nannofossil assemblage composition, the Selli Level has been interpreted as a high productivity event (Premoli Silva et al., 1999). The occurrence, although low, of benthic foraminifera, which are poorly diversified and of very small size throughout the Selli indicate that bottom waters were never totally anoxic but probably only dysoxic (Premoli Silva et al., 1999). This is in agreement with an upwelling system (Valdes et al., 2004). The specific foraminiferal arrangement (with radially elongated chambers) implies that local factors such as upper water column stratification, seasonality, and/or productivity may have been superimposed on the global ecological perturbation related to the Selli Event, thereby controlling the stratigraphical distribution of these forms (Coccioni et al., 2006).

4.1.3.3. The Albian OAE1b

Several expressions of OAE1b are represented in the world, such as in Central Italy (Marche Umbria Basin), southeastern France (Vocontian Basin) and some ODP legs such as 207. Planktonic foraminifera with elongated chambers are also found in the OAE1b with a low abundance and diversity (Coccioni et al., 2006). These authors assume that the relation between increased abundances of elongate-chambered planktonic foraminifera and the OAEs support the hypothesis of eutrophic conditions, coupled with other environmental factors. They propose that although water oxygenation and eutrophic conditions may have been significant controlling factors governing the development of elongated chambers in Early Cretaceous planktonic foraminifera, an interplay of several physical–chemical and ecological factors, including also temperature, salinity, seasonality, productivity, type of food, and trace elements, was likely responsible for the development of such a morphological adaptation.

Biomarker analyses reveal a disturbed depositional mechanism during the OAE1b (Kuypers et al., 2002). Archaea-derived isoprenoidal tetraether membrane lipids and free and macromolecularly bound isoprenoid alkanes are abundant in the investigated black shales. The large difference (up to 12‰) in $^{13}C/^{12}C$ ratio between the algal biomarkers and the much more abundant pelagic archaea-derived biomarkers indicate that the latter were living chemoautotrophically, possibly using ammonium as an energy source.
There seems to be no unifying mechanism for black shale deposition during the middle-Cretaceous OAEs (Kuypers et al., 2002). According to Erbacher et al. (2001), the probable cause of the OAE1b deposition was enhanced by an increased thermohaline stratification 112 Myr ago, supported by stable

isotopic data. OAE1b is associated with an increase in surface-water temperatures and runoff that led to decreased bottom-water formation and elevated carbon burial in the restricted basins of the western Tethys and North Atlantic. Thus, a well mixed, well ventilated, low-nutrient water column with relatively high salinities and cool temperatures increased moderately in temperature at the same time as surface-water salinity decreased, causing pronounced thermohaline stratification of the water column.

4.1.3.4. Other studied OAEs 1b: 113 *and* Urbino *Levels*

Others minor/local OAEs have been discovered above the Selli Level (Fig. 4-6; Baudin et al., 1998): several discrete black marker-beds occur above the Selli Level in the Marne a Fucoidi Formation, i.e., the **113 Level** (5-25 cm thick, latest Aptian), the Monte Nerone Level (2-2.5 m thick, Aptian-Albian boundary) and the **Urbino Level** (15-40 cm thick, Early Albian). The Selli Level appears as one of the major episodes of organic matter accumulation in the Cretaceous succession of the Umbria-Marche Basin. Its geochemical characteristics are similar to those of the Urbino and Bonarelli Levels which show comparable average TOC and HI values. However, these horizons have been so far poorly studied.

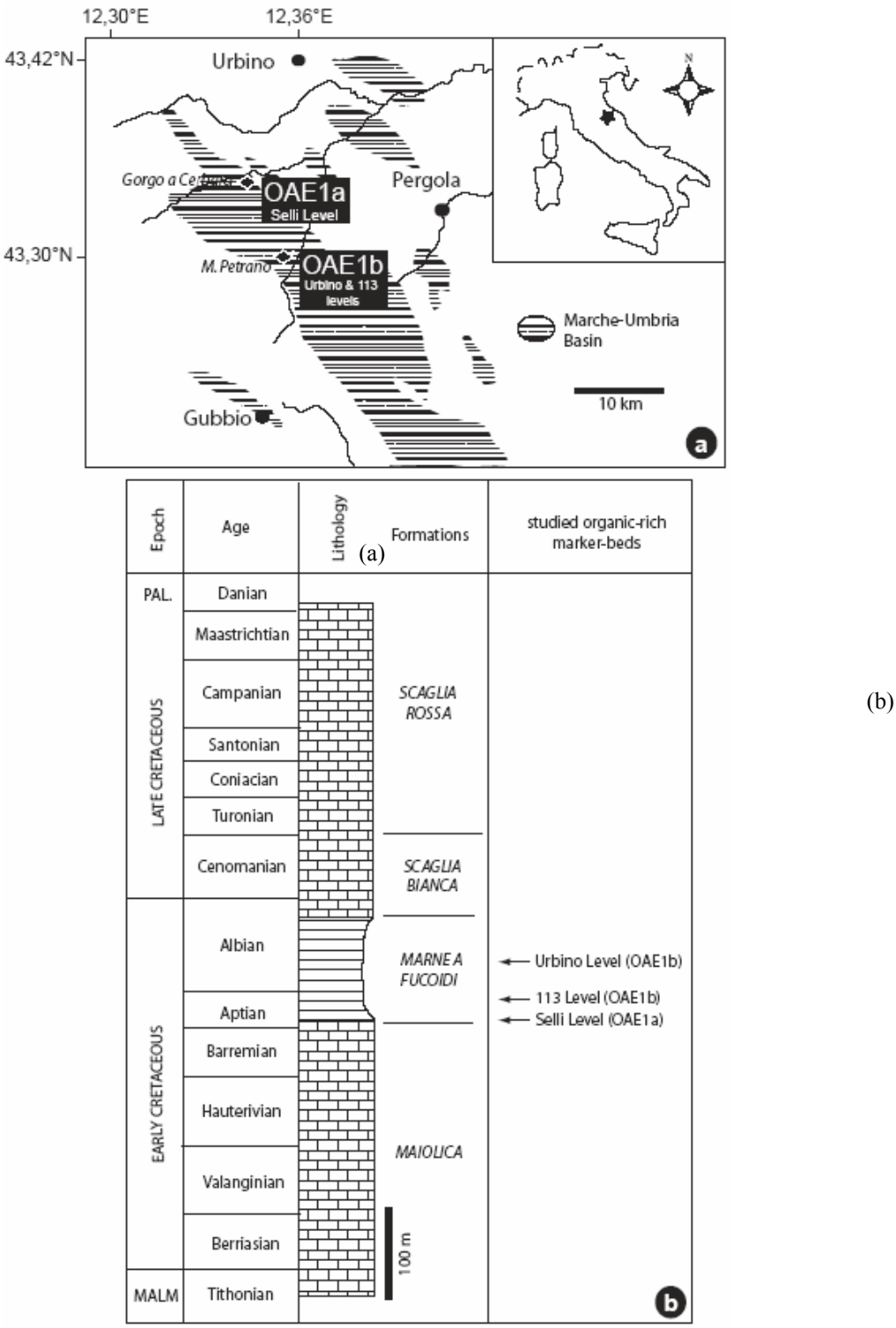

Figure 4-6 : Location map (a) and stratigraphical column (b) of the different studied OAEs.

4.2. Recent analogs: bacterial and continental samples

4.2.1. SULPHUROXIDIZING BACTERIA

Sulphuroxidizing bacteria are found in great abundance in areas with locally high sulfide fluxes such as hydrothermal vents, cold seeps or methane hydrates. They are also especially abundant in most coastal environments and in freshwater. They accumulate nitrate in their large vacuoles and utilize it as terminal electron acceptor for sulphide oxidation to sulphate. Conspicuously high biomasses of sulphur bacteria are found in areas of coastal upwelling where the high primary production leads to an enhanced export of organic material to the sediment and sulphate reduction rates are exceptionally high. The ability to store nitrate is found in three different genera of colourless sulfur bacteria, i.e., *Beggiatoa*, *Thioploca* and *Thiomargarita*. The most abundant seems to be *Beggiatoa*. They are present in continental shelf sediments of the central Chile upwelling, in Tokyo Bay and in Monterey Bay. They could be analogs of fossilized mats in the Monterey Formation. The bacteria depend indirectly on the local primary productivity and the intensity of upwelling. They are consumed by some protozoa (ciliates, amoebas) and meiofauna (nematodes) but the role of these interactions in food web dynamics is relatively unstudied.

4.2.1.1. Beggiatoa spp.

Beggiatoa are gram-negative proteobacteria, which are morphologically similar to some cyanobacteria (though lacking photosynthetic pigments) and are motile by a gliding motion. They include both colonial and filamentous forms, and appear white due to the reflection of light against their sulfur inclusions and may form mats on marine sediments ranging in size from a few millimetres to several meters. *Beggiatoa* spp. occur as intertwining masses of elongate filaments that bind detrital and organic matter together. A mat sample from the anaerobic zone exhibits a foamy texture with bacterial filaments binding detrital matter into cohesive balls. The framework of the mat appears as a mass of intertwining filaments binding terrigenous clays and fine silts, AOM and diatom frustules in an open porous network (Grant, 1991).
Mat communities can include photosynthetic microorganisms, and in areas where sulphide and oxygen concentrations overlap at the sediment surface, the sulfur bacteria perform diurnal vertical migrations, appearing at the sediment surface during darkness. Their metabolism is essentially chemolithotrophic. They oxidize sulphide into elemental sulfur or sulfate, and can use nitrate in the absence of oxygen.
However, it was proven that marine *Beggiatoa* can grow lithoautotrophically, inorganic sulfur compounds having been used as energy metabolism in microgradient cultures (Nelson, 1989; Nelson et al., 1986). Moreover, the strain isolated by Grabovich et al. (1998) from a freshwater stream is capable of mixotrophic and strictly lithoheterotrophic growth, with sulfur compounds used as electron donors. In a way metabolism is aerobic or microaerophilic with oxygen as the terminal electron acceptor in respiration. Sulfur may substitute as the terminal electron acceptor for a short period in the absence of oxygen. The substitution of sulfur for oxygen is usually thought to be used while the bacteria glide to a new area where oxygen can be acquired. Marine *Beggiatoa* spp. can live anaerobically and conserve energy by coupling sulphide oxidation with the reduction of nitrate to dinitrogen and/or ammonia (Muβmann et al., 2003). In general, their presence in shallow water areas is considered as an indication of environmental deterioration like in Lake Geneva.

4.2.1.2. *Thioploca spp.*

Thioploca spp. are very close to *Beggiatoa* but they are unculturable; they are found in shelf sediments along the coast of southern Peru and northern to central Chile within the oxygen minimum zone, reach a high biomass of up to 1 kg/m2 (fresh weight including sheaths) (Gallardo, 1977). Studies on partially purified mixed cultures of *Thioploca* spp. showed that they oxidize sufide to sulfate while reducing nitrate to ammonium (Otte et al., 1999). The marine *Thioploca* spp. commute up and down in their sheaths between the sediment surface, where they take up nitrate from the overlying seawater, and deeper parts of the sediment, where free hydrogen sulfide is available (Sayama, 2001).
The bacteria have a uniseriate filament with distinct crosswalls, consisting of a row of cylindrical, disk-shaped cells with diameters of 5-9 µm and with many sulphur globules. Otte et al. (1999) confirm that *Thioploca* species are facultative chemolithoautotrophs capable of mixotrophic growth. The *Thioploca* recharge their "lungs" with nitrate at the surface and oxidize sulphide at depth, thereby storing elemental sulfur globules as an energy reserve (Jorgensen and Gallardo, 1999).

Unlike *Beggiatoa*, filaments often have tapered ends and occurred as bundles surrounded by a common sheath. The cell length of the marine *Thioploca* spp. is generally 0.5-1.5 times the cell diameter and a single filament many contain more than a thousand cells. The cells are separated by septa formed by the cytoplasmic membranes and the innermost layer of the complex, four-layered cell wall (Maier and Murray, 1965; Strohl et al., 1981). Pasteris et al. (2001) showed that the red autofluorescence of membrane material reveals relatively thick outer cell walls and much thinner internal cell membranes, i.e., septa, within the trichomes. Numerous sulphur inclusions are found in the cytoplasm, most probably formed by intrusions of the outer cytoplasmic membrane (Maier and Gallardo, 1984; Maier and Murray, 1965; Maier et al., 1990). Most of the sulphur spherules are localized in or adjacent to the cell walls and do not occur in the central portion of an individual cell, most of which is a fluid-filled vacuole (Pasteris 2001).
A unique cellular structure was observed by Maier and Gallardo (1984) and Maier et al. (1990). Inside each cell of the filaments they found a central liquid vacuole which filled more than 80% of the total cellular volume and which was bounded by a membrane. The active cytoplasm was thus distributed as only a thin layer along the periphery of each cell (Jorgensen and Gallardo, 1999). It was previously assumed that *Thioploca* would reduce their intracellular NO_3^- to N_2 (denitrification), but the incubation experiments of washed *Thioploca* sheaths with ^{15}N compounds showed that although conversion to N_2 cannot be ruled out, dissimilatory reduction of NO_3^- to NH_4^+ is the preferred pathway in *Thioploca* (Otte et al. 1999).

4.2.2. MICROBIAL MATS

4.2.2.1. *Hassi Jerbi (Southern Tunisia) near the sabkha El Melah.*

The southern Tunisian coast is characterized by a semi-arid climate. In the study area, the tidal range is up to 1.5 m during spring tides and winter storms. Because the bathymetric gradient is low, wide intertidal zones are often exposed. The island of Jerba is connected to the coastline by a well-developed barrier-island system cut by two tidal channels (Fig. 4-7).
Characteristic morphological features include lagoonal basins partially closed by coastal spits. When groundwater salinity increases, this environment grades into a sabkha.. Sabkha are exposed to a high degree of environmental fluctuation. They are characterized by flat and very saline areas of sand or silt lying just above the water-table. This environment favours the development of microbial mats, which are adapted to hypersaline conditions. The horizontal distribution of surface sea water results in a characteristic sequence of increasing salinity from the lagoon towards the higher lying sabkha [measurements during the study revealed a range from 40‰ (lagoon) to 180‰ (further inland sites of microbial mat growth) (Gerdes et al., 2000). They often contain soft nodules and enderolithic veins of

gypsum or anhydrite. A thin crust of halite and gypsum may be present in some parts. Subsurface, chicken-wire gypsum is common in the inner parts of the sabkhas.
Cyanobacterial mats have been sampled in supratidal marshes (Davaud and Septfontaine, 1995).

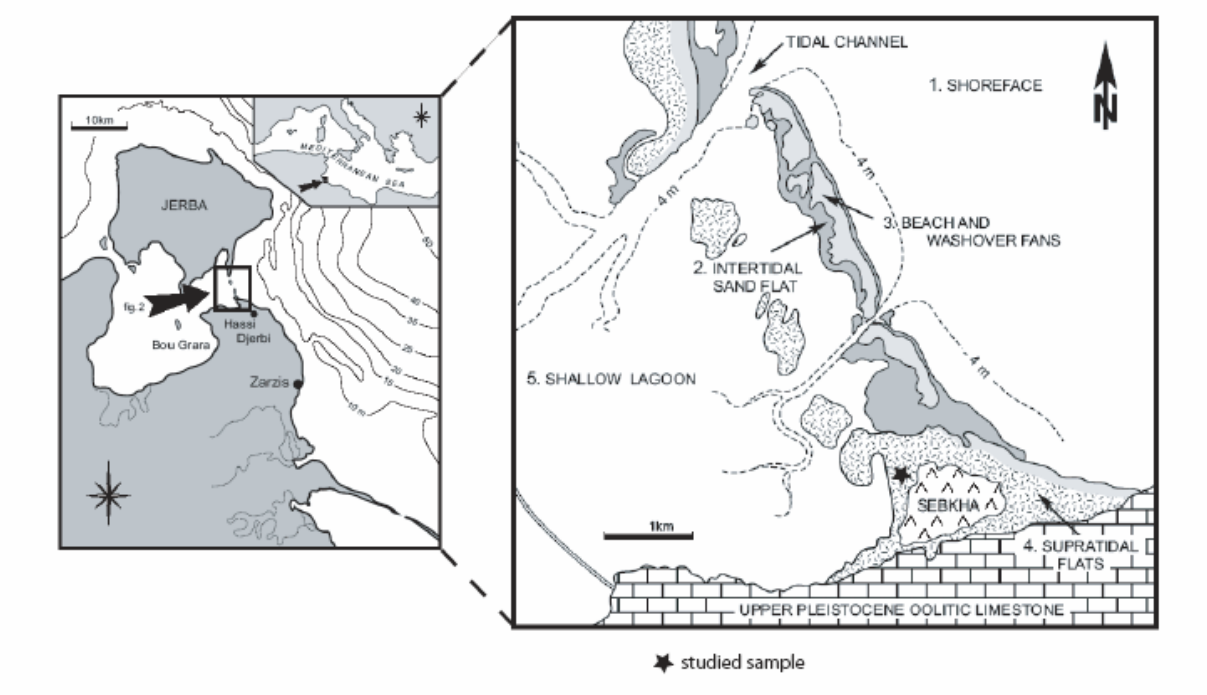

Figure 4-7 : Geological map of Hassi Jerbi region and location of studied samples; modified from Davaud and Septfontaine (1995).

4.2.2.2. Lagoa Vermelha (Brazil)

Lagoa Vermelha is a coastal hypersaline lagoon located about 100 km east of Rio de Janeiro city (Brazil), between the municipalities of Saquarema and Araruama at some 22°51'S and 42°25'W (Fig. 4-8). The region is characterized by the presence of a geological evolution linked to the oscillation of the sea level during the late Quaternary. Numerous studies on microbial mats in this area led to the first evidence of dolomite mediated by bacteria (Vasconcelos and McKenzie, 1997), and sulphate-reducing bacterial cultures from the lagoon have been shown to mediate dolomite precipitation in the laboratory (Warthmann et al., 2000). The upper 1 m of Lagoa Vermelha sediment is characterized by alternating carbonate and organic carbon-rich layers. Low Mg-calcite, aragonite, high Mg-calcite (7–35 mol.% $MgCO_3$) and Ca-dolomite (42–48 mol.% $MgCO_3$) are the carbonate mineral phases present in the lagoon sediment (Hohn et al., 1986; Vasconcelos and McKenzie, 1997; Vasconcelos, 1994). In microbial mats, twenty-three species of cyanobacteria have been recognized (Silva e Silva et al., 2004).

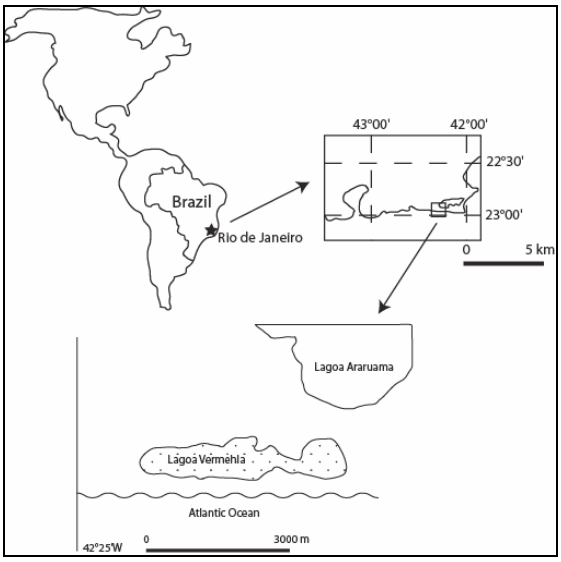

Figure 4-8 : location of the Lagoa Vermelha (Brazil).

4.2.3. CONTINENTAL SEDIMENTS: PEAT BOG AND MASOKO LAKE (TANZANIA)

4.2.3.1. Sample location

Both sampling sites are located in Tanzania. The peat bog is situated at 9°21'S-33°47'E at a height of 663 m, near the village named Kambangunguru (Fig. 4-9) and the lake Masoko (9°20'S-33°45'E, 800 m.a.s.l., 36,5 m water depth) is in the Rungwe highland volcanic area (Bergonzini et al., 2001).
This lake is characterized by anoxic conditions prevailing at the sediment–water interface (de Mesmay et al., 2007). Three samples have been taken in each site.

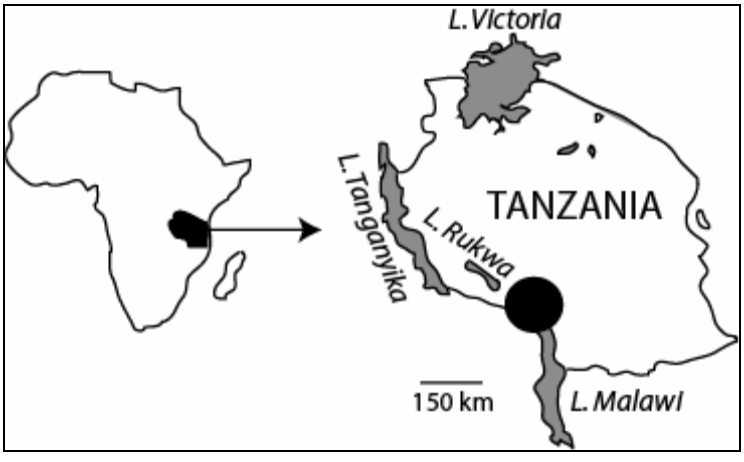

Figure 4-9 : location of Tanzanian samples (black point).

4.2.3.2. Peat bog

a) definition

Peat bog belongs to wetlands in general, which are characterized by three: i) the presence of water, ii) unique soil conditions and especially low oxygen content and iii) specialized biota (Charman, 2002).
A bog is a nutrient-poor, acid peatland with vegetation in which peat mosses, ericaceous shrubs, and sedges play a prominent role (Charman, 2002; Dammon and French, 1987). From a pedological point of view, peat bog deposits are included into the Histosols order, characterized by reduced biological activity and a complex abiotic control of OM transformation. Peat accumulation occurs when annual primary productivity in peat-forming systems exceeds the rate of mineralization.
As a bog matures peat begins to accumulate. This peat layer is formed by the semi-consolidated remains of plant material, constituting a precursor to coal.
Peat in fens, bogs and marshes, contains worldwide 0.5 10^{11} mg C (Succow and Jeschke, 1990) because anoxic conditions retard microbial decay rates of OM relative to the annual C input rates by vegetation (Moore, 1989). Bogs are challenging environments for plant life because they are low in nutrients and very acidic. The high acidity of bogs and the adsorption of water by sphagnum moss reduce the amount of water available for plants (Brake et al., 1999).

Damman and French (1987) have established a classification of bogs based on i) the method of water supply, ii) the landforms where the bog development occurs and iii) the landform produced by the bog.

b) process of formation/development

Peat bog deposits were formed in peculiar paleoecosystems where the slow biodegradation of plant residues depends on a series of pedo-climatic and hydromorphic factors leading to a progressive accumulation of OM stabilized in different evolutionnary stages (Clymo, 1983). It can be classified depending on the type of plant material from which it was derived. Damman and French (1987) recognize the five following types of peat based on their vegetal origin:
- Sphagnum peat, which consists primarily of Sphagnum with minor amounts of vascular plant material;
- moss and moss-sedge peat, which is primarily derived from mosses;
- reed and sedge peat, which is derived from a mixture of reeds, cattails, and large sedges;
- wood peat, which originates in forested peatlands and contains wood in various stages of decay
- limnic peat, which develops in lakes as a result of the deposition of organic matter from aquatic organisms.

As decay and compaction occur, the peat becomes more humid. Humification is a measure of the degree of decomposition that has occurred.

Peat formation processes are slow and the macromolecular organic components are particularly recalcitrant against biodegradation (Clymo, 1983).
The efficiency of degradation in this anoxic environment is low, then polysaccharides are utilised preferentially over lignin (Beguin and Aubert, 1994; Kirk and Farrell, 1987; Young and Frazer, 1987). Thus, the OM selective preservation pathway is highly effective in such environments.

Development of sphagnum peat (Painter, 1998): *Sphagnum* mosses and relatively young peat (<1000 years old) absorb up to 20–25 times their own weight of water, and their porous surfaces facilitate rapid evaporation. Most of those that have preservative properties are produced by the growth of *Sphagnum* in water that has collected in basins in impervious rocks (Clymo and Hayward, 1982). In the first stage of peat formation, the moss grows over the surface of the lake from the sides. As successive generations die, they sink beneath the surface, gradually increasing the thickness of the floating raft of vegetable matter until the whole basin is filled with peat containing at least 96% of water. During this stage, which may take 2000 years or more, depending upon the depth of the lake,

anything thrown into the bog will sink and come into immediate contact with soluble, brown products of decay of the dead mosses on the surface (Moore and Bellamy, 1974).
In the second stage of bog development, the living moss on the surface grows up above the level of the groundwater, while the layers of dead moss underneath become steadily compressed.
From this point onwards, the peat becomes ‘ombrogenous' (rain-fed). Ombrogenous peat is especially noted for its preservative properties.
Sphagnum mosses, like other bryophytes, have no roots, and like most mosses they have leaves that are only one cell thick and able to absorb nutrients directly from the ambient water. In the living moss that carpets the surface of the bog, sphagnan is covalently cross-linked to other cell-wall glycans and is an integral part of the structure of the holocellulose. As such, it is completely insoluble in water.

c) specific intertropical case: Tanzania

In modern intertropical wetlands, permanent flooding and the litter quality appear as major factors controlling the mineralization and methane production rates (Miyajima et al., 1997). The plants forming peat in intertropical wetlands, such as that studied in Tanzania, include C3 trees and sedges, and C4 sedges. These two categories of plants can be clearly characterized by their $^{13}C/^{12}C$ ratios (Smith and Epstein, 1971), with the C3 and C4 terrestrial plants having $\delta^{13}C$ values around −26 and −13‰, respectively (Deines, 1980). In most cases, C3 plants have $\delta^{13}C$ values between −28 and −25‰, but their overall range of δ-values is much larger (from −34 to −22‰). The large ^{13}C shifts observed have been shown to be due to major variations in the C4/C3 ratio of the source organic matter. Intertropical peat deposits show large variations in their stable carbon isotope compositions, as demonstrated by Aucour et al. (1999). These changes are primarily related to the C3/C4 ratio of the source plants for the peat.

5. RESULTS

5.1. Recent analogs

5.1.1. OPTICAL AND CHEMICAL CHARACTERIZATION

5.1.1.1. Sulphuroxidizing bacteria

Macroscopically, these bacteria appear in a whitish gelatineous mass with dark grains (s) corresponding to sulphur (Plate 1a/1-2). In palynological slides, they display a colourless mass characterized by an "alveolar" network made of various holes with different orders of magnitude (Plate 1a/3). They show a strong fluorescence (FS6, Plate 1a/4) associated different constitution depending on the amount present on the slide: they appear as a continuous membrane, a granular or alveolar network. Only the TOC can be measured, i.e., 0.59 % with Rock-Eval pyrolysis.
The studied sample is dominated by two categories of bacteria: filaments and coccoids embedded in the alveolar network, i.e. EPS.

- filaments

The average width is 6 to 7 µm, sometimes 10 to 15 µm and the length varies from a few µm to 1 mm (Plate 1b/1-2). They are constituted of nanofilaments or microtubules (50 nm in diameter) (Plate 1b/3-4). The surface is characterized by "bumpiness" and some isolated rounded bodies called "balls" or "nanoballs" (80 to 100 nm in diameter). They are sometimes twisted with joints (Plate 1b/5). Ultrathin section in TEM shows 230 nm thick microtubules (Plate 1b/6).
Balls are aligned perpendicularly to the filament.

- coccoids

They have an ovoid form and are 2 to 4 µm wide. They are stacked together through the EPS they produced (Plate 1c/1-2).
Some of them are joined up with filaments and contain small balls called "nanoballs" (10 to 120 nm in diameter) with a random distribution (Plate 1c/3-4). In AFM, they are characterized by an association of fragments showing clear boundaries and an average size of 250 nm (Plate 1c/5). They are also distributed along filaments with a stratified appearance; their size varies from 80 to 150 nm (Plate 1c/6).
In ultrathin section, these round bacterial bodies are characterized by a double-space membrane with two distinct morphologies: one is smooth (Plate 1d/1) and the other presents undulations with an interval of about 100-130 nm (Plate 1d/2-3). Bacteria are globally in a stress-state and contain some 150 nm wide vesicles (Plate 1d/4). Isolated nanoballs are also observed, with a diameter of 100-120 nm (Plate 1d/5). Typical structures such as ghosts and membrane accumulation (resembling lysosoms) are present (Plate 1d/6). They contain no material but just concentric circles (physical equilibrium in response to mechanical constrains). Sometimes the external membrane is burst.

- secretions

When there are several layers constituting a film, they form a compact mass, which broke into an alveolar network with a high bacterial density (Plate 1e/1-6). They are characterized by 50-100 nm large nanofilaments, randomly distributed with some rounded holes (Plate 1e/7). In ultrathin section, filaments are undulating and get in a tangle with a maximum thickness of 120 nm (Plate 1e/8-9).
For FTIR spectra interpretations, the identification of absorption bands was achieved based on data published by Barancikova et al. (1997), Francioso et al. (2002), Schnitzer and Khan (1972, 1978), Silverstein et al. (1991), Stevenson (1994).

Three intervals of the FTIR spectra were used for quantification: 1100-950, 1700-1600 and 3000-2890 cm^{-1}, which correspond respectively to polysaccharides, aromatic and aliphatic compounds.
The spectrum is characterized by a strong absorbance in the range 4000-1500 cm^{-1} that corresponds to alcohols and phenols. Shoulder at 1141 cm^{-1} is associated to C – O of alcohol (annexe A4).

5.1.1.2. Cyanobacterial biofilm

A thin green biofilm has been developed from a microbial mat (Brazil) in laboratory conditions (with freshwater) for several months. It is attached to the edges of the culture compartment.
This biofilm is composed of different communities of microorganisms, which are embedded in EPS. It can be described macroscopically as a continuous soft green film with a thickness of several micrometers (Plate 2a/1). Small white crystals are visible and form a bumpy surface (Plate 2a/2). In a palynological slide (Plate 2a/3) after acid attack, OM can be mainly described as amorphous. The texture is gelified, sometimes granular and the colour beige to orange with sharp outlines. This complex OM is composed of an accumulation of different particles with small dark geometric forms of variable thickness. Among the amorphous particles, some specific structures are identifiable such as twisted filaments and ligneous fragments. Particles in general are strongly fluorescent, i.e., FS6 (Plate 2a/4-5): they are composed of different dark constituents within a fluorescent alveolar network with different fluorescence intensities. Filamentous organisms show a moderate fluorescence.
Microscopical investigations permit the identification of some components:

- bacteria and diatoms

In SEM, coccoid and filamentous bacteria are visible, in particular those of the genus *Spirulina* (Plate 2b/1). In TEM, some of them show typical internal components such as thylakoid membranes (with phycobilisoms for cyanobacteria; Plate 2b/2-3) and spores (size smaller than 250 nm; Plate 2b/4). Differences between gram positive and gram negative bacteria can be made based on structure of cell wall. AFM only shows the form but not precise details about the bacterial surface (Plate 2b/5-6).

- algae

The distinction between green algae and cyanobacteria is not always clear. There are two types of algae, encrusting and not encrusting. Generally the length and width is more important than those of bacteria. Small cubic crystals on the surface are associated to calcite in symbiotic algae (Plate 2c/1,3). Typical thylakoid membranes locally stacked to form grains are reminiscent of the green algal type (Plate 2c/2) and cytoplasmic inclusions (starch grains, carboxysoms, etc, Plate 2c/3). The other types of algae are characterized by individual cells forming the filament (Plate 2c/4). The cell wall is different from that of bacteria and is characterized by a dense thick layer sometimes containing internal structures (Plate 2c/5).

- secretions

Secretions are produced by different bacterial communities and are compacted into a dense mass with all microorganisms (Plate 2d/1). At surface, they form a dendroid network. In TEM they are characterized by curly-like filaments (Plate 2d/2), whereas they appear as non-organized filaments at free state (Plate 2d/3). AFM shows small alveoli with small topographic variations (2 to 40 nm deep, Plate 2d/4). When bacterial concentration is low, EPS form a flat surface with local holes (Plate 2d/5-6). Diatoms are concentrated within EPS.
Different types of ultralaminae have been recognized: i) some 100 nm thick layers have been observed (Plate 18a). After acid etching, no entire algal cell was observed. Only dense layers sometimes characterized by diffuse outlines were preserved, the thickness of which ranges from 80 to 170 nm (Plate 18b); ii) typical organisms (Plate 21a) were characterized by a complex cell wall showing the following constituents: an undulating, 13 nm thick outer membrane; a dense 4.5 nm thick layer with sharp outlines: a diffuse, 14 nm thick layer showing the same contrast as the outer membrane. The total thickness of the cell wall was 57 nm. After acid etching, only the outer membranes were preserved, with a total thickness of 140 nm (Plate 21b); iii) a third kind of ultralaminae appeared as homogeneous, 70 nm thick membrane pairs, which were parallel to the cell (Plate 23a). They were placed side by side, possessed sharp outlines and contained small dark grains. The space between each membrane was constant and some 30 nm thick. They could sometimes present a diffuse aspect, but

their thickness was smaller, i.e., 35 nm (Plate 21a). The recent biofilm also contained organisms where thin membranes were randomly placed in the cell (Plate 23b). They were 40 nm thick and locally stacked to each other. The same distribution was observed in other cells where these thin membranes were about 50 nm thick and locally stacked in a pack (Plate 23c & d). After acid etching, these membranes were denser but with a similar size (60 nm) (Plate 23e).

Rock-Eval data indicate a TOC content of 10%, a T_{max} of 417°C; and a HI of 398 mg HC/g TOC. On the HI-T_{max} diagram this sample would correspond to thermally immature Type II marine OM. The isotope composition is defined as $\delta^{13}C = -18.5‰$ and $\delta^{15}N = 0.4‰$.
FTIR data are summarized in annexe A4.

5.1.1.3. Microbial mats

♦ *Lagoa Vermelha*

This mat is mainly soft with a purple colour inside (Plate 3a/1). From top to bottom, it consists of: i) a 3 mm thick green layer typical of photosynthetic microorganisms; ii) a 4 mm thick purple layer characterizing heterotrophic organisms, mainly N_2 reducers; iii) a 1 mm thick white crystalline layer associated with a thin green layer; iv) a 5 mm thick white granulous zone located on the top of a 1 cm thick orange zone. Minerals concentrated in white zones are typical of hypersaline conditions, i.e, 87% halite, 8% dolomite, 4% calcite and 1% gypsum.
In palynological slides, OM in the upper part is characterized by up to 5 mm long particles which are beige and amorphous (Plate 3a/2). Organic matter appears stringy or granular; when dense, its aspect is gelified. Particles are surrounded by long contorted green filaments giving a green aspect to the particles (Plate 3a/3). The interior of the microbial mat is composed of amorphous particles with a colour varying from beige to brown (Plate 3a/4). The texture of particles is similar to that in the upper part. Long rigid translucent filaments are visible. After acid etching, the numerous amorphous beige to green particles are smaller with respect to their initial size. Terrestrial fragments are more visible and include cuticles, tracheids, spores and pollen (Plate 3a/5). Filaments are separated from particles.
In general, particles show a strong fluorescence, i.e., FS5, as for example filaments forming loops, fibrous structures and alveolar networks (Plate 3a/6). At the edge of particles, a dendroid network displays a moderate fluorescence as well as long filaments (Plate 3a/7). Non-fluorescent twisted filaments seem to link organic particles (Plate 3a/8).
In microview (Plate 3b/1), fern-shaped particles with locally filamentous structures made it difficult to aquire pictures. There are different kinds of particles: smooth particles showing small topographic variations and a globular aspect with a height difference of 10 nm (Plate 3b/2). Some of them display some 250 nm wide geometric forms (Plate 3b/3). Small stratified particles show 50 nm wide nanoballs at their surface (Plate 3b/4-5). Long filaments display an irregular texture. Small, 160 nm wide filaments are also present with nanoballs at their surface (Plate 3b/6). Irregularities on the filaments are constituted of nanoballs and of larger than 85 nm geometric forms (Plate 3b/7).
In TEM without acid etching, numerous communities of microorganisms are embedded in EPS and associated to crystals of different nature.
Microbial secretions present more or less defined different aspects, i.e., finely entangled filaments creating regular alternation of dense and light zones (Plate 3c/1) or very thin parallel filaments (Plate 3b/2).
Organisms show a different degree of evolution. Most of the prokaryotes (bacteria) are characterized by a small size, a simple content and a double-space membrane in the process of sporulation (Fig. c18). They promote mineralization on their outer membrane: crystals are located on the bacterial or algal surface (Plate 3c/3) or largely distributed to form granulations between some bacteria (Plate 3c/4). Filamentous bacteria containing lipidic grains with other smaller bacteria are in the process of sporulation (Plate 3c/5). Very organized cells are commonly observed. This distribution resembles thallus organization in algae with a size of about 15 µm. Each internal cell contains many, 1-2 µm wide lipidic grains (Plate 3c/6). A colony of circular individuals is observed. These organisms are characterized by a thick outer-membrane and a resistant content with lipidic inclusions and maybe

metals (Plate 3c/7). In some cases, the division process is visible (Plate 3c/8). They are located beside another kind of organisms reminiscent of thallus arrangement (Plate 3c/9).
The isotope composition is defined as $\delta^{13}C = -11.9‰$ and $\delta^{15}N = 8.7‰$.
FTIR data are summarized in annexe A4.

♦ *Hassi Jerbi*

This microbial mat is characterized by a dark-coloured, several mm thick anoxic zone in the upper part. At depth, it appears as light-coloured, laminated and not really cohesive sediment (Plate 4a/1). There is an important detrital contribution in these carbonate sediments: 60% quartz, 16% halite, 14% aragonite and 10% calcite. Geochemical data indicate a TOC content of only 0.59%, (and therefore a high mineral content, a T_{max} of 426°C and a HI of 416 mg HC/g TOC. On the HI-Tmax diagram this sample plots as Type II, thermally immature, marine OM.
In thin sections, the mat appears to be made of brown organic paralell laminae with other organic clasts and rare foraminifera.

Palynological preparations (Plate 4a/2) show translucent to beige-coloured particles, heterogeneous in size and type of constituents. Amorphous particles can be larger than 5 mm. They contain structured elements such as spores and pollen, filamentous organisms likely algae, other twisted translucent filaments, structured membranes and some fibrous structures. Apart from the structured elements, the rest of the OM appears amorphous (Plate 4a/3).When the AOM density is low in the slide, a translucent alveolar network is commonly observed, pigmented by small particles.
In general, this sample is characterized by a moderate to strong fluorescence, i.e., FS4 (Plate 4a/4) depending on the constituents: grumose matter displays a strong fluorescence, unlike the twisted filaments (Plate 4a/5). Moreover, strong fluorescence is associated with membrane-like matter, fibrous structures and diffuse mass around elements, but spores and pollen are the most fluorescent constituents (Plate 4a/6).
The ultrastructure of OM reveals different kinds structures:

1) A diffuse, not well-contrasted mass appearing as “curly” or sometimes forming an alveolar network (Plate 4b/1). It can be located around balls or randomly distributed. This texture is typical of EPS. Another kind of secretions is characterized by an alveolar network with different orders of magnitude (Plate 4b/2).
2) Homogeneous, strongly contrasted and rounded circular structures, which can be up to of 150 nm in diameter and sometimes translucent (Plate 4b/3). This is typical of algal or bacterial membranes.
3) Specific organisms such as i) filamentous 1 µm wide constituents, with an external envelope and internal structures which are not well-preserved (Plate 4b/4); ii) 800 nm long bacillus with internal vacuoles resembling bacteria in the process of sporulation (Plate 4b/5).
4) 30 nm large nanoballs with a translucent aspect (Plate 4b/6).

Ultralaminae can be defined as i) dense, 175 nm thick concentrically layered particles (Plate 18c). Sometimes, they appeared as contorted layers with “sharp” outlines and a thickness ranging from 120 to 180 nm (Plate 18d); ii) this sample exhibited some 500 to 900 nm thick, filamentous forms, which were less contrasted (Plate 21c) than forms previously observed (e.g., plate 18d). They appeared not well preserved; iii) finally, a mixture of different layers with variable thicknesses could be observed (Plate 21d): when thick (up to 155 nm), their aspect was translucent; when thin, layers were dense and dark, with a thickness ranging from 15 to 50 nm. This sample contained less dense contorted forms, of variable thickness, with an average thickness of 180 nm (Plate 25a).

The nanostructure of this sample is mainly composed of globular bodies and filaments. Globular matter is composed of nanoballs with a size of about 70 nm (Plate 4c/1). Nanoballs are present in bunches on filaments (Plate 4c/2), together with other geometric forms (50-90 nm) (Plate 4c/3). Typical 27 nm wide nanobodies are found forming an ovoid body (Plate 4c/4). These bodies are oriented in the same direction (Plate 4c/5).
The isotope composition is defined as $\delta^{13}C = -13.2‰$ and $\delta^{15}N = 2.1‰$.

FTIR data are summarized in annexe A4.

5.1.1.4. Continental sediments from Tanzania

Macroscopically, peat bog and caldera lake samples appear as non consolidated organic matter where phytoclasts like wood, stems, plants, etc are visible. They are dark-coloured and minerals are in minor quantity and represented by clays and quartz.

♦ *Lake Masoko*

The palynofacies is made of terrestrial structured elements and amorphous particles (Plate 5a/1). Structured elements are composed of numerous constituents including spores and pollen. Before acid attack, diatoms form a colony in chains (filament) and are abundant, as well as cuticles and tracheids. Amorphous particles are brown and granular with sharp outlines (Plate 5a/2). After acid treatment, amorphous particles have the same aspect, i.e., granular, brown-coloured with sharp outlines and made of different components. Dark tracheids are well-preserved, whereas orange fibrous particles appear more degraded (Plate 5a/3).
Particles exhibit a locally strong fluorescence, i.e., FS4 (Plate 5a/4) or are patchily fluorescent when they are granular (Plate 5a/5). Some figured elements such as woody fragments are strongly fluorescent (Plate 5a/6).
In SEM, OM seems heterogeneous and is characterized by terrestrial fragments with different degradation states, heterogeneous matter in background, membranes of spores and framboidal pyrite. Tracheids can be well-preserved (Plate 5b/1) or strongly degraded whith only the general structure visible (Plate 5b/2). Terrestrial cuticles reveal numerous holes (Plate 5b/3) and when strongly degraded, an alveolar network is observed at surface (Plate 5b/4). At surface, 500 nm wide filaments are entangled and have secondary thin filaments (Plate 5b/5). The background is constituted of irregular, heterogeneous matter, which drapes some balls and other fragments (Plate 5b/6). Framboidal pyrite is concentrated within the irregular matter (Plate 5b/7).
In AFM, 300 nm wide filaments contain bunches of nanoballs at surface (Plate 5c/1). The background is composed of many nanoballs with an average diameter of 30 nm (Plate 5c/2-3). Other kinds of particles are characterized by oriented nanoballs (40 nm) (Plate 5c/4-5). Big nanoballs (larger than 100 nm) are rare (Plate 5c/6).
In TEM, OM is mainly characterised by lamellar structures close to ultralaminae with bacterial bodies, organized alveolar structures and other types of membranes. It can be further detailed as:

1) Contorted, dark-coloured, regular, 25-30 nm wide structures are sometimes stacked and form a stack some of 140 nm large. They are up to several μm long (Plate 5d/1).
2) Strongly contrasted to quasi-translucent membranes depending on the thickness, from 30 nm to 150 nm. These lamellar structures are rolled up or sometimes twisted (Plate 5d/2).
3) Kinds of filaments sometimes associated to “beehive” structures or with ornamentations at surface are typical of cuticular membranes (Plate 5d/3-4).

Numerous coccoid or rod forms are found with a size ranging from 500 nm to 1 μm in diameter (Plate 5d/5). They contain rounded forms, are characterized by a double-spaced membrane (Plate 5d/6), some of them being retracted (Plate 5d/7). They are assimilated to bacteria, with retracted forms and rounded internal bodies characterizing a process of sporulation. Other organisms seem more evolved, i.e., with a bigger size and like a nuclear space (Plate 5d/8) or appear as individual cells in a filamentous organism (Plate 5d/9). They are assimilated to algae. Alveolar networks with different orders of magnitude are also observed (Plate 5d/10).
Ligneous material is characterized by geometrical strips and strong contrast (Plate 5d/11). 30 to 50 nm wide nanoballs are observed (Plate 5d/12).
The isotope composition is defined as $\delta^{13}C = -25.3‰$ and $\delta^{15}N = 3.8‰$.
FTIR data are summarized in annexe A4. Differences between both samples are minor as KAM 450. The acid etching induces a more pronounced deouble-peak at 2900 cm^{-1}, partial disappearance

(shoulder) at 2360 cm^{-1}, a weaker absorbance in the range 1000-1400 cm^{-1} corresponding to C – O stretching of alcohol and phenol.

♦ *Peat bog*

Palynological slides indicate numerous terrestrial constituents composed of AOM, cuticles, spores and pollen, tracheids, translucent membranes and ligneous structures (Plate 6a/1). AOM shows different types: granular (Plate 6a/1), light to dark-brown coloured and containing inertinite fragments (Plate 6a/2). However, it appears granular in background.
This sample is composed of various components showing different intensities of fluorescence. In general, particles are weakly fluorescent (FS3) with small internal dark bodies (Plate 6a/3). Granular particles exhibit a patchy fluorescence (Plate 6a/4).
In SEM, OM is mainly composed of identifiable terrestrial particles such as wood, charcoal, spores, pollen and cuticles. The background mass is heterogeneous, made of numerous discontinuities and drape other structures (Plate 6b/1). This mass comprises elongated fibrous structures and fragments of different nature (Plate 6b/2). Charcoal is characterised by a regular network made of rectangular holes (Plate 6b/3). Remnants of filaments form a dendroid network. These structures contrast with vegetal structures, which present an alveolar network at surface when degraded (Plate 6b/4). Coatings on filaments are made of a stretched film besides nanoballs (Plate 6b/5). Charcoal is formed when wood is heated in oxygen-depleted conditions. It is chemically highly inert and not subject to microbial attack.
Structures comparable to *Botryococcus braunii* are well-preserved (Plate 6b/6).
Different nanostructures are visible with AFM. Edges of particles are globular, made of 80 nm wide nanoballs (Plate 6c/1). Nanoballs widely cover the surface (Plate 6c/2) with a size ranging from 40 to 150 nm (Plate 6c/3). They are sometimes aligned (Plate 6c/4). Particles made of some 210 nm wide microtubules (Plate 6c/5) are characterized by bunches of nanoballs perpendicular to them; a bunch is made of different, 20 to 50 nm large elements (Plate 6c/6).
In TEM, lamellar structures are the most important and present different aspects:

1) filamentous, 150-200 nm long, not strongly contrasted structures, contain sometimes some dark grains resembling cytoplasmic inclusions. This morphology is attributed to algae such as *Botryococcus braunii* (also see in SEM) (Plate 6d/1).
2) An accumulation of more or less thin filaments, which are well-defined and dense, is typical of algal cell walls in general (Plate 6d/2).
3) Other types of filamentous structures are characterized by translucent twisted forms with variable thickness (Plate 6d/3). These filaments resemble cell wall membranes.
4) Lamellar structures showing specific surficial ornementations are attributed to cuticle (or more generally vegetal) ultrastructure (Plate 6d/4). They are accompanied by a regular alveolar network (Plate 6d/5).

Other structures such as 800 nm wide fibrous elements are less abundant. They are characterised by a strong contrast (completely dark) with small regular holes and are connected with twisted filaments having the same contrast (Plate 6d/6); they are typical of terrestrial components. Microbial secretions are also represented by an alveolar network. Here they are stacked to form undulating membranes (Plate 6d/7).
Few bacteria have been observed: they are about 500 nm in diameter and contain some 300 nm wide rounded voids (Plate 6d/8). This could be an endospore or the result of germination. A large cell (3 µm wide) contains a 800 nm wide sphere, itself containing bodies resembling endospores (Plate 6d/9). This is either a symbiosis between organism and bacterium, or an ingestion by the host organism called phagocytosis. Another ovoid to rounded form containing alveolar matter and a diffuse cell wall is probably degraded algae where specific organization is close to that of thallus (Plate 6d/10).
The isotope composition is defined as $\delta^{13}C = -26.2‰$ and $\delta^{15}N = 2.6‰$.
FTIR data are summarized in annexe A4. There is no real difference between the sample before and after acid etching: the acid etching induces a more pronounced double-peak at 2900 cm^{-1}, partial disappearance (shoulder) at 2360 cm^{-1}, a weaker absorbance in the range 1000-1400 cm^{-1} marked by several peaks corresponding to C – O stretching of alcohol and phenol. A peak appears at 1500 cm^{-1}.

5.1.2. EFFECTS OF ACID TREATMENT

5.1.2.1. Recent bacteria

♦ Sulphuroxidizing bacteria

Before acid attack, these bacteria appear made of a whitish gelatinous mass with dark grains. After acid etching, the colour is similar, but the texture is more granular, in bunches.
In palynological slides, bacteria embedded in EPS appear made of a translucent stringy network, which has the same aspect after acid etching. The network is sometimes alveolar (Plate 7a/1) in both cases. Material shows a strong fluorescence in both cases: natural bacteria are made of a fluffy alveolar network (Plate 7a/2), sometimes granular or with a smooth aspect. With acid attack, there is no modification in the fluorescence intensity. However, the alveolar network becomes more pronounced.
With combined microscopical methods, some differences are visible in different bacterial communities:
Filaments seem to conserve their general structure. However, a destructuration is observed when it is broken showing the distribution of microtubules or protofilaments (Plate 7a/3-4). The nanostructure in AFM reveals a smooth wall (less surface coarseness) (Plate 7a/5). Acid treatment has no impact on the size of bacterial bodies.
Coccoid bacteria are preserved with similar sizes after acid treatment but with a more geometrical outline in SEM (Plate 7b/1-2). However, this structuration disappears as shown in AFM (Plate 7b/3-4), with a specific dehydration treatment. The surface seems to be smoother and surrounded by a lesser amount of EPS (locally entirely destroyed). The observed fragmentation in plaques and geometrical forms in SEM is probably due to dehydration (Plate 7b/2). Nevertheless, bacterial density is lower with ghosts of coccoid bacteria (0.5 to 1 μm) (Plate 7b/5). The double-spaced membrane is totally preserved (Plate 7b/6).
Secretions are usually partially destroyed; they are preserved only when they are bound to bacterial cells at their ends (Plate 7c/1). They are also present at nanoscale and characterized by 100 nm large holes and organic matter forming an alveolar network (Plate 7c/2-4). Moreover, the dimensions of alveoli are relatively amplified through this treatment (30 nm prior to acid attack)
Comparison of FTIR spectra shows no notable difference: the general tendency is similar but with the appearance of two weak bands: 840 and 640 cm^{-1}. Absorbance is maximal from 2000 to 4000 cm^{-1}.

♦ Cyanobacterial biofilm

Before acid etching, this biofilm is constituted of a continuous, soft, green film with a thickness of several micrometers and small white crystals. After acid etching, the biofilm appears macroscopically fragmented in small, light-coloured particles. After acid etching, the biofilm shows mostly a strong fluorescence. Highly fluorescent filaments are probably degraded algae or cyanobacteria. Other particles are made of different constituents such as coccoid, filamentous organisms embedded in EPS with some non-fluorescent elements. Some particles are weakly fluorescent and bound to others strongly fluorescent by a non-fluorescent diffuse gel. It seems that EPS can or can not be fluorescent.
In SEM and TEM, an alveolar network is observed (before and after acid etching), with different orders of magnitude, which corresponds to EPS (Plate 7d/1,5). Several microorganisms are intact including bacteria (Plate 7d/2) and coccoid algae (Plate 7d/3), but in general, only cell walls are preserved, sometimes with cytoplasmic inclusions (Plate 7d/4).
Acid treatment has some effects on the biofilm (A4) and particularly, the appearance of several bands such as double peak at 2930-2863 due to aliphatic C – H stretching, 1384 aliphatic C – H stretching, 1214 C – O stretching and OH bending of COOH groups, 1111 and 1074 C – O of alcohol. The large band at 3380 is more restricted after acid treatment. The disappearance of the band at 2090 associated to OH stretch of OH groups is noted.

♦ *Microbial mat: Lagoa Vermelha (Brazil)*

Natural microbial mat shows a strong fluorescence: large particles are made of distinguishable filamentous forms and with an amorphous mixture between elements (fluorescent and non fluorescent). After acid attack, particles have the same aspect with some exceptions: the dendroid network is well-defined and strongly fluorescent. Fluffy filaments on the edge of particles disappear. Connections between particles are weakly fluorescent (Plate 7e/1) and some particles appear granular (Plate 7e/2).
The intensity of bands is more pronounced after acid treatment (A4), characterized by the appearance of double peak at 2930 and 2850 corresponding aliphatic O – H stretching, 1730 C ═ O stretching of COOH and ketones and 1266 C – O stretching and OH bending of COOH groups.

♦ *Microbial mat: Hassi Jerbi (Tunisia)*

Organic matter is diluted in an important mineral matrix, without specific colour, except in the anoxic upper part. After acid attack, OM appears as beige-coloured and as fluffly particles. There is no real difference based on FTIR results due to acid treatment (A4). However, double peak at 2930-2850 (aliphatic C – H stretching) is more pronounced with 2350. The appearance of peak at 1266 C – O stretching and OH bending of COOH groups and the disappearance of the peak at 2520 are observed. Iarom/aliph is of 12 before and 4.3 after acid treatment.

5.1.2.2. Continental sediments from Tanzania

In palynological slides after acid attack, no change has been observed in this type of material (Plate 7e/3): amorphous particles have the same aspect, i.e., granular, brown-coloured with sharp outlines and made of different components. Dark tracheids are well-preserved, whereas orange fibrous particles appear more degraded.
From a chemical point of view, FTIR spectra show some differences especially in the Iarom/aliph. In the lake Masoko, there is no real difference between natural and acid treated samples (A4): the acid attack induces a more pronounced double-peak at 2900 cm^{-1}, partial disappearance (shoulder) at 2360 cm^{-1}, a weaker absorbance in the range 1000-1400 cm^{-1} corresponding to C – O stretching of alcohol and phenol. Iarom/aliph is of 15.3 before and 3.4 after acid etching.
In the peat bog, differences between both samples are minor as C11. The acid etching induces a more pronounced double-peak at 2900 cm^{-1}, partial disappearance (shoulder) at 2360 cm^{-1}, a weaker absorbance in the range 1000-1400 cm^{-1} marked by several peaks corresponding to C – O stretching of alcohol and phenol. A peak appears at 1500 cm^{-1}. Iarom/aliph is of 11.4 before and 5.7 after acid etching.

To summarize, the acid treatment has only a minor impact on recent OM. Consequently, the acid treatment needed to extract fossil OM from rocks can be considered as not affecting significantly the microscopic observations carried out on this OM.

5.2. Fossil OM

5.2.1. THE MONTEREY FORMATION

Three samples have been analyzed, which belong to the phosphatic shale unit: N12, N23 and N35 (see Fig. 4-2). They have been chosen for their lamination and different mineral composition.

Bulk rock

Sample N35: Macroscopically, this sample is finely laminated (Plate 8a/1). In thin section, OM presents a heterogeneous distribution:
In organic-poor intervals, OM is present as parallel orange to brown-coloured lines showing outlines of grains like a sign of deformation (compaction) or varved sediments (Plate 8a/2). In organic-rich intervals, there is stacking of dark-orange to brown-coloured laminae with moulding of grains (Plate 8a/3). Laminae are about 20 µm thick.
Numerous occurrences of foraminifera are encountered.
Microfossils are easily recognizable under SEM, i.e., foraminiferal shells (biseriate, calcitic radial cell walls), coccolithophorids and chitinous tests showing regular holes (Plate 8a/4). On the other hand, a veined membrane is well represented (Plate 8a/5). It shows a radial structure, it is thin as shown by tears due to cubic pyrite and the moulding of underlying material, like framboidal pyrite (Plate 8a/6). Locally, this membrane is compacted in a single filament or combined in alveoli with opal CT inside in small rods. It is intimately associated with phyllosilicates.
Mineralogical analysis indicates a carbonate rock, composed of 81% calcite, 4% quartz for N35 and a higher content in silicates for N23: 3% albite, 31% ankerite, 1.5% apatite, 2.5% phyllosilicates, 7% quartz and 51% calcite. N12 has a higher content in quartz (22%) and evaporites (15% gypsum and 12% halite) ; 14% albite, 27% calcite and 8% phyllosilicates.

Kerogen (after destruction of mineral phase)

Sample N35: In palynological slides, the OM of this sample is composed of more than 95% AOM (Plate 8b/1), the remainding part corresponding to sporomorphs. It shows a grumose aspect, brown to dark-brown colour with particles of variable size. It is characterized by an alveolar or dendroid network. In general, particles have no defined outlines, with sometimes regular and angular edges. Some particles appear made of small spheres.
In general, AOM displays a moderate fluorescence (FS3) as shown by some non-fluorescent particles and more common particles with patchy fluorescence, i.e., strongly fluorescent points in a generally non fluorescent mass (Plate 8b/2).
Particles with patchy fluorescence contain spheres, alveolar network and undetermined forms showing a partially fluorescent background.
Under SEM, the OM appears as heterogeneous and made of filaments (Plate 8b/3), an alveolar network (Plate 8b/4), 2 µm wide balls (Plate 8b/5) and coccolithophorid marks (Plate 8b/6). In AFM, particles appear globular, made of nanoballs with a size of 50 to 100 nm (Plate 8c/1-2). They are arranged like staircases (Plate 8c/3) with a relief varying from 150 nm to 370 nm.
Under TEM, OM appears as diffuse and stringy with different textures: translucent membranes (Plate 8d/1), fluffy alveolar network (Plate 8d/2) and dispersed (Plate 8d/3).
Bacterial bodies, recognizable through their form and/or cell wall are more or less preserved: an ovoid, 100 to 600 nm long form is strongly contrasted and contain no visible structure (Plate 8d/4). The cell wall is not distinct. However, a contorted diffuse filament is attached to the end of the cell, corresponding probably to flagellae. The best preserved bacterium exhibits a typical cell wall containing a thin cytoplasmic membrane, a large interspace and a dark outer membrane which is locally burst and appears translucent (Plate 8d/5). This bacterium is a gram negative coccus. A

succession of numerous circles with a size varying from 50 to 250 nm is observed (Plate 8d/6). They are characterized by a thick contrasted envelope which resembles bacteria or microalgae. Finally, coccoid bodies containing inclusions are ascribed to bacteria (Plate 8d/7).

Sample N12: In palynological slides, OM is mainly composed of AOM and some translucent particles (Plate 9/1). The AOM has a grumose aspect and is dark brown with sharp outlines (Plate 9/2). Particles exhibit a weak fluorescence (FS2), although some of them are completely non-fluorescent (Plate 9/3).
Under TEM, OM appears relatively degraded and heterogeneous. Phytoclasts are recognizable through their strongly contrasted aspect including regular holes (Plate 9/4) and also framboidal pyrite arranged in an ovoid form (Plate 9/5). Round shapes (Plate 9/6), sometimes containing vacuoles (Plate 9/7) are attributed to bacteria. The filamentous colony contains remains of rectangular cells with a partial destruction of the 4 µm long and 1 µm wide external envelope (Plate 9/8). This resembles sulphuroxidizing bacteria. A few ultralaminae are also present and appear strongly degraded.

Sample N23: AOM is dominant with minor elements such as phytoclasts, spores and pollen. Amorphous particles are characterized by a brown to dark brown colour with sharp or blurred edges and heterogeneous sizes (Plate 10a/1).
OM in this sample is characterized by a weak fluorescence (FS2), but with localized strong fluorescence (Plate 10a/2).
The OM is geneally characterized by a heterogenous aspect resembling locally an alveolar network (Plate 10a/3). Two typical structures are recognized:
- Balls: with an average size of 500 nm (Plate 10a/4). In AFM, the alignment of nanoballs (150 nm) is perpendicular to particles in “stairs” (Plate 10a/5), whereas some of them are assembled in bunches at filament surfaces, with a size varying from 50 to 150 nm (Plate 10a/6).
- Filaments: twisted, 315 nm wide filaments divided in several nanofilaments (130 nm in diameter) at the end (Plate 10a/7). They are linked by a smooth film. Thin filaments forming a dendroid network, whereas others collapsed and form thick stack of filaments (Plate 10a/8).

Organic matter shows some 145 nm thick layers, which were sometimes diffuse, with a streamer-like form (Plate 20e). They are considered as degraded ultralaminae. Dark layers with well defined or diffuse outlines are observed (Plate 22e & f). They are stacked, with thicknesses ranging from 85 to 100 nm. When burst, they appear diffuse, and up to 300 nm thick.

Geochemical data

Rock-Eval pyrolysis indicates for samples N35 and N23 respectively a TOC content of 3.33% and 1.98%, a T_{max} of 408°C and 411°C and a HI of 488 mg HC/g TOC and 326 mg HC/g TOC . On the HI-T_{max} diagram (Fig. 6-5), samples plot as thermally immature Type II OM.
The isotope composition is defined as $\delta^{13}C_{ker}$ = –22.2‰ and $\delta^{15}N_{ker}$ = 2.6‰ for N12 and $\delta^{13}C_{ker}$ = –21.5‰ and $\delta^{15}N_{ker}$ = 4.7‰ for N35.

Organo-mineral relations

FTIR data are summarized in annexe A4. For sample N12, Iarom/aliph is 2.97. No notable effect of acid etching has been observed in this sample. The acid etching induces a more pronounced double-peak at 2900 cm^{-1}, a smaller peak at 2360 cm^{-1}, a strong peak at 1384 cm^{-1} and shoulders in the range 1500-1000 cm^{-1} which are more important in absorbance comparing to rock.
For sample N35, Iarom/aliph is 3.99. Bulk rock and kerogen FTIR spectra strongly differ: acid etching implies a stronger absorbance for the broad band at 3400 cm^{-1} and for the double peak near 3000 cm^{-1}. A diminution is also observed for 2360 cm^{-1}. Two peaks at 1700 cm^{-1} and 1635 cm^{-1} appear as well as a large band at 1200 cm^{-1}.

5.2.2. KIMMERIDGIAN LAMINITES: ORBAGNOUX SECTION

Two samples have been studied. They belong to dark-coloured parallel laminae: samples MP5 and MP19 (Plate 11a/1). See figure 4.4 for location.

Bulk rock

Sample MP5: OM is mainly characterized by dark parallel laminae with various colours: golden, orange to dark-brown. They form an entangled network draping detrital clasts (Plate 11a/2). Golden laminae are very thin and are concentrated as "angel hair" (Plate 11a/3). Benthic fauna is rare.
Sample MP19: this sample is less rich in OM (see TOC data below). OM is heterogeneously distributed, characterized by dark parallel laminae (dark-orange to dark-brown) draping detrital clasts or grains (Plate 11a/4). Occurrence of abundant foraminifera (which can be pyritized) and also of degraded phosphatic remains (Plate 11a/5).
Both studied samples are carbonates (88% calcite) with a low content in quartz (12%). No phyllosilicates have been found.

Kerogen (after destruction of mineral phase)

Sample MP5: Most of OM is characterized by AOM (> 95%), which exhibits particles of variable size and light-brown to dark-brown colour (Plate 11b/1). Dark-brown coloured AOM shows a gelified or granular aspect with sharp outlines (Plate 11b/2). When thin, it appears as light-brown coloured with concentration of dark geometrical forms characterzing dense zones (Plate 11b/3). The majority of particles exhibit a strong fluorescence, i.e. FS6 (Plate 11b/4). A fluorescent alveolar network is observable in the background. Some filamentous forms are non-fluorescent. These non-fluorescent zones form patches within a fluorescent particle.
The treatment of rocks by acids led to two types of particles within the residue: a loose and a dense type.

- loose particles are characterized by a geometrical form, are very porous and contain many holes (Plate 11c/1). These alveoli are in fact an assemblage of a filamentous network of several orders of magnitude (Plate 11c/2).

Remnants of organic skeletons are observed within the network (Plate 11c/3); the filamentous aspect is due to the agglomeration of mainly fluffy bodies and also smooth filaments.

- dense particles are more heterogeneous than particles previously described : alveolar network is more fluffy with coccolith imprints (Plate 11c/4). They are characterized by circular depressions surrounded by filaments or spheres (Plate 11c/5).

The nanostructure is heterogeneous in this sample. Edges of alveoli are formed by rounded elements (Plate 11c/6), nanoballs on filaments (Plate 11c/7) and particles entirely composed of nanoballs are ubiquitous (Plate 11c/8).
In SEM, fossil bacteria are very well preserved and have coccoid and filamentous forms (Plate 11d/1-2).
In TEM, the material is characterized by numerous voids and pointed forms (Plate 11d/3). These voids are surrounded mainly by an alveolar network and also by a continuous homogeneous matter. The alveolar network shows different orders of magnitude, i.e., from 50 nm to some µm (Plate 11d/4). Small dense particles are commonly observed: typical, 350 nm large, framboidal pyrite crystals appear completely dark and are grouped in a bunch larger than 2 µm (Plate 11d/5). Other particles are round, greyish, agglomerated within an alveolar network with a diameter varying from 30 to 100 nm (Plate 11d/6). Terrestrial particles are recognizable through their dense and lamellar texture (Plate 11d/7).
Figured elements resembling organisms are present in this sample: filamentous forms resembling a worm, which appear internally structured and dark (Plate 11d/8); filamentous bodies with a 2.5 µm wide, double-spaced membrane, and a cell wall thickness of 600 nm are associated to filamentous bacteria (Plate 11d/9).

Sample MP19: the same observations as for sample MP5 can be made. In palynological slides, OM is mainly composed of AOM. Other figured fragments are rare or absent (Plate 12a/1). AOM appears as light brown when it is thin. Brown AOM is associated with degraded terrestrial elements (Plate 12a/2). Particles show mainly a bright fluorescence, i.e. FS6 (Plate 12a/3), which can be locally very strong (small rods; Plate 12a/4).
In SEM, all particles are characterized by an alveolar network with holes, some 10 to 20 μm in diameter (Plate 12b/1). This network is finely filamentous at the nanoscale (Plate 12b/2).
In AFM, 300 nm wide filamentous particles are made of nanoballs (60 nm in diameter) with a relief of 300 nm (Plate 12b/3). Oriented, 30 nm wide nanoballs are located at the surface of smooth areas (Plate 12b/4). Alveoli at the edge are made of several segmented elements, each one being 100 nm large with a relief of 60 nm (Plate 12b/5). Nanoballs are abundant in this sample (Plate 12b/6).
In TEM, two types are equally represented, i.e., an alveolar network and denser elongated structures (ultralaminae). Textures similar to those encountered in sample MP5 are encountered, such as framboidal pyrite (Plate 12c/1), ligneous particles (Plate 12c/2) and degraded lamellar structures associated with small dark balls (Plate 12c/3). A similar alveolar network with different orders of magnitude (10 nm to 1 μm) is commonly observed (Plate 12c/4). However, dark particles containing small regular holes reflect a trerrestrial origin (Plate 12c/5-6) and are more abundant than in sample MP5.
Typical bacterial bodies are slightly more abundant and better preserved than in sample MP5. They contain internal diffuse membranes, an external cell wall (double-space membrane) and also vacuoles and numerous inclusions. They appear as 1 μm long Gram-positive bacteria and the size of inclusions varies from 25 to 200 nm (Plate 12c/7-8).

Different types of ultralaminae are recognized: i) locally widen and sometimes spread out (Plate 19a): their thickness range from 45 to 90 nm on average, with a maximum of 350 nm. They surround a patch constituted of small dark granules and rod-shaped cellular forms. They could form more than 10 μm long structures (Plate 19b). Layers have the same appearance as those formed in recent microbial mats and range in thickness from 35 to 80 nm (Plate 19c). Their arrangement is similar to that in *Botryococcus braunii* (Plate 18e); ii) a mixture of different types of membranes with variable thicknesses is observed (Plate 22a). Translucent layers are 60 nm thick and homogeneous, whereas dense layers range in thickness from 50 to 140 nm. Their aspect is similar to that of layers in plate 21d, and indicate a certain stage of degradation; iii) thin membranes are characterized by a succession of 80 nm thick, light-colored layers stacked by pairs and 300 nm thick dark-colored laminae (Plate 24a). Each light-layer is 40 nm thick.

Geochemical data

Rock-Eval pyrolysis indicates for samples MP5 and MP19 respectively a TOC content of 6.31% and 4.71%, a T_{max} of 408°C and 411°C and a HI of 809 and 813 mg HC/g TOC. On the HI-T_{max} diagram, both samples plot as thermally immature type I OM (Fig. 6-5).
The isotope composition is defined as $\delta^{13}C_{ker}$ = –26.6‰ and $\delta^{15}N_{ker}$ = 1.5‰ for sample MP19.

Organo-mineral relations

FTIR data are summarized in annexe A4. Iarom/aliph is 0.85. Few differences have been observed between kerogen and bulk rock. It is characterised by a more pronounced double-peak at 2900 cm^{-1}, disappearance at 2360 cm^{-1}, and a large band at 1350-1160 cm^{-1} which is less absorbant.

5.2.3. CRETACEOUS BLACK SHALES (OAES)

5.2.3.1. The Selli level

Two samples with a high HI (see below) have been studied, i.e., samples S20 and S27 (see figure 4.5 for location). These samples were selected with the expectation of encountering a high microbial contribution.

Bulk rock

Sample S20: Thin sections show abundance of OM in undulating entangled laminae (Plate 13a/1). There are 3 colours of laminae: orange, brown and black, which are widely distributed in the organic-richer zones. There are also well-preserved phosphatic remnants showing joints (Plate 13a/2). These irregular wavy laminations may drape thin elongated detrital lenses. Lenses are concentrations of detrital particles, including clay, silt-sized quartz and mica, some feldspar and allochthonous micrite aggregates. Some of the lenses are fecal pellets containing broken phosphatic remains of arthropods and/or fish.

Sample S27: this sample is similar to sample S20 except for phosphatic remains which are relatively less preserved (Plate 13a/3-4).

Kerogen (after destruction of mineral phase)

Sample S20: most of the OM consists of AOM with a brown to dark colour when it is dense (Plate 13a/5). Different textures can be recognized, probably associated to the nature or preservation state of the elements. It includes lumpy or granular and gelified parts in the same particle. Some of them are made of geometric or bony forms (Plate 13a/6). Their size is variable but generally they are some millimetres wide.
Fluorescence appears heterogeneous (FS4). Particles showing a weak fluorescence contain local flashy elements, whereas the rest is completely dark (Plate 13a/7). Others show a patchy fluorescence. A special zone is characterized by a strongly fluorescent typical alveolar network (Plate 13a/8).
Organic matter is characterized by numerous occurrences of large balls (about 10 μm in diametre) on a fluffy surface (Plate 13b/1). These balls are attached to a compact mass forming an alveolar network (Plate 13b/2). Without gold-coating, an alveolar network with holes varying from 5 to 10 μm in diameter (Plate 13b/3), and framboidal pyrite within alveoli (Plate 13b/4) are commonly observed.
Particles are heterogeneous at nanoscale. Nanoballs are present as bunches on a long-limbed particle (Plate 13b/5). Bunches of stratified particles in packet display at surface oriented nanoballs of two sizes, i.e., 40 and 250 nm (Plate 13b/6). It seems that nanoballs are made of single 50-100 nm wide elements, which are packed together forming a 200 nm large set (Plate 13b/7). Typical 220 nm large structures characterized by an opening are attributed to spores or pollen (Plate 13b/8).
Under TEM, various components are observable, including bacteria, terrestrial structures, fragmented organic matter and nanoballs. Bacteria are characterized by a gram negative cell wall with lipidic inclusions (Plate 13c/1-2). When organisms contain separate zones as big components inside the cell, they are thought to be of algal origin (Plate 13c/3). More or less dark nanoballs are present in bunches (Plate 13c/4) or along fragments of OM (Plate 13c/5). Terrestrial structures comprise laminar membranes (Plate 13c/6) and ligneous material (Plate 13c/7). Framboidal pyrite is located within remnants of bacterial cell, characterized by a typical undulating cell wall (Plate 13c/8).

Sample S27: Observations are similar to those in sample S20. In palynological slides, OM is mainly composed of dark brown AOM, which appears grumose (Plate 14a/1) or gelified (Plate 14a/2). In general, particles are weakly (Plate 14a/3) to patchily fluorescent (Plate 14a/4) corresponding to FS3.
Particles in SEM (without coating) are mainly characterized by an alveolar network with numerous, 10 μm large balls (Plate 14a/5). The matter is finely filamentous (Plate 14a/6).

The nanostructure is close to that in sample S20. Bunches of stratified particles show nanoballs oriented in two directions (Plate 14b/1). Other globular particles display locally nanoballs (40 nm) at the edge (Plate 14b/2). Finally, bunches of nanoballs are also observed at the end of particles (Plate 14b/3).
In TEM, some differences are observed with respect to sample S20. Sample S27 contains ultralaminae, bacteria, terrestrial OM, pyrite, nanoballs and fragmented and/or alveolar network. An alveolar/fragmented network appears as a dominant component (Plate 14b/4). Bacteria are more or less preserved with a non characteristic cell wall, a diffuse content (Plate 14b/5) or with lipidic inclusions (Plate 14b/6). Cubic, framboidal pyrite has been found within a remnant of organism (Plate 14b/7) or as pyrotohedron within ultralaminae (Plate 14b/8). The terrestrial fraction is made of resistant matter with holes (Plate 14b/9). Typical algae in symbiosis with bacteria occur in this sample (Plate 14b/10). Translucent to dark nanoballs are present in bunches (Plate 14b/11).

In the Selli level, ultralaminae can be described as i) a concentric arrangement of layers, sometimes forming patches up to 7 x 2.5 μm in size (Plate 19d). Layers have sharp edges with sometimes diffuse, blurred substances inbetween the pigmentation (Plate 19e). They appear as contorted layers surrounding a zone with some granules (Plate 19f). Some are 135 nm thick and resemble those in plate 19a; ii) diffuse layers are observed, sometimes stacked with dark-coloured boundaries (Plate 22b). One is 30 nm thick and the total thickness of the stack ranges from 155 to 330 nm. This probably indicates a certain degradation stage, but different from that in plate 21d. It is maybe specific to the composition of the ultralaminae or due to different degradation conditions prior to diagenesis; iii) fossil OM displays ill-defined, dark, parallel, 60 nm thick layers in a less contrasted patch (Plate 24b). This arrangement can be related to degraded material.
Organic matter in sample S20 appears better preserved than that in sample S27.

Geochemical data

Rock-Eval pyrolysis indicates for samples S20 and S27 respectively a TOC content of 10.13% and 11.69%, a T_{max} of 404°C and 414°C and a HI of 409 and 485 mg HC/g TOC. On the HI-T_{max} diagram, both samples plot as thermally immature Type II OM (Fig. 6-5).
The isotope composition is defined as $\delta^{13}C_{ker}$ = –26.9‰ and $\delta^{15}N_{ker}$ = –0.7‰ for S20 and $\delta^{13}C_{ker}$ = –25.1‰ and $\delta^{15}N_{ker}$ = –0.8‰ for S27.

Organo-mineral relations

FTIR data are summarized in annexe A4. For sample S20, Iarom/aliph is 2.88. FTIR tendancy is globally the same but with some differences. Broad band at 3420 cm^{-1} is more pronounced as well as the double peak at 2920 cm^{-1} and 2360 cm^{-1}. Peaks at 1700 cm^{-1} and 1635 cm^{-1} and 1450 cm^{-1} are more pronounced on the contrary to rock (only shoulders). A large band at 1230 cm^{-1} is distinct from the strong large peak centered at 1050 cm^{-1} in rock.
For sample S27, Iarom/aliph is 4.07. FTIR tendancy is globally the same as S20. Broad band at 3420 cm^{-1} is less pronounced, whereas the double peak at 2920 cm^{-1} and 2360 cm^{-1} are higher in absorbance. Peak at 1700 cm^{-1} appears as well as at 1455 cm^{-1} and 1375 cm^{-1} replacing a large peak at 1422 cm^{-1} in rock. A large band at 1230 cm^{-1} is distinct from the strong large peak centered at 1100 cm^{-1} in rock.

5.2.3.2. The Urbino Level

The two studied samples come from the Monte Petrano and Contessa sections (see figure 4.6 for location). Samples appear laminated and are intercalated between marls (Plate 15a/1).

Bulk rock

Monte Petrano sample: the OM is mainly charcterized by dark parallel laminae (Plate 15a/2) and OM scattered in the matrix (Plate 15a/3) parallel to the laminae. When dense, OM is opaque. Phosphatic fish debris are abundant (Plate 15a/4).
This sample is a carbonate rock composed of 68% calcite, 29% quartz, 4% montmorillonite and 1% illite.
In the Contessa sample, OM agglomerated in grains (Plate 15a/5) and numerous phosphatic remains have been found (Plate 15a/6). In contrast to Monte Petrano, this sample is siliciclastic and composed of 62% quartz, 13% montmorillonite, 22% illite and 2% kaolinite.

Kerogen (after destruction of mineral phase)

Monte Petrano sample

In palynological slides, OM appears as mainly amorphous. It is heterogeneous in size with a dominant brown colour and sharp outlines (Plate 15b/1). Particles are made of rounded elements which can be dark. When thin, it appears as a translucent alveolar network. The other particles are spores and pollen or gelified particles. The majority of OM is non fluorescent, i.e. FS3 (Plate 15b/2). Some particles show an heterogeneous fluorescence from strong to absent. Fluorescent zones can be described as an alveolar network (Plate 15b/3).
In SEM, OM of the Monte Petrano sample is a combination of degraded, figured elements, amorphous organic matter composed of fluffy, smooth and granulous particles where balls are the dominant elementary bodies.
Different kinds of particles are observed: i) particles with an alveolar network (Plate 15b/4) and many balls with a size lower than 200 nm (average between 40 to 90 nm) are widely represented (Plate 15b/5-6); ii) smooth bodies with sharp outlines contain filaments (remnants of bacteria?) (Plate 15c/1). Moreover, there is frequently framboidal pyrite (Plate 15c/2). At nanoscale, locally smooth areas are observed (Plate 15c/3).
TEM observations show heterogeneous OM, mainly composed of a more or less fragmented network and ovoid bodies with thick membranes corresponding respectively to EPS and bacterial cell walls (Plate 15c/4). The alveolar network is characterized by different orders of magnitude (100 nm to several µm) (Plate 15c/5) and contains colonies of bacteria (Plate 15c/6). They seem degraded inside but inclusions are observed in some of them (Plate 15c/7). They are characterized by a relatively small size, i.e., between 200 and 500 nm in width. Well-preserved terrestrial elements are noteworthy, marked by a strong contrast and some holes (Plate 15c/8). Groups of translucent to dark, 30 to 150 nm wide nanoballs are also present (Plate 15c/9).
Bacteria are largely distributed in this sample. They occur either as single elements or in colonies as ovoid, 1 µm long shapes, which are located within an alveolar network. They show a thick cell wall with an internal filling made of some vacuoles. Some of them are relatively diffuse (Plate 15c/7). Some are 2 µm long and 1 µm wide ovoid bodies with no observable cell wall and fragmented diffuse constituents inside. Near the edge, 500 nm long ovoid forms resemble to (Plate 15c/7). They resemble algae containing symbiotic bacteria (Plate 15c/6).

Contessa sample

The same proportion of AOM (> 90%) as the Monte Petrano sample is observed, but its appearance is different: 2 types of AOM are observed with a gelified and granular structure (Plate 16a/1). One type is made of an uniform light-coloured matrix containing dark geometrical bodies (as for example, remnants of filaments; Plate 16a/2). Other well preserved particles such as wood fragments (tracheids), spores and pollen are visible.
Particles are entirely non-fluorescent (except for spores and pollen) and correspond to FS1 (Plate 16a/3).
Organic matter in this sample is characterized by the same material as in the Monte Petrano sample, with some differences. Under SEM, structured elements are less recognizable and are mainly balls. More or less defined membranes are closely associated to balls and form an alveolar network (Plate 16a/4). The surface is locally covered with nanoballs (Plate 16a/5).

AFM pictures indicate locally smooth areas (Plate 16a/6) or irregular structures with nanoballs in the background (Plate 16a/7).
In TEM, this sample is composed of different kinds of bacteria, terrestrial structures, fragmented particles and nanoballs. Bacteria are characterized by: i) gram negative cell wall, dark storage and lipidic inclusions (Plate 16b/1-2); ii) few occurrences of gram positive cell wall with undulating cell wall and cellular content appearing in dark (Plate 16b/3); iii) 100 nm wide forms inclusions with a size smaller than the limiting size for viable bacteria (Plate 16b/4). Round translucent bacterial membranes are also present, assumed to be lysosomes (Plate 16b/5).
Fragmented elements and alveolar networks with different orders of magnitude are widely represented, i.e, EPS (Plate 16b/6). Large, translucent, folded membranes are associated to plant walls (Plate 16b/7), whereas others with strong contrast and regular holes are attributed to terrestrial fragments (Plate 16b/8). Nanoballs (30 to 150 nm) with a translucent to dark aspect occur either in bunches (Plate 16b/9) or along filamentous (algal?) structures (Plate 16b/10).

Various ultralaminae have been identified: i) a 6 x 2 μm patch composed of elongated, contorted, well defined layers, up to 150 nm thick (Plate 20d), which are similar to those in plates 19d and 20a; ii) contorted dark layers with an average thickness of 30 nm are separated by a weakly contrasted and diffuse zone (Plate 22d); iii) a sequence of contorted, dark-colored, 20 nm thick, paired layers separated by light-colored intervals is observed. Layers have a sharp outline (Plate 24d); iv) lamellar structures are found but no relation can be established with the previously described structures. They appear as filamentous, stacked, more than 5 μm long forms and surrounded by a typical layer (Plate 25b). This 75 nm thick layer is radially fragmented (Plate 25c). When broken, they appear as more translucent, twisted membranes. Filaments contain some granules and are surrounded by a more contrasted thin wall. The thickness of filaments is of 120 nm, whereas that of stacked filament walls is of 25 nm.

Geochemical data

Rock-Eval pyrolysis for the Monte Petrano sample indicates a TOC content of 4.28%, a T_{max} of 410°C and a HI of 415 mg HC/g TOC. On the HI-T_{max} diagram the Monte Petrano sample plots as thermally immature Type II OM (Fig. 6-5).
Data are quite different for the Contessa sample compared to Monte Petrano sample: a TOC content of 1.18%, a T_{max} of 437°C and a HI of 70 mg HC/g TOC. On the HI-T_{max} diagram Contessa sample plots in the thermally immature Type III OM (Fig. 6-5).
The isotope composition is defined as $\delta^{13}C_{ker} = -23.8‰$ and $\delta^{15}N_{ker} = -1.1‰$ for U_{mp}.

Organo-mineral relations

FTIR data are summarized in annexe A4. For Ump sample, Iarom/aliph is 6.41. FTIR spectra are strongly different: the broad band at 3420 cm^{-1} is reduced to a shoulder, shoulders near 2000 cm^{-1} disappear in kerogen, peak at 1707 cm^{-1}, 1453 cm^{-1} and 1376 cm^{-1} appear. A large band at 1230 cm^{-1} is distinct from the strong large peak centered at 1100 cm^{-1} in rock.

Molecular biology

DNA extraction has been performed on two Monte Petrano samples, i.e., one in altered rocks at surface and another one at a depth of 50 cm in unweathered rocks. Results show two different bacterial populations between the two samples, which indicates that there is no contamination from weathered to unweathered sediments.
Most of the clone phylotypes in the unweathered sample were similar to sequences typically obtained from marine sedments, whereas the sequences from the surface weathered sample were mainly composed of terrestrial phylotypes. In the unweathered deep sample, proteobacteria, more specifically purple non-sulfur bacteria (PNS) are dominant including *Delftia* (β-proteobacteria), *Variovorax (*β-proteobacteria), *Paracoccus denitrificans (*α-proteobacteria), *Thiobacillus(*β or γ-proteobacteria) and Syntrophaceae which belongs to the sulfate-reducing bacteria (SRB). In the weathered sample

Chryseobacterium, Rubrobacteraceae, *Arthrobacter*, *Pedobacter*, Comamonadaceae, Xanthomonadaceae and Actinomycetes have been found.

5.2.3.3. The 113 Level

One sample has been studied in the Monte Nerone section (see figure 4.6 for location).

Bulk rock

This sample is a calcareous sandstone composed of 60% quartz, 34% calcite, 5% montmorillonite, 1% illite and 0.1% kaolinite.
In thin section, the sediment is laminated and the OM is distributed paralell to laminae within an orange to dark-brown micritic matrix (Plate 17a/1). This sample is characterized by well-preserved phosphatic remains showing radial zonations (Plate 17a/2). Foraminifera are also present.

Kerogen (after destruction of mineral phase)

In palynological slides, AOM is the dominant constituent. Other particles are represented by inertinite, vitrinite, cutinite and soporomorphs (Plate 17a/3). AOM displays several aspects with colours varying from light brown to dark brown. It is made of geometric dark bodies and cutinite (Plate 17a/4). Its texture can be granular or gelified; when dense, it appears black. The size of particles is heterogeneous from micrometers to millimeters.
In SEM without coating, particles are made of a perforated network (Plate 17a/5). Geometrical fragments of different sizes are commonly observed (Plate 17a/6).
The nanostructure is heterogeneous, characterized by globular structures and more or less organized nanoballs. Globular areas contrast with smooth zones containing 50 nm large nanoballs (Plate 17b/1). Stratified particles in bunches display oriented, 40 nm large nanoballs at surface (Plate 17b/2). On the other hand, several 130 nm wide, parallel filaments, with 60 nm wide nanoballs at the end (Plate 17b/3). Isolated, non organized nanoballs (40 nm) were also found on a broken filament (Plate 17b/4).
In TEM, OM is globally characterized by a dominance of lamellar structures resembling ultralaminae. The remaining part comprises patchy, finely, contorted fragments, undefined organic matter and numerous occurrences of small dark balls. A general overview shows degraded lamellar structures without specific form, weakly contrasted material and small dark grains (35 to 80 nm) accumulated in zones up to 3 µm wide (Plate 17b/5). Fibrous structures are typical of ligneous material (Plate 17b/6). They are composed of strongly contrasted regular masses. There are rare occurrences of an alveolar network with different orders of magnitude (100 to 600 nm) (Plate 17b/7). Remnants of 900 nm wide bacteria are characterized by external cell walls and maybe remnants of endospores (Plate 17b/8). Small dark grains range from 35 to 80 nm (Plate 17b/8). Others specific rounded structures are characterized by more diffuse aspect large of 100 to 350 nm (Plate 17b/9). They are either microspores (typical of thick membranes) or remnants of bacterial cells.

Ultralaminae can be described as: i) similar contorted layers forming extensive patches (Plate 20a). At high magnification, layers appear stacked by pairs, which are some 245 nm thick and radially fragmented (Plate 20b). This arrangement is similar to that in Plate 19e, although the fragmented appearance suggests a degraded state; ii) sometimes broken or spread out, 60 to 150 nm thick single layers are also observed (Plate 20c). Fossil OM shows relatively dark, contrasted, contorted, 70 nm thick layers (Plate 22c); iii) a patch of diffuse layers is also observed, sometimes discontinuous and undulating. The layer thickness is about 35 nm (Plate 24c).

Geochemical data

Rock-Eval pyrolysis indicates a TOC content of 3.88%, a T_{max} of 408°C and a HI of 459 mg HC/g TOC. On the HI-T_{max} diagram this sample plots as thermally immature type II OM (Fig. 6-5).

The isotope composition is defined as $\delta^{13}C_{ker} = -18‰$ and $\delta^{15}N_{ker} = -1.4‰$.

Organo-mineral relations

FTIR data are summarized in annexe A4. For this sample, Iarom/aliph is 1.31. Acid etching induces a lesser pronounced band at 3400 cm^{-1} and an accentuation of peaks close to 3000 cm^{-1} and 2360 cm^{-1}. Two distinguish peaks appears comparing a broad band in rock at 1457 cm^{-1} and 1383 cm^{-1}. A band 1050-1350 cm^{-1} with shoulders, which is characterised by a weak absorbance replaces a wide band centred at 1050 cm^{-1}.

6. INTERPRETATION AND DISCUSSION

6.1. Identification of biological structures

Different types of biological structures have been recognized in recent and fossil OM.

6.1.1. PROKARYOTES

Bacteria encountered in the studied samplesare characterized by a size ranging from 200 nm to 2 μm. Their morphology is variable but filamentous and coccoid bodies are the most frequently encountered. Gram-negative bacteria are better preserved because of their outer membrane, composed of LPS, a more resistant compound than peptidoglycan (a major component in Gram-positive bacteria). Internal components observable in recent and fossil bacteria are mainly storage inclusions and vacuoles that are typical: i) polyhedral, dark inclusions (Plate 16b/2) called carboxysomes: they contain enzymes involved in carbon fixation reactions; ii) round, dark inclusions (Plates 2b/3, 2c/3, 12c/7, 16b/1) used for carbon storage; iii) round, light-coloured inclusions (Plates 3c/7, 13c/3, 16b/1) which can be polyhydroxybutyrate granules or glycogen granules (energy reserves); iv) gas vesicles (Plates 4b/5, 9/7, 12c/8, 13c/1, 14c/1, 16b/4) wich are permeable to atmospheric gases, enabling the organism to regulate buoyancy.
When bacteria are exposed to any environmental stress such as nutrient limitation, oxygen depletion, dryness, etc, some of them survive as endospores (Plates 2b/4, 5d/5), i.e., a dormant, tough, and non-reproductive structure. Bacteria will produce a single endospore internally, which is often surrounded by a thin cover.
The cytoskeleton is formed of 100 nm wide filaments called microtubules or protofilaments (Plates 1b/3, 1b/6). They give flexibility to the cell.
Cyanobacteria are characterized by thylakoid membranes (stacked by pair) with pigments called phycobilisomes (Plate 2b/2-3).

6.1.2. EUKARYOTES

Most eukaryotes present in studied samples are algae. In general they are bigger than bacteria (several micrometers in diameter). They are characterized by a thick and homogeneous cell wall and complex cellular structures. They include nucleus and nuclear membrane (Plates 2c/3, 5d/8). Although different cytoplasmic inclusions are present, green algae are recognizable. They contain thylakoid membranes locally stacked in grana (Plate 2c/2) and are sometimes surrounded by cryptocrystalline calcite (Plate 2c/3).
Algae are frequently in close association with bacteria (Plate 6d/9). This could be either a symbiosis or a phagocytosis state.

6.1.3. MICROBIAL SECRETIONS

Microbial secretions called EPS, are produced by most organisms (e.g. Plates 2d/2, 1e). In studied samples, they are mainly found with bacteria. In general, EPS are characterized by a more or less continous muccus (Plate 2d/1), an alveolar network with different orders of magnitude (Plate 1e/4) or agglomerated filaments (Plate 1e/5). They incorporate terrestrial elements when the latter are being degraded (Plate 6b/5).

6.1.4. TERRESTRIAL ELEMENTS

Cuticles (Plate 5b/3) and woody fragments (Plate 5b/1) are characterized by a regular architecture (constant space of holes. In TEM, they appear as translucent membranes with ornamentations (Plate 5d/3-4). Other kinds of structures appear dark in TEM by the presence of geometrical strips (Plate 5d/11). This is typical of lignite.

6.1.5. NANOBALLS

20-150 nm wide balls, observable in SEM (Plate 10/4), AFM (Plates 1c/4, 5c/3, 15b/6) and as dark balls in TEM (Plates 5d/12, 11d/7) are called nanoballs. They are encountered in both recent and fossil samples either as oriented or random bodies. Their origin is still controversial and especially their role in carbonate precipitation as nannobacteria. In this study, they are observable within OM using different techniques. Therefore, artefacts such as metallization (Folk and Lynch, 1997), inorganic precipitates or precursor stages of precipitation in sulfate-reducing bacteria (Aloisi et al., 2006) can be excluded. Although we can not verify their living or non-living status in fossil OM, some features are close to “nannobacteria” observed in OM degradation (Schieber et al., 2003). Depending on studied environments, they could be attributed to macroproteins or nannobacteria.

6.1.6. SIZE CHANGES BETWEEN RECENT AND FOSSIL STRUCTURES

Some biological structures can be recognized in fossil OM based on recent bacteria observations. However, the size of these structures is generally smaller in fossil structures. This size reduction is analyzed in chapter 6.3. Although the behavior of biological structures during early diagenesis is misunderstood, some explanations for this smaller size can be tentatively brought forward: i) loss of water during compaction inducing tissue retraction; ii) oxidation and molecular rearrangement of biomolecules; iii) adsorption and cross-linking with minerals and other molecules.

6.2. Effect of palynological acid treatment: on recent analogs

From a macroscopical point of view, acid treatment has an influence on the consistency and colour of material. Particles are fragmented, lose their fluffy texture and have extenuating colours.
- In sulphuroxidizing bacteria, coccoid species after acid treatment present a smooth aspect with preserved sizes and preserved cellular content. EPS are partially destroyed: they appear smooth at nanoscale, which implies a more regular alveolar network than before treatment (also visible in blue-light fluorescence). Filaments are more easily decomposed, showing internal structures such as protofilaments or microtubules.
No agglomeration of material but partial disappearance has been observed, surface structures deformation are only visible at nanoscale.
- In the cyanobacterial biofilm, it appears that acid attack does not affect fluorescence intensity. A partial destruction of bacterial bodies is observed with a selective preservation of cell walls and maybe thylakoid membranes. At nanoscale, depressions are accentuated and smooth areas are preserved.
It seems that EPS in the biofilm are resistant to chemical hydrolysis compared to those in sulphuroxidizing bacteria.
In the microbial mats, the dendroid network becomes more marked as an alveolar network. Some EPS disappear when they are not attached to other EPS or to organic particles, as it is the case in sulphuroxidizing bacteria.
In continental sediments (where minerals are present), no optical change has been observed, but in FTIR Iarom/aliph is three times lower after acid etching.

Consequently, in optical microscopy no real impact has been observed in the samples of recent analogs, except for the loss of the green colour in photosynthetic organisms. Secretions, i.e., EPS are partially destroyed depending on their fixation to other particles. A smoothing at surface is observed at nanoscale, but no drastic deformation of structures is encountered. EPS become better defined as an alveolar network.
In all recent analogs, acid etching causes an increase in aliphatic C-H stretching and C = O stretching of COOH and ketones.

6.3. Comparison between fossil and recent OM: evidence of microbial activity

Most laminated rocks resemble microbial mats construction at the macroscale, i.e., they display an alternation of organic and mineral layers. Based on comparisons with recent bacterial and continental analogs, organisms and biological structures observed in fossil AOM have been identified, such as remnants of terrestrial and bacterial structures.

6.3.1. MONTEREY FORMATION

In the AOM of the Miocene Monterey Formation, for which sulphuroxidizing bacteria are thought to be the present-day analogue, some bacterial structures are recognized.

- Organisms

➢ Several small filaments with no straight form are found in fossil AOM. The same filaments are encountered in recent filamentous bacteria (Plates 8b/3); they correspond probably to filaments with microtubules or protofilaments, which are structures of cytoskeleton giving flexibility to the cell.

➢ Very organized nanoballs, less than 100 nm in diameter with a specific alignment are perpendicular to the particle arrangement (Plate 10/5). In recent bacteria, linear structures are in fact microtubules or protofilaments (100 nm wide) with aligned nanoballs (50 nm wide) at surface. They correspond to macroproteins, nannobacteria or the accumulation of dead membranes (lysosomes). They are perpendicular to the cytoskeleton.
➢ Coccoid bacteria in fossil AOM are characterized by a homogeneous content with preservation of the outer membrane (Plate 8d/5). In some cases, the cell wall is burst, possibly during sample preparation.

- EPS

In the Monterey samples and recent sulphuroxidizing bacteria, EPS present different aspects:
➢ Filamentous structures with ramifications at the end similar to a fan are observed in fossil AOM. These filaments are twisted with germination at precise locations (Plate 10/7). This morphology is similar to that in recent bacteria with coccoid bodies at one end and, the filament divided in two parts at the other end (Plate 1e/5). This corresponds to agglomerated EPS.
➢ It may appear both as an agglomerated mass (possibly due to compaction) and as a secondary EPS generation with a dendroid form (Plate 10/8).
➢ In TEM, EPS seem to be constituents of their own, characterized by a filamentous alveolar network with some 20 nm wide connections; this kind of EPS is typical of slime layers. It shows a more compact and fluffy aspect than in recent OM, but the general geometry is preserved (Plates 8d/2, 1e/7).
➢ On the contrary to the slime layer, the capsule is more organized (see small rods) and surrounds closely bacteria. The individual size is about 100 nm.
Amorphous organic matter is locally characterized by an alveolar network with recognizable filaments (Pacton et al., 2007).
Structures observed in fossil OM are 6.5 times as small as those in recent bacteria. In both cases, the smaller size of structures in fossil samples is probably due to diagenetic processes such as dehydration and compaction.

6.3.2. KIMMERIDGIAN LAMINITES

The presence of cyanobacteria in sedimentary rocks has been already observed through organic geochemistry (lipids) and bacterial remains such as sheaths have been observed in SEM (Kazmierczak et al., 1996). Previous studies at Orbagnoux using TEM (Mongenot et al., 1997, 1999) indicate that AOM is entirely composed of gel-like, nanoscopically amorphous, sulphur-rich, organic particles.

- Organisms

Individual bacteria in Kimmeridgian AOM can be compared with recent ones based on morphostructure and ultrastructure.
In fossil OM, 2-5 µm wide coccoid and filamentous bodies (Plate 11d/1-2) are similar in size and arrangment to recent bacteria (Plate 2b/1). Other microorganisms are also present: long filamentous bodies resembling nematods. The partly destroyed membrane may be probably gram negative cell wall. Moreover, typical algal structures are recognizable through the thickness of the cell wall and the dark grains corresponding to cytoplasmic inclusions (Plate 12c/7).
The same distribution of nanoballs as in the Monterey Formation is observed in these samples. They are probably remains of bacterial filaments with macroproteins, nannobacteria or accumulation of membranes (lysosomes) at their surface.

- EPS

Fossil AOM is heterogeneous, characterized by circular depressions surrounded by filaments. In the recent biofilm, similar depressions correspond to EPS between communities of filamentous bacteria.
In TEM, AOM is characterized by an alveolar microstructure with different orders of magnitude (from several µm to 100 nm, Fig. 9a). Both AOM and the recent biofilm exhibit a similar alveolar structure with the same size range (Plates 11d/4, 12b/2; 7d/5). The biofilm structure is constituted by EPS and, consequently, that observed in fossil AOM can be interpreted as relicts of a biofilm framework. This

correlation precludes that this morphology may be related to diagenesis. Moreover, the ubiquitous presence of alveoli in the recent biofilm (which contains less than 5% calcite) makes it highly improbable that most of the alveoli observed in the fossil AOM might be attributed to solution cavities resulting from the loss of mineral phases.
Alveolar structures are also recognizable with AFM (Plate 11c/6). The nanostructure of AOM indicates an association of elements constituting the edges of alveoli. Fossil bacteria display the samerange of size than recent bacteria.

6.3.3. CRETACEOUS BLACK SHALES

6.3.3.1. Selli

- Organisms

SEM observations of the organic network after destruction of the mineral matrix show the remains of coccoid bodies resembling recent bacteria. Observations of ultrathin sections in TEM support a bacterial origin based on the size (several μm), the internal structures characterized by a well-preserved cell envelope and some cytoplasmic inclusions (Plate 13c/1-3).

- EPS

SEM photographs of fossil kerogen isolated by palynological preparation clearly illustrate coccoid-shaped bacteria associated with a spongeous to granular organic mass (Plate 13/b-1-2), similar to an alveolar network. In TEM, fragments are dispersed between structured elements (e.g. algal cell walls).
SEM observations of fossil kerogen particles show evidence of bacterial colonization of an organic substrate or remnants of different bacterial communities embedded in EPS. The latter are either the product of bacterial degradation or original EPS.

6.3.3.2. L113

- Organisms

Under SEM and TEM, structures resembling filaments are assimilated to rods, i.e., a morphological type of bacteria. Bacterial bodies are only preserved as remains of cell walls (Plate 17b/8-9).

- EPS

EPS in fossil OM are present as an alveolar network with different orders of magnitude (in TEM) and as fragments of residual EPS (Plate 17b/7), commonly occurring in recent microbial mats.

6.3.3.3. Urbino

The contribution of bacteria in the OAE1b formation has so far never been reported. The identification of bacterial structures in the fossil AOM is based on the morpho- and ultrastructures of previously studied recent bacteria, i.e., microbial mats and sulphuroxidizing bacteria:

- Organisms

Whole bacteria are surprisingly preserved in the fossil AOM (Plate 16b/1-3), with the thickening of cell walls and presence of cellular content, perhaps genetic material. The size of fossil bacterium is 1.5 times smaller than recent analogue.
Different types of bacteria are observed, which contain sometimes inclusions and vacuoles, and are even in colony. The best preserved fossil bacteria clearly show the type of cell wall (Gram-negative because of the presence of inter-membrane space).

Moreover, bacterial products such as membranes are characteristic of enzymatic degradation (Plate 16b/5). Lysosomes which are concentric accumulations of dead bacteria membranes are very well preserved.

- EPS

In fossil AOM, alveolar networks associated with sometimes dendroid filaments are typical of EPS (Plate 15c/5). In SEM they are associated with a high concentration of bacteria.
The biofilm architecture is also preserved as smooth areas correspond to EPS. The size of EPS networks (also observed in the Selli and 113 levels) is similar to those observed in recent bacteria.

6.3.3.4. Summary

Present-day bacteria seem to be good analogs to attempt to identify their presence in fossil OM. Indeed, in fossil OM:

- remnants of filamentous bacteria can be associated with sulphuroxidizing bacteria;
- the presence of biofilms is identified through EPS, characterized by an alveolar network and smooth areas, and also by communities of coccoid and filamentous bacteria in the Kimmeridgian laminites;
- typical EPS within microbial mats are visible only in SEM and are characterized by an alveolar network;
- the bacterial preservation is due to cell wall and cellular content. In general, bacteria contain dark storage and lipidic inclusions or undulating cell walls characterizing respectively ideal growth conditions or a stressed-environment;
- The size of biological structures observed in fossil OM is relatively close to those in living bacteria for OM in Orbagnoux and OAEs. This implies a microenvironment protecting from dessication and hydrolysis sauch as microbial mats.

6.4. Evaluation of microbial activity: implication for OM preservation

Through the water column, OM degradation is mainly governed by bacteria with a specific metabolism (phototrophic, chemoautotrophic, etc.) depending on the redox conditions. Under oxic conditions, heterotrophic bacteria metabolize cyanobacterial products, as shown by lysosomes in modern microbial mats. The preservation of such structures in fossil OM implies specific OM preservation processes. Microbial secretions, i.e., EPS, are major components in microbial mats. They could be the preservation agent in the OAEs and Kimmeridgian samples, where they are characterized by a nanostructured OM, i.e., an alveolar network. The latter occurs through a physical protection (crosslinking) and EPS play the same role as clays in the sorptive preservation pathway (Pacton et al., 2007).
In the Urbino level, despite available data on small areas using TEM, bacteria are characterized by a gram negative cell wall, lipidic and dark storage inclusions indicating good conditions required for microbial growth. In the Selli level, bacteria are present as endospores. Formation of spores is not a normal part of the bacterial life cycle, but rather a defense mechanism used to survive nutritional deprivation. Spores are resistant to temperature, desiccation, organic solvents, ultraviolet light, and most other agents. Unlike the Urbino level, osmotic exchanges may have occurred during the Selli event in the microbial mats, thereby decreasing nutrients supply and increasing the stress of bacteria. Absence of degradation and stress on bacteria in the Urbino samples implies a physical protection and a confinement of microbial mats. The preservation is exceptional, becauseof: i) the preservation of bacteria with intact cell walls and internal inclusions; ii) the preservation of fossil DNA older than 1

Ma the maximum theory survival DNA. Therefore, in this case EPS are not the only factor responsible for OM preservation as in the Kimmeridgian laminites.

Kimmeridgian laminites and OAEs samples are characterized macroscopically by an alternation of organic and mineral laminae. The same observation can be made in the recent microbial mats. The conjunction of microbial mat architecture and EPS contributes to the accumulation and preservation of OM with respect to others organic-rich sediments (OAEs).

6.5. Classification of AOM based on its genetic identity and optical aspects: a high-resolution paleogeographical tool

6.5.1. MORPHOLOGY: NANOSTRUCTURATION

Nanoscale investigations using AFM on recent analogs indicate a strong occurrence of nanoballs. In particular, these cover the surface of the OM in continental samples, the Hassi Jerbi microbial mat and sulphuroxidizing bacteria. They appear also as bunches attached to filaments. In oxic/dysoxic samples (cyanobacterial biofilm and Brazilian microbial mat), nanoballs are rare and present only at surface. Organic matter in Lake Masoko seems less affected by bacterial degradation as shown by SEM and TEM observations. Indeed, nanoballs are abundant and cover most of the OM in anoxic or dysoxic samples, where bacterial degradation is active. Some authors (Schieber and Arnott, 2003) have tested the action of bacteria on organic tissues. They have exposed proteinaceous organic tissues to protein degrading enzymes (either through bacterial activity or via immersion into purified enzyme solutions). They have obtained nanoballs as a natural byproduct of the ensuing degradation process. In both cases the enzymes act as catalysts or chemical “knifes” that break up large, complex, molecular structures, such as cell walls and muscle fibers, into smaller, simpler pieces. The ubiquitous occurrence of balled-up nanoscale subunits is possibly related to elastic forces inherent in larger structures (such as muscle fibers or cell walls) that are composed of coiled and folded up proteins or crystalline and non-crystalline zones of cellulosic fibers. When the structure is cut into smaller subunits, unbalanced forces cause the latter to deform and contract into sphere-like structures. However, other samples have been analized with the same methods and do not present the same distribution of nanoballs. Therefore, a biological origin is proposed here for this type of nanoballs, thereby supporting the hypothesis of nanobacteria proposed by Schieber and Arnott (2003). Those perpendicular to particle orientation are ascribed to either macroproteins or stressed bacterial forms responding to environmental conditions. The distribution of these putative nanobacteria increases with bacterial degradation. The geometrical arrangment of these nanoballs and their ubiquitous presence in samples before and after acid treatment support the interpretation that these nanoballs are not artefacts.

In fossil sediments, the occurrence of nanoballs varies depending on the depositional environment. In the Monterey Formation, nanoballs are locally present as bunches or aligned according to particle orientation. In the Kimmeridgian laminites, nanoballs are the main OM constituting particles at nanoscale. Filamentous structures are completely covered by them (Plate 11d/6). Nanoballs occur as bunches in sample S20 of the Selli Level, but are rare in samples S27 and L113. The Urbino level displays the greatest occurrence of nanoballs of all studied OAEs, particularly in the Contessa sample.
Based on comparisons with recent analogs, the Urbino level and the Kimmeridgian laminites are considered as environments where the inprint of bacterial degradation is preserved. Nanoballs in these levels are interpreted as nannobacteria. Nanoballs are another proof of well-preserved OM and of its

formation in anoxic conditions. Therefore, OM is not completely transformed and, based on microscopical investigations, it can be said that the degradation/recondensation pathway plays a minor role in OM accumulation. This is in agreement with others studied samples, e.g., the Monterey Formation. Consequently, macroproteins are more easily preserved than putative nanobacteria in fossil OM.

6.5.2. FLUORESCENCE

Blue-light fluorescence studies performed on recent bacteria generally show a strong fluorescence with some weakly fluorescent zones, depending on the specific nature of bacteria. Bacterial cells strongly fluoresce, whereas EPS may or may not fluoresce. This is particularly true for microbial mats with respect to the biofilm or sulphuroxidizing bacteria. Non-fluorescent EPS appear as a diffuse mass, containing some thin filaments linking other organic particles. In the continental sediments, OM is in both cases highly heterogeneous and displays different degrees of fluorescence. Consequently, in recent bacteria, the ubiquitous, strongly fluorescent material is represented more by a dominant bacterial species than by EPS. In the case of communities (microbial mats), OM shows various intensities of fluorescence, from weak to strong.
In fossil OM, the fluorescence of AOM varies depending on the depositional environment. In the Monterey Formation, AOM is patchily fluorescent, which is a typical response of Type II OM. The bituminous shales in Orbagnoux contain strongly fluorescent AOM, whereas AOM in OAEs is mainly weakly fluorescent. In the Selli and Urbino levels, a strong fluorescent alveolar network is observed, as well as a weakly fluorescent diffuse mass. The latter probably corresponds to EPS in a microbial mat, whereas AOM in the bituminous shales is attributed to a cyanobacterial biofilm. This implies that weakly fluorescent AOM does not automatically reflect a strongly degraded material (i.e., reworked by bacteria) or a terrestrial input (Tyson, 1995). It could also be associated to non-fluorescent EPS. This interpretation is in agreement with the microscopically well-preserved OM, for example bacteria and ultralaminae encountered in OAEs.

Correlations of Rock-Eval data with microscopy have been made according to Tyson (2006). Although Tyson recommends at least 20 samples for a good correlation between microscopy and geochemistry, only few samples (2-3 per environment) have been analysed in this study. Indeed, correlations are just a rough estimation and not a proper quantitative analysis. Figure A2 shows a ternary AOM-palynomorph-phytoclasts (APP) plot of all studied fossil and recent samples. According to Tyson (2006), the AOM pole refers to a dysoxic-anoxic distal facies. Recent analogs are located near the phytoclast group which corresponds to a proximal or oxic facies. As expected, a good correlation is observed between fluorescence scale index (FSI) and HI. Variations are attributed to the degree of AOM preservation and the redox conditions during early diagenesis (Tyson 2006).

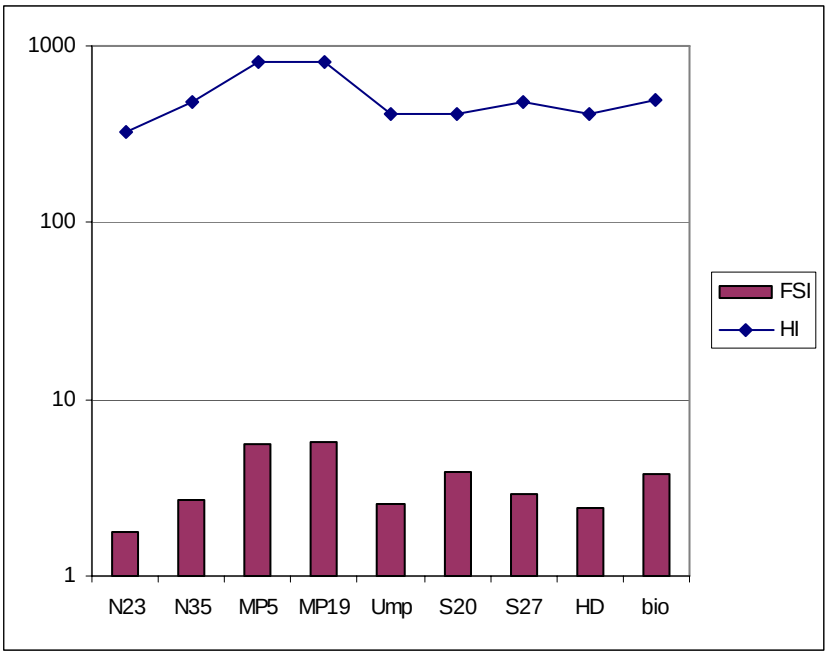

Figure 6-1 : Relationship between mean whole-rock sample hydrogen index (HI) and fluorescence scale index (FSI)

6.5.3. ULTRALAMINAE

6.5.3.1. Recognition of the different types of ultralaminae in fossil and recent material

Ultralaminae are typical, 10-30 nm thick, lamellar structures encountered in fossil SOM. So far, they have been associated to microalgal cell walls with highly resistant, algaenan compounds. Their pyrolysates, i.e. alkylnitriles, are used as a proof of the OM selective preservation pathway. The comparison of fossil ultralaminae with recent microbial analogs, containing green algae and cyanobacteria, sheds new light on their possible multiple origin. Four classes have been identified, which do not contradict the published biological information obtained from organic geochemistry after extraction of soluble constituents in fossil OM. Based on microscopic observations, the specific characteristics of each class (especially width, texture and degradation aspect) can be specifically determined (table 6-1):

Algal cell walls.— Algal cell walls are commonly 100-200 nm thick and have a particular dense and homogeneous texture. In both recent and fossil material, outlines are sharp. They occurr as elongated spirals or contorted layers associated with small granules, which can be inclusions and granules serving as specific storage sites (Konhauser, 2007). Their length of about 10 µm is significant. When they are degraded, they appear as layers locally diffuse and, in some cases, a radial fragmentation is observed.

Bacterial cell walls.— Bacterial cell walls are characterized by a wide size range (50-150 nm), depending on the nature of the cell wall (Gram-negative or -positive bacteria). The texture is heterogeneous, dense or translucent. No significant difference is observed between fossil and recent bacteria. The length is not a significant parameter because some filamentous bacteria could be several µm long. They occur as single or contorted layers but can be differentiated from algal cell walls through their more diffuse aspect. The thin or burst parts are interpreted as resulting from the degradation of bacterial cell walls both in recent bacteria and fossil OM.

Thylakoid membranes.— Thylakoid membranes are typically thin layers, i.e., ranging from 35 to 70 nm in thickness. Another important parameter is their occurrence: they are grouped by pair or stacked

depending on the cyanobacterial or algal origin. Their outline is generally sharp, but their internal texture is not always dense. It could be related to the presence or absence of pigments. Their length is variable because of the organisms' form (filamentous, coccoid or bacillus). No change has been observed in the recent material after the acid treatment. In fossil OM, they can be fragmented.

Organisms and others.— Organisms on their own are characterized by a typical 25 nm thick membrane separated from a 120 nm thick internal cell. The occurrence of such well-preserved structures is rare and, if degraded, they can be mixed up with the classes cited above. They were differentiated from simple cell walls because of their complex constitution including outer membranes. They are architecturally too evolved to be cell walls similar to those previously described.

parameters	*cell wall*				*thylakoid*	
	algal		bacterial		recent	fossil
	recent	fossil	recent	fossil		
thickness	80 -200 nm	commonly 100-150 nm, rare 35 nm	~60 nm; 150 nm when burst	variable: 30-150 nm	40-70 nm	35-60 nm
texture	dense, homogeneous with sharp outlines	dense, homogeneous with sharp outlines	dense or translucent depending on their nature	not always well-defined, blurred; sometimes dense	dense, sharp outlines	sharp outlines
occurrence	contorted layers or elongated spirals	patch; contorted, elongated spirals or linear with granule layers	linear or contorted layers	linear or contorted layers	linear or randomly distributed contorted string-like layers: stacked by pair (cyanobacteria) or associated in grana (for algae)	stacked contorted lines; by pair
length	7 μm	10 μm	1 μm to some μm	several μm	several μm	several μm
degradation	locally diffuse	rarely diffuse; radially fragmented	burst	burst	no change	sometimes fragmented

Table 6-1: Summary of the main characteristics of ultralaminae types distinguished in fossil and recent OM.

6.5.3.2. Resistance of ultralaminae to degradation

In all the studied fossil environments, algal and bacterial cell walls are more frequent than thylakoids. The latter seem to be more affected by degradation (fig. 6-2). Bacterial cell walls can be better preserved than thylakoids because of their lipidic content (more abundant in Gram-negative bacteria), but they are more sensitive to degradation than algal cell walls. Thylakoids associated to photosynthetic pigments can be preserved, because, although they are rich in degradable proteins, they contain a small amount of lipids. In some cases, this preservation might be due to encapsulation. This process is based on intrinsically reactive biochemical compounds encapsulated in some protective matrix (Eglinton, 1998; Knicker et al., 1996). The preservation of these specific membranes, separated from other cellular components such as cell wall and storage inclusions, could be the result of either separation during OM isolation treatment and/or lysis.

The resistance to degradation of each class of ultralaminae is closely related to their chemical nature. Microscopic observations do not contradict organic geochemical data because ultralaminae produce molecular compounds which are common in OM. Indeed, cell walls and thylakoids can be characterized by biomarkers such as n-alkanes, hopanes and more specifically maleimides and isorenieratene depending on source organisms (Kuypers et al., 2002; Pancost et al., 2004; Philp, 1985). This is in agreement with their biochemical nature described above: algae are preferentially preserved because of their non hydrolysable compounds, i.e., algaenans.

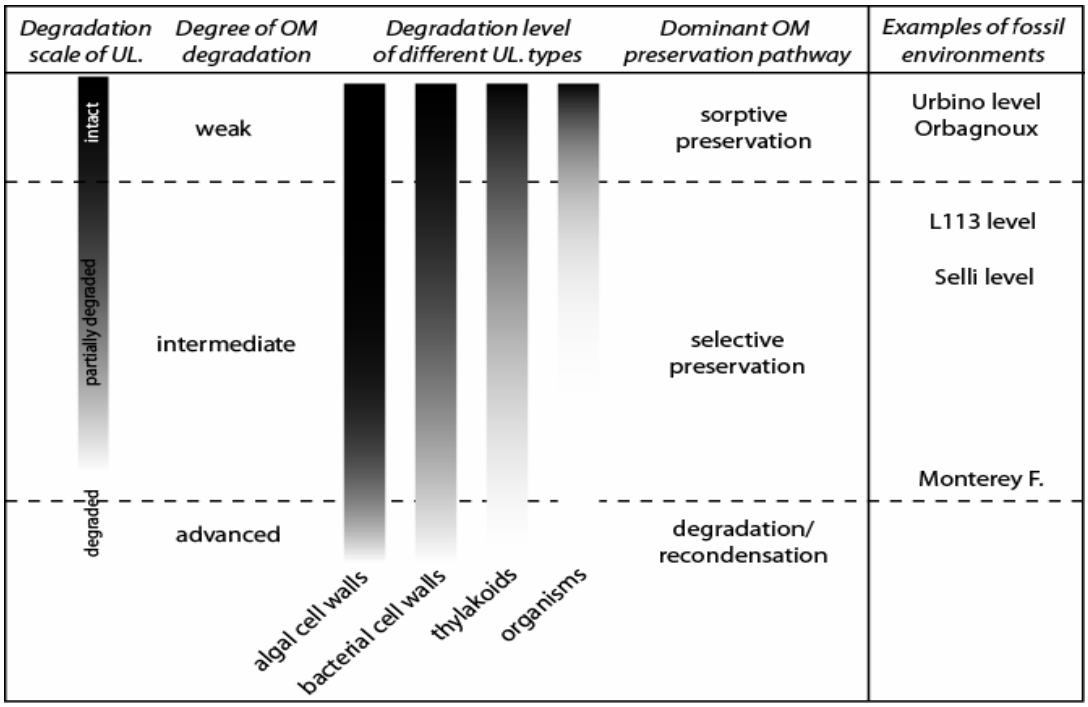

Figure 6-2: Degradation level of different ultralaminae types with respect to degree of OM degradation and dominant OM preservation pathways.

6.5.3.3. Relation between ultralaminae and OM preservation pathways

This study shows a variety of ultralaminae, which cannot be distinguished in biomarker studies. Until now, ultralaminae were solely associated to pyrolysates of algaenans, i.e., alkylnitriles, and therefore, reflecting the role of the selective preservation pathway. In the five studied environments, the degradation stage of ultralaminae is closely associated to OM preservation processes (fig. 6-3). In the upper part of figure 6-3, the weak degradation of OM is related to the sorptive preservation pathway (well-preserved structures are always found with dominant EPS), because of the lability of thylakoid compounds. It implies automatically the concomitant contribution of the selective preservation pathway because algae are not submitted to hydrolysis. The evolution towards degraded ultralaminae implies an increasing contribution of the degradation/recondensation pathway. According to microscopic observations, the latter coincides with degraded OM.
Classically, the preservation of algaenans is thought to result from the selective preservation pathway. However, this is not the case in Kimmeridgian laminites where geochemical analyses indicate that vulcanization is the dominant preservation process. On the other hand, selective preservation is interpreted as playing an important role in the Monterey Formation (Schimmelmann et al., 2001), where structures are less well-preserved with respect to the other studied fossil environments.

6.5.3.4. Paleoenvironmental significance of ultralaminae

Although the different types of ultralaminae highlight the evidence of relative proportion of eukaryotic and prokaryotic organisms, thylakoids are an indicator of paleobathymetry. They are components of phototrophic organisms, which constrain water depth to the photic zone (about 200 m). OM accumulation begins with photosynthesizers at the water surface. In most cases, they are degraded and metabolized throughout the water column, and therefore absent in SOM. Moreover, thylakoids are highly prone to hydrolysis and physical reactions. The presence of such structures in specific

environments supports that photosynthetic/trophic organisms live at the specific depth where thylakoids have been found, i.e. at sea bottom. They cannot be the result of degradation through transport. Their preservation is also due to a low degradation thanks to EPS in a protected environment such as microbial mats.

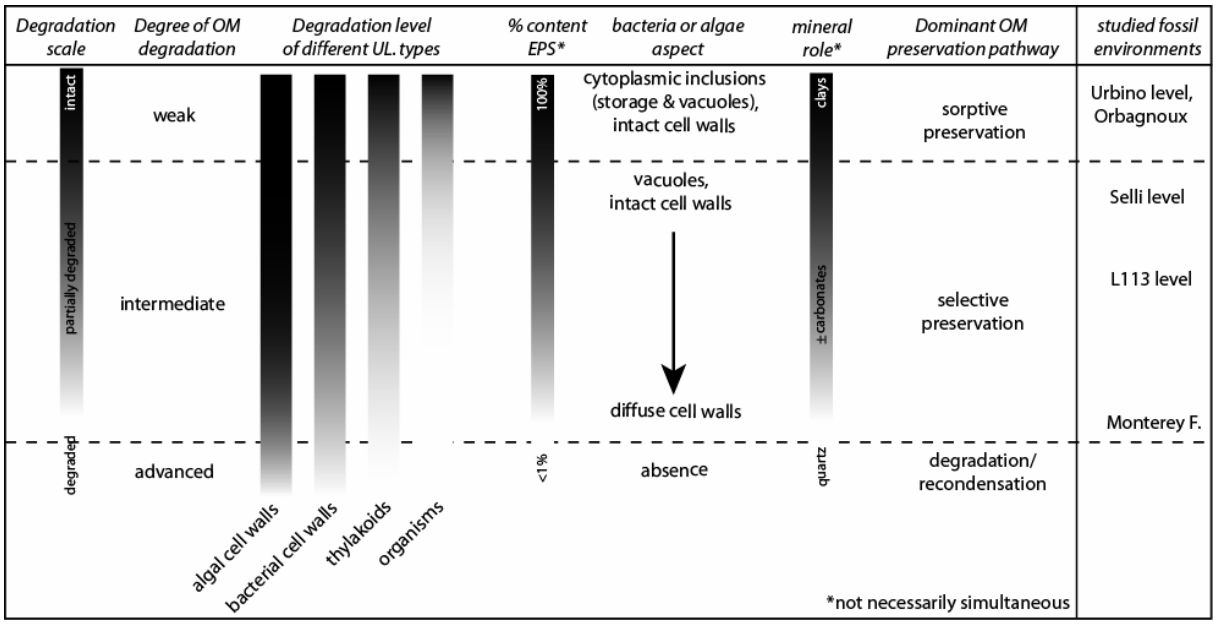

Figure 6-3: Palaeoenvironmental significance of AOM in relation with preservation pathways (UL = ultralaminae)

Consequently, ultralaminae can be considered as a new indicator, besides organic geochemistry and optical microscopy, for identifying the paleoenvironment and preservation pathways of SOM. The multiple origin of ultralaminae implies new considerations about OM preservation and depositional conditions. In particular, the ultralaminae scale of degradation can be associated with the degree of OM degradation and the dominant OM preservation pathway.

6.6. Mineral effect on OM preservation

The mineralogical content of all studied samples is shown in figure 6-4.

6.6.1. THE MONTEREY FORMATION

Samples belonging to the phosphatic unit shale are characterized by a heterogeneous composition: samples N23 and N35 are rich in carbonates (80%), have the same proportion of quartz, a weak content in clay (2%) and other accessory minerals. Sample N12 is characterized by an equal proportion of carbonates, quartz and evaporites (about 30% for each one), with 10% of clays and the remaining mineral fraction being composed of feldspars.
Sample N35 is comparable to sample N23, showing the same proportion of quartz and carbonates, but N35 contains interstratified illite/chlorite. OM is poorly preserved in the latter sample.
Sample N12 appears as the best preserved of the Monterey samples. It has an equal proportion of illite and chlorite which indicates that clays have probably played a role in OM preservation. The hypothesis of this "better" preservation is attributed either to evaporites or to clays and specifically illite.

6.6.2. THE KIMMERIDGIAN LAMINITES

These bituminous shales and more particularly carbonate samples do not contain clay. Both samples have an important content of carbonates (more than 80%), and the remaining fraction is composed of quartz. Organic matter appears well-preserved but the carbonate content is similar to that in the Monterey samples. Therefore, carbonates at Orbagnoux do not seem to play a role in OM preservation, which excludes mineralogy as a potential factor of preservation.

6.6.3. CRETACEOUS BLACK SHALES (OAES)

Microscopic data indicate well-preserved OM at all sites, and the Urbino level (Contessa) seems to be the interval with the best preservation. Samples Ump and L113 are characterized by the same lithology including quartz and clays. Clay contents are similar, but sample Ump is twice as rich in carbonate as sample L113. Samples Uk and S20 display a similar content in quartz and clays with phosphates (i.e. hydroxyapatite) corresponding to arthropod and fish remains. Sample S20 is composed of illite, interstratified illite-smectite and a weak proportion of chlorite.
Sample Uk has the highest content in montmorillonite (15%), samples L113 and Ump have a lower, similar proportion (about 5%) and sample N23 has a low content.
Sample Uk has the highest content in illite (20%), sample N12 has 7%. In samples Ump and L113, the illite content is minor (<0.5%). Kaolinite is found in low quantities in samples Uk and N12 (2%).
Sample Uk demonstrates the best preserved OM with respect to other samples, with a relatively important proportion of clays (illite and montmorillonite).

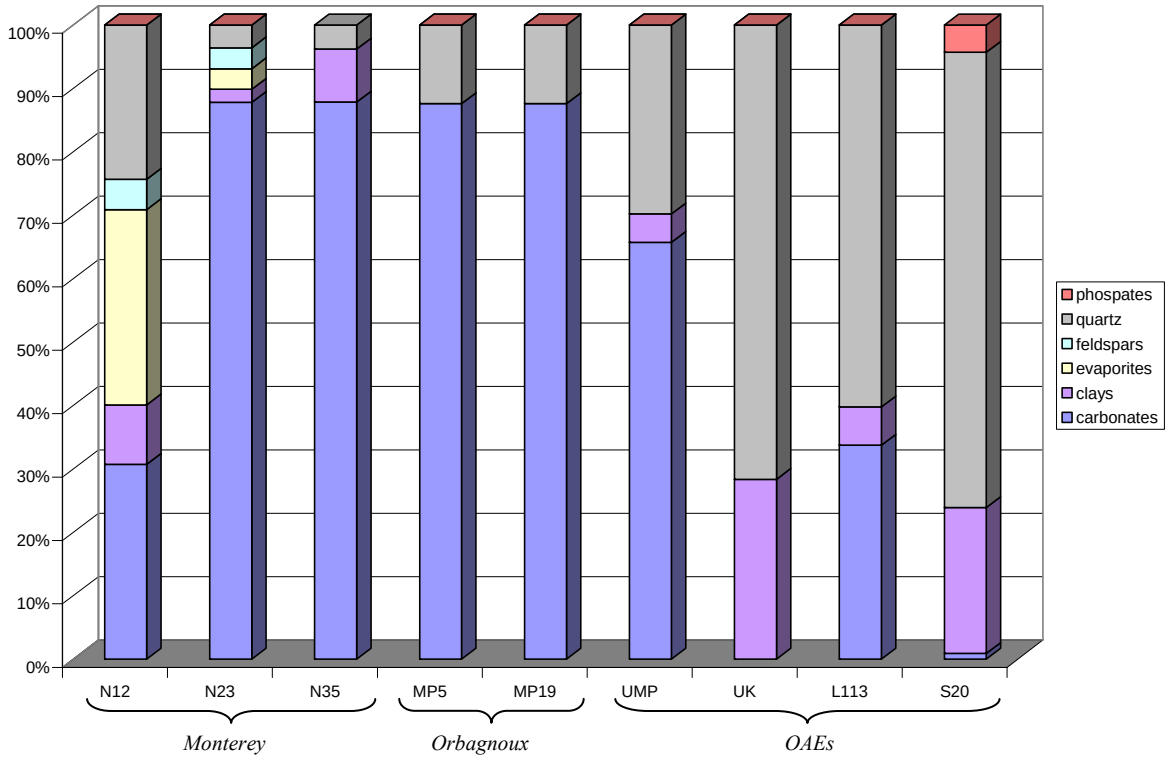

Figure 6-4 : mineralogical content of fossil studied samples.

Comparison of mineralogical content (Fig 6-1) of the different fossil samples indicates that mineralogy seems to play an important role in OM preservation of specific environments:
Samples MP19-MP5-N23 and N35 have a similar proportion of carbonates (80%). Orbagnoux samples (MP5 & MP19) have the highest quartz content compared to samples N23 and N35.

Sample Uk is the only one that contains no carbonate, but a high proportion in quartz (70%) and clays. In the Orbagnoux samples, OM is well-preserved whereas there is no clay.
The preservation in OAEs samples is not due to carbonate, because sample N35 displays the same proportion in carbonates and shows a badly preserved OM. In this case, the mineralogy plays no role in terms of preservation.
Sample N12 has a similar proportion of illite and chlorite, which indicates that clays have probably played a role in OM preservation.

The sorptive preservation pathway through specific clays seems to be an important agent in OM preservation. Samples Ump and L113 present the same clay distribution with montmorillonite being the main factor in OM preservation, with a minor contribution for illite. Montmorillonite has a cation exchange capacity (CEC) of 800m^2/g and illite of 120m^2/g. Both have the property to incorporate water and montmorillonite can form a stable colloidal suspension. However, a better OM preservation is not always related only to mineralogy as shown by samples with a similar mineralogy but very different types of OM preservation (Ump, N23, N35 and Orbagnoux samples).

6.7. Relation between organic geochemistry and OM preservation

Rock-Eval pyrolysis data (Fig. 6-5) indicate some analogies between fossil samples and recent microbial analogs. HI shows the importance of aliphatic compounds in the samples, increasing from Type III to Type I OM. The Orbagnoux samples have the most aliphatic compounds (cyanobacteria as main source of OM), whereas the others are relatively similar (Type II).
The cyanobacterial biofilm, which seems to be a good analogue for the Orbagnoux samples, plots in the Type II OM, close to other fossil samples.

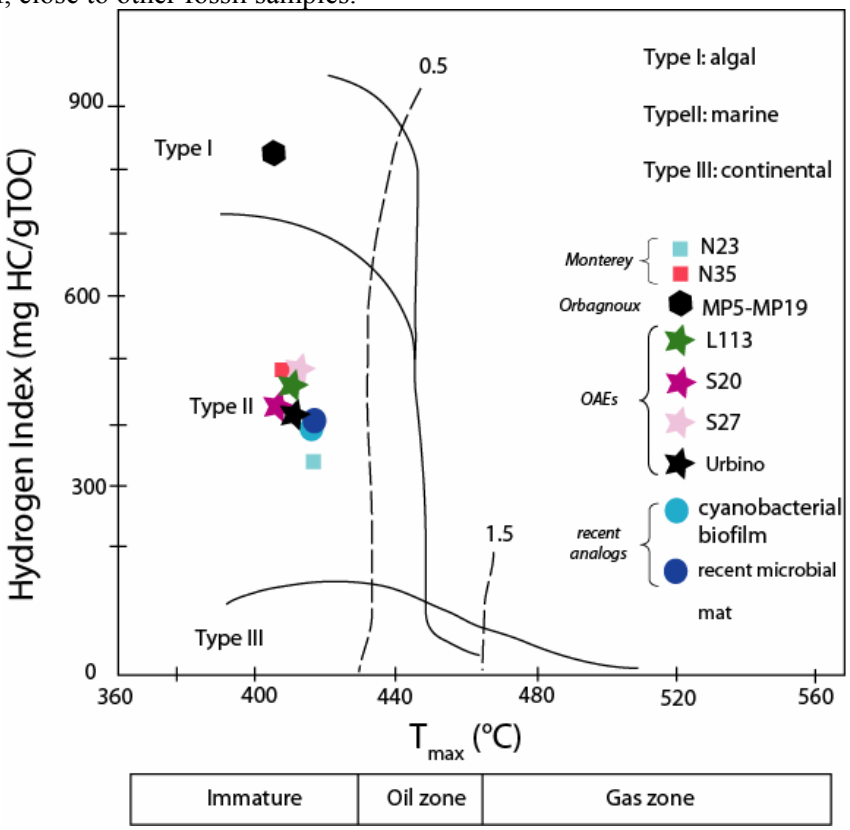

Figure 6-5 : Rock-Eval data of fossil and recent samples.

Comparison of FTIR spectra derived from rocks and OM shows some differences which correlate with the differences in preservation of the studied samples (Fig. 6-6). Two are considered as well-preserved i.e., the Kimmeridgian laminites, essentially constituted of EPS and the Urbino sample (DNA and bacterial bodies). In the Kimmeridgian laminites, the band at about 2300 disappears with respect to other samples, but this band is not mentioned in the literature. In the rock sample of the Urbino level, a broad and strong peak at 1640 cm^{-1} corresponds to vibrations of aromatic C = C and anti-symmetrical stretching of COO^- groups. This corresponds also to the band of illite-montmorillonite. It indicates that illite-montmorillonite contribute to a better preservation of aromatic skeletons. This implies a role of the sorptive preservation pathway by this kind of clay.

Comparisons between fossil OM and recent analogs show some common properties: the spectra of Monterey samples and sulphuroxidizing bacteria are not similar, thereby indicating that OM is strongly degraded and remineralized, which is coherent with microscopic observations. However, all fossil OM display a band at 1450 cm^{-1} corresponding to aliphatic C - H stretching, occurring also in the Brazilian microbial mat and the biofilm. This is a marker of photosynthetic organisms, such as cyanobacteria, thereby confirming the presence of the latter in all sediments.
The range 1100-950 cm^{-1} corresponds to polysaccharides, occurring in microbial mats and biofilm, which are also found in all sediments except the Urbino level. This absence could explain a non incorporation of these compounds into humic substances characterizing a biodegradation of OM less important in this level.
The microbial mats are characterized by a band at 1250 cm^{-1}, which is not the case for the biofilm. It corresponds to EPS secreted by mixed bacterial communities. The same band appears only in the OAEs samples, thereby indicating a contribution of microbial mats in these sediments (coherent with microscopical observations). This corresponds to C – O stretching.

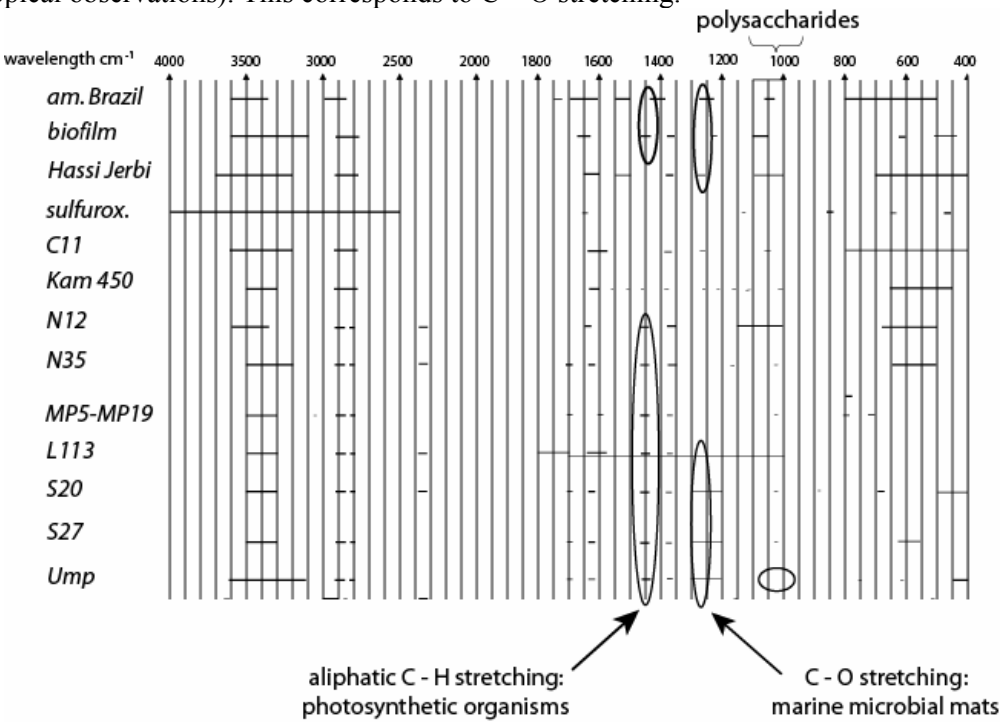

Figure 6-6 :FTIR identification of spectrometric compounds in acid treated samples.

The FTIR investigations permit the establishment of an index comparing the ratio of aromatic to aliphatic compounds (Arom/aliph index) in a sample. The arom/aliph index is variable depending on samples. Samples MP19 (and MP5) and L113 have the lowest value (<2) and contain a highly aliphatic material. On the contrary, sample Ump shows the highest value (>6) indicating a major contribution of aromatic compounds. Samples N12 and S20 are similar (~3) whereas samples N35 and

S27 (~4) are richer in aromatic chains. Sample S27 is relatively richer in aromatic compounds compared to S20.
Hydrogen index does not automatically reveal the real content in aromatic compounds (e.g., samples Ump and L113). It is just a bluk average parameter and it is not a specific type of OM since real samples are always mixtures. Aliphatic structures characterizing type II OM (all samples except MP5) comprise abundant chains and ring systems. Sample Ump displays a value close to that of microbial mat. Among OAEs values, there is an enrichment in aliphatic compounds of sample Ump, Selli (S20 and S27) and to L113. According to Tyson (2006), FSI values have been plotted with HI values (Fig. 6-7), where a good correlation is observed ($r^2 = 0.8$).

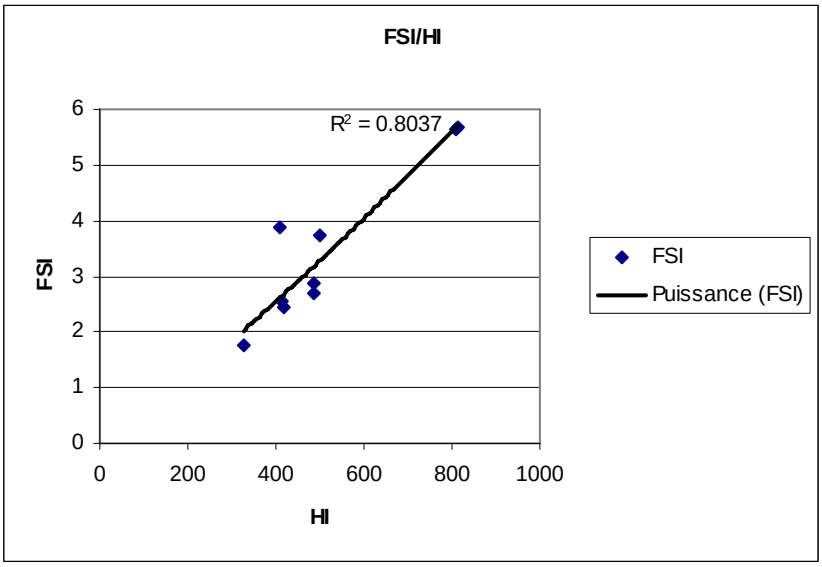

Figure 6-7 : diagram showing comparisons betwwen HI values and FSI of studied samples.

In summary, FTIR investigations highlight the role of the sorptive preservation pathway by protecting aromatic skeletons in the Urbino sample. It suggests the presence of photosynthetic organisms in all studied samples. Microbial mats contribute to OM preservation with a typical band corresponding to C – O stretching. Although HI values and Iarom/aliph should reflect hydrogen compounds in OM, it appears that Rock-Eval data are not always coherent with other chemical investigations. Maybe the classification proposed by Espitalié et al. (1985, 1986) is oversimplified and the bacterial contribution to OM accumulation is more complex than hydrogen-rich compounds.

6.8. Relation between AOM and paleoenvironment

6.8.1. MONTEREY FORMATION

In the Miocene Monterey Formation, the contribution of EPS in OM preservation seems to be minor: OM is locally characterized by filaments and an altered alveolar network related to stretching. Bacteria appear strongly degraded. This is in agreement with previous studies (deep-water conditions, Fig. 6-8), which show recycling of nutrients through the water column mediated through oxydo-reduction and bacteria. In this way, sulphuroxidizing bacteria have been degraded and relatively preserved via interaction with clays (i.e. illite) by the sorptive preservation pathway. The recondensation and the vulcanization processes seem to be the dominant pathways involved in OM preservation.

Isotopic analyses confirm previous palaeoenvironmental indications. Marine algal lipids are reported to have a mean $\delta^{15}N$ value of about +6‰ and an intermediate $\delta^{13}C$ value of about -21 to -22‰, which are in agreement with values of the fossil record. In this way, marine lipids may be the predominant precursor material for OM in the Monterey Formation.

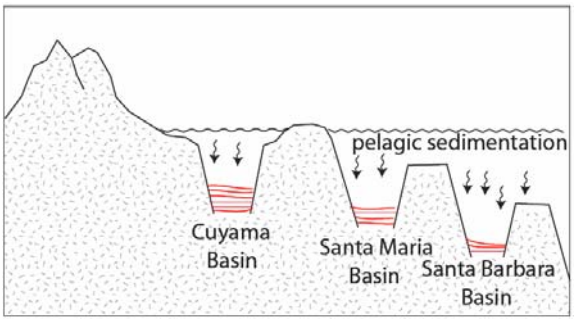

Figure 6-8 : paleoenvironmental reconstruction of the Monterey Formation; modified from Gorsline and Emery (1959).

6.8.2. KIMMERIDGIAN LAMINITES

The investigation of samples through a combination of TEM and SEM methods reveals that in fact AOM has a complex structure at the nanoscale (Pacton et al., 2006).
The presence in fossil AOM of ultralaminae and other structured elements such as filamentous and coccoid bacteria sheds new light on OM preservation mechanisms. Previously, the AOM of Orbagnoux has been described as gel-like and amorphous at the nanoscale by Mongenot et al. (1997 and 1999). This "amorphization" is commonly attributed to the vulcanization preservation pathway, which is well identified through organic geochemistry (Sinninghe Damsté et al., 1988; 1989; Mongenot et al., 2000). The better resolution of the data presented here permits the distinction of structures that can be attributed to cyanobacterial biofilms. The presence of these structures indicates that the selective preservation pathway (Derenne et al., 1991) of Orbagnoux dark laminae has been strongly underestimated and/or that the vulcanization pathway in the Orbagnoux palaeoenvironment does not result in OM "amorphization". Ultralaminae are composed of well-preserved algal cell walls and thylakoids (by pair: → cyanobacteria) and relatively degraded bacterial cell walls. This implies that the paleoenvironment was dominated by soft cyanobacterial biofilms (or photosynthetic microbial mats) in high-salinity shallow water (excluding the presence of grazing macrofauna, Fig. 6-9). Therefore, the sorptive preservation pathway (EPS) could have played a major role in OM preservation.
The carbon and nitrogen isotope composition of the kerogen from the Orbagnoux sample ($\delta^{13}C_{ker}$ = –26.6‰, $\delta^{15}N_{ker}$ = +1.5‰) and for the recent biofilm ($\delta^{13}C$ = –18.5‰, $\delta^{15}N$ = 0.4‰) suggests that marine algae/bacteria were the main source of organic carbon. The $\delta^{15}N$ values close to those of modern atmospheric N_2 ($\delta^{15}N \approx 0$ ‰), suggest primary contribution of molecular nitrogen fixers, such as photosynthetic cyanobacteria, which have $\delta^{15}N$ values between –2 to +4 per mil (Fogel and Cifuentes, 1993).

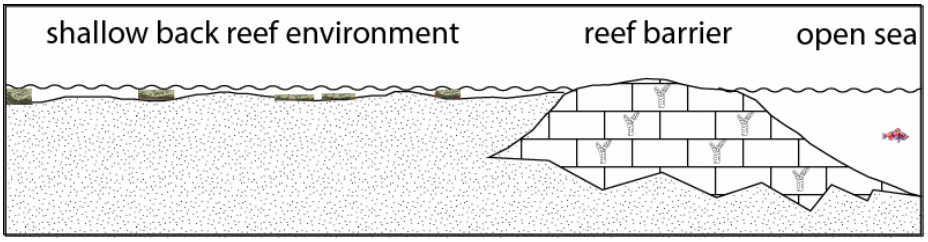

Figure 6-9 : Paleoenvironmental reconstruction of Kimmeridgian laminites with local microbial mats; modified from Tribovillard et al. (1999).

6.8.3. CRETACEOUS BLACK SHALES (OAES)

6.8.3.1. Palaeoenvironmental reconstruction

In the Cretaceous period, the study of different OAEs shows the same macroscopic architecture but some differences are visible at the microscale. This is due to a different preservation pathway and paleoenvironmental conditions: the detrital supply plays a role in the degradation of OM, as well as the nature of OM itself. The ultrastructure reveals differences in microbial activity.
Based on comparisons with the recent microbial mat, geochemical and microscopic data of both environments are similar and point to local microbial mats as the source of AOM in studied OAEs (Fig. 6-10). Indeed, macroscopic observations reveal an alternation of OM and minerals, i.e., laminites, commonly occurring in microbial mats. Mat development is permitted in areas where grazing macrofauna is rare or absent, which is coherent with obervations in the studied OAEs. Palynofacies are similar, with a dominance of AOM in both environments displaying the same characteristics. The dominance of the alveolar network reveals the presence of EPS, which have probably contributed to the fossilization and preservation of OM (Pacton et al., 2006). The presence in SEM, TEM and AFM of EPS, bacteria, remains of bacterial degradation (lysosomes) and ultralaminae strongly suggests a protected environment with a high physical protection of OM, such as in a microbial mat. Organic geochemistry and isotopes indicate the role of microbes (bacteria and algae) as important contributors to OM accumulation, where values are close to those in the microbial mat. This is another proof that microorganisms greatly contribute to the AOM. Moreover, others classes of ultralaminae correspond to thylakoids, which are membranes contributing to photosynthesis. Photosynthetic evidences shown by cyanobacteria (geochemistry and isotopes) and ultralaminae (microscopy) imply a limited water depth corresponding to the photic zone. The hypothesis of cyanobacteria developing at sea surface is excluded considering the high preservation state of OM with respect to other paleoenvironments. Therefore, AOM could be derived from photosynthetic microbial mats where cyanobacteria, diatoms and other microalgae are dominant in the upper part of the mat. It becomes slowly enriched in a variety of organic compounds due to the overproduction of carbon during photosynthesis and lysis of the primary producers (characterized by lysosomes). These compounds are degraded by fermentative and heterotrophic bacteria. A mat is governed by complex pathways in which primary production of organic carbon and nitrogen fixation by phototrophy and chemoautotrophy in the upper part of the mat are balanced by heterotrophic decomposition below. Therefore, in a photosynthetic mat where anoxia occurs, the ammonium may be directly utilized by some microorganisms as a nitrogen source, whereas the remainder is oxidized to nitrate by nitrifying bacteria (Konhauser, 2007). This hypothesis is in agreement with biomarkers found in an equivalent level, i.e., in the Vocontian Basin (Kuypers et al., 2002).
The carbon and nitrogen isotope composition of the kerogen from the black shales ($\delta^{13}C_{ker}$ = –23.8‰, $\delta^{15}N_{ker}$ = –1.1‰) and for the recent microbial mat ($\delta^{13}C$ = –13.2‰, $\delta^{15}N$ = 2.1‰) suggests that marine algae/bacteria were the main source of organic carbon. The $\delta^{15}N$ values close to those of modern atmospheric N_2 ($\delta^{15}N \approx 0$ ‰), suggest primary contribution of molecular nitrogen fixers, such as photosynthetic cyanobacteria. These isotopic values results during times of elevated marine production and accompanying drawdown of dissolved $^{12}CO_2$ for subsequent assimilation by primary producers (Hayes, 1993).

The fragility of thylakoids implies that OM cannot support a transport throufg the water column. Another hypothesis for the location of the development of the microbial mats could be redox interfaces, then a sinking to sea bottom. However, no indication of discontinuities between pelagic deposits and occasional microbial mats has been observed on the field and in thin sections. Moreover, the continuity of laminae and the importance of the mat in term of weight does not support this hypothsesis. Thus, the development of shallow-water benthic microbial mats is favored.

Differences in ultralaminae types are noteworthy: algal and cyanobacterial structures are dominant in the 113 level, thylakoids seem to be less important in the Selli level, and OM in the Urbino level appears as the best preserved with occurrences of the four types including thylakoids which are rarely

degraded. This indicates a difference in the microbial mats communities and increase in water depth as shown by the disappearance of thylakoids.
Therefore, the Urbino, Selli and 113 levels have been deposited in the photic zone (Fig. 6-10), the Urbino being the shallowest and the 113 the deepest. In terms of preservation, the selective preservation pathway coupled with the protective role of EPS are dominant in the OAEs, thereby corresponding to the expansion of microbial mats.

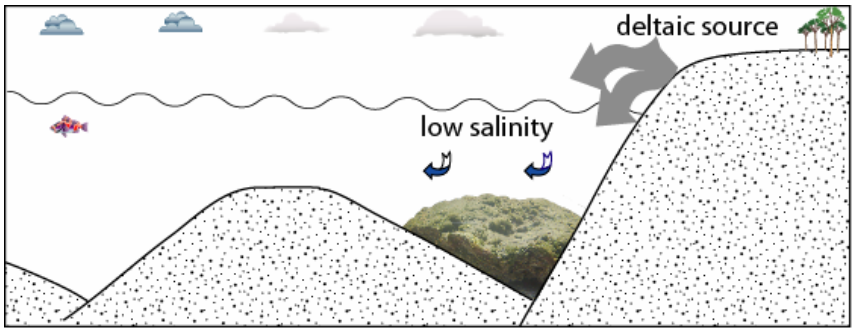

Figure 6-10 : Paleoenvironmental reconstruction of OAEs showing occurrence of microbial mats.

Organic matter in the studied OAEs displays a certain degree of preservation (presence of bacteria and ultralaminae), especially in the Urbino level. In order to determine which processes are involved in the OM preservation, typical structures or molecules of known pathways have been examined. In particular, structures as ultralaminae have been shown to originate from the selective preservation of algaenans. The latter are non-hydrolyzable, highly aliphatic macromolecular constituents, which build up very thin (10-30 nm) chemically resistant outer walls in a number of green microalgae (Derenne et al., 1991; Tegelaar et al., 1989). The occurrence of well-preserved ultralaminae in both fossil OM and recent microbial mat confirms the presence of algae and photosynthetic organisms in OM and the role of the selective and sorptive preservation pathway in recent and fossil studied samples.
The exceptional OM preservation implies another factor than EPS, as is demonstrated in another study (Pacton et al., 2006). The presence of clays, especially illite, could have played a role through the sorptive protection pathway. This mechanism involves a protective role by minerals. In addition to a physical protection from biodegradation (the small size of the pores prevents the action of hydrolytic enzymes), OM adsorption onto pores should favour subsequent condensation reactions by concentrating the reactants (Collins et al., 1995). Some minerals such as clays are known to have catalytic properties (Degens and Ittekkot, 1984). As observed by Salmon et al. (2000), adsorption on the mineral phase possibly played a role, coupled with a physical protection mechanism.

There is a terrestrial supply composed of clays, quartz and palynomorphs and a marine fraction mainly composed of phytoplankton. At the sea bottom benthic microbial mats develop, producing most of the organic compounds. Consequently, a model is proposed for the deposition of OM in the Urbino level (Fig. 6-11):
The studied microbial mats are photosynthetic in their upper part and anoxic in their lower part, which are not in agreement with deep-water deposits described for OAEs. At surface, oxidation and oxic biodegradation occur through cyanobacteria and photosynthetic organisms. Within the microbial mat, where there is anoxia, nitrate and sulfate reduction and methanogenesis take place by anoxygenic organisms which metabolize cyanobacterial products, as shown by the presence of lysosomes. During diagenesis, AOM is well protected from chemical and physical degradation by the concomitant presence of EPS and clays through the sorptive preservation pathway. The selective preservation pathway also plays an important role in the OM preservation, characterized by the abundance and preservation state of ultralaminae. The development of such microbial mats restricts the water depth to the photic zone.

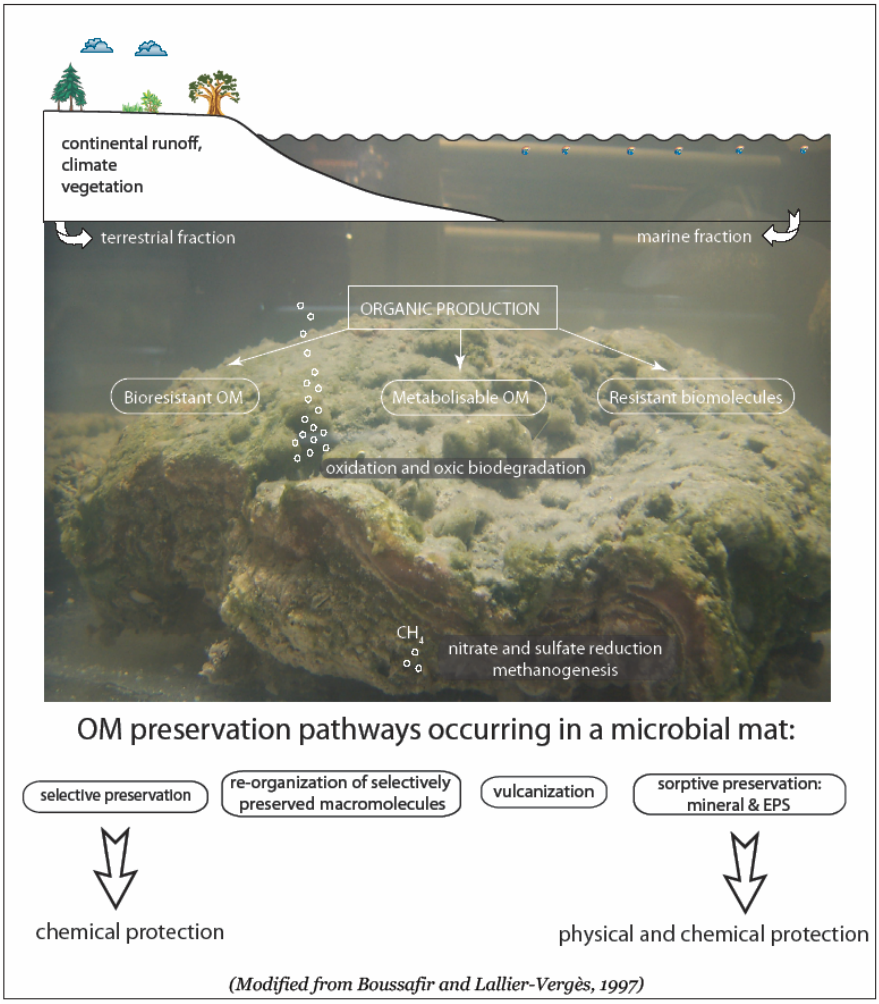

Figure 6-11 : Model of OM deposition during the formation of the Urbino level.

Comparisons with Black Sea environment show that conditions prevailing OAEs seem different, i.e., microbial mats have been found in relation with methane oxidation and aromatic degradation (Kube et al., 2005). These microbial mats are typically attached to the carbonate towers (Michaelis et al., 2002; Pimenov et al., 1997; Reitner et al., 2005; Tourova et al., 2002). In studied OAEs no evidence of methanogenesis has been found but only anaerobic photosynthesis indicators. In this way, it can be compared to Black Sea environment.
According to Meyers (2006), a shift in dominant made of photosynthesis from algae to microbes would be much towards resolving the question of high levels of OM production. However, this model implies a destruction of thylakoids and a rapid recycling of OM which contradict observations made in studied OAEs. Although there is a good correlation between Mediterranean sapropels and Mid-Cretaceous black shales (Meyers, 2006), the hypothesis of surface salinity stratification that enhanced microbial primary production and magnified OM is in adequation with the development of microbial/photosynthetic mats.

6.8.3.2. The paleome

Although ancient DNA is highly debated because the oldest preserved DNA is supposed to date back to between 50 ky to one million years, sequences found in the Urbino level are estimated to date about 100 Ma. They are compatible with marine communities while this level is actually at a height of 1000 m. Sequences give more information about the environment where bacteria lived.

Bacterial sequences extracted from the unweathered sample seem to indicate a reducing marine environments in the zone of anoxygenic photosynthesis (Fig. 6-12) as indicated by the purple non-sulfur bacteria (PNS): i) *Delftia* and *Variovorax* (Gram-negative β-Proteobacteria) are known to reduce nitrate to nitrite; ii) *Paracoccus denitrificans* (Gram-negative α-Proteobacteria) can be aerobic or denitrifying under anoxic conditions with nitrate as the respiratory oxidant and organic compounds as the carbon and energy sources (Kelly et al., 2000). *Paracoccus denitrificans* is now being exploited as a model organism for the study of poorly characterized sulfur compound transformations (Baker et al., 1998); iii) Thiobacillus (Gram-negative β-Proteobacteria) use oxygen as an electron acceptor under aerobic conditions and under anoxic conditions, *T. denitrificans* oxidize reduced sulphur to sulphate while reducing nitrate. Syntrophaceae (δ-Proteobacteria) are a family of sulphate-reducing bacteria (SRB) and are known to live in close association with purple bacteria (Tonolla et al., 2004). SRB members within the δ-Proteobacteria are widely distributed in marine sediments (Jorgensen, 1982) and are especially dominant in various water discharging euxinic conditions such as hydrocarbon seeps (Inagaki et al., 2002; Li et al., 1999; Orphan et al., 2001). These results confirm those found in an equivalent horizon of an OAE1b, i.e., γ-Proteobacteria and δ-Proteobacteria related to SRB (Inagaki et al., 2006).

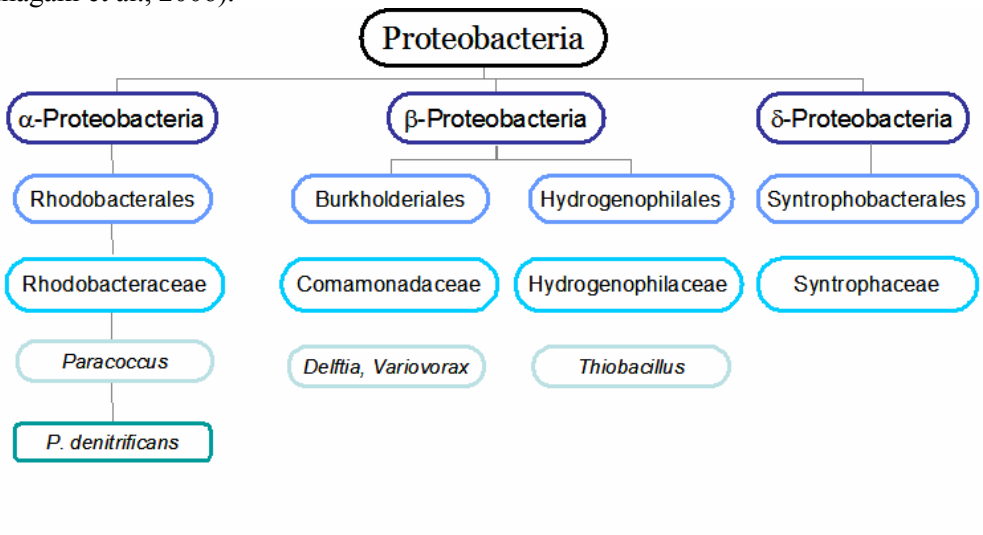

Figure 6-12 : Phylogenetic relationship between the 16S rRNA gene clone sequences from the unweathered sample of the Urbino level.

Sequences found in the weathered sample are different from those identified in the unweathered sample. They display a strong affinity with soil environment: i) Chryseobacterium (Gram-negative Flavobacteria) is associated to degradation of various organic substrates (cellulose, pectin, chitin, fungi or insect) for freshwater or soil species; ii) Rubrobacteraceae (Gram-positive Actinobacteria) have been isolated from soil; iii) Arthrobacter (Gram-positive Actinobacteria) is widespread in soil and contribute to recycling OM, breaking down environmental pollutants and transforming heavy metals. Most species of *Arthrobacter* are obligate aerobes, but all exhibit a pure respiratory, never fermentative metabolism; iv) Pedobacter (Gram-negative Sphingobacteria) is found in widespread environment; v) Comamonadaceae (Gram-negative β-Proteobacteria); vi) Xanthomonadaceae (Gram-negative γ-Proteobacteria) is always plant-associated (Brunings and Gabriel, 2003); and vii) Actinomycetes (Gram-positive Actinobacteria) are non marine, found in soil.
Based on microscopic and geochemical data, it has been established that microbial mats could be the main origin for OM accumulation in the studied OAEs. The bacterial DNA signatures lead to precise the composition of microbial mats living at the time of the Urbino level deposition, which are dominantly anoxic photosynthetic (Fig. 6-13). The top of the mats is composed of cyanobacteria (as suggested by thylakoids and biomarkers). Colourless sulfuroxidizing bacteria are usually below cyanobacteria. They are microaerophilic and their extraction remains difficult at the present time. Therefore, it is not surprising to have no sequences in the fossil record. The purple non sulfur bacteria

(PNS) cannot tolerate high sulfur concentrations. They are photoheterotrophs and just below colourless sulfuroxidizing bacteria. *Delftia*, *Variovorax* and *Paracoccus denitrificans* contribute to the nitrogen cycle in this zone. Thiobacillus releases sulfate from oxidation of sulfide compounds. The purple (PSB) and green sulfur bacteria (GSB) are associated with PNS but produce large amounts of H_2S. Because PNS cannot live with high sulfur concentrations, PSB and GSB have been probably poorly represented in the mats. The bottom of the mats is constituted of SRB as shown by the presence of Syntrophaceae. No evidence of methanogenesis has been found, which is coherent with shallow-water microbial mats.

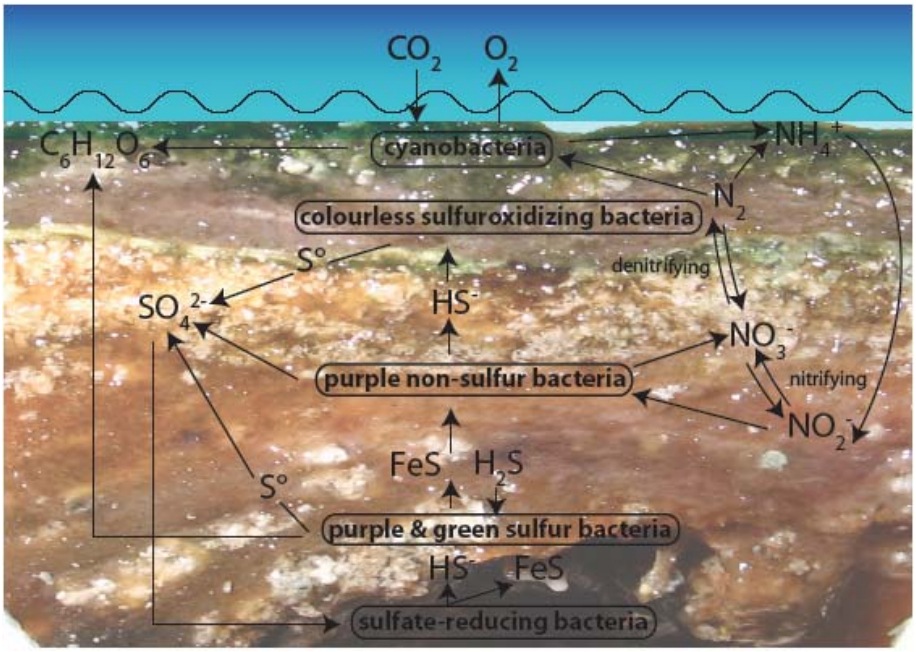

Figure 6-13 : Proposed reconstruction of Cretaceous microbial mats occurring during the Urbino level.

Correlations with microscopical observations can be made based on phylogenetic data. Under anoxic conditions and associated with OM (sludges), Acidothiobacillus ferroxidans contains no carboxysomes but PHB and other dark storage inclusions, which are compatible with fossil observed bacteria (Gram-negative). This is coherent with an anaerobic environment. Other fossil Gram-negative bacterium contain polyhedral dark inclusions characteristic of carboxysomes. They are usually found in all cyanobacteria and some nitrifying bacteria. Because no thylakoids have been found, this bacterium observed could be *Delftia* or *Variovorax*.

The hypothesis of endolithic bacteria is non favored to explain microbial presence in OM. Most of them are known to be extremophiles and have a slow procreation cycle. Based on microscopy, EPS generated by bacteria are widely distributed and bacteria are also randomly distributed (not in local colonies). These evidences do not support local occurences of endolithic bacteria.

6.9. Model of organic matter preservation

Based on the comparisons between fossil OM and their recent microbial counterparts, new parameters have been added, thereby modifying the model of OM degradation proposed by Boussafir and Lallier-Vergès (1997) (Fig. 6-14). This model takes into account the biological and physico-chemical processes occurring in the photic zone. The organic accumulation is initiated through biological primary productivity. The main producers of OM in the marine environment are unicellular phytoplanktonic organisms such as diatoms, dinoflagellates, green algae, cyanophytes, phytoflagellates and nanoflora (Lalli and Parsons, 1993). These living organisms producing OM are also present in the photosynthetic part of the microbial mats. Bacteria occur at different stages of OM accumulation: as producers in aerobic and anaerobic conditions and in the degradation of OM. They

provide the three types of OM, i.e., bioresistant, metabolizable OM and resistant biomolecules (including EPS).
Recycling of OM begins in the photic zone where phytoplankton is being grazed and because of oxidation. All organisms contribute to the flux of metabolisable OM exported to the sea floor. Organisms with "organic tests" and bacteria possess naturally bioresistant biomolecules. The metabolisable OM is generally recycled in the oxic zone. Metabolizable and resistant biomolecules are rearranged in selectively preserved macromolecules through bacteria acting as agents of degradation. Both minerals and EPS play a physical protection role for resistant molecules. Interactions between OM and minerals or EPS are stronger than degrading bacteria or hydrolysis. In this way, this leads to nanostructured AOM, whereas others molecules form nanoscopically amorphous OM through anoxic bacterial degradation.
Part of the H_2S reacts to form sulfides, commonly pyrite (Berner and Raiswell, 1983; Berner and Westrich, 1985). Excess HS^- is incorporated within free lipids of metabolizable OM by the way of vulcanization (Mongenot et al., 1997). The vulcanization pathway can lead to nanoscopically amorphous OM (cf. the Kimmeridge Clay Formation, Boussafir and Lallier-Vergès, 1997) or can have no impact on OM morphology (demonstrated in the Kimmeridgian laminites). Selective preservation keeps both biological and molecular structures: ultralaminae, i.e., microalgal and bacterial cell walls, and thylakoids, dinocysts and terrestrial OM. In the case of bacteria, the preservation process acts through a re-organisation of "selectively preserved" molecules. Only the molecular structure is preserved.

All these processes also occur in microbial mats, which contain an anoxic part below their surface. This implies that these microenvironments mimick all processes occurring in the OM degradation/preservation through the water column. Therefore, microbial mats are considered as a model of SOM deposition in the OAEs and Kimmeridgian laminite.

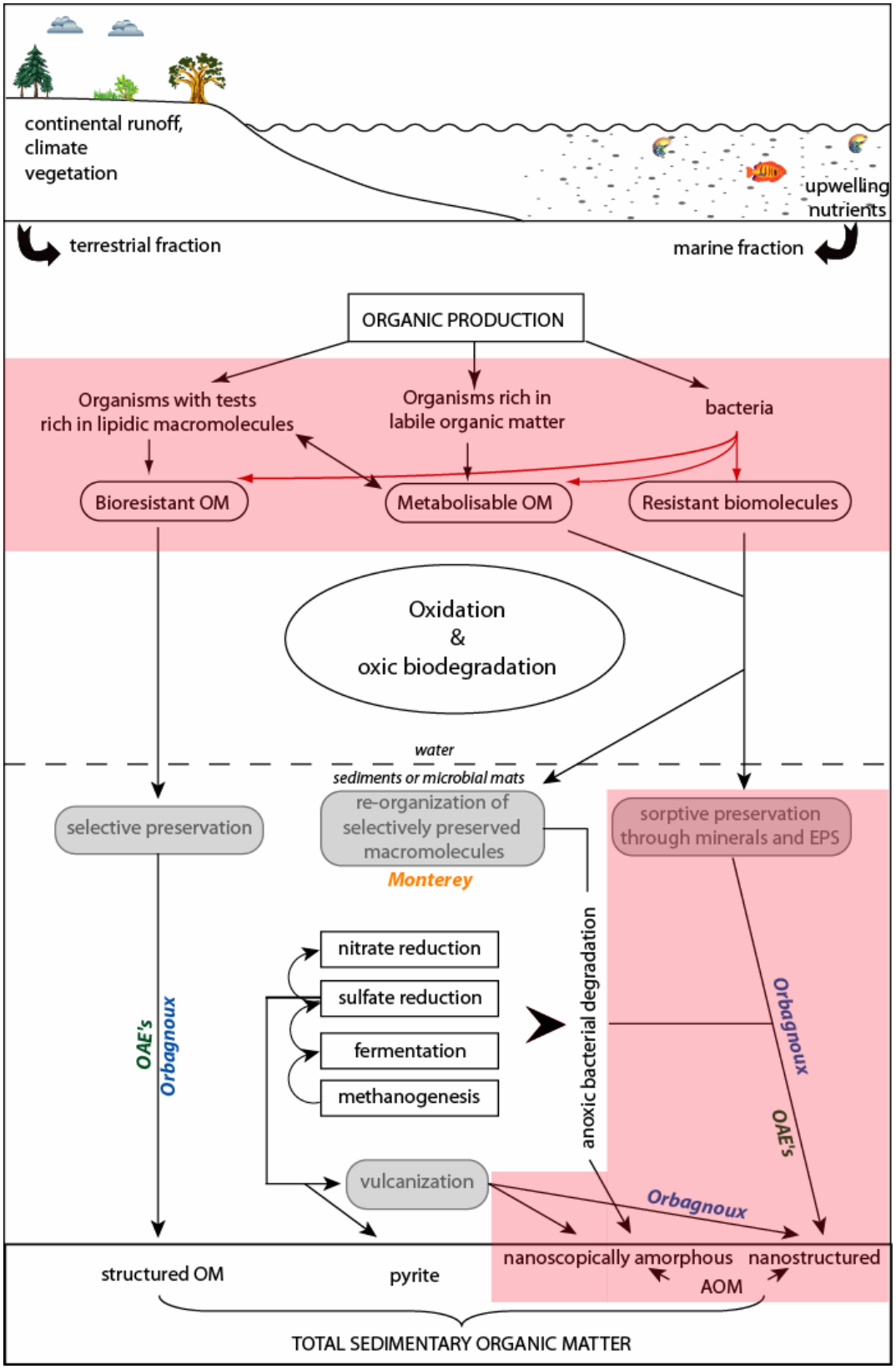

Figure 6-14 : a depositional model of OM in organic-rich sediments showing processes of degradation/preservation occurring in the water column and sediments/microbial mats. The main contribution of this study is related with the items highlighted in red; modified from Boussafir and Lallier-Vergès (1997).

7. CONCLUSIONS

The aim of this study was to determine the paleoenvironmental significance of AOM in organic-rich fossil sediments using comparisons with present-day analogs. Three extensively studied palaeoenvironments have been considered: i) the Monterey Formation related with sulphuroxidizing bacteria; ii) the Kimmeridgian laminites where OM originates from cyanobacteria and where vulcanization plays a major role and leads to the "amorphization" of OM down to the nanoscale; iii) three Cretaceous OAEs including the Selli level (OAE1a) and two less studied levels of OAE1b, i.e., the Urbino and 113 levels. Whereas OAEs origins are widely debated, the paleoenvironment of the two other selected sedimentary intervals are better defined. Therefore, investigations on AOM have been oriented towards finding specific parameters related to depositional conditions. In order to estimate the role of microbial activity in AOM formation, respective analogs have been studied in the same way. A multidisciplinary approach has been used combining microscopical tools (optical microscopy in transmitted light and blue-light fluorescence, SEM, TEM and AFM) and geochemical tools (FTIR, Rock-Eval pyrolysis, organic geochemistry and DNA extraction).

The study of sedimentary organic matter requires the elimination of the mineral fraction through acid treatment. In order to estimate the impact of this chemical attack on OM, recent microbial and continental analogs have been exposed to the same treatment. It shows no real impact in optical microscopy, except for the loss of the green colour in photosynthetic organisms. EPS are partially destroyed depending on their fixation to other particles. A smoothing of the surface was observed at nanoscale but no drastic deformation of structures. EPS becomes better defined as an alveolar network.
In all present-day analogs, acid attack causes an increase in aliphatic C-H stretching and C = O stretching of COOH and ketones.

Microbial activity can play different roles in OM accumulation, depending on depositional conditions. Bacteria are known to metabolize and recycle OM through the water column. Thanks to comparisons with recent microbial analogs, OM preservation pathways have been revisited. Depending on studied environments, EPS entirely condition OM structuration as shown in microscopy. In some cases, structured elements such as bacteria and ultralaminae are well-preserved. Recent studies indicate that EPS fix metal ions or other molecules by cross-linkings. Therefore, it plays a physical and chemical barrier by adsorption. Consequently, EPS are supposed to play the same role as clays and are considered as a new preservation agent in the sorptive preservation pathway. A model based on microscopic observations is proposed to explain the nanomorphology of OM. This alveolar network commonly observed in most AOM could be the result of mechanical constraints because of the hydrated nature of EPS.

TEM investigations of recent and fossil samples highlight the importance of ultralaminae, so far ascribed to microalgal cell walls, as a high resolution paleogeographical tool. This comparison reveals different types of ultralaminae:

1) algal cell walls are characterized by 100-200 nm thick dense layers, chemically composed of algaenans;
2) bacterial cell walls with 60-150 nm thick layers, which have a more heterogeneous texture. They are composed of phospholipids and proteins, and in the case of Gram-negative bacteria, of lipopolysaccharides;
3) thylakoid membranes (membranes acting in the photosynthetic process) are typically thin: they form 35-70 nm thick string-like layers, which appear stacked or in pairs. They are composed of proteins and lipids. They are associated to photosynthetic pigments which can be preserved or not, depending on their nature;
4) filamentous organisms can be distinguished from the others categories through their typical cell wall.

Therefore, they indicate a contribution of algae and /or bacteria. In the case of thylakoids, the water depth can be limited to the photic zone and consequently, they can be used as an indicator of paleobathymetry. Their respective chemical composition is compatible with that shown by biomarkers.

Fluorescence studies have shown that a non-fluorescent marine OM does not automatically imply a strongly degraded OM. EPS in recent bacteria can show a diffuse, weak fluorescence. This is coherent with well preserved structures such as bacteria and ultralaminae in TEM associated with a weak fluorescent fossil AOM.

At nanoscale, "nanoballs" are widely represented when a strong microbial activity is observed in both recent material (i.e., microbial mats and continental sediments) and in fossil anoxic samples (i.e., Kimmeridgian laminites and the Urbino level). Based on comparisons with recent analogs, they seem to indicate a low level of OM degradation and are always associated with bacteria. Shieber et al. (2003) proposed that nannobacteria are a by-product or early organic degradation. Therefore, their ubiquitous presence in these samples as random nanoballs could indicate that they are in fact nannobacteria. Other nanoballs specifically oriented on organic particles are attributed to macroproteins and seem more resistant to degradation.

Although the number of samples studied in the different palaeoenvironments is very low (because of the time consuming methods used), the results of this research pa the way for a reevaluation of paleoenvironmental conditions:

1) OM in the Monterey Formation shows locally identifiable filamentous sulfuroxidizing bacteria, a weak contribution of EPS and a large proportion of undetermined OM. These results lead to validate suggested hypotheses emerged from this work for the microbial role in OM accumulation/diagenesis.
2) In the Kimmeridgian laminites, comparison with a recent cyanobacterial biofilm suggests that AOM is in fact nanostructured and presetns EPS morphology. Cyanobacterial thylakoids also confirm that cyanobacteria have been the main OM producers as suggested by previous authors (Tribovillard et al., 1999, 2000). However, these observations contradict previous interpretations and lead to a reevaluation of OM preservation pathways. The presence of ultralaminae and EPS implies a major role of the selective preservation and sorptive pathways. Vulcanization seems to have no impact on OM morphology. The occurrence of many nanoballs attests of an early diagenesis deposit.
3) Based on microscopical and geochemical data, AOM in OAEs is interpreted to be derived from marine microbial communities and EPS suggesting the existence of microbial mats. Cyanobacteria defined both in microscopy (ultralaminae derived from thylakoids) and in organic geochemistry (methylhopanes and short-chains isoprenoids) indicate that OM was produced within the photic zone. Comparisons of the studied black shale samples seem to indicate that they are all deposited in the photic zone, but with a palaeowater depth increasing from the Urbino level to the Selli level and down to the 113 level. Therefore two hypotheses can be proposed for OM accumulation, i.e., either as shallow-water benthic microbial mats or as microbial mats living at the interface between 2 water masses with different salinity, and then, sinking to sea bottom. However, the first hypothesis is favored at the present time because of the lability of components like thylakoids and DNA, which cannot withstand transport through the water column. These results shed new light on the interpretation of OAEs, which have so far been considered only as deep-water deposits.
4) Microscopical and geochemical evidences of photosynthesis have been encountered in the Urbino level, and are supported by molecular biology. The DNA identification of organisms points to four genus/species belonging to purple non-sulfur bacteria (PNS) which are anaerobic photosynthesizers and the Syntrophaceae family (sulfate-reducing bacteria) which live in close association with PNS bacteria. This exceptional

preservation state is not only due to the physical protection of EPS (also present in other studied black shales), but could also be enhanced by mineralogy, especially illite and montmorillonite, as shown by FTIR and XRD. These clays are known to physically protect OM by sorption. Therefore, the sorptive preservation pathway through EPS and clays has certainly played a major role in this OAE level.

The paleoenvironmental reconstruction of an organic-rich sediment requires a multidisciplinary approach. TEM investigations turn out to be a high-resolution tool for structures in organic particles down to the nanoscale (terrestrial components, EPS, bacteria, ultralaminae). Organic geochemistry can not detect the preservation of OM through EPS, because of their highly hydrated nature and the presence of ultralaminae (common components in the bulk signal, e.g., polysaccharides, lipids,…).
This study sheds a new light on the role of bacteria: they are considered more as a preservation than a degradation agent in specific environments such as the Kimmeridgian laminites or OAEs.
Finally, this study highlights the role of microbial activity in OM accumulation by showing good correlations between fossil and recent bacteria but the transition phases during diagenesis can not be demonstrated. Further work is required to better understand how OM is be transformed. It includes:

- the simulation of the diagenesis of a microbial mat with an anoxic chamber in order to evaluate the microbial arrangement and the relationship between O_2 deficiency and AOM formation. It should be performed using microscopical and geochemical methods including molecular biology;
- the simulation of compaction during diagenesis using a diamond press;
- the measure of the efficiency of EPS and clay in OM protection using an experimental device;
- the investigation of more samples in particular with different TOCs and HIs in the studied OAEs to infirm/confirm the microbial hypothesis and in other OAE black shales using the same techniques in order to define whether microbial mats have only a local or a more regional extent during the Lower Cretaceous.

8. REFERENCES

ADAM, P., SCHMID, J.C., MYCKE, B., STRAZIELLE, C., CONNAN, J., HUC, A., RIVA, A., and ALBRECHT, P., 1993, Structural investigation of nonpolar sulphur macromolecules in petroleum: Geochimica et Cosmochimica Acta, v. 57, p. 3395-3419.

AGUADO, R., CASTRO, J.M., COMPANY, M., and ALFONSO DE GEA, G., 1999, Aptian bio-events--an integrated biostratigraphic analysis of the Almadich Formation, Inner Prebetic Domain, SE Spain: Cretaceous Research, v. 20, p. 663-683.

AHMED, M., SCHOUTEN, S., BAAS, M., and DE LEEUW, J.W., 2001, Bound lipids in kerogens from the Monterey Formation, Naples Beach, California, *in* Rullkötter, C.M.I.a.J., ed., The Monterey Formation : From Rocks to Molecules: New York, Columbia University Press, p. 189-205.

ALOISI, G., GLOTER, A.,KRÜGER, M.,WALLMANN, K.,GUYOT, F.,ZUDDAS, P., 2006, Nucleation of calcium carbonate on bacterial nanoglobules: Geology, v. 34, p. 1017-1020.

ALPERIN, M.J., BLAIR, N.E., ALPERT, T.M., HOEHLE, T.M., and MARTENS, C.S., 1992, Factors that control the stable carbon isotopic composition of methane in an anoxic marine sediment.: Global Biogeochem. Cycles, v. 6, p. 271-291.

ARP, G., HOFMANN, J., and REITNER, J., 1998, Microbial fabric formation in spring mounds ("microbialites") of alkaline salt lakes in the Badain Jaran sand sea, PR China.: Palaios., v. 13, p. 581-592.

ARTHUR, M.A., BRUMSACK, H.-J., JENKYNS, H.C., and SCHLANGER, S.O., 1990, Stratigraphy, geochemistry, and paleoceanography of organic carbon-rich Cretaceous sequences., *in* Baudoin, R.N.G.a.B., ed., Cretaceous resources, events and rhythms.: Dordrecht, Kluwer Academic Publishers, p. 75-119.

ARTHUR, M.A., DEAN, W.E., and SCHLANGER, S.O., 1985, Variations in the global carbon cycle during the Cretaceous related to climate, volcanism, and changes in atmospheric CO_2., *in* Sundquist, E.T.a.B., W.S., ed., The carbon cycle and atmospheric CO_2: natural variations Archean to present.: Washington, Geophysical Monograph, p. 504-529.

ARTHUR, M.A., SCHLANGER, S.O., and JENKYNS, H.C., 1987, The Cenomanian–Turonian oceanic anoxic event: II. Paleoceanographic controls on organic matter production and preservation., *in* Fleet, J.B.a.A.J., ed., Marine Petroleum Source Rocks, p. 401-420.

AUCOUR, A.-M., BONNEFILLE, R., and HILLAIRE-MARCEL, C., 1999, Sources and accumulation rates of organic carbon in an equatorial peat bog (Burundi, East Africa) during the Holocene: carbon isotope constraints: Palaeogeography, Palaeoclimatology, Palaeoecology, v. 150, p. 179-189.

AUERBACH, I.D., SORENSEN, C., HANSMA, H.G., and HOLDEN, P.A., 2000, Physical morphology and surface properties of unsaturated *Pseudomonas putida* biofilms: Journal of bacteriology, v. vol 182, p. 3809-3815.

AUSTIN, J.J., ROSS, A.J., SMITH, A.B., FORTEY, R.A., and THOMAS, R.H., 1997a, Problems of reproducibility - does geologically ancient DNA survive in amber-preserved insects?: Proc. R. Soc. Lond. B. Biol. Sci., v. 264, p. 467-474.

AUSTIN, J.J., SMITH, A.B., and THOMAS, R.H., 1997b, Palaeontology in a molecular world: the search for authentic ancient DNA.: Trends in Ecology & Evolution, v. 12, p. 303-306.

AZAM, F., 1998, Microbial control of oceanic carbon flux: The plot thickens: Science, v. 280, p. 694-696.

AZAM, F., SMITH, D.C., STEWARD, C.F., and HAGSTROM, A., 1993, Bacteria–organic matter coupling and its significance for ocean carbon cycling.: Microbial Ecology, v. 28, p. 167-179.

BAKER, S.C., FERGUSON, S.J., LUDWIG, B., PAGE, M.D., RICHTER, O.-M.H., and VAN SPANNING, R.J.M., 1998, Molecular genetics of the genus *Paracoccus*: metabolically versatile bacteria with bioenergetic flexibility.: Microbiology and Molecular Biology Reviews, v. 62, p. 1046-1078.

BARANCIKOVA, G., SENESI, N., and BRUNETTI, G., 1997, Chemical and spectroscopic characterization of humic acids isolated from different Slovak soil types: Geoderma, v. 78, p. 251-266.

BARRON, E.J., and PETERSON, W.H., 1990, Mid-Cretaceous ocean circulation: results from model sensitivity studies: Paleoceanography, v. 5, p. 319-337.

BATTEN, D.J., 1983, Identification of amorphous sedimentary organic matter by transmitted light, *in* Brooks, J., ed., Petroleum geochemistry and exploration of Europe, Geological society of London special publication, p. 275-87.

BATTEN, D.J., 1996, Chapter 7C colonial chlorococcales: American association of stratigraphic palynologists foundation, v. 1, 191-203 p.

BAUDIN, F., FIET, N., COCCIONI, R., and GALEOTTI, S., 1998, Organic matter characterisation of the Selli Level (Umbria-Marche Basin, central Italy): Cretaceous Research, v. 19, p. 701-714.

BEERLING, D.J., LOMAS, M.R., and GRÖCKE, D.R., 2002, On the nature of methane gas-hydrate dissociation during the Toarcian and Aptian oceanic anoxic events: American Journal of Science, v. 302, p. 28-49.

BEGUIN, P., and AUBERT, J.-P., 1994, The biological degradation of cellulose: FEMS Microbiology Reviews, v. 13, p. 25-58.

BELLANCA, A., ERBA, E., NERI, R., PREMOLI SILVA, I., SPROVIERI, M., TREMOLADA, F., and VERGA, D., 2002, Paleoceanographic significance of the Tethyan 'Livello Selli' (early Aptian) from the Hybla Formation, northwestern Sicily: biostratigraphy and high-resolution chemostratigraphic records.: Palaeogeography, Palaeoclimatology, Palaeoecology, v. 185, p. 175-196.

BERGAMASCHI, B.A., TSAMAKIS, E., KEIL, R.G., EGLINTON, T.I., MONTLUCON, D.B., and HEDGES, J.I., 1997, The effect of grain size and surface area on organic matter, lignin and carbohydrate concentration, and molecular compositions in Peru Margin sediments: Geochimica et Cosmochimica Acta, v. 61, p. 1247-1260.

BERGONZINI, L., GIBERT, E., WINCKEL, A., and MERDACI, O., 2001, Bilans hydrologique et isotopiques (18O et 2H) du lac Massoko, Tanzanie. Quantification des échanges lac-eaux souterraines: Compte Rendu de l'Académie des Sciences., v. 333, p. 617-623.

BERNER, R., and RAISWELL, R., 1983, Burial of organic carbon and pyrite sulphur in sediments over Phanerozoic time: a new theory.: Geochimica et Cosmochimica Acta, v. 47, p. 855-862.

BERNER, R.A., 1994, GEOCARB II: a revised model of atmospheric CO2 over Phanerozoic time: American Journal of Science, v. 294, p. 56-91.

BERNER, R.A., and WESTRICH, J.T., 1985, Bioturbation and the early diagenesis of carbon and sulphur.: American Journal of Science, v. 285, p. 193-206.

BERNIER, P., 1984, Les formations carbonatées du Kimméridgien et du Portlandien dans le Jura méridional. Stratigraphie, micropaléontologie et sédimentologie, Docum. Labo. Géol. Lyon, p. 803 pp.

BERNIER, P., and COURTINAT, B., 1979, La matière organique des calcaires d'arrière-récifs du Kimméridgien supérieur dans le Jura méridional. Systématique, conditions de genèse et d'environnement, Docum. LAbo. Géol. Lyon, p. 95-117.

BERNIER, P., GAILLARD, C., BARALE, G., BOURSEAU, J.P., BUFFETAUD, E., and WENZ, S., 1991, Morphogenetic impact of microbiological mats on surface structures of Kimmeridgian micritic limestone (Cerin, France). Sedimentology, v. 38, p. 127-136.

BERTRAND, P., BERNER, U., and LALLIER-VERGÈS, E., 1986, Organic sedimentation in Celebes and Sulu basins: type of organic matter and evaluation of organic carbon accumulation rates, *in* E.A. Silver, C.R., M.T. von Beymann et al., ed., Proceedings of the ocean drilling program, scientific results: College Station Texas, p. 217-25.

BICE, K.L., BARRON, E.J., and PETERSON, W.H., 1997, Continental runoff and early Cenozoic bottom-water sources: Geology, v. 25, p. 951-954.

BOETIUS, A., RAVENSCHLAG, K., SCHUBERT, C., RICKERT, D., WIDDEL, F., GIESEKE, A., AMANN, R., JØRGENSEN, B.B., WITTE, U., and PFANNKUCHE, O., 2000, A marine microbial consortium apparently mediating anaerobic oxidation of methane: Nature, v. 407, p. 623-626.

BOONE, D.R., WHITMAN, W.B., and ROUVIÈRE, P., 1993, Diversity and taxonomy of methanogens.: Methanogenesis: Ecology, Physiology, Biochemistry and Genetics.: New York, Chapman & Hall, 35-82 p.

BOUDAGHER-FADEL, M.K., BANNER, F.T., and WHITTAKER, J.E., 1997, The Jurassic Favusellacea, the earliest Globigerinina.: The Early Evolutionary History of Planktonic Foraminifera.: New York, Chapman & Hall, 17-52 p.

BOUSSAFIR, M., GELIN, F., LALLIER-VERGES, E., DERENNE, S., BERTRAND, P., and LARGEAU, C., 1995, Electron microscopy and pyrolysis of kerogens from the Kimmeridge Clay Formation, UK: Source organisms, preservation processes and origin of microcycles.: Geochimica et Cosmochimica Acta, v. 59, p. 3731-3747.

BOUSSAFIR, M., and LALLIER-VERGES, E., 1997, Accumulation of organic matter in the Kimmeridge Clay Formation (KCF): an update fossilisation model for marine petroleum source-rocks: Marine and petroleum geology, v. 14, p. 75-83.

BRAKE, M., HOPER, H., and JOERGENSEN, R.G., 1999, Land use-induced changes in activity and biomass of microorganisms in raised bog peats at different depths: Soil Biology and Biochemistry, v. 31, p. 1489-1497.

BRALOWER, T., J. , and THIERSTEIN, H.R., 1984, Low productivity and slow deep-water circulation in mid-Cretaceous oceans: Geology, v. 12, p. 614-618.

BRASS, G.W., SOUTHAM, J.R., and PETERSON, W.H., 1982, Warm saline bottom water in the ancient ocean.: Nature, v. 296, p. 620-623.

BRASSELL, S.C., and FARRIMOND, P., 1986, Fluctuations in biological marker compositions within a Cenomanian black shale from the Angola Basin.: Biogeochemistry of black shales, v. 60, E.T. Degens, P.A. Meyers and S.C. Brassell, 311-338 p.

BRÉHÉRET, J.G., 1994, The Mid-Cretaceous organic-rich sediments from the Vocontian Zone of the French Southeast Basin., *in* Mascle, A., ed., Hydrocarbon and Petroleum Geology of France., Special Publication of the European Association of Petroleum Geoscientists., p. 295-320.

BRUNINGS, A.M., AND GABRIEL, D.W., 2003, Xanthomonas citri: Breaking the surface: Mol Plant Pathol, v. 4, p. 41-57.

BUJAK, J.P., BARSS, M.S., and WILLIAMS, G.L., 1977, Offshore east Canada's organic type and color and hydrocarbure potential: the Oil and Gas Journal, v. 75, p. 198-201.

CANO, R.J., and BORUCKI, M.K., 1995, Revival and identification of bacterial spores in 25- to 40-million year-old Dominican amber.: Science, v. 268, p. 1060-1064.

CANO, R.J., POINAR, H.N., PIENIAZEK, N.J., ACRA, A., and POINAR, G.O., 1993, Enzymatic amplification and nucleotide sequencing of DNA from 120-135 million year old weevil.: Nature, v. 363, p. 336-338.

CANO, R.J., POINAR, H.N., and POINAR, G.O., 1992a, Isolation and partial characterisation of DNA from the bee *Proplebeia dominicana* (Apidae: Hymenoptera) in 25-40 million year old amber.: Med. Sci. Res., v. 20, p. 249-251.

CANO, R.J., POINAR, H.N., ROUBIK, D.W., and POINAR, G.O., 1992b, Enzymatic amplification and nucleotide sequencing of portions of the 18S rRNA gene of the bee *Proplebeia dominicana* (Apidae: Hymenoptera) isolated from 25-40 million year old Dominican amber.: Med. Sci. Res., v. 20, p. 619-622.

CASTRO, H.F., WILLIAMS, N.H., and OGRAM, A., 2000, Phylogeny of sulfate-reducing bacteria.: FEMS Microbiol. Ecol., v. 31, p. 1-9.

CECCA, F., FARAONI, P., MARINI, A., and PALLINI, G., 1995, Field trip across the representative sections for the Upper Hauterivian-Barremian ammonite biostratigraphy in the Maiolica exposed at Monte Nerone, Monte Petrano and Monte Catria (Umbria-Marche Apennines). Memorie Descrittive della Carta Geologica d'Italia, v. 51, p. 187-211.

CHALANSONNET, S., LARGEAU, C., CASADEVALL, E., BERKALOFF, C., PENIGUEL, G., and COUDERC, R., 1998, Cyanobacterial resistant biopolymers. Geochemical implications of the properties of *Schizothrix* sp. resistant material., *in* Novelli, L.M.e.L., ed., Advances in Organic geochemistry: Pergamon press, Oxford, Organic Geochemistry, p. 1003-1010.

CHARMAN, D., 2002, Peatlands and environmental change, *in* Sons, J.W., ed., p. 301.

CHIN, W.-C., ORELLANA, M.V., and VERDUGO, P., 1998, Spontaneous assembly of marine dissolved organic matter into polymer gels: Nature, v. 391, p. 568-572.
CLYMO, R.S., 1983, Mires: Swamp, Bog, Fen and Moor, Ecosystems of the World: Amsterdam, Elsevier, 159-224 p.
CLYMO, R.S., and HAYWARD, P.M., 1982, The ecology of Sphagnum: Bryophyte ecology: London, Chapman and Hall., 229-289 p.
COBIANCHI, M., LUCIANI, V., and MENEGATTI, A., 1999, The Selli Level of the Gargano Promontory, Apulia, southern Italy: foraminiferal and calcareous nannofossil data: Cretaceous Research, v. 20, p. 255-269.
COCCIONI, R., ERBA, E., and PREMOLI SILVA, E., 1992, Barremian-Aptian calcareous plankton biostratigraphy from the Gorgo a Cerbara section (Marche, Central Italy) and implications for plankton evolution.: Cretaceous Research, v. 13, p. 517-537.
COCCIONI, R., FRANCHI, R., NESCI, O., PERILLI, N., WEZEL, F., and BATTISTINI, F., 1989, Stratigrafia, micropaleontologia e mineralogia delle Marne a Fucoidi (Aptiano inferiore-Albiano superiore) delle sezioni di Poggio le Guaine e del fiume Bosso (Appennino umbro-marchigiano). Fossili, evoluzione, ambiente ", Atti del secondo convegno internazionale: Pergola (Italy), 163-201 p.
COCCIONI, R., and LUCIANI, V., 2004, Planktonic foraminifera and environmental changes across the Bonarelli event (OAE2, latest Cenomanian) in its type area: a high-resolution study from the Tethyan reference Bottaccione section (Gubbio, central Italy)
10.2113/0340109: Journal of Foraminiferal Research, v. 34, p. 109-129.
COCCIONI, R., and LUCIANI, V., 2005, Planktonic foraminifers across the Bonarelli Event (OAE2, latest Cenomanian): The Italian record: Palaeogeography, Palaeoclimatology, Palaeoecology Paleobiotic changes in Earth History and their causes - Paleobiotic changes in Earth History and their causes, v. 224, p. 167-185.
COCCIONI, R., LUCIANI, V., and MARSILI, A., 2006, Cretaceous oceanic anoxic events and radially elongated chambered planktonic foraminifera: Paleoecological and paleoceanographic implications: Palaeogeography, Palaeoclimatology, Palaeoecology
Causes and Consequence of Marine Organic Carbon Burial Through Time, v. 235, p. 66-92.
COCCIONI, R., NESCI, O., TRAMONTANA, M., WEZEL, F.C., and MORETTI, E., 1987, Descrizione di un livello-guida "radiolaritico-bituminoso-ittiolitico" alla base dell Marne a Fucoidi nell'Appennino Umbro-Marchigiano: Bollotino della Societa Geologica Italiana, v. 106, p. 183-192.
COGHLAN, A., 1996, Slime City: New Scientist, v. 15, p. 32-36.
COLLINS, M.J., BISHOP, A.N., and FARRIMOND, P., 1995, Sorption by mineral surfaces: Rebirth of the classical condensation pathway for kerogen formation?: Geochimica et Cosmochimica Acta, v. 59, p. 2387-2391.
COMBAZ, A., 1980, Les kérogènes vus au microscope, *in* Durand, B., ed., Insoluble organic matter from sedimentary rocks: Paris, Eds. Technip, p. 55-111.
COSTERTON, J.W., LEWANDOWSKI, Z., CALDWELL, D.E., KORBER, D.R., and LAPPIN-SCOTT, H.M., 1995, Microbial Biofilms: Ann. Rev. Microbiol., v. 49, p. 711-745.
COSTERTON, J.W., LEWANDOWSKI, Z., DE BEER, D., CALDWELL, D., KORBER, D., and JAMES, G., 1994, Biofilms, the customized microniche: Journal of bacteriology, v. 176, p. 2137-2142.
COURTINAT, B., 1989, Les organoclastes des formations lithologiques du Malm dans le Jura méridional. Systématique, biostratigraphie et éléments d'interprétation paléoécologique, Docum. LAbo. Géol. Lyon, p. 361 pp.
DAMMON, A.W.H., and FRENCH, T.W., 1987, The ecology of peat bogs of the glaciated Northeastern United States: Fish and Wildlife Service Biological Report, v. 85, p. 7-16.
DAVAUD, E., and SEPTFONTAINE, M., 1995, Post-mortem onshore transportation of epiphytic foraminifera: recent example from the Tunisian coastline.: Journal of Sedimentary Research, v. A65, p. 136-142.
DE LEEUW, J.W., and LARGEAU, C., 1991, A review of macromolecular organic compounds that comprise living organisms and their role in kerogen, coal and petroleum formation, *in* M.H., E.a.S.A., Macko, ed., Organic Geochemistry: New York, Plenum publishing Corp.
DE MESMAY, R., GROSSI, V., WILLIAMSON, D., KAJULA, S., and DERENNE, S., 2007, Novel mono-, di- and tri-unsaturated very long chain (C37-C43) n-alkenes in alkenone-free lacustrine sediments (Lake Masoko, Tanzania): Organic Geochemistry, v. 38, p. 323-333.
DECHO, A.W., VISSCHER, P.T., and REID, R.P., 2005, Production and cycling of natural microbial exopolymers (EPS) within a marine stromatolite: Palaeogeography, palaeoclimatology, palaeoecology, v. 219, p. 71-86.
DEGENS, E.T., and ITTEKKOT, V., 1984, A new look at clay-organic interaction: Mitteilungen aus dem Geologisch-Palantologischen Instut der Universitat, v. 56, p. 229-248.
DEINES, P., 1980, The isotopic composition of reduced inorganic carbon.: Handbook of environmental isotope geochemistry, v. 1: Amsterdam, The terrestrial environment A. Elsevier, 329-406 p.
DEKKER, M.L., 1988, Infrared Microspectroscopy, Theory and Applications, *in* R.G.Messerschmidt, M.A.H., ed., Practical Spectroscopy series: New York and Basel.
DERENNE, S., LARGEAU, C., CASADEVALL, E., BERKALOFF, C., and B., R., 1991, Chemical evidence of kerogen formation in source rocks and oil shales via selective preservation of thin resistant outer walls of microalgae: origin of ultralaminae: Geochimica et Cosmochimica Acta, v. 55, p. 1041-1050.
DESALLE, R., 1994, Implications of ancient DNA for phylogenetic studies.: Experientia., v. 50, p. 543-550.
DESALLE, R., BARCIA, M., and WRAY, C., 1993, PCR jumping in clones of 30-million-year-old DNA fragments from amber preserved termites (*Mastotermes electrodominicus*). Experientia., v. 49, p. 906-909.
DESALLE, R., GATESY, J., WHEELER, W., and GRIMALDI, D., 1992, DNA sequences from a fossil termite in Oligo-Miocene amber and their phylogenetic implications.: Science, v. 257, p. 1933-1936.
DIDYK, B.M., SIMONEIT, B.R.T., BRASSELL, S.C., and EGLINTON, G., 1978, Organic geochemical indicators of palaeoenvironmental conditions of sedimentation: Nature, v. 272, p. 216-222.

DONEGAN, D., and SCHRADER, H., 1981, Modern analogues of the Miocene diatomaceous Monterey Shale of California: Evidence from Sedimentologic and Micropaleontologic Study., *in* Garrison, R.E.a.D., R.G., ed., The Monterey Formation and related siliceous rocks of California., SEPM Pacific Sect. Symp., p. 149-157.
DUNN, K.A., MCLEAN, R.J.C., UPCHURCH, G.R.J., and FOLK, R.L., 1997, Enhancement of leaf fossilization potential by bacterial biofilms.: Geology, v. 25, p. 1119-1122.
DURAND, B., and MONIN, J.C., 1980, Elemental analysis of kerogens (C, H, O, N, S, Fe). *in* Durand, B., ed., Kerogen: Insoluble Organic Matter from Sedimentary Rocks.: Paris, Editions Technip, p. 113-142.
DURAND, B., and NICAISE, G., 1980, Procedures of kerogen isolation, *in* Durand, B., ed., Insoluble Organic Matter from Sedimentary Rocks.: Paris, Editions Technip, p. 35-53.
EGLINTON, G., 1998, The archaeological and geological fate of biomolecules, *in* Greenblatt, C.L., ed., Digging for pathogens: Rehovot, Balaban publishers.
EGLINTON, G., and CALVIN, M., 1967, Chemical fossils: Sci. Am., v. 261.
EGLINTON, G., SCOTT, P.M., BELSKY, T., BURLINGAME, A.L., and CALVIN, M., 1964, Hydrocarbons of a biological origin from a one-billion-year-old sediment.: Science, v. 145, p. 263-264.
EHRLICH, H.L., 1996, Geomicrobiology, Marcel Dekker.
ERBA, E., 1994, Nannofossils and superplumes: the early Aptian "nannoconid crisis". Paleoceanography, v. 9, p. 483-501.
ERBA, E., 2004, Calcareous nannofossils and Mesozoic oceanic anoxic events: Marine Micropaleontology
Calcareous nannofossil palaeoecology and palaeocenographic reconstructions, v. 52, p. 85-106.
ERBACHER, J., 1994, Entwicklung und Paläoozeanographie mittelkretazischer Radiolarien der westlichen Tethys (Italien) und des Nordatlantiks.: Tübinger Mikropaläontol. Mitt., v. 12, p. 120.
ERBACHER, J., HUBER, B.T., NORRIS, R.D., and MARKEY, M., 2001, Increased thermohaline stratification as a possible cause for an ocean anoxic event in the Cretaceous period: Nature, v. 409, p. 325-327.
ERBACHER, J., THUROW, J., and LITTKE, R., 1996, Evolution patterns of radiolaria and organic matter variations: a new approach to identify sea-level changes in mid-Cretaceous pelagic environments: Geology, p. 499-502.
ERLANDSEN, S.L., KRISTICH, C.J., DUNNY, G.M., and WELLS, C.L., 2004, High-resolution visualization of the microbial glycocalyx with low-voltage scanning electron microscopy : dependence on cationic dyes.: Journal of Histochemistry and Cytochemistry., v. 52, p. 1427-1435.
ESPITALIE, J., DEROO, G., and MARQUIS, F., 1985a, La pyrolyse Rock-Eval et ses applications: Première partie.: Rev. Instit. Fr. Pétr., v. 40, p. 563-579.
ESPITALIE, J., DEROO, G., and MARQUIS, F., 1985b, La pyrolyse Rock-Eval et ses applications: Deuxième partie.: Rev. Instit. Fr. Pétr., v. 40, p. 755-784.
ESPITALIE, J., DEROO, G., and MARQUIS, F., 1986, La pyrolyse Rock-Eval et ses applications: Troisième partie.: Rev. Instit. Fr. Pétr., v. 41, p. 73-89.
ESPITALIÉ, J., MADEC, M., TISSOT, B.P., MENNING, J.J., and LEPTL, P., 1977, Source rock characterization method for petroleum exploration.: Proc. 9th Annual Offshore Technol. Conference Houston, p. 439-448.
FALAH, M., and GUPTA, R.S., 1994, Cloning of the hsp70 (dnaK) genes from *Rhizobium meliloti* and *Pseudomonas cepacia*: phylogenetic analyses of mitochondrial origin based on a highly conserved protein sequence.: J. Bacteriol., v. 176, p. 7748-7753.
FARRIMOND, P., EGLINTON, G., BRASSELL, S.C., and JENKYNS, H.C., 1990, The Cenomanian/Turonian anoxic event in Europe: an organic geochemical study: Marine and Petroleum Geology, v. 7, p. 75-89.
FASSEL, T.A., and EDMISTON, C.E., 1999, Bacterial Biofilms : Strategies for Preparing Glycocalyx for Electron Microscopy: Methods in Enzymology., v. 310, New York, Academic Press, 194-205 p.
FENCHEL, T., 2002, Review: microbial behavior in a heterogeneous world: Science, v. 296, p. 1068-1071.
FIET, N., 1998, Stratigraphie intégrée d'une série pélagique à horizons enrichis en matière organique (black shales). L'Aptien-Albien du bassin de Marches-Ombrie (Italie centrale). [unpublished Ph.D. thesis], 283 p.
FISH, S.A., SHEPHERD, T.J., MCGENITY, T.J., and GRANT, W.D., 2002, Recovery of 16S ribosomal RNA gene fragments from ancient halite.: Nature, v. 417, p. 432-436.
FOGEL, M.L., and CIFUENTES, L.A., 1993, Isotope fractionation during primary production., *in* Engel, M.H.a.M., S.A., ed., Organic Geochemistry: New York, Plenum Press, p. 73-98.
FOLK, R., and LYNCH, L., 2001, Organic matter, putative nannobacteria and the formation of ooids and hardgrounds: Sedimentology, v. 48, p. 215-229.
FÖLLMI, K.B., BADERTSCHER, C., KAENEL, E., STILLE, P., JOHN, C.M., ADATTE, T., and STEINMANN, P., 2005, Phosphogenesis and organic-carbon preservation in the Miocene Monterey Formation at Naples Beach, California - The Monterey hypothesis revisited: Geological Society of America Bulletin, v. 117, p. 589-619.
FRANCIOSO, O., SANCHEZ-CORTES, S., CASARINI, D., GARCIA-RAMOS, J.V., CIAVATTA, C., and GESSA, C., 2002, Spectroscopic study of humic acids fractionated by means of tangential ultrafiltration: Journal of Molecular Structure, v. 609, p. 137-147.
FRANZEN, J.L., 1994, Bacterial preservation of the digestive system in Messel equoids.: Kaupia-Darmstätder Beiträge zur Naturgeschichte, v. 4, p. 3-11.
FREEMAN, K.H., and HAYES, J.M., 1992, Fractionation of carbon isotopes by phytoplankton and estimates of ancient CO_2 levels: Global Biogeochemical Cycles, v. 6, p. 185-198.
FREEMAN, K.H., HAYES, J.M., TRENDEL, J.M., and ALBRECHT, P., 1990, Evidence from carbon isotope measurements for diverse origins of sedimentary hydrocarbons.: Nature, v. 342, p. 254-256.
GALEOTTI, S., 1998, Planktic and benthic foraminiferal distribution patterns as a response to changes in surface fertility and ocean circulation: a case study from the Late Albian "Amadeus Segment" (Central Italy). Journal of Micropalaeontology, v. 17, p. 87-96.

GALLARDO, V.A., 1977, Large benthic microbial communities in sulphide biota under Peru-Chile subsurface countercurrent.: Nature, v. 268, p. 331-332.
GELPI, E., SCHNEIDER, H., MANN, J., and ORO, J., 1970, Hydrocarbons of geochemical significance in microscopic algae: Phytochemistry, v. 9, p. 603-612.
GERDES, G., KLENKE, T., and NOFFKE, N., 2000, Microbial signatures in peritidal siliciclastic sediments: a catalogue.: Sedimentology, v. 47, p. 279-308.
GERDES, G., KRUMBEIN, W.E., and REINECK, H.E., 1991, Biolaminations - Ecological versus depositional dynamics., *in* G., E., W., Ricken & A., Seilacher, ed., Cycles and Events in Stratigraphy, Springer-Verlag, p. 238-266.
GOLENBERG, E.M., GIANNASI, D.E., CLEGG, M.T., SMILEY, C.J., DURBIN, M., HENDERSON, D., and ZURAWSKI, G., 1990, Chloroplast DNA sequence from a Miocene *Magnolia* species.: Nature, v. 344, p. 656-658.
GORIN, G., GÜLAÇAR, F., and CORNIOLEY, Y., 1989, Organic geochemistry, maturity, palynofacies and paleoenvironment of Upper Kimmeridgian and Lower Tertiary organic-rich samples in the southern Jura (Ain, France) and Subalpine massifs (Haute-Savoie, France): Eclog. Geol. Helv., v. 82, p. 491-515.
GOTH, K., DE LEEUW, J.W., PÜTTMANN, W., and TEGELAAR, E.W., 1988, Origin of the Messel oil shale kerogen: Nature, v. 336, p. 759-761.
GRABOVICH, M.Y., DUBININA, G.A., LEBEDEVA, V.Y., and CHURIKOVA, V.V., 1998, Mixotrophic and lithoheterotrophic growth of the freshwater filamentous sulfur bacterium *Beggiatoa Leptomitiformis* D-402.: Microbiology, v. 67, p. 383-388.
GRANT, C., 1991, Lateral and vertical distributions of filamentous bacterial mats (Beggiatoa spp.) in Santa Barbara Basin, California : a modern analog for Monterey Formation [unpublished Thesis of master of Science thesis], 201 p.
GREGORY, W.A., CHINN, E.W., SASSEN, R., and HART, G.F., 1991, Fluorescent microscopy of particulate organic matter: Sparta Formation and Wilcox Group, south central Louisiana.: Organic Geochemistry, v. 17, p. 1-9.
GUBLER, Y., and LOUIS, M., 1956, Etude d'un certain milieu du Kimméridgien bitumineux de l'est de la France.: Rev. Instit. Fr. Pétr., v. 11, p. 1536-1543.
GUPTA, R.S., 2000, The phylogeny of proteobacteria: relationships to other eubacterial phyla and eukaryotes: FEMS Microbiology Reviews, v. 24, p. 367-402.
HALLAM, A., 1985, A review of Mesozoic climates.: Journal of the Geological Society, v. 142, p. 433-445.
HEBSGAARD, M.B., PHILLIPS, M.J., and WILLERSLEV, E., 2005, Geologically ancient DNA: fact or artefact?: TRENDS in Microbiology., v. 13, p. 212-220.
HEIMHOFER, U., HOCHULI, P.A., HERRLE, J.O., ANDERSEN, N., and WEISSERT, H., 2004, Absence of major vegetation and palaeoatmospheric pCO2 changes associated with oceanic anoxic event 1a (Early Aptian, SE France): Earth and Planetary Science Letters, v. 223, p. 303-318.
HEIMHOFER, U., HOCHULI, P.A., HERRLE, J.O., and WEISSERT, H., 2006, Contrasting origins of early Cretaceous black shales in the Vocontian basin: evidence from palynological and calcareous nannofossil records: Palaeogeography, Palaeoclimatology, Palaeoecology, v. 235, p. 93-109.
HERBERT, T.D., 1992, Paleomagnetic calibration of Milankovitch cyclicity in Lower Cretaceous sediments.: Earth and Planetary Science Letters, v. 112, p. 15-28.
HOCHULI, P.A., MENEGATTI, A.P., WEISSERT, H., RIVA, A., ERBA, E., and SILVA, I.P., 1999, Episodes of high productivity and cooling in the early Aptian Alpine Tethys: Geology, v. 27, p. 657-660.
HOEHLER, T.M., ALPERIN, M.J., ALBERT, D.B., and MARTENS, C.S., 1994, Field and laboratory studies of methane oxidation in an anoxic marine sediment: evidence for a methanogen-sulfate reducer consortium.: Global Biogeochem. Cycles, v. 8, p. 451-463.
HOFREITER, M., SERRE, D., POINAR, H.N., KUCH, M., and PÄÄBO, S., 2001, Ancient DNA.: Nature Reviews Genetics, v. 2, p. 353-360.
HOHN, A., TOBSCHALL, H.J., and MADDOCK, J.E.L., 1986, Biogeochemistry of a hypersaline lagoon east of Rio-De-Janeiro, Brazil: Science of the Total Environment, v. 58, p. 175-185.
HOLD, I.M., BRUSSEE, N.J., SCHOUTEN, S., and SINNINGHE DAMSTE, J.S., 1998, Changes in the molecular structure of a Type II-S kerogen (Monterey Formation, U.S.A.) during sequential chemical degradation: Organic Geochemistry, v. 29, p. 1403-1417.
HOLTZAPFFEL, T., 1985, Les minéraux argileux. Préparation, analyse diffractométrique et détermination.: Société Géologique du Nord., v. 12, p. 136pp.
HOPFGARTNER, G., VEUTHEY, J.-L., GÜLAÇAR, F.O., and BUCHS, A., 1990, Extraction of biomarkers from sediments with supercritical carbon dioxide: a comparative study with solvent extraction and thermodesorption methods.: Organic Geochemistry, v. 15, p. 397-402.
HUBER, B.T., HODELL, D.A., and HAMILTON, C.P., 1995, Middle-late Cretaceous climate of the southern high latitudes: stable isotopic evidence for minimal equator-to-pole thermal gradients: Geological Society of America Bulletin, v. 107, p. 1164-1191.
HUGHES, W.B., HOLBA, A.G., MILLER, D.E., and RICHARDSON, J.S., 1985, Geochemistry of greater Ekofisk crude oils., *in* B.M., T., A.G., Doré, S.S., Eggen, P.C., Home and R.M., Larsen., ed., Petroleum geochemistry in exploration of the Norwegian shelf.: London, Graham and Trotman., p. 75-92.
INAGAKI, F., OKADA, H., TSAPIN, I., and NEALSON, K.H., 2005, The paleome: a sedimentary genetic record of past microbial communities.: Astrobiology, v. 5, p. 141-153.
INAGAKI, F., SAKIHAMA, Y., INOUE, A., KATO, C., and HORIKOSHI, K., 2002, Molecular phylogenetic analysis of reverse-transcribed bacterial rRNA obtained from deep-sea cold seep sediments.: Environ. Microbiol., v. 4, p. 277-286.
INGLE, J.C.J., 1981, Cenozoic depositional history of the northern continental borderland of southern California and the origin of associated Miocene diatomites.: Guide to the Monterey Formation in the California coastal area, Ventura to San Luis Obispo, Pacific section AAPG, 1-7 p.

ISAACS, C.M., 2001, Depositional framework of the Monterey Formation, California.: C.M. Isaacs and J. Rullkötter.: New York, Columbia University Press., p.1-30 p.
JENKYNS, H.C., 1995, Carbon-isotope stratigraphy and paleoceanographic significance of the Lower Cretaceous shallow-water carbonates of Resolution Guyot, Mid-Pacific Mountains., *in* E.L., W., W.W., Sager, J.V., Firth & J.M., Sinton, ed., Proceedings of ODP, Scientific Results, Ocean Drilling Program, College Station., p. 99-104.
JENKYNS, H.C., 1999, Mesozoic anoxic events and paleoclimate: Zbl. Geol. Paläont. Teil, p. 943-949.
JENKYNS, H.C., 2003, Evidence for rapid climate change in the Mesozoic–Palaeogene greenhouse world.: Philos. Trans. R. Soc. Lond. Ser. A: Math. Phys. Sci., v. 361, p. 1885-1916.
JORAND, F., BOUÉ-BIGNE, F., BLOCK, J.C., and URBAIN, V., 1998, Hydrophobic/hydrophilic properties of activated sludge exopolymeric substances: Water Science and Technology, v. 37, p. 307-315.
JORGENSEN, B.B., and GALLARDO, V.A., 1999, *Thioploca* spp.: filamentous sulfur bacteria with nitrate vacuoles: FEMS microbiology letters, v. 28, p. 301-313.
KAISER, K., and GUGGENBERGER, G., 2003, Mineral surfaces and soil organic matter.: Eur. J. Soil Sci., v. 54, p. 1-18.
KATZ, B.J., and ELROD, L.W., 1983, Organic geochemistry of DSDP site 467, offshore California, Middle Miocene to Lower Pliocene strata.: Geochimica et Cosmochimica Acta, v. 47, p. 389-396.
KATZ, B.J., and ROYLE, R.A., 2001, Variability of source rock attributes in the Monterey Formation, California: The Monterey Formation: From Rocks to Molecules: New York, Columbia Univesity Press, 107-130 p.
KAZMIERCZAK, J., COLEMAN, M.L., GRUSZCZYNSKI, M., and KEMPE, S., 1996, Cyanobacterial key to the genesis of micritic and peloidal limestones in ancient seas: Acta Palaeontologica Polonica, v. 41, p. 319-338.
KEIL, R.G., MONTLUÇON, D.B., PRAHL, F.G., and HEDGES, J.I., 1994a, Sorptive preservation of labile organic matter in marine sediments: Nature, v. 370, p. 549-552.
KEIL, R.G., TSAMAKIS, E., FUH, C.B., GIDDINGS, J.C., and HEDGES, J.I., 1994b, Mineralogical and textural controls on the organic composition of coastal marine sediments: Hydrodynamic separation using SPLITT-fractionation: Geochimica et Cosmochimica Acta, v. 58, p. 879-893.
KELLY, D.P., RAINEY, F.A., and WOOD, A.P., 2000, The genus *Paracoccus.*, *in* M., D., N., Falkow, H., Rosenberg, K. H., Schleifer & E., Stackebrandt., ed., The Prokaryotes: an Evolving Electronic Resource for the Microbiological Community.: New York, Springer.
KENIG, F., SINNINGHÉ DAMSTÉ, J.S., FREWIN, N.L., HAYES, J.M., and DE LEEUW, J.W., 1995, Molecular indicators for palaeoenvironmental change in a Messinian evaporitic sequence (Vena del Gesso, Italy). II: High-resolution variations in abundances and ^{13}C contents of free and sulphur-bound carbon skeletons in a single marl bed: Organic Geochemistry, v. 23, p. 485-526.
KENNEDY, M.J., READER, S.L., and SWIERCZYNSKI, L.M., 1994, Preservation records of microorganisms: evidence of the tenacity of life.: Microbiology, v. 140, p. 2513-2529.
KERR, A.C., 1998, Oceanic plateau formation: a cause of mass extinction and black shale deposition around the Cenomanian-Turonian boundary?: Journal of the Geological Society, v. 155, p. 619-626.
KILLOPS, S.D., and KILLOPS, V.J., 2006, An introduction to organic geochemistry, *in* technical, L.S., ed., p. 244.
KIM, S., SOLTIS, D.E., SOLTIS, P.S., and SUH, Y., 2004, DNA sequences from Miocene fossils: an *ndh*F sequence of *Magnolia Latahensis* (Magnoliaceae) and an *rbc*L sequence of *Persea pseudocarolinensis* (Lauraceae). Am. J. Bot., v. 91, p. 615-620.
KIRK, T.K., and FARRELL, R.L., 1987, Enzymatic "combustion": the microbial degradation of lignin: Annual Review of Microbiology, v. 41, p. 465-505.
KNICKER, H., SCARONI, A.W., and HATCHER, P.G., 1996, ^{13}C and ^{15}N NMR spectroscopic investigation on the formation of fossil algal residues.: Organic Geochemistry, v. 24, p. 661-669.
KOHNEN, M.E.L., SCHOUTEN, S., DAMSTE, J.S.S., DE LEEUW, J.W., MERRITT, D.A., and HAYES, J.M., 1992, Recognition of paleobiochemicals by a combined molecular sulfur and isotope geochemical approach: Science, v. 256, p. 358-362.
KOHNEN, M.E.L., SINNINGHE DAMSTÉ, J.S., and DE LEEUW, J.W., 1991, Biases from natural sulphurization in palaeoenvironmental reconstruction based on hydrocarbon biomarker distributions: Nature, v. 349, p. 775-778.
KONHAUSER, K., 2007, Introduction to Geomicrobiology., Blackwell Publishing.
KRUMBEIN, W.E., 1983, Stromatolites - the challenge of a term in space and time.: Precambrian Res., v. 20.
KUBE, M., BECK, A., MEYERDIERKS, A., AMANN, R., REINHARDT, R., and RABUS, R., 2005, A catabolic gene cluster for anaerobic benzoate degradation in methanotrophic microbial Black Sea mats.: Systematic and Applied Microbiology., v. 28, p. 287-294.
KUYPERS, M.M.M., BLOKKER, P., HOPMANS, E.C., KINKEL, H., PANCOST, R.D., SHOUTEN, S., and SINNINGHÉ DAMSTÉ, J.S., 2002, Archeal remains dominate marine organic matter from the early Albian oceanic event 1b: Palaeogeography, Palaeoclimatology, Palaeoecology, v. 185, p. 211-234.
LALLI, C.M., and PARSONS, T.R., 1997, Biological Oceanography, An Introduction (2nd edition): the Open University, 314 pp.
LAMBERT, L.H., COX, T., MITCHELL, K., ROSSELLO-MORA, R.A., DEL CUETO, C., DODGE, D.E., ORKAND, P., and CANO, R.J., 1998, *Staphylococcus succinus sp.*, isolated from Dominican amber.: Int. J. Syst. Bacteriol., v. 48, p. 511-518.
LARGEAU, C., 1995, Formation of refractory organic matter from biological precursors in role of nonliving organic matter in the Earth's carbon cycle., John Wiley & Sons.
LARGEAU, C., DERENNE, S., CLAIRAY, C., CASADEVALL, E., RAYNAUD, J.F., LUGARDON, B., BERKALOFF, C., COROLLEUR, M., and ROUSSEAU, B., 1990, Characterization of various kerogens by scanning electron microscopy (SEM) and transmission electron microscopy (TEM) - Morphological relationships with resistant outer walls in extant micro-organisms: Meded. Rijks Geol. Dienst, v. 45, p. 91-101.
LARSON, R.L., 1991a, Geological consequences of superplumes: Geology, v. 19, p. 963-966.
LARSON, R.L., 1991b, Latest Pulse of Earth: evidence for a mid-Cretaceous superplume.: Geology, v. 19, p. 547-550.

LARSON, R.L., and ERBA, E., 1999, Onset of the mid-Cretaceous greenhouse in the Barremian-Aptian: igneous events and the biological, sedimentary, and geochemical responses.: Paleoceanography, v. 14, p. 663-678.
LAWRENCE, J.R., SWERHONE, G.D.W., LEPPARD, G.G., ARAKI, T., ZHANG, X., WEST, M.M., and HITCHCOCK, A.P., 2003, Scanning transmission X-Ray, laser scanning, and transmission electron microscopy mapping of the exopolymeric matrix of microbial biofilms: Applied and Environmental Microbiology, v. 69, p. 5543-5554.
LECKIE, R.M., BRALOWER, T.J., and CASHMAN, R., 2002, Oceanic anoxic events and plankton evolution: biotic response to tectonic forcing during the mid-Cretaceous.: Paleoceanography, v. 17, p. 1-29.
LI, L., KATO, C., and HORIKOSHI, K., 1999, Microbial diversity in sediments collected from the deepest cold-seep area, the Japan Trench.: Mar. Biotechnol., v. 1, p. 391-400.
LIEBIG, K., 1998, Fossil microorganisms from the Eocene Messel Oil-Shale of Southern Hesse, Germany.: Kaupia-Darmstätder Beiträge zur Naturgeschichte, v. 7, p. 1-95.
LINDAHL, T., 1993, Instability and decay of the primary structure of DNA: Nature, v. 362, p. 709-715.
LINDBERG, B., 1990, Components of bacterial polysaccharides.: Advances in Carbohydrate Chemistry and Biochemistry., v. 48, p. 279-318.
LUCIANI, V., COBIANCHI, M., and JENKYNS, H.C., 2001, Biotic and geochemical response to anoxic events: the Aptian pelagic succession of the Gargano promontory (Southern Italy). Geological Magazine, v. 138, p. 277-298.
MADIGAN, M.T., MARTINKO, J.M., and PARKER, J., 2003, Biology of microorganisms, 1019 pp. p.
MAGNIEZ-JANNIN, F., 1998, Chamber elongation in Early Cretaceous planktic foraminifera: an adaptive response to oxygen depleted sea water?: Comptes Rendus de l'Academie des Sciences - Series IIA - Earth and Planetary Science, v. 326, p. 207-213.
MAIER, S., and GALLARDO, V.A., 1984, *Thioploca araucae* sp. nov. and *Thioploca chileae* sp. nov.: International Journal of Systematic Bacteriology, v. 34, p. 414-418.
MAIER, S., and MURRAY, R.G.E., 1965, The fine structure of *Thioploca ingrica* and a comparison with *Beggiatoa*: Canadian Journal of Microbiology, v. 11, p. 645-656.
MAIER, S., VÖLKER, H., BEESE, M., and GALLARDO, V.A., 1990, The fine structure of *Thioploca araucae* and *Thioploca chileae*: Canadian Journal of Microbiology, v. 36, p. 438-448.
MARGULIS, L., 1993, Symbiosis in Cell Evolution, 2nd Edition.: New York.
MARTILL, D.M., 1987, Prokaryote mats replacing soft tissues in Mesozoic marine reptiles.: Mod. Geol., v. 11, p. 265-269.
MARTILL, D.M., and WILBY, P.R., 1994, Lithified prokaryotes associated with fossil soft tissues from the Santana Formation (Cretaceous) of Brazil. Kaupia: Darmstätder Beiträge zur Naturgeschichte, v. 4, p. 71-77.
MASRAN, T.C., and POCOCK, S.A.J., 1981, The classification of plant-derived particulate organic matter in sedimentary rocks: ed. J. Brooks: London, Academic press, 145-176 p.
MAYER, C., MORITZ, R., KIRSCHNER, C., BORCHARD, W., MAIBAUM, R., WINGENDER, J., and FLEMMING, H.C., 1999, The role of intermolecular interactions : studies on model systems for bacterial biofilms.: International Journal of Biological Macromolecules, v. 26, p. 3-16.
MAYER, L.M., 1994a, Relationships between mineral surfaces and organic carbon concentrations in soils and sediments: Chemical Geology, v. 114, p. 347-363.
MAYER, L.M., 1994b, Surface area control of organic carbon accumulation in continental shelf sediments: Geochimica et Cosmochimica Acta, v. 58, p. 1271-1284.
MAYER, L.M., MACKO, S.A., and CAMMEN, L., 1988, Provenance, concentration and nature of sedimentary organic nitrogen in the Gulf of Maine.: Marine Chemistry, v. 25, p. 291-304.
MCCAFFREY, M.A., FARRINGTON, J.W., and REPETA, D.J., 1989, Geochemical implications of the lipid composition of *Thioploca* spp. from the Peru upwelling region-15°S.: Organic Geochemistry, v. 14, p. 61-68.
MCPHILEMY, B., 1988, The value of fluorescence microscopy in routine palynofacies analysis: Lower Carboniferous succession from counties Armagh and Roscommon, Ireland.: Review of Palaeobotany and Palynology, v. 56, p. 345-359.
MEYERS, P.A., 2006, Paleoceanographic and paleoclimatic similarities between Mediterranean sapropels and Cretaceous black shales.: Palaeogeogr., Palaeoclimatol., Palaeoecol., v. 235, p. 305-320.
MICHAELIS, W., SEIFERT, R., NAUHAUS, K., TREUDE, T., THIEL, V., BLUMENBERG, M., KNITTEL, K., GIESEKE, A., PETERKNECHT, K., PAPE, T., BOETIUS, A., AMANN, R., JORGENSEN, B.B., WIDDEL, F., PECKMANN, J., PIMENOV, N.V., and GULIN, M.B., 2002, Microbial reefs in the Black Sea fueled by anaerobic oxidation of methane.: Science, v. 297, p. 1013-1015.
MISRA, C.M., 1991, Organic matter distribution pattern in the deeper part of central west coast and northeast Arabian Sea.: Proceedings of the conference on integrated exploration research, achievements and perspectives,: Dehra Dun, Keshava Deva Malaviya Institute of Petroleum Exploration, 233-245 p.
MIYAJIMA, T., WADA, E., HANBA, Y.T., and VIJARNSORN, P., 1997, Anaerobic mineralization of indigenous organic matter and methanogenesis in tropical wetland soils.: Geochimica et Cosmochimica Acta, v. 61, p. 3739-3751.
MONGENOT, T., BOUSSAFIR, M., DERENNE, S., LALLIER-VERGES, E., LARGEAU, C., and TRIBOVILLARD, N., 1997, Sulphur-rich organic matter from bituminous laminites of Orbagnoux (France, Upper Kimmeridgian). The role of early vulcanization: Bulletin de la Société Géologique de France, v. 168, p. 331-341.
MONGENOT, T., DERENNE, S., LARGEAU, C., TRIBOVILLARD, N., LALLIER-VERGES, E., DESSORT, D., and CONNAN, J., 1999, Spectroscopic, kinetic and pyrolytic studies of kerogen from the dark parallel laminae facies of the sulphur-rich Orbagnoux deposit (Upper Kimmeridgian, Jura): Organic Geochemistry, v. 30, p. 39-56.
MONGENOT, T., TRIBOVILLARD, N.-P., ARBEY, F., LALLIER-VERGÈS, E., DERENNE, S., LARGEAU, C., PICHON, R., DESSORT, D., and CONNAN, J., 2000, Comparative studies of a high resolution sampling of the different facies of the organic-rich Orbagnoux deposit (Upper Kimmeridgian, Jura): petrographic and bulk geochemical approach. Extent and origin of interfacies and intrafacies variations: Bulletin de la Société Géologique de France, v. 171, p. 23-26.

MOORE, P.D., and BELLAMY, D.J., 1974, Peatlands, Springer.
MOORE, T.R., 1989, Plant production, decomposition and carbon efflux in a subarctic patterned fen.: Arctic and Alpine Research, v. 21, p. 156-162.
MORITA, R.Y., 2000, Is H_2 the universal energy source for long-term survival?: Microb. Ecol., v. 38, p. 307-320.
MUBMANN, M., SCHULZ, H., STROTMANN, B., KJAER, T., NIELSEN, L., ROSSELLO-MORA, R., AMANN, R., and JORGENSEN, B.B., 2003, Phylogeny and distribution of nitrate-storing *Beggiatoa* spp. in coastal marine sediments.: Environmental Microbiology, v. 5, p. 523-533.
NELSON, D.C., 1989, Physiology and biochemistry of filamentous sulfur bacteria, *in* bacteria, A., ed., sci. tech. publ., p. 219-238.
NELSON, D.C., JORGENSEN, B.B., and REVSBECH, N.P., 1986, Growth pattern and yield of a chemoautotrophic *Beggiatoa* sp. in oxygen-sulfide microgradients.: Applied and Environmental Microbiology, v. 52, p. 225-233.
NELSON, D.C., WATERBURY, J.B., and JANNASCH, H.W., 1982, Nitrogen fixation and nitrate utilization by marine and freshwater *Beggiatoa*.: Arch. Microbiol., v. 133, p. 172-177.
NICHOLSON, W.L., MUNAKATA, N., HORNECK, G., MELOSH, H.J., and SETLOW, P., 2000, Resistance of *Bacillus* endospores to extreme terrestrial and extraterrestrial environments.: Microbiol. Mol. Biol. Rev., v. 64, p. 548-572.
NOFFKE, N., GERDES, G., KLENKE, T., and KRUMBEIN, W.E., 2001, Microbially induced sedimentary structures indicating climatological, hydrological and depositional conditions within recent and Pleistocene coastal facies zones (southern Tunisia). Facies, v. 44, p. 23-30.
NOLD, S.C., and ZWART, G., 1998, Patterns and governing forces in aquatic microbial communities.: Aquatic Ecology, v. 32, p. 17-35.
ORPHAN, V.J., HINRICHS, K.U., USSLER, W.I., PAULL, C.K., TAYLOR, L.T., SYLVA, S.P., HAYES, J.M., and DELONG, E.F., 2001a, Comparative analysis of methane-oxidizing archaea and sulfate-reducing bacteria in anoxic marine sediments.: Appl. Environ. Microbiol., v. 67, p. 1922-1934.
ORPHAN, V.J., HOUSE, C.H., HINRICHS, K.U., MCKEEGAN, K.D., and DELONG, E.F., 2001b, Methane-consuming archaea revealed by directly coupled isotopic and phylogenetic analysis.: Science, v. 293, p. 484-487.
OSCHMANN, W., 2000, Microbes and black shales., *in* RIDING; R.E. & AWRAMIK, S.M.e., ed., Microbial sediments, Springer-Verlag Berlin Heidelberg, p. 137-148.
OTTE, S., KUENEN, J.G., NIELSEN, L.P., PAERL, H.W., ZOPFI, J., and SCHULZ, H.N., 1999, Nitrogen, carbon and sulfur metabolism in natural *Thioploca* samples.: Applied Environmental Microbiology., v. 65, p. 3148-3157.
OZALAS, K., SAVRDA, C.E., and FULLERTON, R.R.J., 1994, Bioturbated oxygenation-event beds in siliceous facies: Monterey Formation (Miocene), California.: Palaeogeogr., Palaeoclimatol., Palaeoecol., v. 112, p. 63-83.
PÄÄBO, S., POINAR, H.N., SERRE, D., JAENICKE-DESPRÉS, V., HEBLER, J., ROHLAND, N., KUCH, M., KRAUSE, J., VIGILANT, L., and HOFREITER, M., 2004, Genetic analyses from ancient DNA: Annu. Rev. Genet., v. 38, p. 645-679.
PÄÄBO, S., and WILSON, A.C., 1991, Miocene DNA sequences - A dream come true?: Current Bology., v. 1, p. 45-46.
PACTON, M., FIET, N., and GORIN, G., 2007, Bacterial activity and preservation of sedimentary organic matter: the role of exopolymeric substances.: Geomicrobiology Journal, v. 24, p. 571-581.
PAINTER, T.J., 1998, Carbohydrate polymers in food preservation: an integrated view of the Maillard reaction with special reference to discoveries of preserved foods in *Sphagnum*-dominated peat bogs: Carbohydrate Polymers, v. 36, p. 335-347.
PALMER, J., ROBERT J, and STERNBERG, C., 1999, Modern microscopy in biofilm research: confocal microscopy and other approaches: Current Opinion in Biotechnology, v. 10, p. 263-268.
PANCOST, R.D., CRAWFORD, N., MAGNESS, S., TURNER, A., JENKYNS, H.C., and MAXWELL, J.R., 2004, Further evidence for the development of photic-zone euxinic conditions during Mesozoic oceanic anoxic events: Journal of the Geological Society, London, v. 161, p. 353-364.
PANCOST, R.D., FREEMAN, K.H., PATZKOWSKY, M.E., WAVREK, D.A., and COLLISTER, J.W., 1998, Molecular indicators of redox and marine photoautotroph composition in the late Middle Ordovician of Iowa, U.S.A.: Organic Geochemistry, v. 29, p. 1649-1662.
PASTERIS, J.D., FREEMAN, J., GOFFREDI, S., and BUCK, K., 2001, Raman spectroscopic and laser scanning confocal microscopic analysis of sulfur-precipitating marine bacteria: Chemical Geology, v. 180, p. 3-18.
PAULL, C.K., CHANTON, J.P., NEUMANN, A.C., COSTON, J.A., MARTENS, C.S., and SHOWERS, W., 1992, Indicators of methane-derived carbonates and chemosynthetic organic carbon deposits: examples from the Florida escarpment.: Palaios., v. 7, p. 361-375.
PEDERSEN, T.F., and CALVERT, S.E., 1990, Anoxia vs. productivity: what controls the formation of organic-carbon rich sediments and sedimentary rocks?: American Association of Petroleum Geologists Bulletin., v. 74, p. 454-466.
PELLATON, C., 2003, distribution of sedimentary organic matter with respect to paleoenvironmental conditions : two case histories from the Miocene of the USA. [unpublished vol.43 thesis]: Genève, Genève.
PETERS, K.E., and MOLDOWAN, M.J., 1993, The biomarker guide., 451 p.
PHILP, R.P., 1985, Fossil fuel biomarkers - Applications and spectra: Series : Methods in Geochemistry and Geophysics, v. 23, 294 p.
PIMENOV, N.V., RUSANOV, I.I., POGLAZOVA, M.N., MITYUSHINA, L.L., SOROKIN, D.Y., KHMELENINA, V.N., and TROTSENKO, Y.A., 1997, Bacterial mats on coral-like structures at methane seeps in the Black Sea.: Microbiology, v. 66, p. 354-360.
PISCIOTTO, K.A., and GARRISON, R.E., 1981, Lithofacies and Depositional Environments of the Monterey Formation, California.: The Monterey Formation and related siliceous rocks of California., v. 15, SEPM, Pacific section,special publications, 97-122 p.
POCOCK, S.A.J., 1982, Identification and recording of particulate sedimentary organic matter: Society of economic paleontologists and mineralogists, short course, p. 13-131.

POINAR, H.N., CANO, R.J., and POINAR, G.O., 1993, DNA from an extinct plant.: Nature, v. 363, p. 677.
POINAR, H.N., HÖSS, M., BADA, J.L., and PÄÄBO, S., 1996, Amino acid racemization and the preservation of ancient DNA.: Science, v. 272, p. 864-866.
POWELL, T.G., GREANEY, S., and SNOWDON, L.R., 1982, Limitations of use of organic petrographic techniques for identification of petroleum source rocks.: American Association of Petroleum Geologists Bulletin., v. 66, p. 430-435.
PRATT, L.M., and KING, J.D., 1986, Variable marine productivity and high eolian input recorded by rhythmic black shales in Mid-Cretaceous pelagic deposits from central Italy.: Palaeoceanography, v. 1, p. 507-522.
PREMOLI SILVA, I., ERBA, E., SALVINI, G., LOCATELLI, C., and VERGA, D., 1999, Biotic changes in Cretaceous oceanic anoxic events of the Tethys: Journal of foraminiferal research, v. 29, p. 352-370.
PREMOLI SILVA, I., and SLITER, W.V., 1999, Cretaceous paleoceanography: evidence from planktonic foraminiferal evolution., *in* Barrera E., J.C.C., ed., Evolution of the Cretaceous Ocean-Climate system., Geological Society of America. Special Paper, p. 301-328.
PRIGENT-COMBARET, C., VIDAL, O., DOREL, C., and LEJEUNE, P., 1999, Abiotic surface sensing and biofilm-dependent regulation of gene expression in Escherichia Coli: Journal of bacteriology, v. 181, p. 5993-6002.
RAYNAUD, J.F., LUGARDON, B., and LACRAMPE-COULOUME, G., 1989, Structures lamellaires et bactéries, composants essentiels de la matière organique amorphe des roches mères.: Soc. Nat. Elf Aquitaine, v. 13, p. 1-21.
REITNER, J., PECKMANN, J., BLUMENBERG, M., MICHAELIS, W., REIMER, A., and THIEL, V., 2005, Concretionary methane-seep carbonates and associated microbial communitiees in Black Sea sediments.: Palaeogeogr., Palaeoclimatol., Palaeoecol., v. 227, p. 18-30.
RIBOULLEAU, A., DERENNE, S., LARGEAU, C., and BAUDIN, F., 2001, Origin of contrasting features and preservation pathways in kerogens from the Kashpir oil shales (Upper Jurassic, Russian Platform). Organic Geochemistry, v. 32, p. 647-665.
RICHE, A., 1904, Feuille de Lyon au 320 000ème: Bull. Carte Géol. fr., v. 13, p. 1-7.
ROBERT, P., 1988, Organic metamorphism and geothermal history: microscopic study of organic matter and thermal evolution of sedimentary basins.: Dordrecht, 311 p.
ROGERS, J.R., BENNETT, P.C., and CHOI, W.J., 1998, Feldspars as a source of nutrients for microorganisms.: American Mineralogist, v. 83, p. 1532-1540.
ROHMER, M., BISSERET, P., and NEUNLIST, S., 1992, The hopanoids, prokaryotic triterpenoids and precursors of ubiquitous molecular fossils.: Biological Markers in Sediments and Petroleum, Prentice-Hall, Englewood Cliffs, NJ, 1-17 p.
RUMPEL, C., RABIA, N., DERENNE, S., QUENEA, K., EUSTERHUES, K., KOGEL-KNABNER, I., and MARIOTTI, A., 2006, Alteration of soil organic matter following treatment with hydrofluoric acid (HF): Organic Geochemistry, v. 37, p. 1437-1451.
SALMON, V., DERENNE, S., LALLIER-VERGÈS, E., LARGEAU, C., and BEAUDOIN, B., 2000, Protection of organic matter by mineral matrix in a Cenomanian black shale: Organic Geochemistry, v. 31, p. 463-474.
SARRET, G., MONGENOT, T., CONNAN, J., DERENNE, S., KASRAI, M., MICHAEL BANCROFT, G., and LARGEAU, C., 2002, Sulfur speciation in kerogens of the Orbagnoux deposit (Upper Kimmeridgian, Jura) by XANES spectroscopy and pyrolysis: Organic Geochemistry, v. 33, p. 877-895.
SAUER, K., 2003, The genomics and proteomics of biofilm formation.: Genome Biology, v. 4.
SAYAMA, M., 2001, Presence of nitrate-accumulating sulfur bacteria and their influence on nitrogen cycling in a shallow Coastal marine sediment.: Applied Environmental Microbiology., v. 67, p. 3481-3487.
SCHIEBER, J., and ARNOTT, H.J., 2003, Nannobacteria as a byproduct of organic tissue degradation by bacteria.: Lunar and Planetary Science, v. 34.
SCHIMMELMANN, A., LAWRENCE, M., and MICHAEL, G.E., 2001, Stable isotope ratios of organic H, C and N in the Miocene Monterey Formation, California., *in* Rullkötter, C.M.I.a.J., ed., The Monterey Formation : From Rocks to Molecules: New York, Columbia University Press, p. 86-106.
SCHLANGER, S.O., and JENKYNS, H.C., 1976, Cretaceous oceanic anoxic events: causes and consequences.: Geologie & Mijnbouw., v. 55, p. 179-184.
SCHNITZER, M., and KHAN, S.U., 1972, Humic Substances in the Environment., *in* Dekker, M., ed.: New York.
SCHNITZER, M., and KHAN, S.U., 1978, Soil Organic Matter.: Amsterdam, Elsevier.
SCHOELL, M., MCCAFFREY, M.A., FAGO, F.J., and MOLDOWAN, M.J., 1992, Carbon isotopic compositions of 28,30-bisnorhopanes and other biological markers in a Monterey crude oil.: Geochimica et Cosmochimica Acta, v. 56, p. 1391-1399.
SCHOUTEN, S., SINNINGHE DAMSTE, J.S., and DE LEEUW, J.W., 1995, Occurrence and distribution of low-molecular-weight sulphoxides in polar fractions of sediments extracts and petroleum.: Organic Geochemistry, v. 23, p. 129-138.
SIESKIND, O., JOLY, G., and ALBRECHT, P., 1979, Simulation of the geochemical transformations of sterols: Superacid effect of clay minerals.: Geochimica et Cosmochimica Acta, v. 43, p. 1675-1679.
SILVA E SILVA, L.H., SENRA, M.C.E., FARUOLO, T.C.L.M., CARVALHAL, S.B.V., ALVES, S.A.P.M.N., DAMAZIO, C.M., SHIMIZU, V.T.A., SANTOS, R.C., and IESPA, A.A.C., 2004, Composição paleobiológica e tipos morfológicos das construções estromatolíticas da lagoa Vermelha, RJ, Brasil: Revista Brasileira de Paleontologia, v. 7, p. 193-198.
SILVERSTEIN, R.M., BASSLER, G.C., and MORRILL, T.C., 1991, Spectrometric Identification of Organic Compounds., *in* Wiley, ed.: New York.
SILVERSTEIN, R.M., and WEBSTER, F.X., 1996, Spectrometric identification of organic compounds., Wyley.
SINNINGHÉ DAMSTÉ, J.S., EGLINTON, T.I., DE LEEUW, J.W., and SCHENCK, P.A., 1989, Organic sulphur in macromolecular sedimentary organic matter: I. Structure and origin of sulphur-containing moieties in kerogen, asphaltenes and coal as revealed by flash pyrolysis: Geochimica et Cosmochimica Acta, v. 53, p. 873-889.
SINNINGHÉ DAMSTÉ, J.S., EGLINTON, T.I., RIJPSTRA, C., and DE LEEUW, J.W., 1990, Characterization of organically bound sulfur in high-molecular weight, sedimentary organic matter using flash pyrolysis and Raney Ni desulfurization., *in*

White, W.L.O.a.C.M., ed., Geochemistry of sulfur in fossil fuels.: Washington, American Chemical Society Symposium Series, p. 486-528.
SINNINGHÉ DAMSTÉ, J.S., IRENE, W., RIJPSTRA, C., DE LEEUW, J.W., and SCHENCK, P.A., 1988, Origin of organic sulphur compounds and sulphur-containing high molecular weight substances in sediments and immature crude oils: Organic Geochemistry, v. 13, p. 593-606.
SKJEMSTAD, J.O., CLARKE, P., TAYLOR, J.A., OADES, J.M., and NEWMAN, R.H., 1994, The removal of magnetic materials from surface soils: a solid state 13C CP/MAS NMR study.: Australian Journal of Soil Research, v. 32, p. 1215-1229.
SMITH, B.N., and EPSTEIN, S., 1971, Two categories of $^{13}C/^{12}C$ ratios for higher plants.: Plant Physiol., v. 47, p. 380-384.
SMITH, C.I., CHAMBERLAIN, A.T., RILEY, M.S., COOPER, A., STRINGER, C.B., and COLLINS, M.J., 2001, Neanderthal DNA: not just old but old and cold?: Nature, v. 410, p. 771-772.
SOLTIS, P.S., SOLTIS, D.E., NOVAK, S.J., SCHULTZ, J.L., and KUZOFF, R.K., 1995, Fossil DNA: its potential for biosystematics., *in* Hoch, P.C.a.S., A.G., ed., Experimental and molecular approaches to plant biosystematics.: St. Louis, Missouri, USA., Missouri Botanical Garden., p. 1-13.
SOLTIS, P.S., SOLTIS, D.E., and SMILEY, C.J., 1992, An *rbc*L sequence from a Miocene Taxodium (bald cypress). Proc. Natl. Acad. Sci. U.S.A., v. 89, p. 449-451.
SOUTAR, A., JOHNSON, S., and BAUMGARTNER, T., 1981, In search of modern depositional analogs to the Monterey Formation., *in* Garrison, R.E.P., K., ed., The Monterey Formation and Related Siliceous Rocks of California, Society of Economic Paleontologists and Mineralogists Special Publication, Pacific Section, p. 123-147.
STANKIEWICZ, B.A., KRUGE, M.A., MASTALERZ, M., and SALMON, G.L., 1996, Geochemistry of the alginite and amorphous organic matter from Type II-S kerogens: Organic Geochemistry, v. 24, p. 495-509.
STAPLIN, F.L., 1969, Sedimentary organic matter, organic metamorphism, and oil and gas occurrence.: Bulletin of Canadian Petroleum Geology, v. 17, p. 47-66.
STARKEY, M., GRAY, K.A., CHANG, S.-I., and PARSEK, M.R., 2004, A sticky business: the extracellular polymeric substance matrix of bacterial biofilms.: Microbial biofilms: Washington, ASM Press, 174-191 p.
STEFFEN, D., and GORIN, G., 1993, Palynofacies of the Upper Tithonian-Berriasian deep-sea carbonates in the Vocontian Trough (SE France). Bull. Centres Rech. Explor. Prod. Elf-Aquitaine, v. 17, p. 235-247.
STEVENSON, F.J., 1994, Humus Chemistry: Genesis, Composition, Reactions., *in* Wiley, ed.: New York.
STRASSER, A., CARON, M., and GJERMENI, M., 2001, The Aptian, Albian and Cenomanian of Roter Sattel, Romandes Prealps, Switzerland: a high-resolution record of oceanographic changes: Cretaceous Research, v. 22, p. 173-199.
STROHL, W.R., GEFFERS, I., and LARKIN, J.M., 1981, Structure of the sulfur inclusion envelopes from four *Beggiatoas*.: Current Microbiology, v. 6, p. 75-79.
SUCCOW, M., and JESCHKE, L., 1990, Moore in der landschaft: Frankfurt/Main.
SUTHERLAND, I.W., 1990, Biotechnology of microbial exopolysaccharides., *in* Press, C.U., ed.: Cambridge, p. 163 pp.
SUTHERLAND, I.W., 2001, Biofilm exopolysaccharides : a strong and sticky framework: Microbiology, v. 147, p. 3-9.
TEGELAAR, E.W., DE LEEUW, J.W., DERENNE, S., and LARGEAU, C., 1989, A reappraisal of kerogen formation: Geochimica et Cosmochimica Acta, v. 53, p. 3103-3106.
TOKITA, M., and TANAKA, T., 1991, Friction coefficient of polymer networks of gels: Journal of Chemical Physics, v. 95, p. 4613-4619.
TONOLLA, M., PEDUZZI, S., DEMARTA, A., PEDUZZI, R., and HAHN, D., 2004, Phototrophic sulfur and sulfate-reducing bacteria in the chemocline of meromictic Lake Cadagno, Switzerland.: Journal of Limnology., v. 63, p. 161-170.
TOPORSKI, J.K.W., STEELE, A., WESTALL, F., AVCI, R., MARTILL, D.M., and MCKAY, D.S., 2002, Morphologic and spectral investigation of exceptionally well-preserved bacterial biofilms from the Oligocene Enspel formation, Germany.: Geochimica et Cosmochimica Acta, v. 66, p. 1773-1791.
TORNAGHI, M.E., PREMOLI SILVA, I., and RIPEPE, M., 1989, Lithostratigraphy and planktonic foraminiferal biostratigraphy of the Aptian-Albian "scisti a fucoidi" in the Piobbico core, Marche, Italy: background for cyclostratigraphy.: Riv. It. Paleont. Strat., v. 95, p. 223-264.
TOUROVA, T.P., KOLGANOVA, T.P., KUSNETSOV, K.B., and PIMENOV, N.V., 2002, Phylogenetic diversity of the Archeal component of bacterial mats on coral-like structures in znes of methane seeps in the Black Sea.: Microbiology, v. 71, p. 196-201.
TRIBOVILLARD, N., 1998, Bacterially mediated peloids in laminated, organic-matter rich, limestones: an unobtrusive presence.: Terra Nova, v. 10, p. 126-130.
TRIBOVILLARD, N., BIALKOWSKI, A., TYSON, R.V., LALLIER-VERGÈS, E., and DECONINCK, J.-F., 2001, Organic facies and sea level variation in the Late Kimmeridgian of the Boulonnais area (northernmost France). Mar. Petrol. Geol., v. 18, p. 371-389.
TRIBOVILLARD, N., DESPRAIRIES, A., LALLIER-VERGÈS, E., and BERTRAND, P., 1994, Sulfur incorporation of lipidic organic matter in reactive-iron deficient environments: a possible enhancement for the storage of hydrogen-rich organic matter: Compte Rendu de l'Académie des Sciences de Paris, v. 319, p. 1199-1206.
TRIBOVILLARD, N., TRICHET, J., DEFARGE, C., and TRENTESAUX, A., 1999, Jurassic lagoonal environments and quasi-abiotic platy limestone accumulation: microbial interventions: Sedimentology, v. 46, p. 1183-1197.
TRIBOVILLARD, N.P., GORIN, G., HOPFGARTNER, G., MANIVIT, H., and BERNIER, P., 1991, Conditions de depot et matière organique en milieu lagunaire d'âge kimméridgien du Jura méridional français (résultats préliminaires): Eclog. Geol. Helv., v. 84, p. 441-461.
TRIBOVILLARD, N.-P., GORIN, G.E., BELIN, S., HOPFGARTNER, G., and PICHON, R., 1992, Organic-rich biolaminated facies from a Kimmeridgian lagoonal environment in the French southern Jura mountains--A way of estimating accumulation rate variations: Palaeogeography, Palaeoclimatology, Palaeoecology, v. 99, p. 163-177.

TRIBOVILLARD, N.T., TRENTESAUX, A., TRICHET, J., and DEFARGE, C., 2000, A Jurassic counterpart for modern kopara of the Pacific atolls: lagoonal, organic matter-rich, laminated carbonate of Orbagnoux (Jura Mountains, France): Palaeogeography, Palaeoclimatology, Palaeoecology, v. 156, p. 277-288.

TYSON, R.V., 1984, Palynofacies investigation of Callovian (Middle Jurassic) sediments from DSDP site 534, Blake-Bahama Basin, western Central Atlantic.: Marine and Petroleum Geology, v. 1, p. 3-13.

TYSON, R.V., 1987, The genesis and palynofacies characteristics of marine petroleum source rocks: marine petroleum source rocks, v. 26: Oxford, Blackwell scientific publications, 74-68 p.

TYSON, R.V., 1989, Late Jurassic palynofacies trends, Piper and Kimmeridge Clay Formations, UK onshore and offshore.: Northwest European Micropalaeontology and Palynology: Chichester, British Micropalaeontological Society Series, 135-172 p.

TYSON, R.V., 1995, Sedimentary organic matter: Organic facies and palynofacies: London, 615 pp. p.

TYSON, R.V., ESHERWOOD, P., and PATTISON, K.A., 2005, Organic facies variations in the early Valanginian to mid-Hauterivian interval of the Agrio Formation (Chos Malal area, Neuquen, Argentina): local significance and global context., *in* Spalletti, L., Veiga, G., Schwarz, E., & Howell, J,, ed., The Neuquen Basin: A Case Study in Sequence Stratigraphy and Basin Dynamics., Geological Society of London, Special Publications, p. 251-266.

VALDES, J., SIFEDDINE, A., LALLIER-VERGES, E., and ORTLIEB, L., 2004, Petrographic and geochemical study of organic matter in surficial laminated sediments from an upwelling system (Mejillones del Sur Bay, Northern Chile): Organic Geochemistry, v. 35, p. 881-894.

VALENTINE, D.L., and REEBURGH, W.S., 2000, New perspectives on anaerobic methane oxidation: Environ. Microbiol., v. 2, p. 477–484.

VASCONCELOS, C., and MCKENZIE, J.A., 1997, Microbial mediation of modern dolomite precipitation and diagenesis under anoxic conditions, Lagoa Vermelha, Rio De Janeiro, Brazil: Journal of Sedimentary Research, v. 67, p. 378-390.

VASCONCELOS, C.O., 1994, Modern dolomite precipitation and diagenesis in a coastal mixed water system (Lagoa Vermehla, Brazil): a microbial model for dolomite formation under anoxic conditions: Eidgenössische Technische Hochschule, Zürich.

VENKATACHALA, B.S., 1981, Differentiation of amorphous organic types in sediments., *in* Brooks, J., ed., Organic Maturation Studies and Fossil Fuel Exploration.: London, Academic Press, p. 277-200.

VENKATACHALA, B.S., 1984, Finely divided organic matter-its origin and significance as a hydrocarbon source material.: Bulletin of the Oil and Natural Gas Commission, v. 21, p. 23-45.

VERDUGO, P., 1994, Polymer gel phase transition in condensation–decondensation of secretory products.: Advances in Science, v. 110, p. 145-156.

VINCENT, H., and BURGER, W.H., 1985, Carbon dioxide and polar cooling in the Miocene: the Monterey Hypothesis: The Carbon Cycle and Atmospheric CO2: Natural Variations Archean to Present., v. 32, American Geophysical Union, Monograph, 455-469 p.

VOLKMAN, J.K., 1986, A review of sterol markers for marine and terrigenous organic matter: Organic Geochemistry, v. 9, p. 83-99.

VOLOSHIN, S.A., and KAPRELYANTS, A.S., 2004, Cell-cell interactions in bacterial populations: Biochemistry, v. 69, p. 1268-1275.

VREELAND, R.H., and ROSENZWEIG, W.D., 2002, The question of uniqueness of ancient bacteria.: J. Ind. Microbiol. Biotechnol., v. 28, p. 32-41.

VREELAND, R.H., ROSENZWEIG, W.D., and POWERS, D.W., 2000, Isolation of a 250 million-year-old halotolerant bacterium from a primary salt crystal: Nature, v. 407, p. 897-900.

WARTHMANN, R., VAN LITH, Y., VASCONCELOS, C., MCKENZIE, J.A., and KARPOFF, A.M., 2000, Bacterially induced dolomite precipitation in anoxic culture experiments: Geology, v. 28, p. 1091-1094.

WEISSERT, H., LINI, A., FOLLMI, K.B., and KUHN, O., 1998, Correlation of early Cretaceous carbon isotope stratigraphy and platform drowning events: a possible link?: Palaeogeography, Palaeoclimatology, Palaeoecology, v. 137, p. 189-203.

WERNE, J.P., HOLLANDER, D., BEHRENS, A., SCHAEFFER, P., ALBRECHT, P., and SINNINGHÉ DAMSTÉ, J.S., 2000, Timing of early diagenetic sulfurization of organic matter: a precursor-product relationship in Holocene sediments of the anoxic Cariaco Basin, Venezuela: Geochimica et Cosmochimica Acta, v. 64, p. 1741-1751.

WHITAKER, M.F., 1984, The usage of palynology in definition of Troll Field geology: Reduction of uncertainties in innovative reservoir geomodelling, 6th offshore northern seas conference and exhibition, p. 44p.

WHITCHURCH, C.B., TOLKER-NIELSEN, T., RAGAS, P.C., and MATTICK, J.S., 2002, Extracellular DNA required for bacterial biofilm formation.: Science, v. 295, p. 1487.

WIDDEL, F., and BAK, F., 1992, Gram-negative mesophilic sulfate-reducing bacteria., The Prokaryotes, 2nd ed.: A. Balows, H. G. Trüper, M. Dworkin, W. Harder, and K.-H. Schleifer, eds, Springer, p. 3352-3378.

WILLERSLEV, E., and COOPER, A., 2005, Ancient DNA.: Proc. R. Soc. B., v. 272, p. 3-16.

WILLERSLEV, E., HANSEN, A.J., and POINAR, H.N., 2004a, Isolation of nucleic acids and cultures from fossil ice and permafrost.: Trends in Ecology & Evolution, v. 19, p. 141-147.

WILLERSLEV, E., HANSEN, A.J., RONN, R., BRAND, T.B., BARNES, I., WIUF, C., GILICHINSKY, D.A., MITCHELL, D.J., and COOPER, A., 2004b, Long-term persistence of bacterial DNA.: Current Biology., v. 14, p. R9-R10.

WILLIAMS, L.A., 1984, Subtidal stromatolites in Monterey Formation and other organic-rich rocks as suggested source contributors to petroleum formation.: American Association of Petroleum Geologists, v. 68, p. 1879-1983.

WILLIAMS, L.A., and REIMERS, C., 1983, Role of bacterial mats in oxygen-deficient marine basins and coastal upwelling regimes: preliminary report: Geology, v. 11, p. 267-269.

WILSON, P.A., and NORRIS, R.D., 2001, Warm tropical ocean surface and global anoxia during the mid-Cretaceous period: Nature, v. 412, p. 425-428.

WOOD, S.E., and GORIN, G.E., 1998, Sedimentary organic matter in distal clinoforms of Miocene slope sediments : site 903 of ODP leg 150, offshore New Jersey: Journal of Sedimentary Research, v. 68, p. 856-868.
WOODWARD, S.R., WEYAND, N.J., and BUNNELL, M., 1994, DNA sequence from Cretaceous period bone fragments.: Science, v. 226, p. 1229-1232.
WUTTKE, M., 1983, Weichteilerhaltung durch lithifizierte mikoorganismen bei mittel-eozänen vertebraten aus dem ölschiefer der "Grube Messel" bei Darmstadt.: Senck. Leth., v. 64, p. 503-527.
YOUNG, L.Y., and FRAZER, A.C., 1987, The fate of lignin and lignin derived compounds in anaerobic environment.: Geomicrobiology, v. 5, p. 261-293.

9. ANNEXES

Samples			Palynology			Microscopy				Geochemistry											
location		N°	LN	fluo.	thin sect.	SEM	SEMroc	TEM	AFM	HI	TOC	T_{max}	$\delta^{34}S$	biomarkers	$\delta^{13}C$	$\delta^{15}N$	µfluoX	FTIR		XRDcl	XRD
fossil	Monterey F.	N12	✓	✓				✓					+ 33 ‰	•	-22,2	6		b	k	✓	✓
		N23	✓			✓	✓		✓	326	1,98	419						b		✓	✓
		N35	✓	✓	✓	✓	✓	✓	✓	488	3,33	408			-21,5	4,7	X	b	k	✓	✓
	Orb.	MP5	✓	✓	✓	✓		✓	✓	809	6,31	408	•	•				b		✓	✓
		MP19	✓	✓	✓			✓	✓	813	4,71	411	+ 47.7 ‰	•	-26,6	1,5		b	k		✓
	Black shales	Urbino MP	✓	✓	✓	✓	✓	✓	✓	415	4,28	410	- 5.7 ‰	•	-23,8	-1,1		b	k	✓	✓
		Urbino Ko	✓	✓	✓	✓	✓	✓	✓				+ 11.8 ‰					b		✓	✓
		L113	✓		✓			✓	✓	459	3,88	408	•		-18	-1,4		b	k	✓	✓
		Selli S20	✓		✓			✓	✓	409	10,13	404	•		-26,9	-0,7		b	k		
		Selli S27	✓		✓			✓	✓	485	11,69	414			-25,1	-0,8		b	k		

Samples			Palynology			Microscopy				Geochemistry									
location		N°	nat.	etched	fluo.	SEM	SEM cp	TEM	AFM	$\delta^{13}C$	$\delta^{34}S$	$\delta^{15}N$	HI	TOC	T_{max}	µfluoX	FTIR		XRD
recent	lake Tanzania	C4	✓	✓															
		C11	✓	✓		✓		✓	✓	-25,3		3,8					b	k	✓
		C21	✓	✓															
	peat bog Tanzania	KAM 100d																	
		KAM 250																	
		KAM 450		✓		✓		✓	✓	-26,2		2,6					b	k	✓
	micr. mat Tunisia	Hassi Djerbi		✓				etched	etched	-13,2		2,1	416	0,59	426		b	k	✓
	micr. mat Brazil	biofilm		✓			✓	N & R	✓	-18,5		0,4	398	10,07	417		b	k	
		Lagoa Vermelha	✓	✓					✓	-11,9		8,7				✓	b	k	✓
	bacteria	sulfurox.	✓	✓	✓	N & R	✓	N & R	N & R		+ 29.2 ‰		-	0,57	-		b	k	
		E. Coli																	

A1: database of the different techniques used in each sample

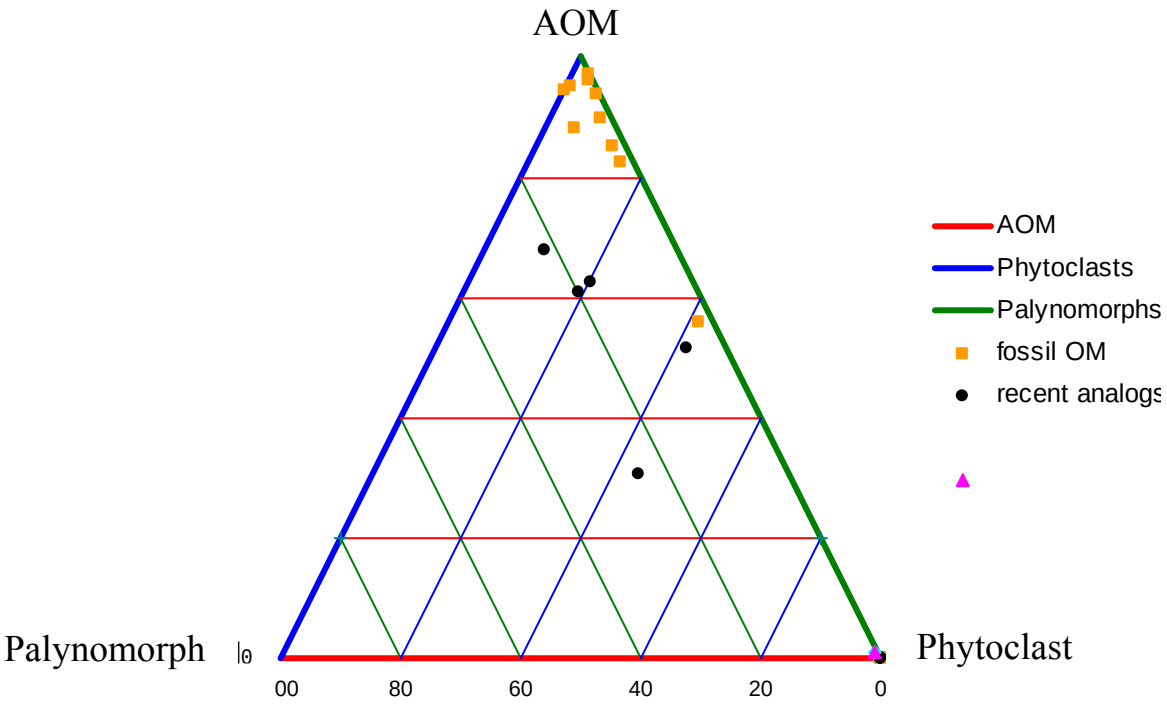

A2: ternary AOM-palynomorph-phytoclasts (APP) diagram

methods		Samples									
		N12		N23		N35		MP5		MP19	
microscopy	specificity	preservation degree	frequency	preservation degree	frequency	preservation degree	frequency	preservation degree	frequency	preservation degree	frequency
standard	palynomorphs			degraded	6.7%	degraded	1.7%		0.4%		
	phytoclasts	weakly degraded	4.1%		5.0%		8.5%	weakly degraded	5.6%	weakly degraded	5.5%
	AOM	-	95.1%	-	88.3%		89.8%		94.0%		94.5%
fluorescence	type	2		2		3		6		6	
SEM	alveolar network				30%		10%		85%		90%
	microorganisms			weakly degraded	30%	weakly degraded	20%	well-preserved	10%		-
	terrestrial st.				-		-		-		-
	undefined				40%		70%		5%		10%
TEM	alveolar network		-			fluffy	30%		40%		30%
	algae	degraded	40%				-	degraded	3%		-
	bacteria					degraded	20%			well-preserved	10%
	ultralaminae		-			strongly degraded	<1%	variable	30%	variable	30%
	terrestrial st.	intact	20%				-		2%		10%
	nanoballs		-				-		20%		20%
	undefined		40%				~50%		5%		-
AFM	smooth surface				-		-		-		20%
	nanoballs				30%		20%		80%		60%
	filaments				20%		-		-		10%
	undefined				50%		80%		20%		10%

methods		Samples									
		Ump		Uk		S20		S27		L113	
microscopy	specificity	preservation degree	frequency	preservation degree	frequency	preservation degree	frequency	preservation degree	frequency	preservation degree	frequency
standard	palynomorphs		2.0%		2.2%				0.5%		2.0%
	phytoclasts	weakly degraded	12.8%	weakly degraded	41.8%	degraded	2.9%		3.2%	weakly degraded	15.5%
	AOM		85.2%		56.0%		97.1%		96.3%		82.5%
fluorescence	type	3		1		4		3			
SEM	alveolar network		40%		40%		60%		60%		60%
	microorganisms	well-preserved	20%	well-preserved	20%	weakly degraded	30%		-		-
	terrestrial st.		-		-		-		-		-
	undefined		40%		40%		10%		40%		40%
TEM	alveolar network		15%		3%		25%		30%		20%
	algae		-		-	well-preserved	5%	degraded	<1%		-
	bacteria	weakly degraded	30%	well-preserved	40%	well-preserved	10%	degraded	5%		5%
	ultralaminae	well-preserved	40%	well-preserved	50%	variable	50%	variable	50%	variable	60%
	terrestrial st.	intact	2%	intact	1%	intact	5%	intact	7%		10%
	nanoballs		10%		5%		3%		5%		4%
	undefined		3%		1%		2%		3%		1%
AFM	smooth surface		10%		10%		15%		30%		5%
	nanoballs		80%		70%		20%		30%		50%
	filaments		-		15%		30%		15%		20%
	undefined		10%		5%		35%		25%		25%

methods		biofilm		microbial mat (Brazil)		microbial mat (Tunisia)		sulfurox. Bacteria		peat bog		Masoko lake	
microscopy	specificity	preservation degree	frequency	preservation degree	frequency	preservation degree	frequency	preservation degree	frequency	preservation degree	frequency	preservation degree	frequency
standard	palynomorphs	intact	17.2%	intact	22.0%	intact	19.8%	alveolar network	100.0%	degraded	25.0%	weak degraded	6.5%
	phytoclasts		20.3%		10.1%		19.4%				44.5%		41.9%
	AOM		62.5%	intact	67.9%	intact	60.8%		-		30.5%		51.6%
fluorescence	type	6		5		4		6		3		4	
SEM	alveolar network	intact	30%					intact	40%	intact	10%	intact	10%
	microorganisms	intact	65%					stressed	60%	intact	20%	intact	20%
	terrestrial st.	intact	5%						-	degraded	60%	intact to weakly degraded	70%
	undefined		-						-		10%		-
TEM	alveolar network	intact	30%	intact	50%	intact	50%	intact	30%		-	intact	10%
	algae	intact	35%	intact	40%	weak degraded	20%		-	weakly degraded	20%	intact	10%
	bacteria	intact	30%	intact	10%			stressed	70%	intact	5%	intact	10%
	ultralaminae		-		-		20%		-	weakly degraded	20%	intact	10%
	terrestrial st.	intact	5%		-	weak degraded	-		-	weakly degraded	50%	intact	50%
	nanoballs		-		-	intact	10%		-	intact	5%	intact	10%
	undefined		-		-		-		-		-		-
AFM	smooth surface	intact	60%	intact	40%	intact	10%		-		-		-
	nanoballs	intact	5%	intact	30%	intact	70%	intact	5%	intact	80%	intact	80%
	filaments	intact	30%	intact	30%	intact	20%	intact	80%	intact	20%	intact	20%
	undefined		5%		-		-		15%		-		-

A3: semi-quantitative estimation of the different elements observed in microscopy

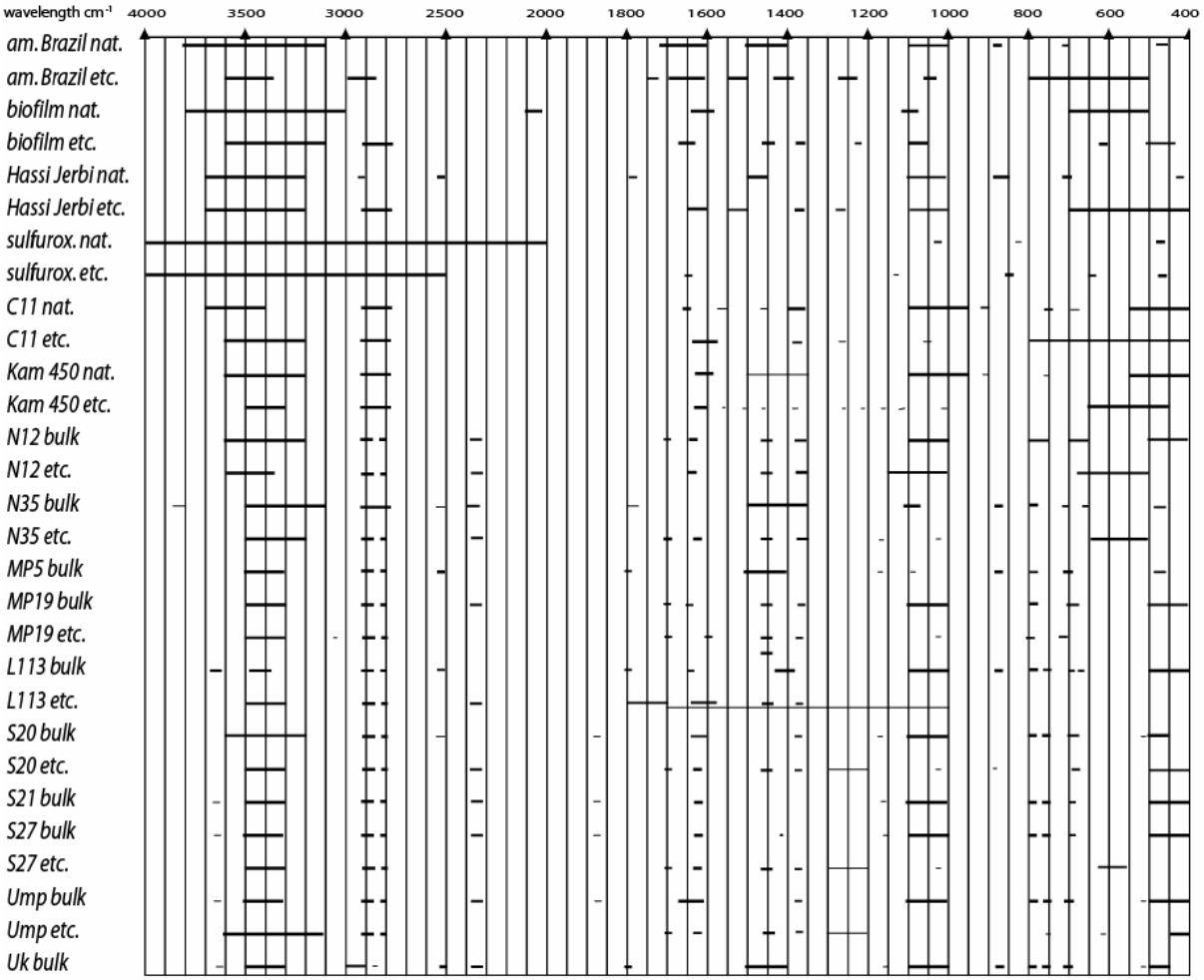

A4: FTIR database for bulk and acid treated samples

PLATES

SEM: Scanning Electron Microscopy
TEM: Transmission Electron Microscopy
AFM: Atomic Force Microscopy

Plate 1a: sulfuroxidizing bacteria:

1-2) White gelatineous mass with dark sulfur granules (s) in macroscopical view
3) Translucent alveolar network in transmitted light
4) Strongly fluorescent alveolar network in blue-light fluorescence

Plate 1b: sulfuroxidizing bacteria: filaments

1-2) Filamentous bodies showing microtubules forming the cytoskeleton in SEM
3-4) Microtubules and some nanoballs in AFM
5) Joined up filament in SEM
6) Microtubules ans dark sulfur inclusions in TEM

Plate 1c: sulfuroxidizing bacteria: coccoids

1-2) Coccoid bacteria surrounded by alveolar networks characterizing EPS in SEM
3) Bunch of nanoballs joined to filaments in AFM
4) Nanoballs in AFM
5) Nanoballs characterized by an association of fragments showing clear boundaries in AFM
6) Oriented nanoballs on the particle edge in AFM

Plate 1d: sulfuroxidizing bacteria: coccoids in TEM

1) Bacterial cell showing typical cell wall and diffuse DNA
2-3) Stressed forms characterized by an undulating cell wall
4) Different cytoplasmic inclusions
5) Translucent nanoballs
6) Lysosomes corresponding to microbial degradation

Plate 1e: sulfuroxidizing bacteria: EPS

1) Continuous veil in SEM
2-3) Alveolar networks at different scales in SEM
4-5) Agglomerated EPS due to mechanical constraints in SEM
6) « curly-form » EPS in AFM
7) Alveolar network in AFM
8) Entangled filaments (i.e. capsule) in TEM

Plate 2a: cyanobacterial biofilm

1-2) Green film with white crystals in macroscopical view
3-4) Structured elements and light-brown granular AOM in transmitted light
5) Strongly fluorescent EPS and bacteria in blue-light fluorescence
6) Strongly fluorescent filamentous organisms in blue-light fluorescence

Plate 2b: cyanobacterial biofilm: bacteria

1) Different microorganisms like diatoms, cyanobacteria (e.g. *Spirulina*) and coccoids which are embedded in EPS in SEM

2-3) Cyanobacteria showing thylakoids and phycobilisomes in TEM
4) Endospores in TEM
5) Smooth area on the biofilm surface in AFM
6) Rare nanoballs in AFM

Plate 2c: cyanobacterial biofilm: algae

1) Algal filament with calcite crystals on its sheath in SEM
2) Green alga showing thylakoids lockally stacked into grana in TEM
3) Dark storage inclusions in alga; the cell is surrounded by cryptocrystaline calcite in TEM
4) Filamentous alga in TEM
5-6) Green alga close to Chlorophyceae family in TEM

Plate 2d: cyanobacterial biofilm: EPS

1) Compact mass; on the top, dendroid network of filaments (microorganisms) in SEM
2) Bacterial cell surrounded by « curly » EPS in TEM
3) « curly » EPS in TEM
4) Alveolar network in AFM
5-6) Smooth area with locally some holes in AFM

Plate 3a: microbial mat, Lagoa Vermelha (Brazil)

1) Laminations characterizing different microbial populations (green, red, brown colours) and mineral layers (in white); scale-bar 1 cm
2) Structured elements and AOM in transmitted light
3) Light-brown granular AOM with green filaments in transmitted light
4) Dark-brown gelified AOM in transmitted light
5) Strongly fluorescent AOM composed of filaments in blue-light fluorescence
6) Non-fluorescent diffuse mass (i.e. EPS) which links bacteria in blue-light fluorescence

Plate 3b: microbial mat, Lagoa Vermelha in AFM

1) Fern-like particles in microview
2) Nanoballs
3) Smooth area locally covered by nanoballs
4) Filaments covered by nanoballs
5) Irregularities on the filament surface

Plate 3c: microbial mat, Lagoa Vermelha in TEM

1) « Curly » EPS
2) Filamentous EPS
3-4) Calcite encrustment around the cells
5) Filamentous bacteria
6-7) Thallus-type arrangement (algae) with lipidic inclusions inside each cell

Plate 4a: microbial mat, Hassi Jerbi (Tunisia)

1) Laminated sediment with anoxic, dark zones. It is colonized by a soft green biofilm
2-3) Structured elements and light-brown and dark-brown granular AOM in transmitted light
4) Patchily fluorescent particle in blue-light fluorescence
5) Strongly fluorescent cutinite; weakly fluorescent filaments and AOM in blue-light fluorescence

Plate 4b: microbial mat, Hassi Jerbi in TEM

1) « Curly » EPS
2) EPS as alveolar network
3) Translucent bacterial membranes
4) Remains of filamentous organism
5) Bacterium with lipidic inclusions or vacuoles
6) Grey to dark nanoballs

Plate 4c: microbial mat, Hassi Jerbi in AFM

1) Nanoballs
2) Bunches of nanoballs on filament surface
3) Nanoballs of varying size
4-5) Oriented particles composed of nanoballs

Plate 5a: continental sediments, Masoko lake (Tanzania)

1) Without acid treatment: structured elements such as cutinite, inertinite, diatoms and AOM in transmitted light
2) With acid treatment: dark-brown granular AOM composed of various inertinite fragments in transmitted light
3) With acid treatment: inertinite and cutinite in transmitted light
4-5) Strongly fluorescent particles with non fluorescent inertinite in blue-light fluorescence

Plate 5b: continental sediments, Masoko lake (Tanzania) in SEM

1) Cutinite (tracheid)
2) Strongly degraded cutinite
3-4) Degraded cutinite fragments
5) Microbial filaments forming an entangled network
6) Surface covered by coccoid bacteria and EPS
7) Framboidal pyrite

Plate 5c: continental sediments, Masoko lake (Tanzania) in AFM

1-2) Bunches of nanoballs on microbial filaments; the rest of the biofilm surface is covered of nanoballs
3) Random nanoballs covering bachground
4) Bi-directionally-oriented nanoballs

Plate 5d: continental sediments, Masoko lake (Tanzania) in TEM
1-2) Ultralaminae: bacterial membranes
3-4) Cuticles membranes
5-6) Endospores
7) Gram-negative bacterium
9) Algae
10) EPS as an alveolar network
11) Ligneous fragments
12) Dark nanoballs

Plate 6a: continental sediments, peat bog (Tanzania)

1-2) Structured elements (cutinite) and light-brown gelified AOM in transmitted light
3) Weakly fluorescent OM in blue-light fluorescence

4) Patchily fluorescent particles in blue-light fluorescence

Plate 6b: continental sediments, peat bog (Tanzania) in SEM

1) Degraded terrestrial stuctures
2) Fibrous fragments associated with coccoid bodies
3) Charcoal fragments with regular holes
4) Alveolar network associated with degraded terrestrial fragments
5) Microbial muccus covering filaments
6) Thallus-arrangement similar to that of algae, i.e. *Botryoccocus braunii*

Plate 6c: continental sediments, peat bog (Tanzania) in AFM

1) Particle edge composed of nanoballs
2) Nanoballs covering surface particle
3) Nanoballs on filaments
4) Oriented nanoballs
5) Nanoballs associated with microtubules
6) Bunches of nanoballs on filaments

Plate 6d: continental sediments, peat bog (Tanzania) in TEM

1) Algal cell walls similar to that of *Botryococcus braunii*
2) Other kinds of algal cell walls
3) Translucent bacterial membranes
4-5) Cuticle membranes with ornamentation
6) Fibrous terrestrial structures
7-8) Bacteria with lipidic inclusions or vacuoles
9) Alga with bacterium containing lipidic inclusions (symbiosis or phagocytosis)

Plate 7a: sulfuroxidizing bacteria after acid treatment

1) Translucent alveolar network in transmitted light
2) Strongly fluorescent alveolar network in blue-light fluorescence
3) Filaments forming the cytoskeleton (i.e. microtubules) associated with coccoid bacteria in SEM
4) Filaments forming the cytoskeleton (i.e. microtubules) with locally oriented nanoballs in SEM
5) Smooth area on a filament in AFM

Plate 7b: sulfuroxidizing bacteria after acid treatment (coccoids)

1) Geometric outlines of coccoid bacteria in SEM
2) Coccoid bacteria on a bacterial filament in SEM
3-4) Smooth surface of coccoid bacteria at nanoscale in AFM
5) Ghosts of coccoid bacteria in TEM
6) Well-preserved bacterium with cell wall in TEM

Plate 7c: sulfuroxidizing bacteria after acid treatment (EPS)

1) EPS attached to bacterial cells in SEM
2) « Curly » EPS in TEM
3-4) EPS as an alveolar network in AFM

Plate 7d: cyanobacterial biofilm after acid treatment

1) Alveolar network in SEM

2) Alveolar network in TEM
3) Bacterium with vacuoles in TEM
4) cell walls with cytoplasmic inclusions in TEM
5) Algal cell walls associated with cytoplasmic inclusions in TEM

Plate 7e: algal mat and continental sediments after acid treatment

1) Fluorescent bacteria with weakly fluorescent EPS in a microbial mat (Lagoa Vermelha, Brazil) in blue-light fluorescence
2) Fluorescent granular OM in a microbial mat (Lagoa Vermelha) in blue-light fluorescence
3) Palynofacies showing vitrinite and gelified AOM in the Masoko lake in transmitted light (sample C11)

Plate 8a: the Monterey Formation, sample N35 (bulk rock)

1) Finely laminated rock
2) Brown, parallel laminae with detrital and carbonate lenses (thin section)
3) OM-richer zone with dark-brown laminae and foraminifera (thin section)
4) Well-preserved foraminifera tests(bi-seriate) in SEM
5-6) Organic membranes surrounded by radial test (5) and some pyite crystals (6) in SEM

Plate 8b: the Monterey Formation, sample N35 (kerogen)

1) Palynofacies showing dark-brown granular AOM in transmitted light
2) Strongly and non-fluorescent particles in blue-light fluorescence
3) Microbial filaments in SEM
4-5) Alveolar network associated with coccoid bodies in SEM
6) Coccolith imprints in OM in SEM

Plate 8c: the Monterey Formation, sample N35 (kerogen) in AFM

1-2) Heterogeneous OM locally with nanoballs
3) Stair-shaped particle edge

Plate 8d: the Monterey Formation, sample N35 (kerogen) in TEM

1) Translucent bacterial membranes
2) Fluffy alveolar network (EPS)
3) Bacterium with a flagellum
4) Bacterium with distorted translucent outer membrane
5) Bacterial cell walls (in colony) or microspores
6) Bacteria with vacuoles or inclusions

Plate 9: the Monterey Formation, sample N12 (kerogen)

1) Palynofacies showing some vitrinite and mainly dark-brown granular AOM in transmitted light
2) Dark-brown granular AOM in transmitted light
3) Weak patchily fluorescent particle in blue-light-fluorescence
4) Terrestrial particles in TEM
5) Framboidal pyrite in TEM
6) Bacterium with vacuoles in TEM
7) Remnant of filamentous sulfuroxidizing bacteria

Plate 10: the Monterey Formation, sample N23 (kerogen)

1) Palynofacies showing some vitrinite and mainly dark-brown granular AOM in transmitted light
2) Non-fluorescent AOM in blue-light-fluorescence
3) Heterogeneous OM in SEM
4) Nanoballs (100-500 nm wide) in AFM
5) Oriented nanoballs perpendicular to stair-shaped particles in AFM
6) Bunches of nanoballs on filaments in AFM
7) Ramifications at the end of a filament in SEM
8) Agglomerated filament and secondary dendroid network (EPS) in SEM

Plate 11a: Kimmeridgian laminites

1) Laminites in the field with dark, parallel, organic-rich laminae
2) Orange to dark-brown parallel organic laminae in sample MP19 in thin section
3-4) Gold and dark-brown fine parallel organic laminae in sample MP5 in thin section
5) Phosphatic debris in sample MP19 in thin sections

Plate 11b: Kimmeridgian laminites

1-2) Palynofacies showing mainly light-brown to dark-brown granular AOM in sample MP5, transmitted light
3) Strongly fluorescent particles in sample MP5 in blue-light fluorescence
4) Palynofacies showing inertinite, vitrinite and light-brown to dark-brown granular AOM in sample MP19, transmitted light
5) Strongly fluorescent particles (locally alveolar network visible) in sample MP19 in blue-light fluorescence

Plate 11c: Kimmeridgian laminites, sample MP5

1-2) Alveolar network in loose bodies in SEM
3) Remain of organic skeleton in loose bodies in SEM
4) Alveolar network and coccolith imprints in dense bodies in SEM
6) 600 nm wide alveolus in AFM
7) Particles entirely made of nanoballs in AFM

Plate 11d: Kimmeridgian laminites, sample MP5

1-2) Filamentous and coccoid bodies in SEM
3) Alveolar network in TEM
4) Framboidal pyrite in TEM
5) Dark nanoballs within alveolar network in TEM
6) Terrestrial fragment within alveolar network in TEM
7) Filamentous body resembling nematods
8) Gram-negative filamentous organism in TEM

Plate 12a: Kimmeridgian laminites, sample MP19

1-2) Alveolar network in most of the particles in SEM
3) Nanoballs on filaments in AFM
4) Oriented nanoballs on a smooth surface in AFM
5) Edge of an alveolus in AFM

Plate 12b: Kimmeridgian laminites, sample MP19 in TEM

1) Framboidal pyrite
2) Structured terrestrial fragment
3) Dark nanoballs within linear structures
4) Alveolar network (EPS)
5) Terrestrial structures
6) Bacteria with dark storage and lipidic inclusions
7) Bacteria containing vacuoles

Plate 13a: Selli level (OAE1a)

1) Dark-brown parallel organic laminae forming an entangled network with detrital lenses in sample S20 (thin section)
2) Phosphatic arthropods remains in sample S27 (thin section)
3-4) Palynofacies showing vitrinite and dark-brown granular AOM in sample S20 in transmitted light
5) Patchily fluorescent particle in sample S2x in blue-light fluorescence
6) Strongly fluorescent alveolar network in sample S2x in blue-light fluorescence

Plate 13b: Selli level (OAE1a), sample S20

1) 10 µm wide coccoid bodies in the size range of big bacteria or algae in SEM
2) Coccoid bodies associated with an alveolar network in SEM
3) Alveolar network without metallization in SEM
4) Framboidal pyrite within alveoli without metallization in SEM
5) Bunches of nanoballs on filaments in AFM
6) Different kinds of nanoballs (in bunches and oriented) in AFM
7) Sutures in nanoballs in AFM
8) Microspores in AFM

Plate 13c: Selli level (OAE1a), sample S20 in TEM

1) Bacteria containing vacuoles
2-3) Gram-negative bacteria containing lipidic inclusions
4) Dark nanoballs
5) Bacterial membranes
6) Terrestrial fragments
7) Framboidal pyrite within bacterium ghost

Plate 14a: Selli level (OAE1a), sample S27

1-2) Palynofacies showing vitrinite associated with dark-brown granular AOM in transmitted light
3) Non-fluorescent particle in blue-light fluorescence
4) Patchily fluorescent particle in blue-light fluorescence
5-6) Alveolar network associated with 5 µm wide coccoid bodies in SEM without metallization

Plate 14b: Selli level (OAE1a), sample S27

1) Oriented nanoballs on smooth surface in AFM
2) Bunches of nanoballs in AFM
3) Alveolar network in TEM
5) Bacterium in TEM

Plate 14c: Selli level (OAE1a), sample S27 in TEM

1) Bacterium containing dark storage inclusions and vacuoles
2) Framboidal pyrite within a bacterium ghost
3) Pyrite crystal within ultralaminae
4) Terrestrial structure
5) Bacteria within a cell (symbiosis with alga)
6) Dark nanoballs

Plate 15a: Urbino level (OAE1b), samples Ump and Uk

1) Finely laminated shale, outcrop section
2) Dark-brown, parallel organic laminae with detrital and carbonate lenses in thin section in sample Ump (perpendicular to laminae)
3) Phosphatic remains in thin section in sample Ump (parallel to laminae)
5-6) Thin sections in sample Uk parallel to laminae

Plate 15b: Urbino level (OAE1b), sample Ump

1) Palynofacies showing mainly dark-brown granular AOM in transmitted light
2) Non-fluorescent particle in blue-light fluorescence
3) Strongly fluorescent alveolar network within a particle in blue-light fluorescence
4) Alveolar network in heterogeneous material in SEM
5) Coccoid bodies and nanoballs in SEM
6) Particle composed of non oriented nanoballs in AFM

Plate 15c: Urbino level (OAE1b), sample Ump

1) texture similar to organism membrane in SEM
2) Framboidal pyrite in SEM
3) Smooth surface and nanoballs in AFM
4) Alveolar network in TEM
5) Remains of bacteria in TEM
6) Bacteria in colony in TEM
7) Terrestrial structures in TEM
8) Dark nanoballs in TEM

Plate 16a: Urbino level (OAE1b), sample Uk

1) Palynofacies showing dark-brown granular AOM in transmitted light
2) Light-brown gelified AOM containing vitrinite, inertinite and granular AOM fragments in transmitted light
3) Non-fluorescent particles in blue-light fluorescence
4) Alveolar network associated with coccoid bodies in SEM
5) Nanoballs in SEM
6) Smooth area in AFM
7) Nanoballs in AFM

Plate 16b: Urbino level (OAE1b), sample Uk in TEM

1) Gram-negative bacteria containing dark storage and lipidic inclusions
2) Gram-negative bacterium containing carboxyzomes
3) Bacterium with dark cellular content and undulating cell wall
4) « Nanobacterium » containing vacuoles
5) Bacterial membranes close to lysosomes

6) Alveolar network
7) Terrestrial fragment
8) Dark nanoballs

Plate 17a: 113 level (OAE1b)

1) Dark-brown OM in thin section (parallel to laminae)
2) Phosphatic remains in thin sections (parallel to laminae)
3) Palynofacies showing cutinite, inertinite and AOM in transmitted light
4) Dark-brown granular AOM in transmitted light
5) Heterogeneous OM in SEM without metallization
6) Alveolar network in SEM without metallization

Plate 17b: 113 level (OAE1b)

1) Oriented nanoballs on smooth surface in AFM
2) Nanoballs on filaments in AFM
3) Dark nanoballs in TEM
4) Terrestrial fragment in TEM
5) Alveolar network in TEM
6) Remain of bacterium in TEM
7) Bacteria or microspores associated with dark nanoballs in TEM

Plate 18: ultralaminae: recent algal cell walls in TEM

a) In the biofilm (Chlorophyte genus)
b) In the biofilm after acid etching
c-d) In the microbial mat of Hassi Jerbi (southern Tunisia) after acid etching
e) *Botryococcus braunii* after acid etching

Plate 19: ultralaminae: fossil algal cell walls in TEM

a) Associated with granules (g) and symbiotic bacteria (b) in Kimmeridgian laminites
b) Long linear layers in Kimmeridgian laminites
c) Arrangement similar to Botryococcus brauni in Kimmeridgian laminites
d-e) Contorted layers in the Selli level
f) Layers associated with granules (g) in the Selli level

Plate 20: ultralaminae: fossil algal cell walls in TEM

a) Extensive patch of contorted layers in the 113 level
b) Amplification of contorted layers showing a radial fragmentation layer in the 113 level
c) Linear layers in the 113 level
d) Patch of contorted layers in the Urbino level
e) Degraded contorted layers in the Monterey Formation

Plate 21: ultralaminae: recent bacterial cell walls in TEM

a) Gram-negative cell wall of cyanobacteria in the biofilm
b) Same Gram-negative cell wall in the biofilm after acid etching
c) Remnants of filamentous bacteria in the Hassi Jerbi microbial mat after acid etching
d) Burst translucent layers attached to dense thin membranes in the Hassi Jerbi microbial mat after acid etching

Plate 22: ultralaminae: fossil bacterial cell walls in TEM

a) Mixture of cell walls in Kimmeridgian laminites
b) More or less diffuse contorted layers in the Selli level
c) Contorted layers in a diffuse mass in the 113 level
d) Thin contorted layers in the Urbino level
e-f) Dense, locally burst layer in the Monterey Formation

Plate 23: ultralaminae: recent thylakoid membranes in TEM

a) Presence of phycobilisome (p, dark) in a cyanobacterium within the biofilm
b-d) Thylakoids asembled in grana in different species of algae within the biofilm
e) Thylakoids associated with granules in the biofilm after acid etching

Plate 24: ultralaminae: fossil thylakoid membranes in TEM

a) Pair of thylakoids alternating with dark zones in the Kimmeridgian laminites
b) Several thin layers in the Selli level
c) Discontinuous, contorted lines in the 113 level
d) Contorted pair of layers in the Urbino level

Plate 25: ultralaminae: organisms and cuticles in TEM

a) Contorted layers in the Hassi Jerbi microbial mat (Tunisia) after acid etching
b-c) Stacked filamentous bodies surrounded by a typical layer in the Urbino level

Plate 1a: sulfuroxidizing bacteria

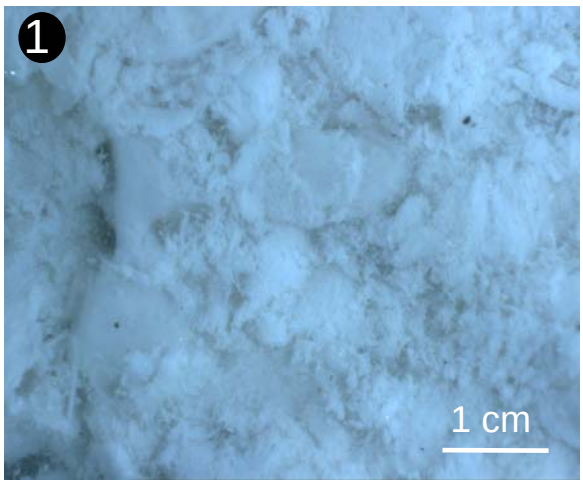

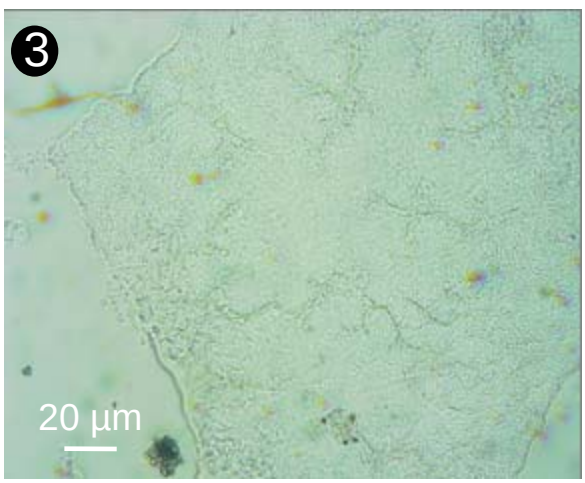

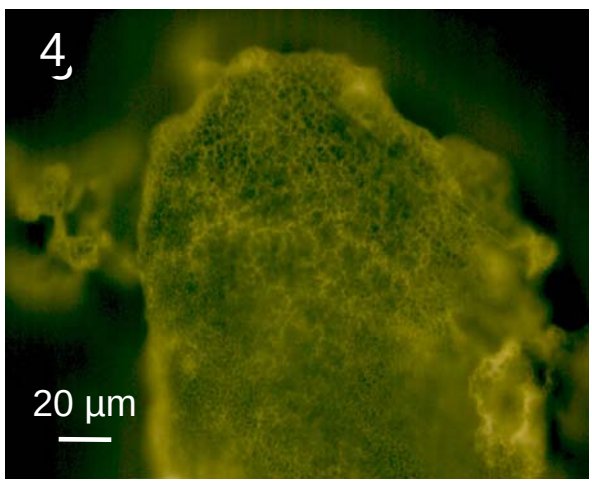

Plate 1b: sulfuroxidizing bacteria: filaments

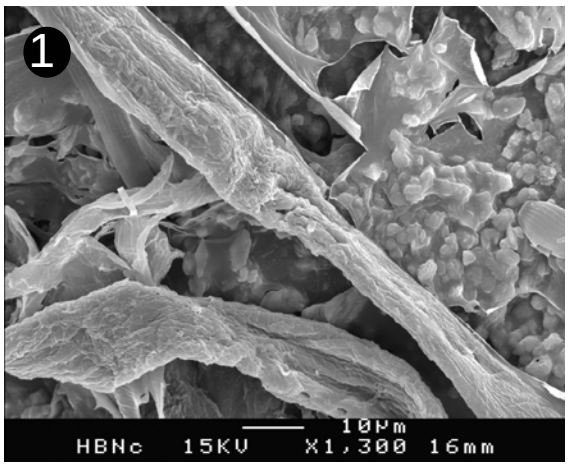

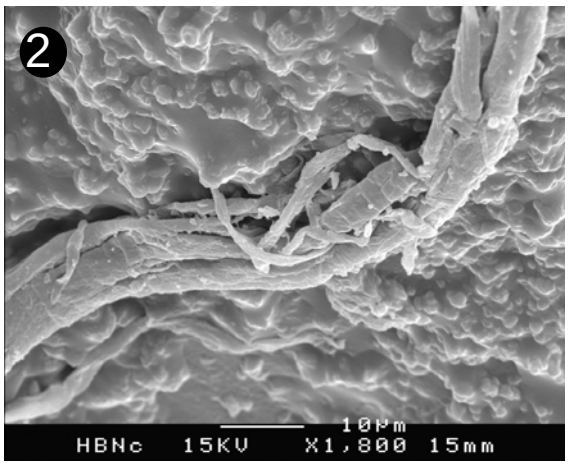

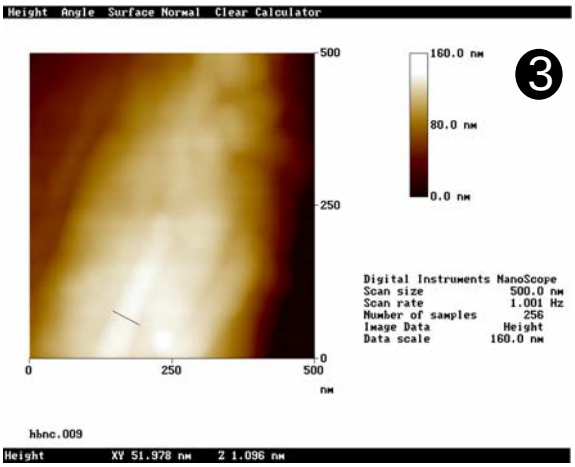

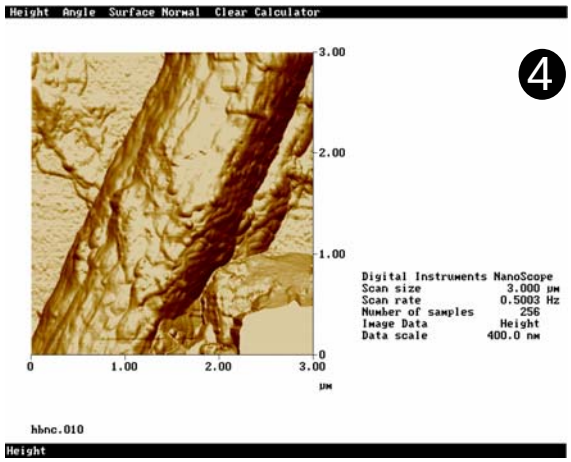

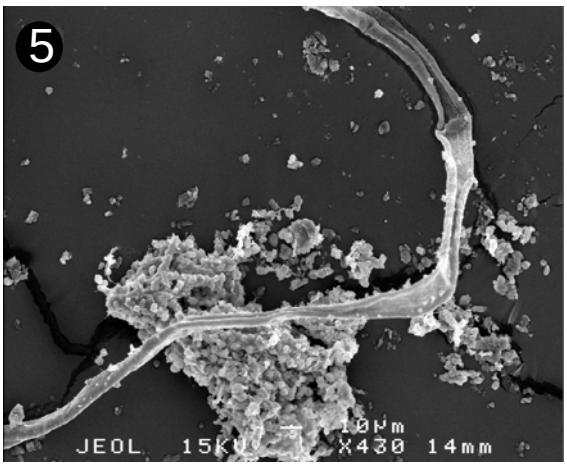

Plate 1c: sulfuroxidizing bacteria: coccoids

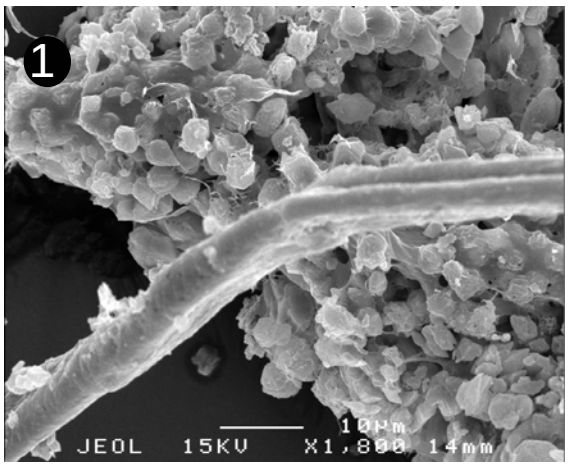

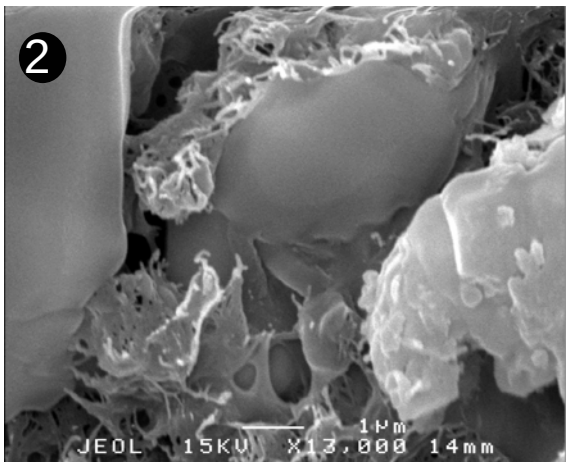

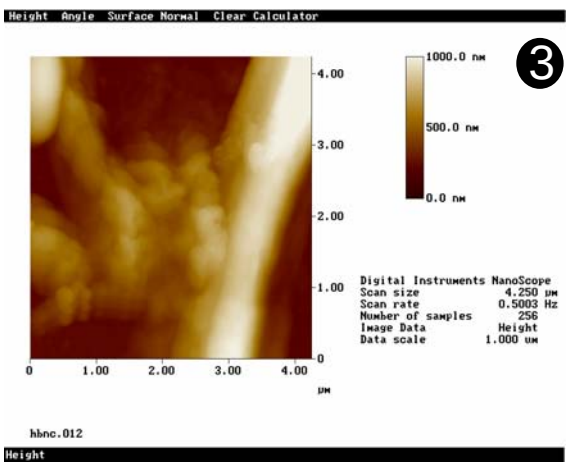

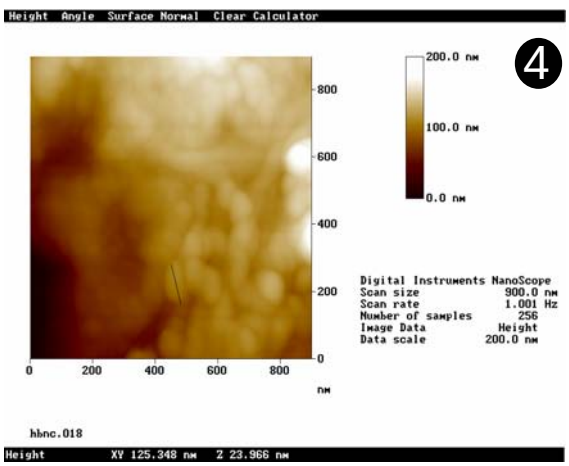

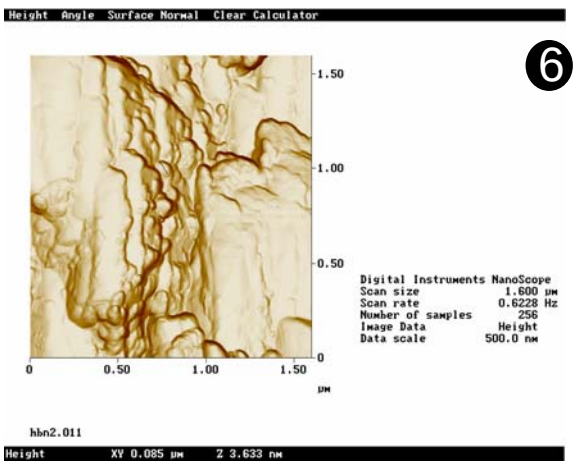

Plate 1d: sulfuroxidizing bacteria: coccoids in TEM

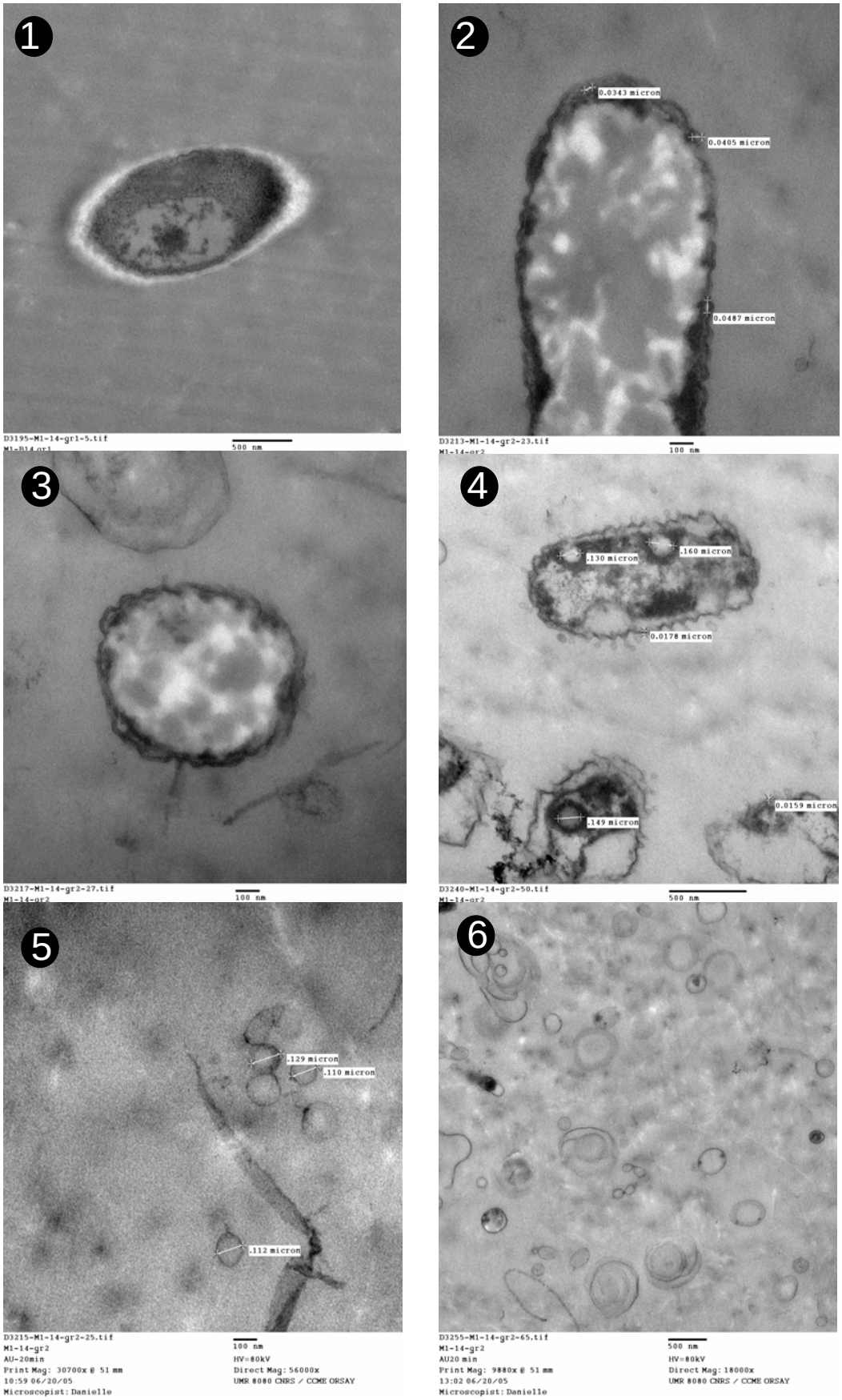

Plate 1e: sulfuroxidizing bacteria: EPS

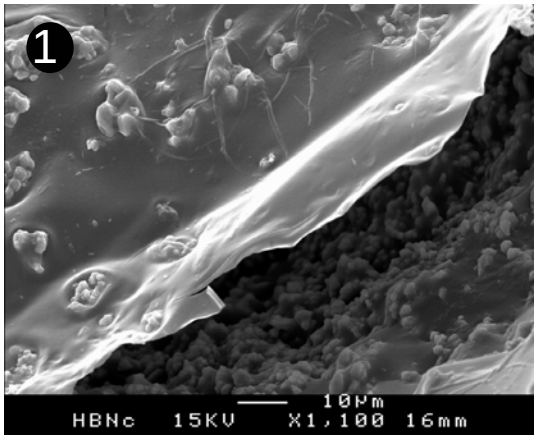

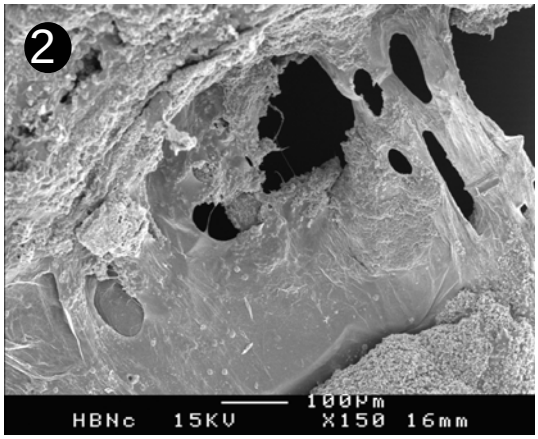

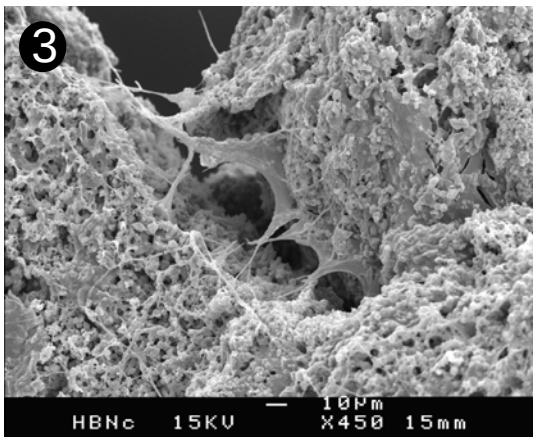

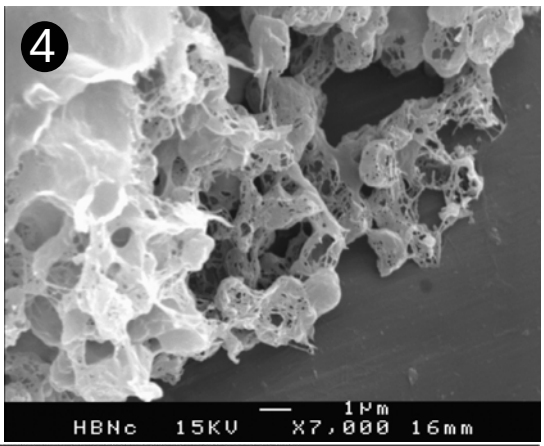

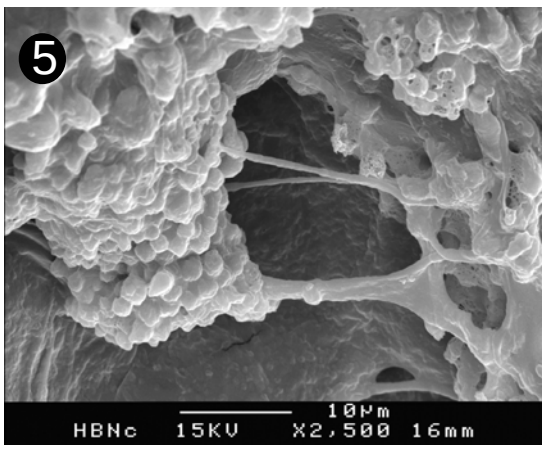

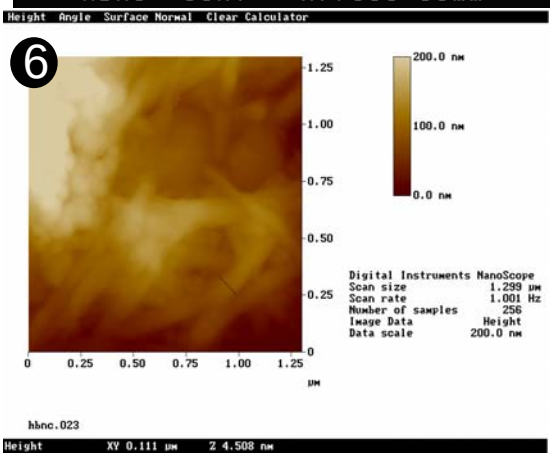

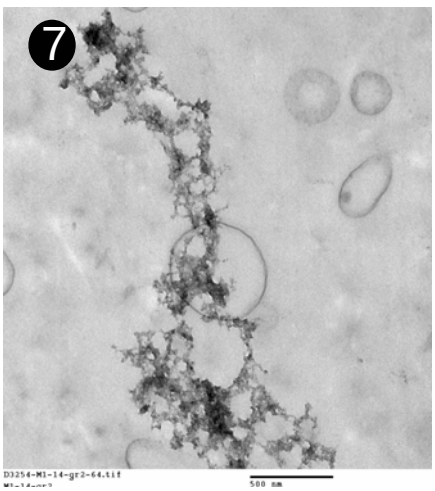

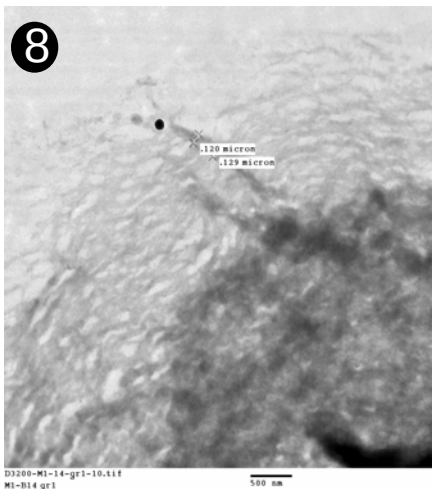

Plate 2a: cyanobacterial biofilm

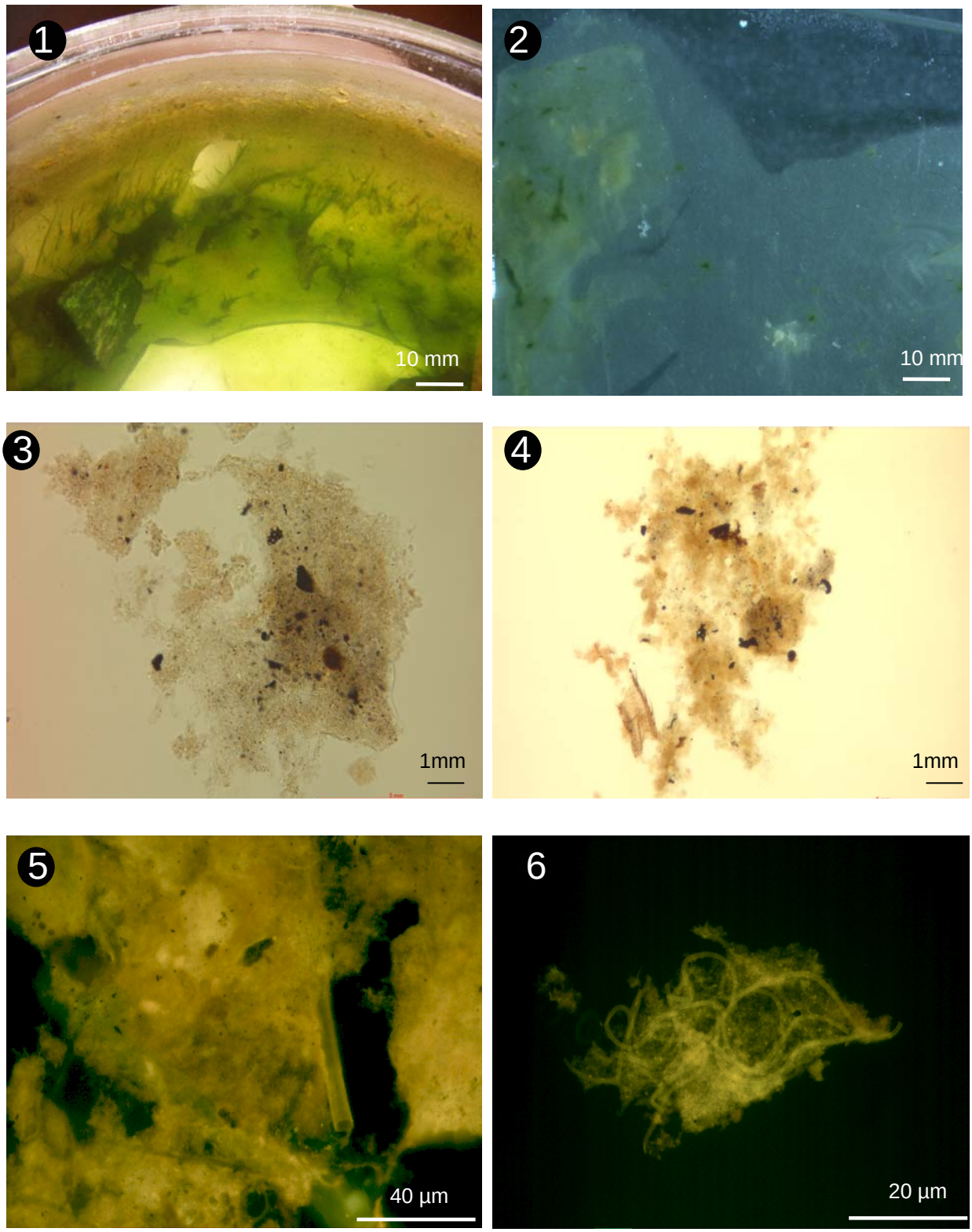

Plate 2b: cyanobacterial biofilm, i.e. bacteria

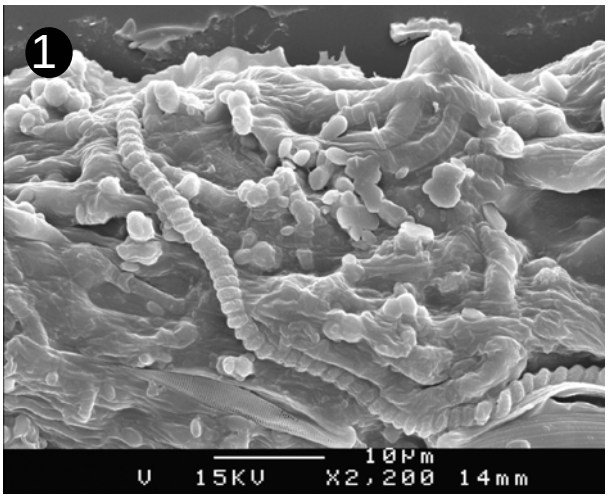

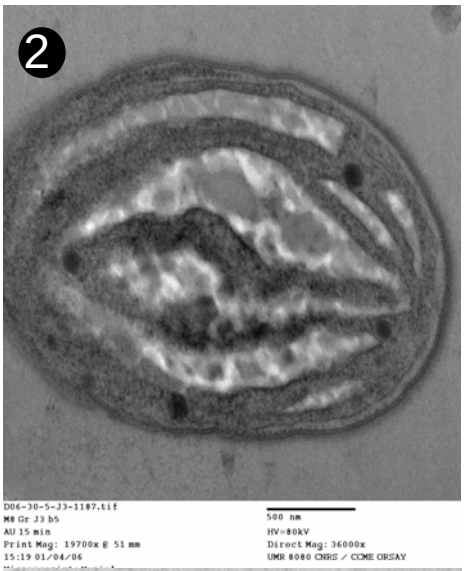

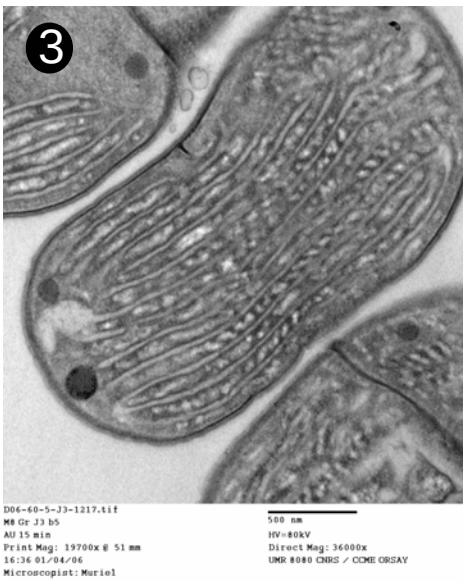

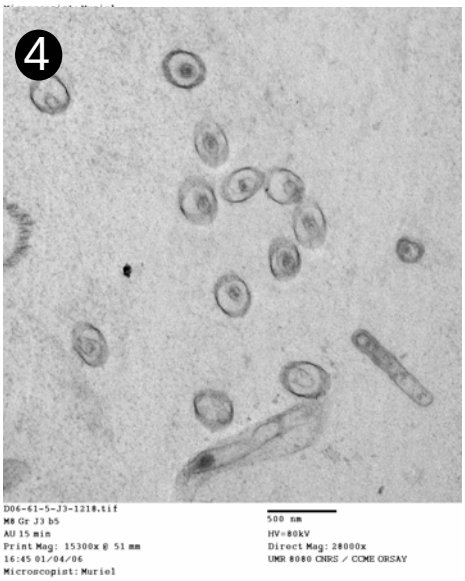

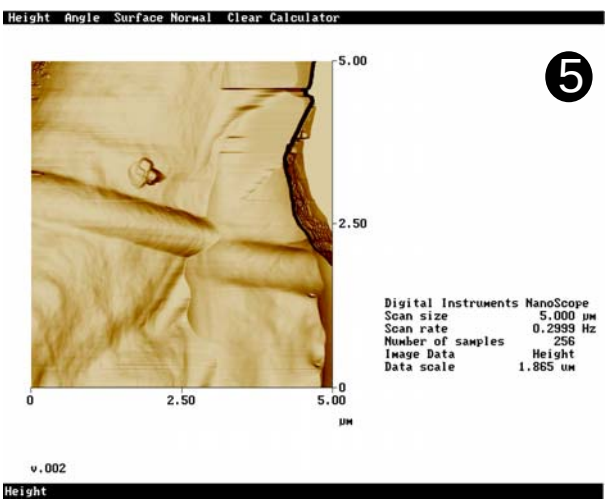

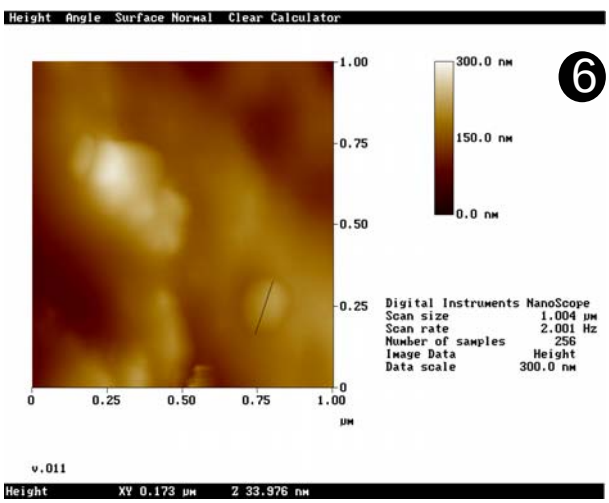

Plate 2c: cyanobacterial biofilm, i.e. algae

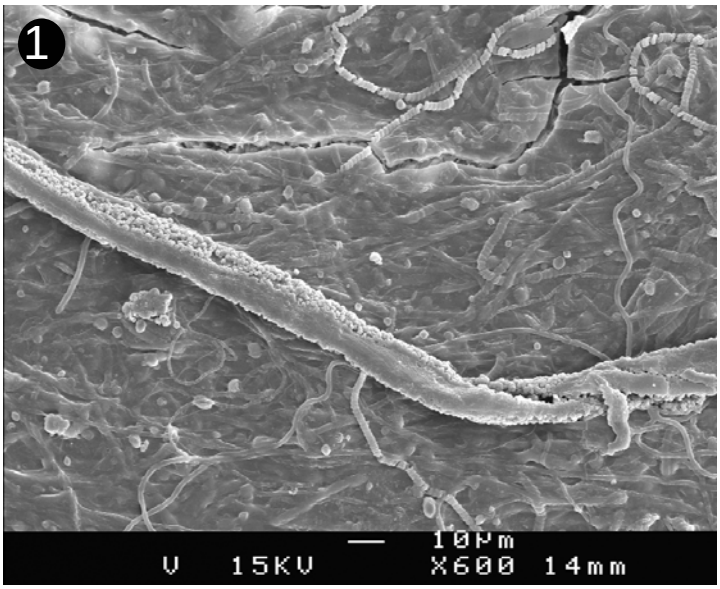

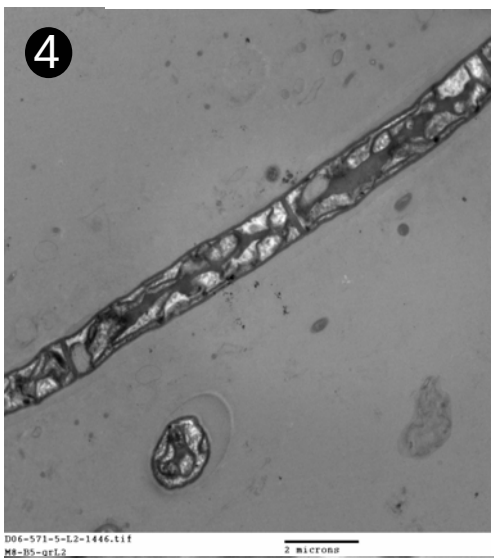

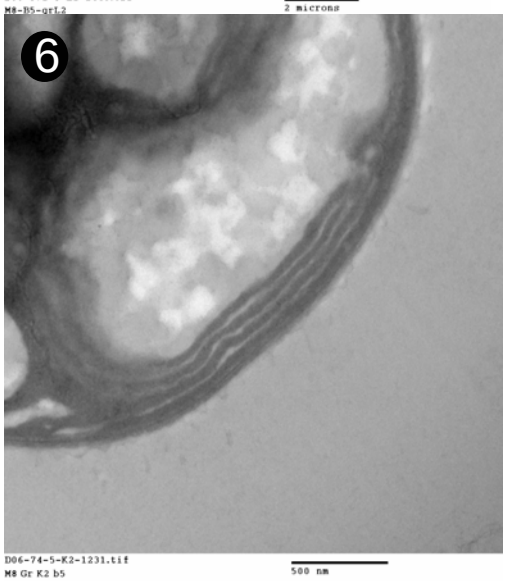

Plate 2d: cyanobacterial biofilm, i.e. EPS

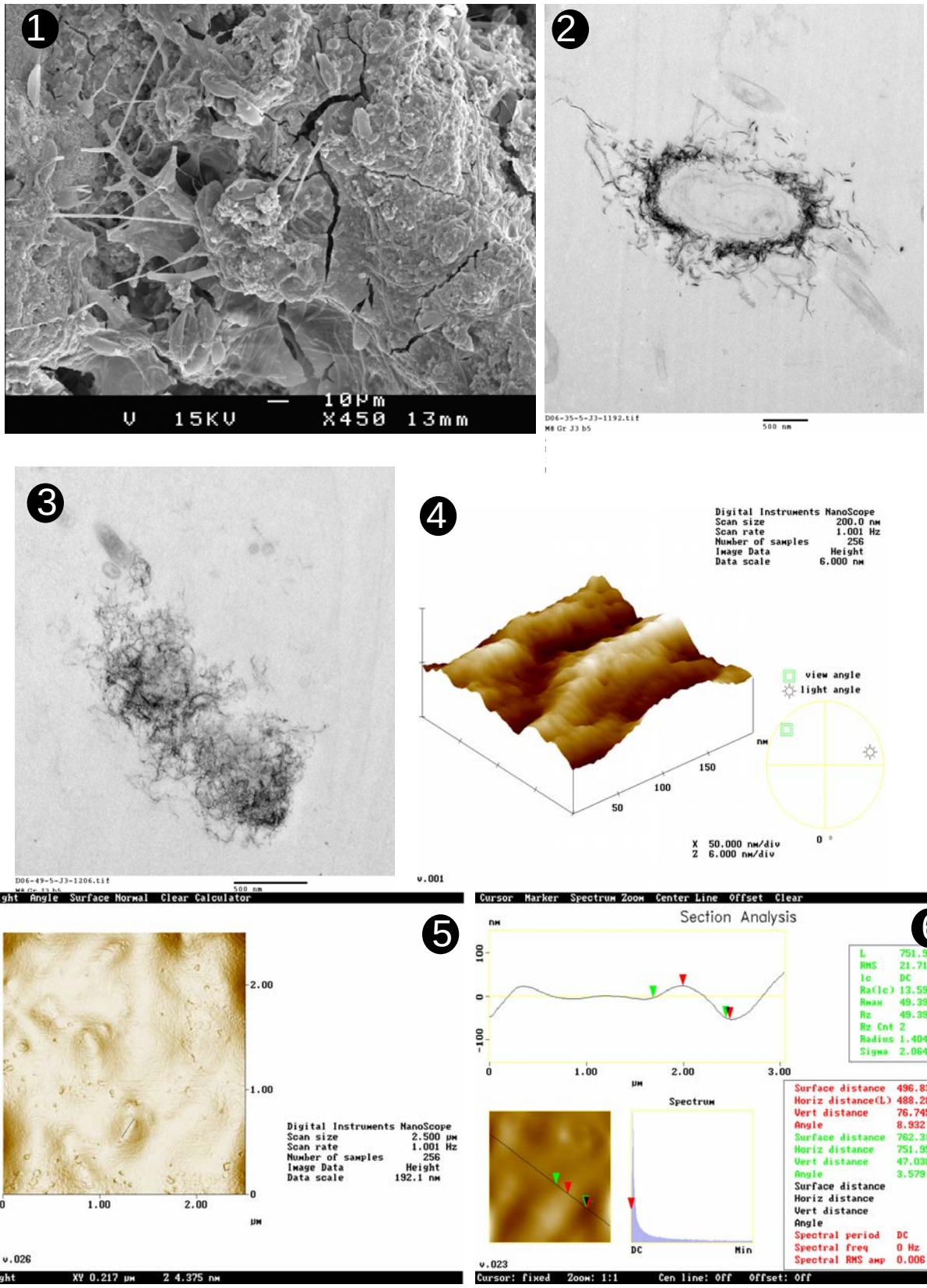

Plate 3a: microbial mat, Lagoa Vermelha

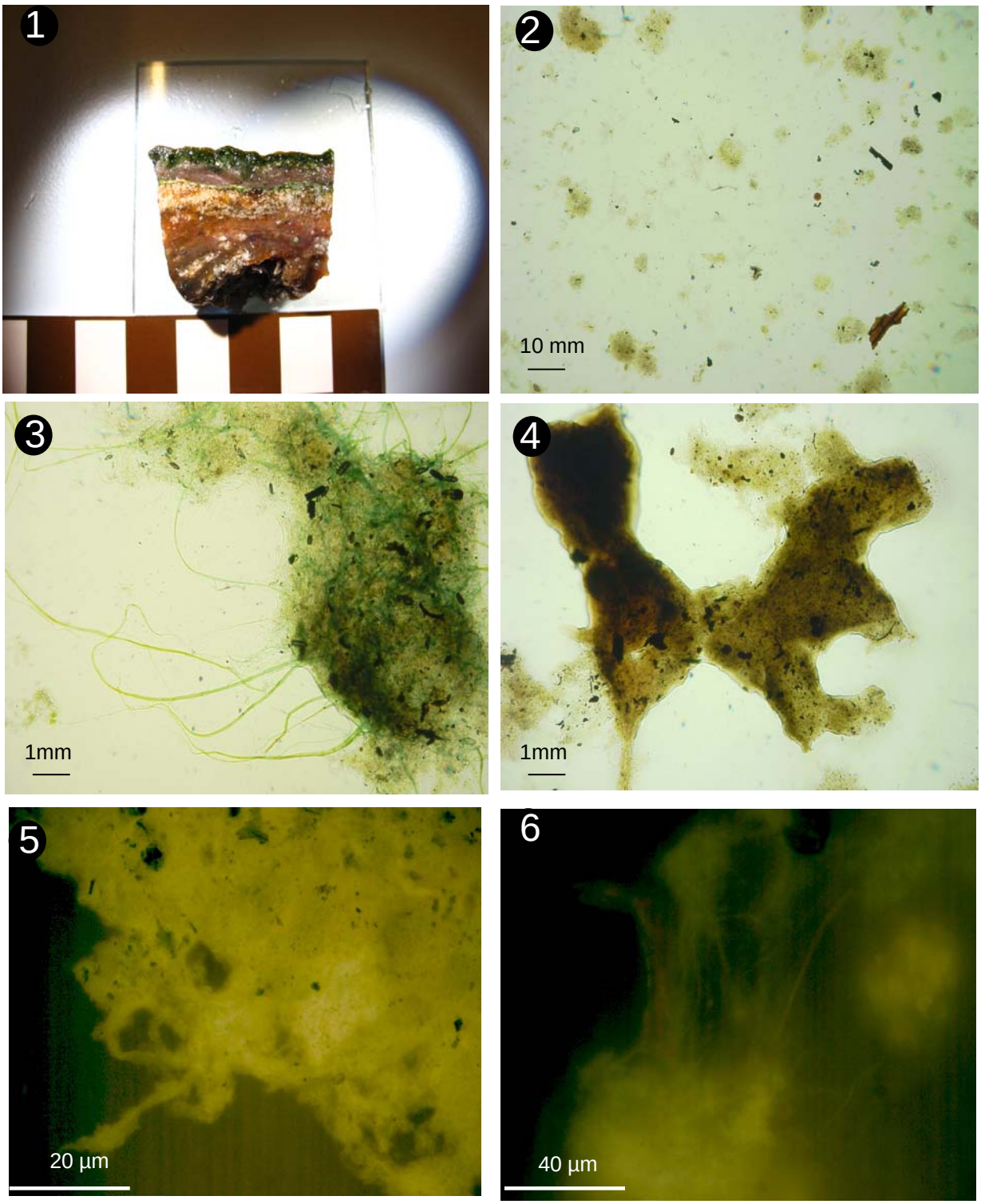

Plate 3b: microbial mat, Lagoa Vermelha in AFM

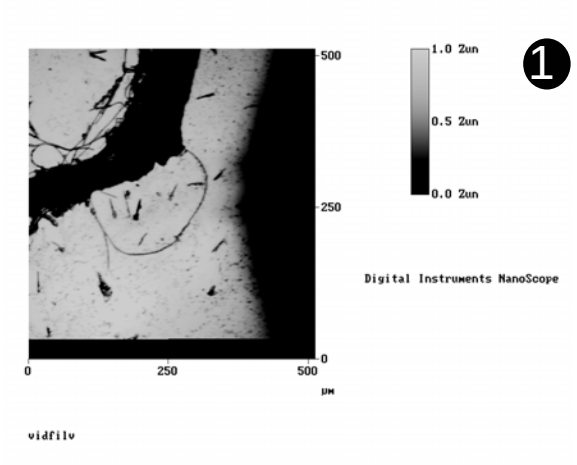

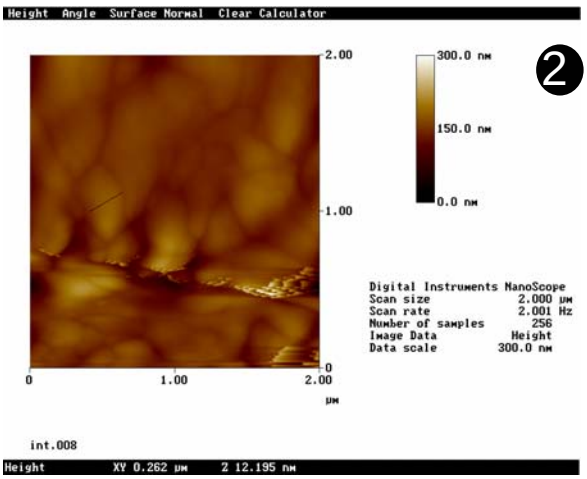

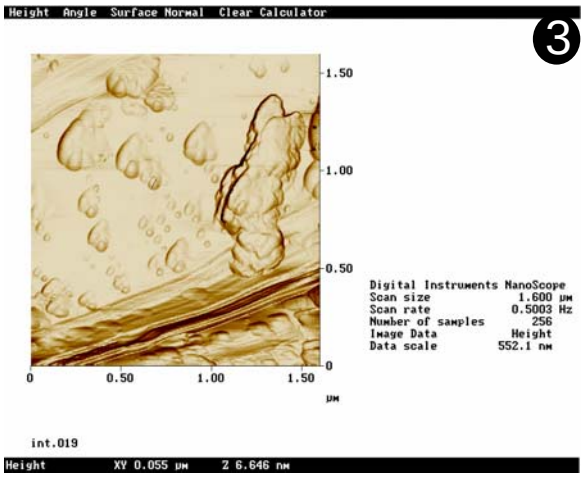

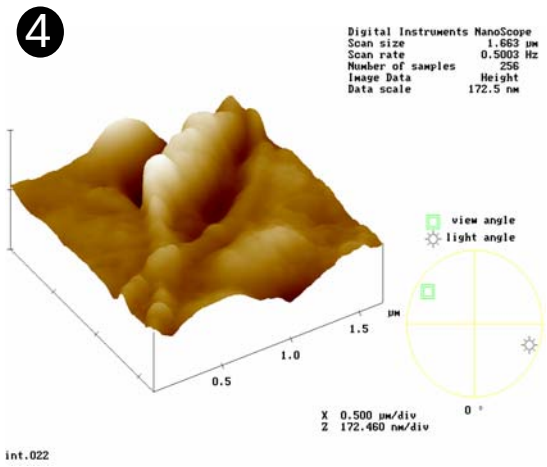

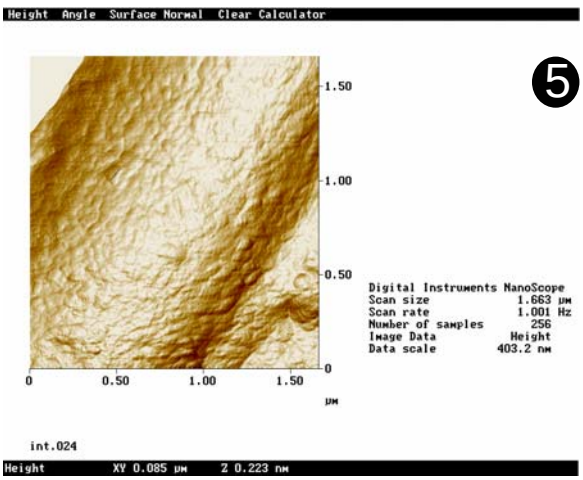

Plate 3c: microbial mat, Lagoa Vermelha in TEM

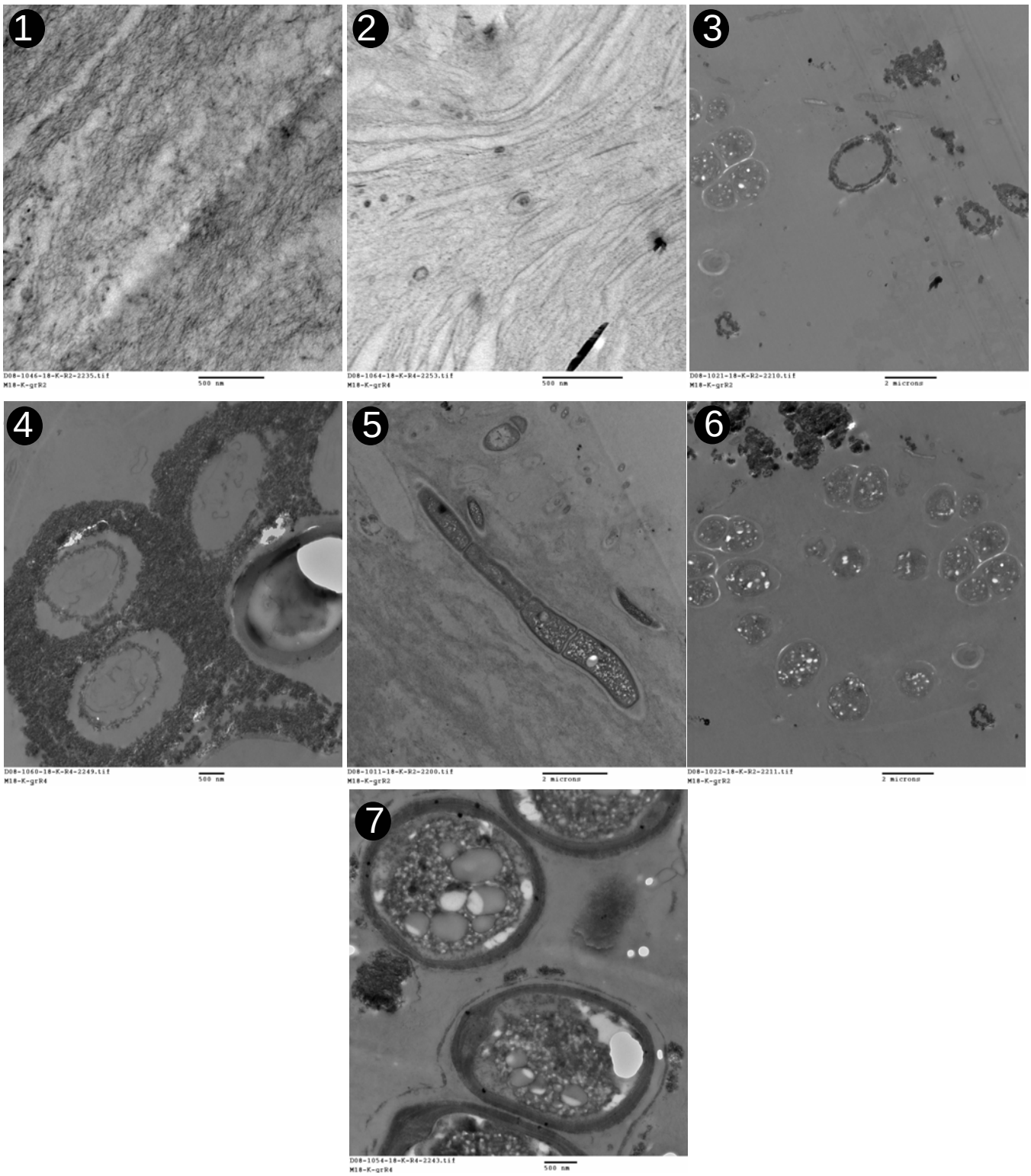

Plate 4a: microbial mat, Hassi Jerbi

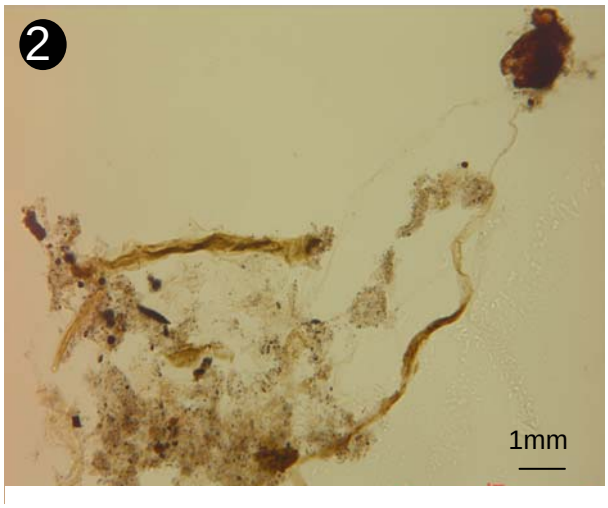

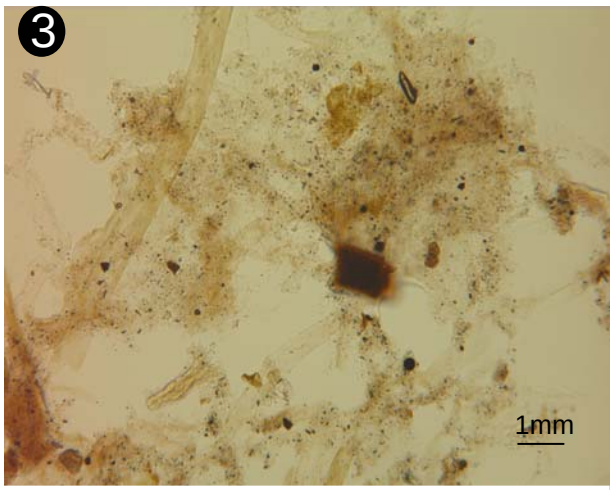

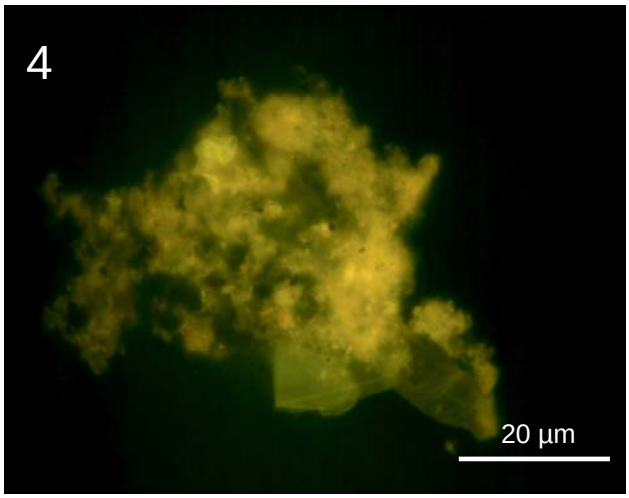

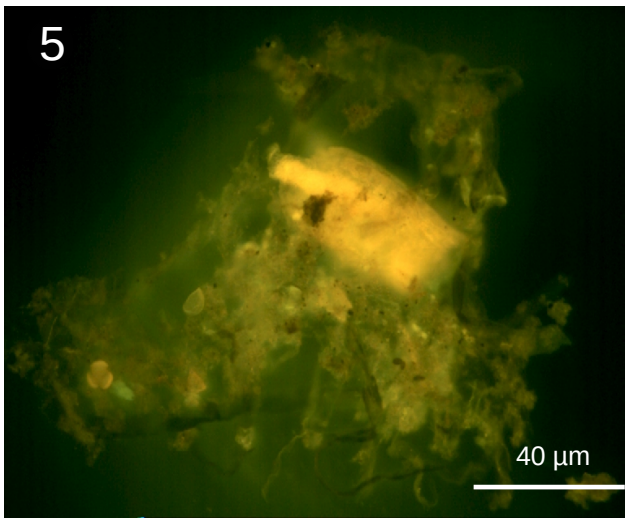

Plate 4b: microbial mat, Hassi Jerbi in TEM

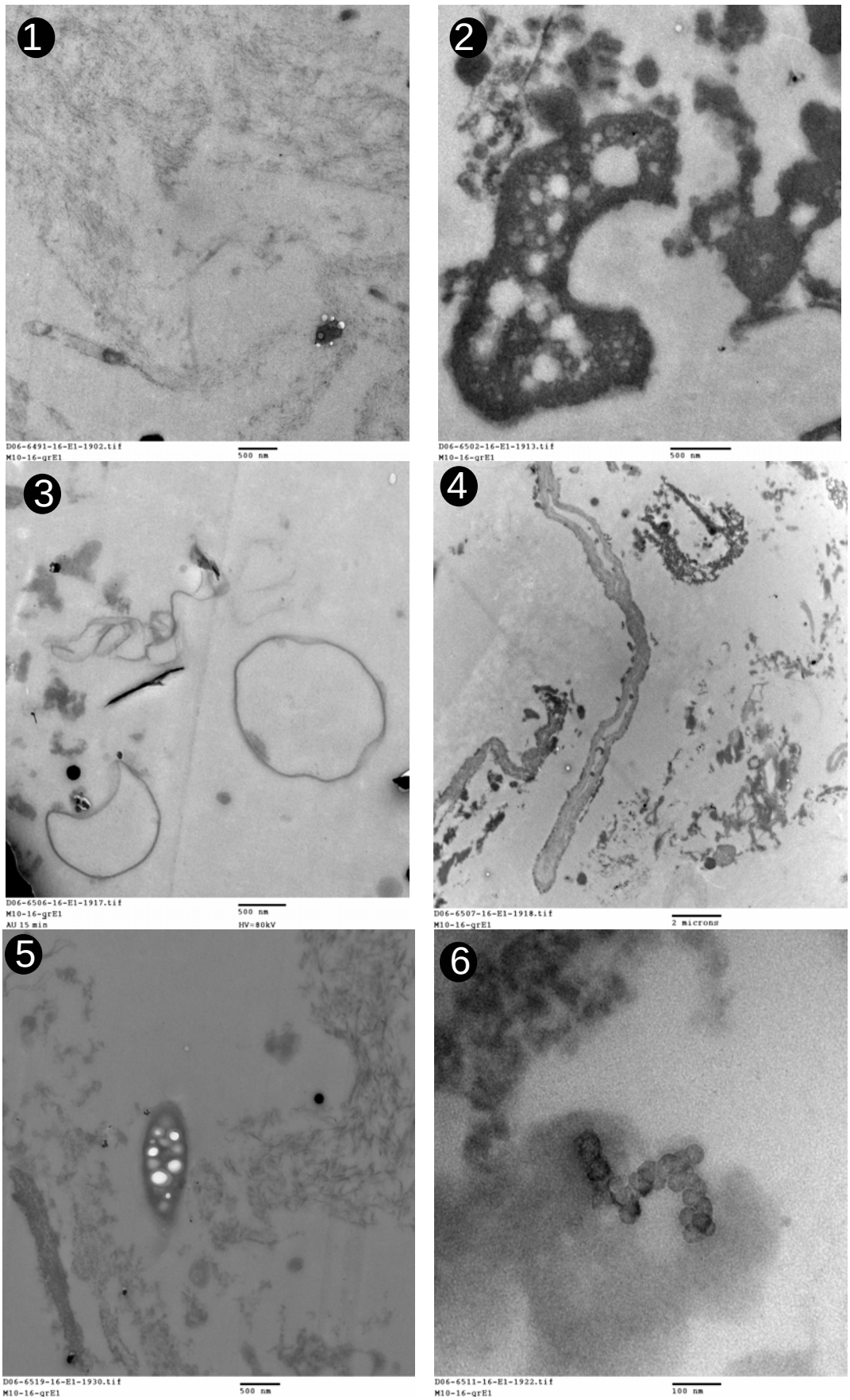

Plate 4c: microbial mat, Hassi Jerbi in AFM

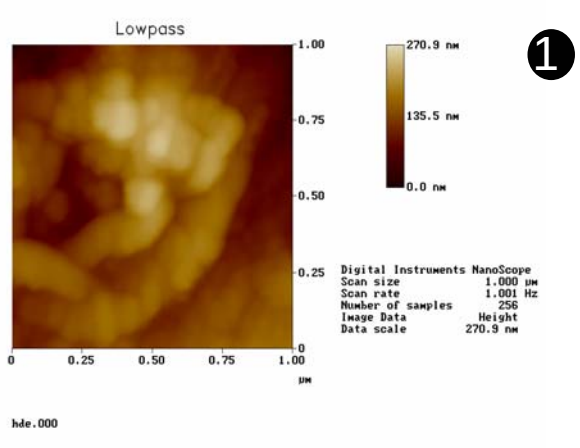

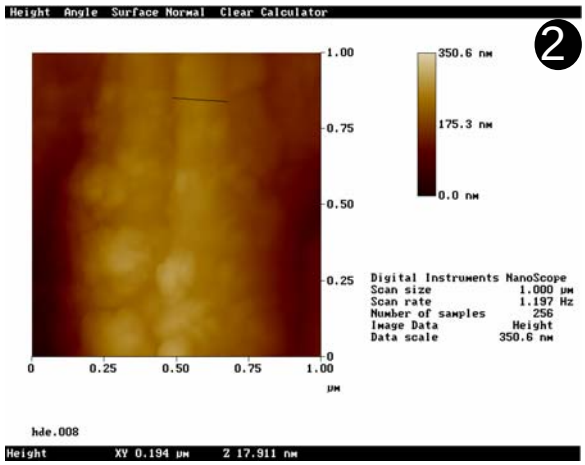

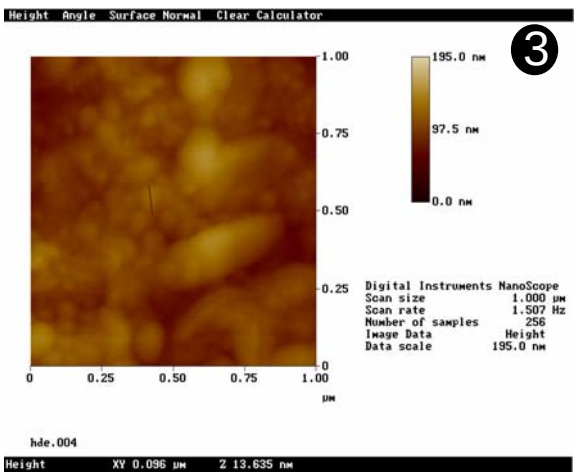

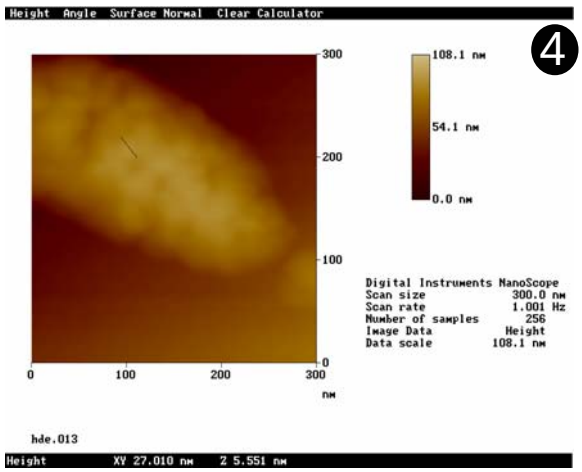

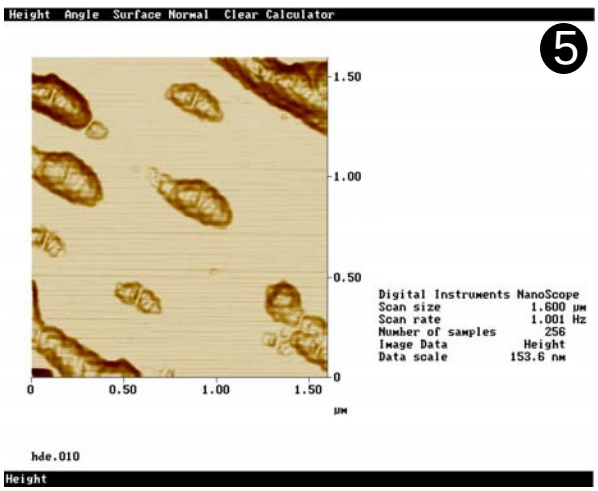

Plate 5a: continental sediments (Tanzania), Masoko lake

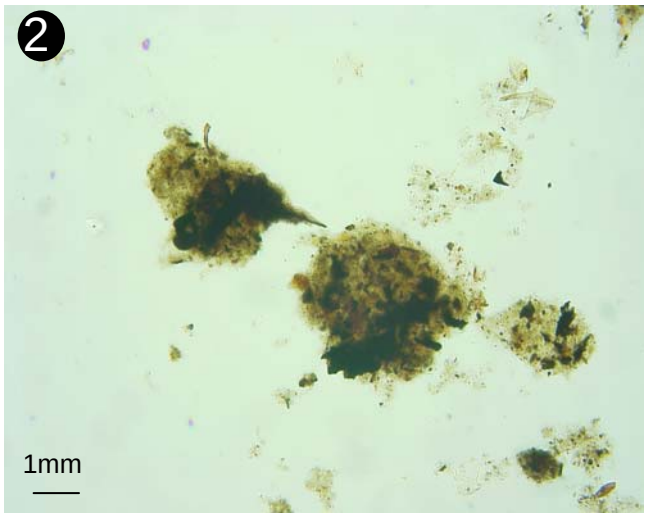

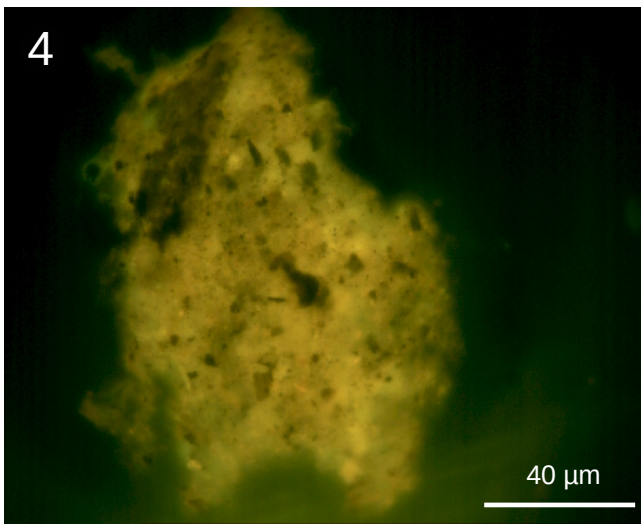

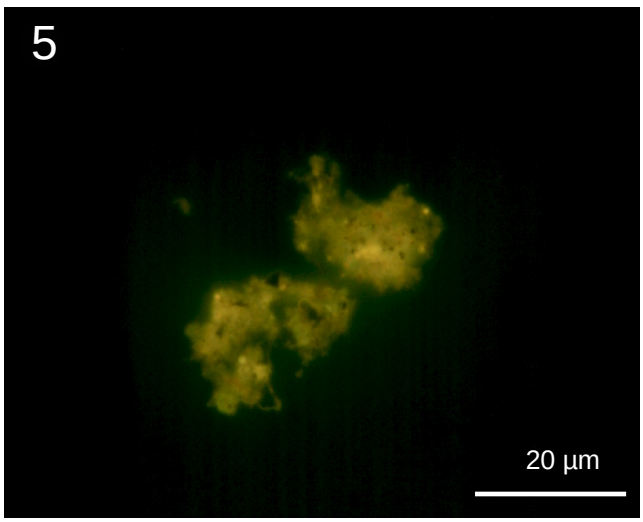

Plate 5b: continental sediments (Tanzania), Masoko lake in SEM

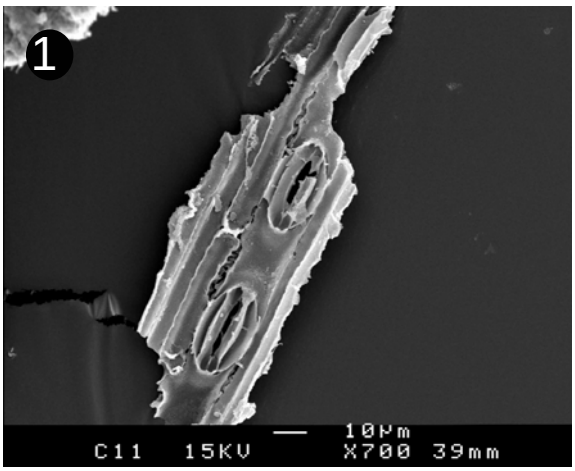

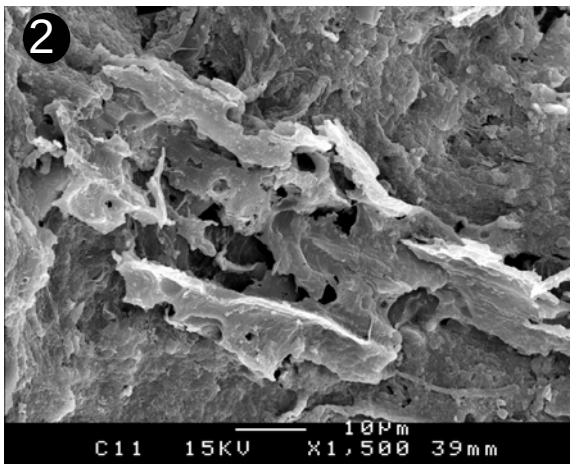

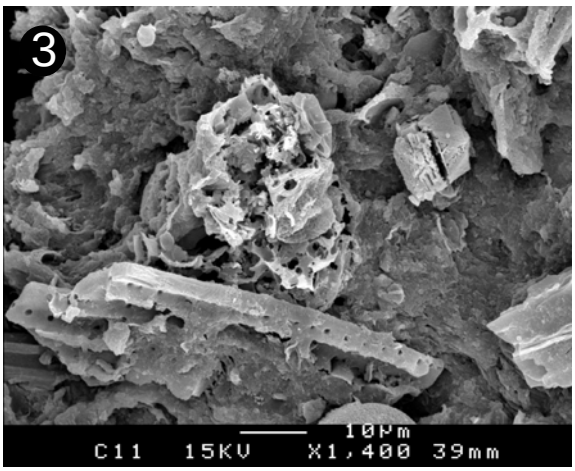

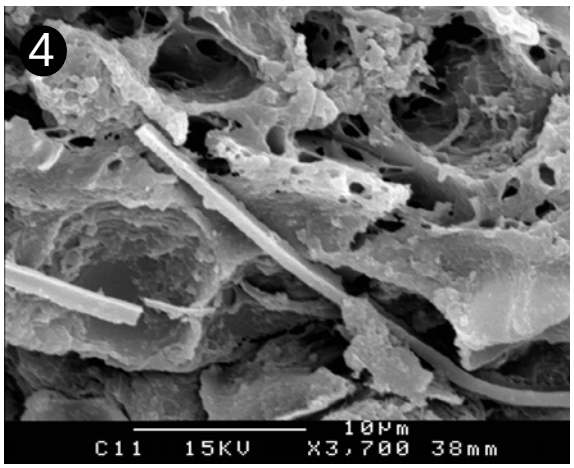

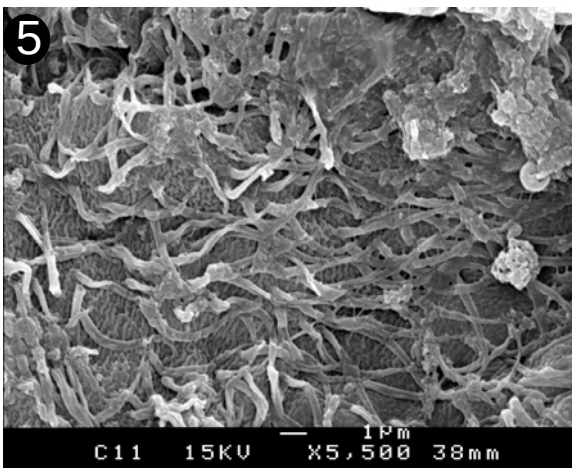

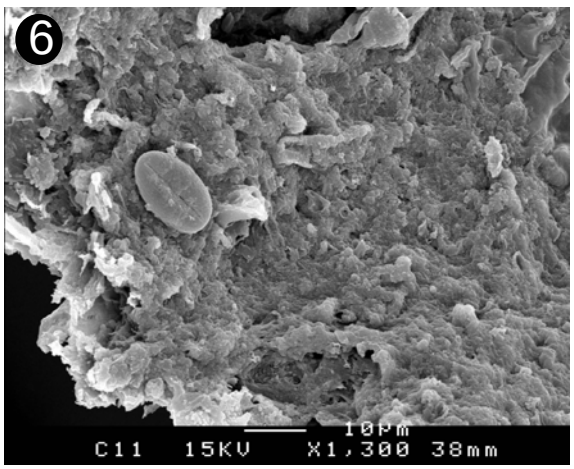

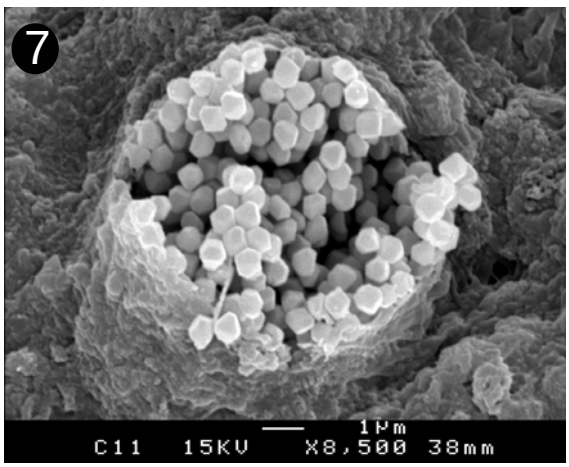

Plate 5c: continental sediments (Tanzania), Masoko lake in AFM

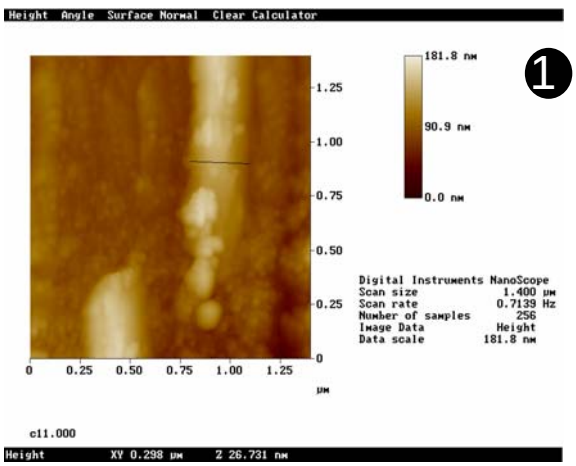

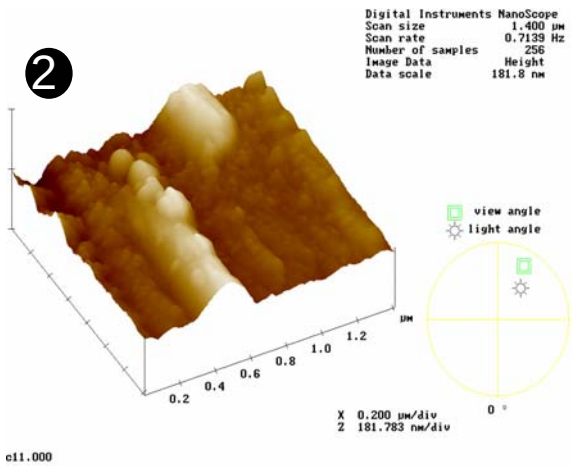

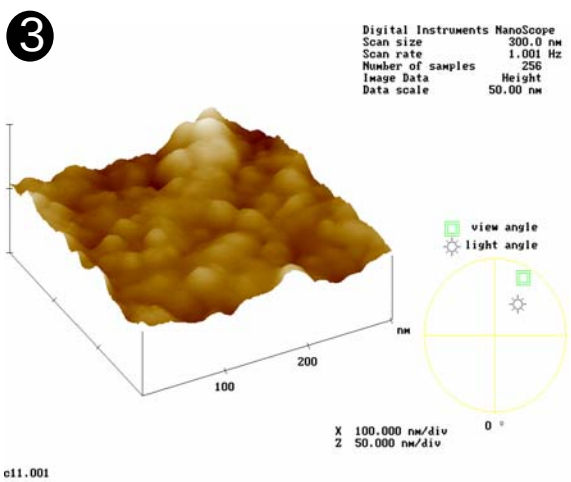

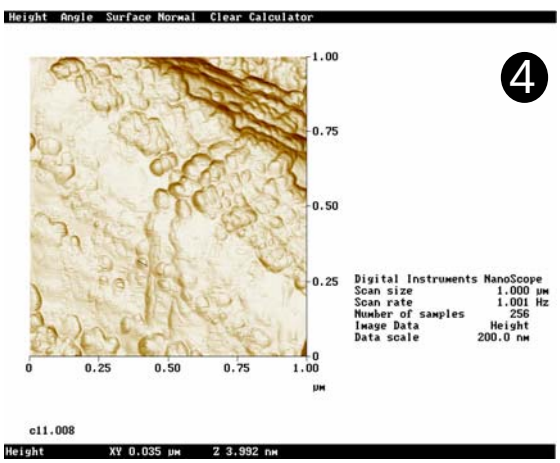

Plate 5d: continental sediments (Tanzania), Masoko lake in TEM

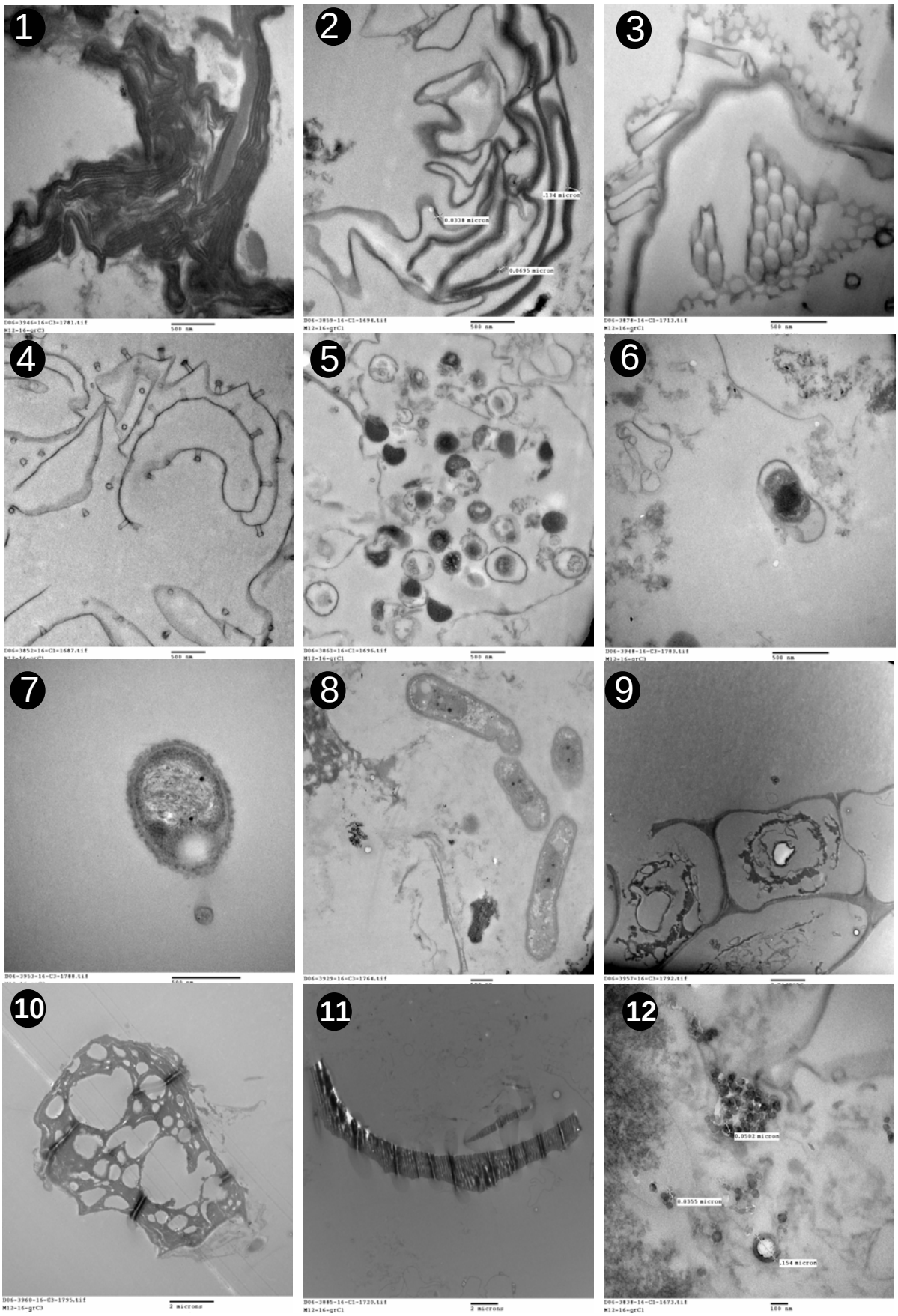

Plate 6a: continental sediments (Tanzania), peat bog

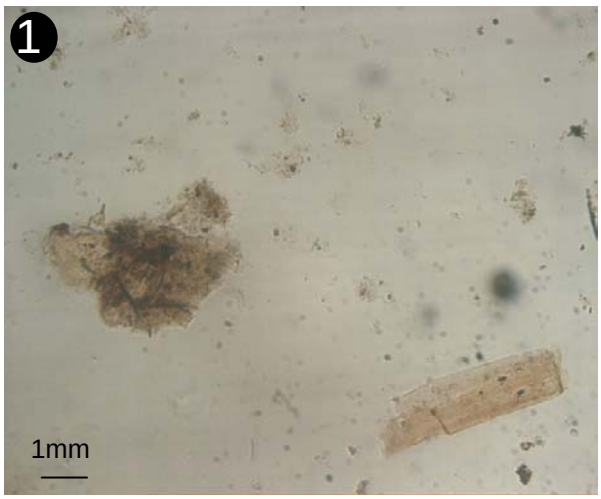

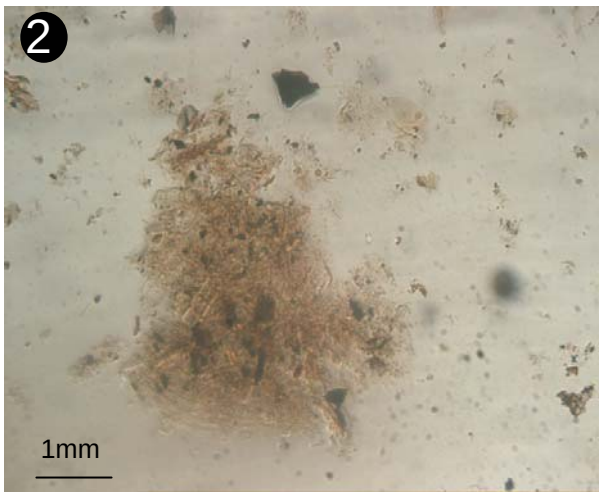

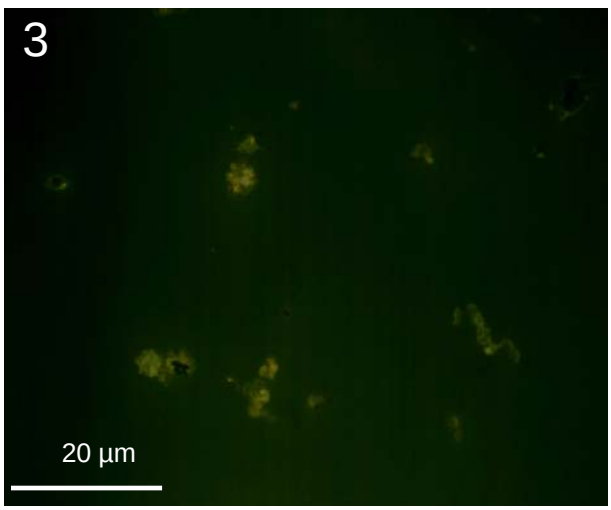

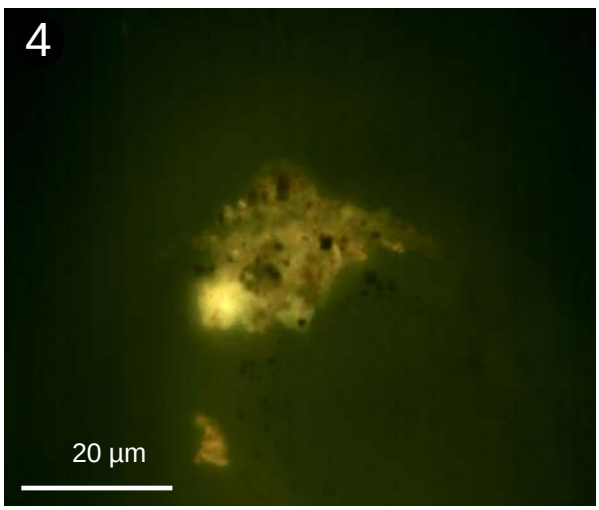

Plate 6b: continental sediments (Tanzania), peat bog in SEM

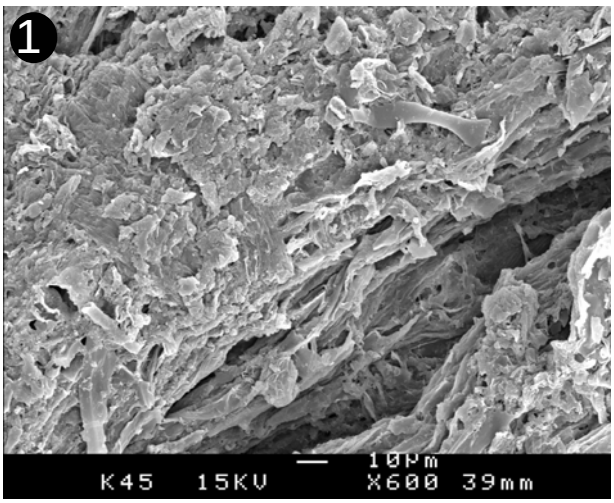

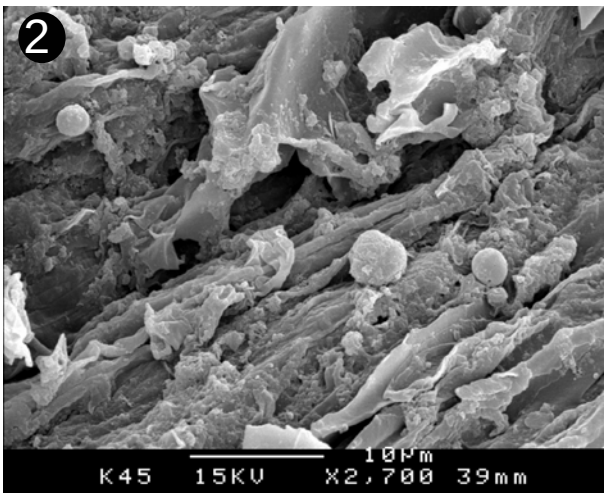

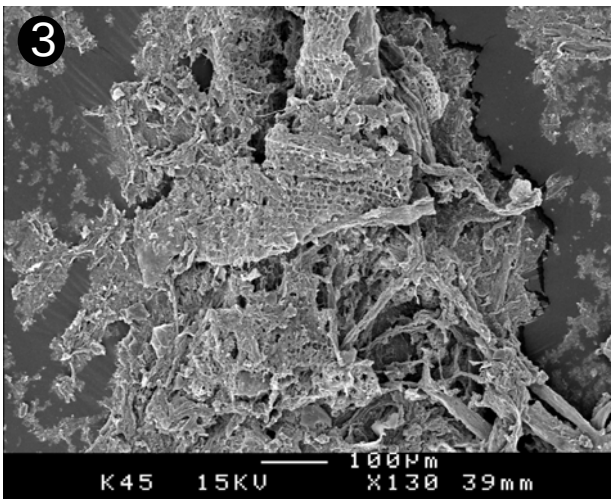

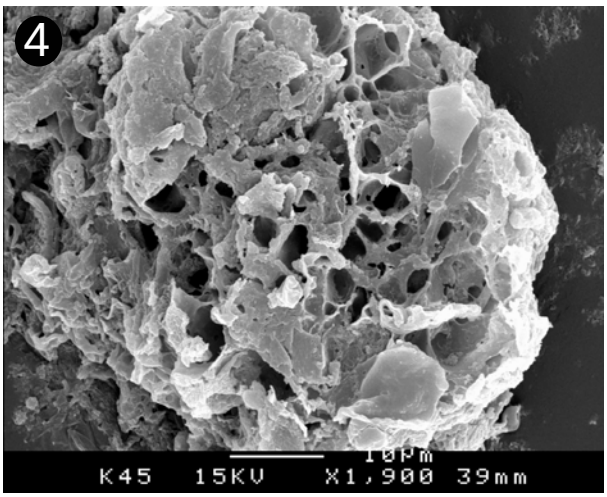

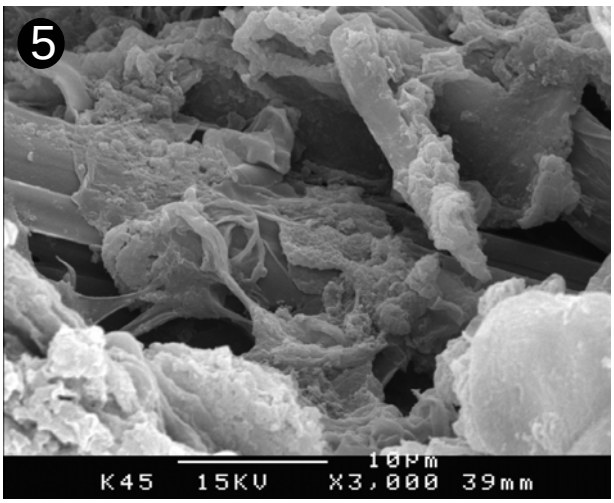

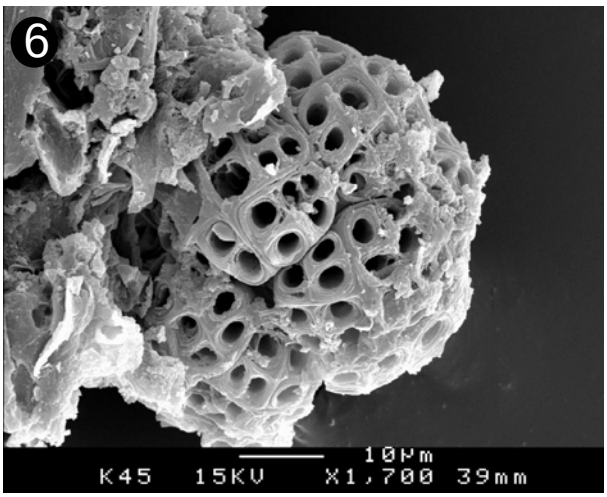

Plate 6c: continental sediments (Tanzania), peat bog in AFM

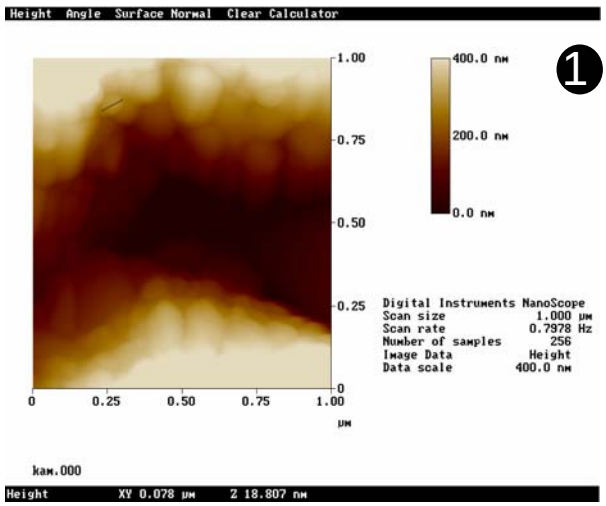

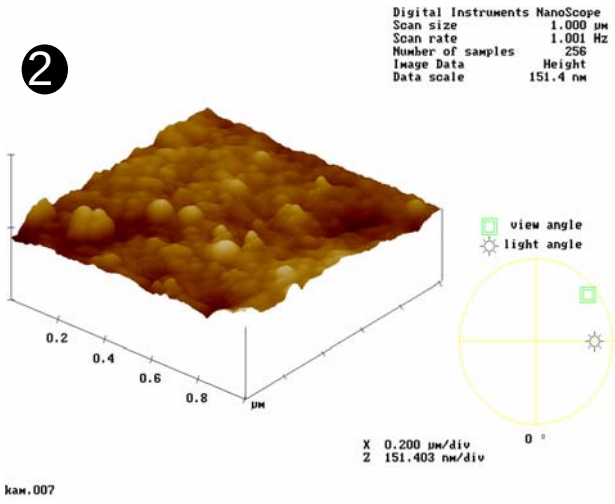

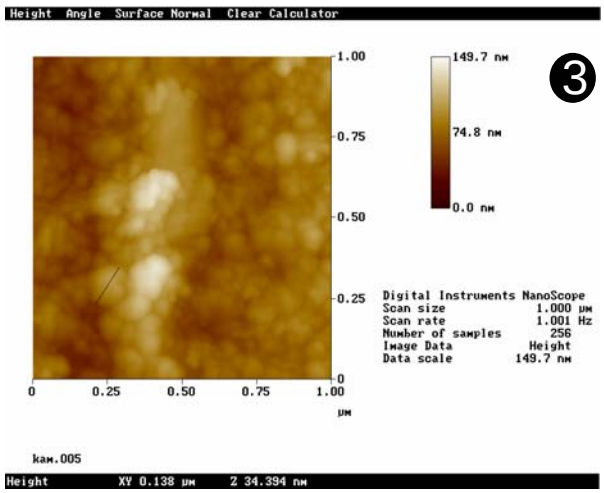

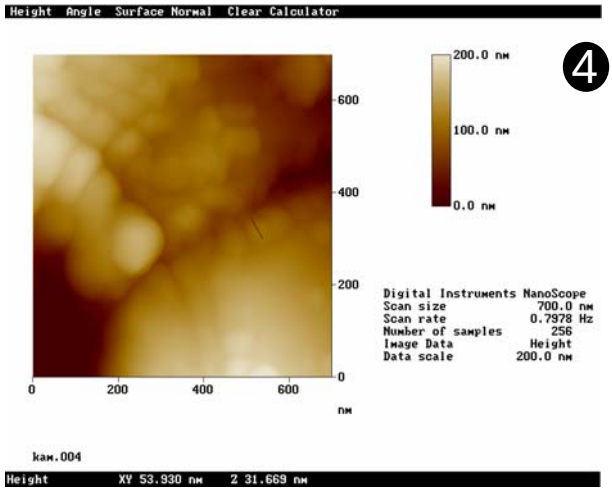

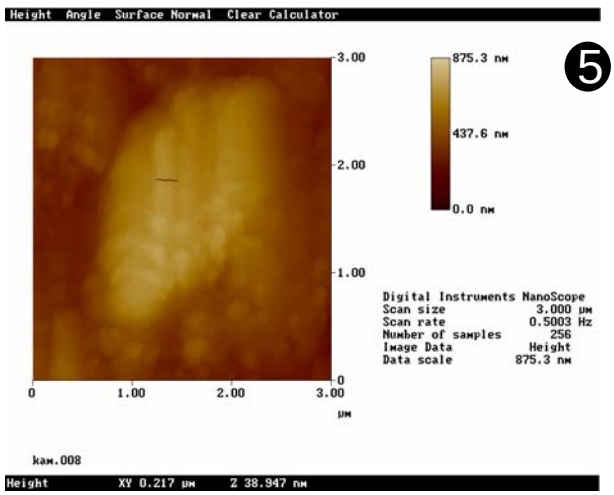

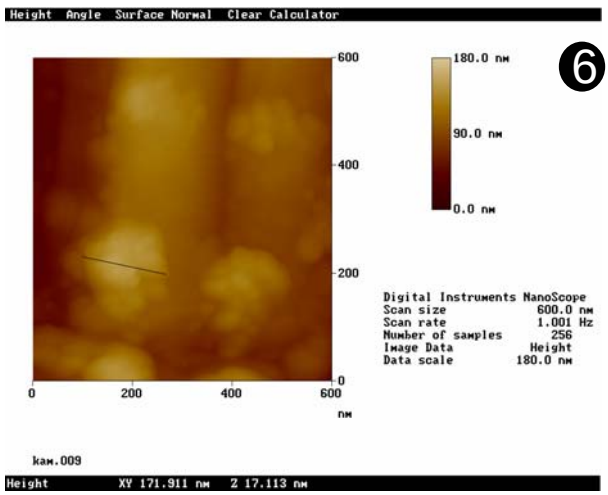

Plate 6d: continental sediments (Tanzania), peat bog in TEM

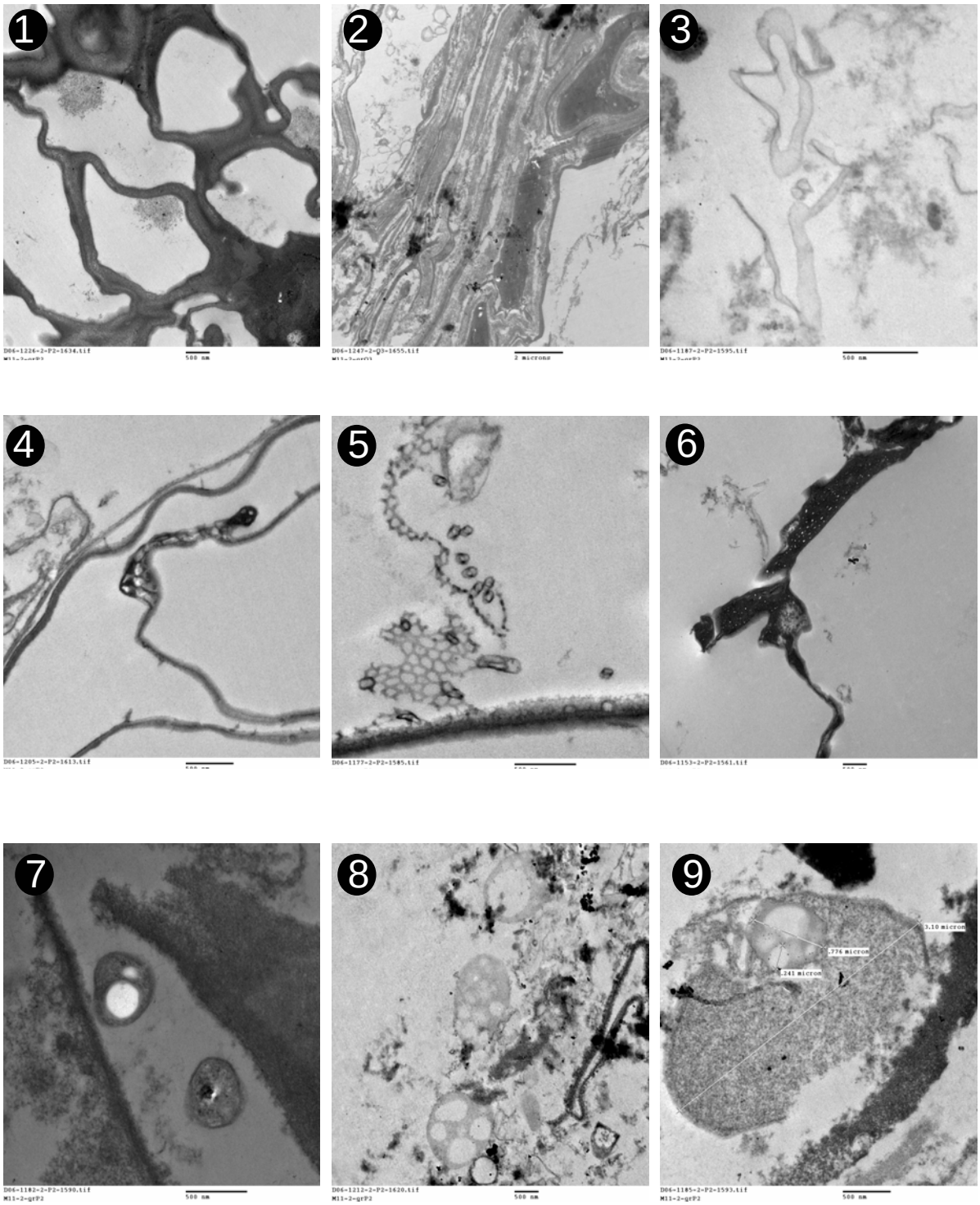

Plate 7a: sulfuroxidizing bacteria after acid treatment

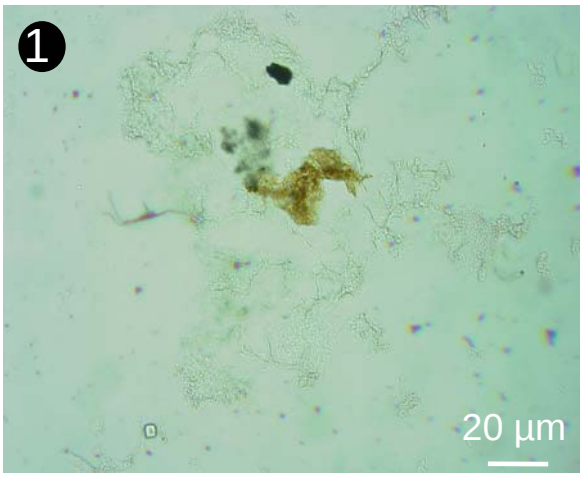

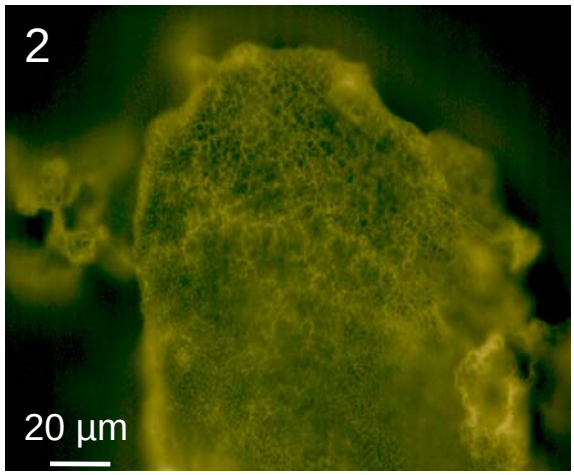

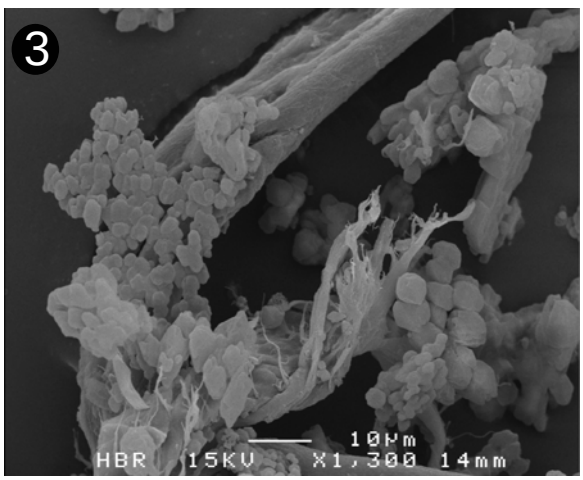

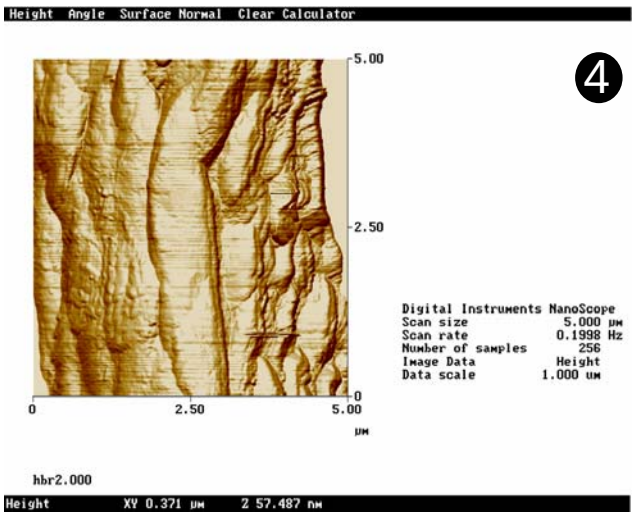

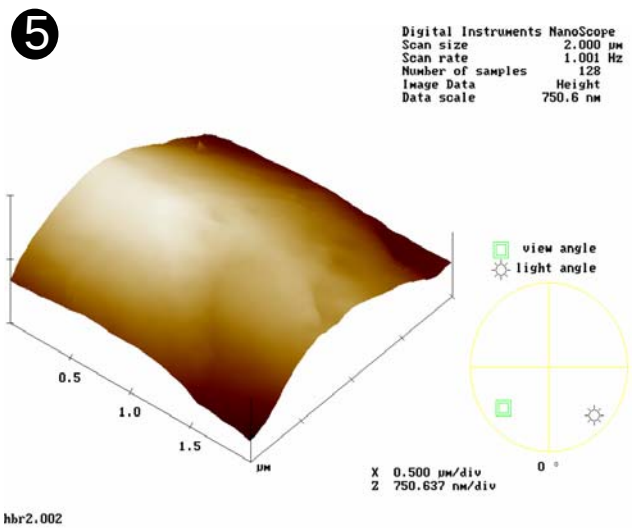

Plate 7b: sulfuroxidizing bacteria after acid treatment (coccoids)

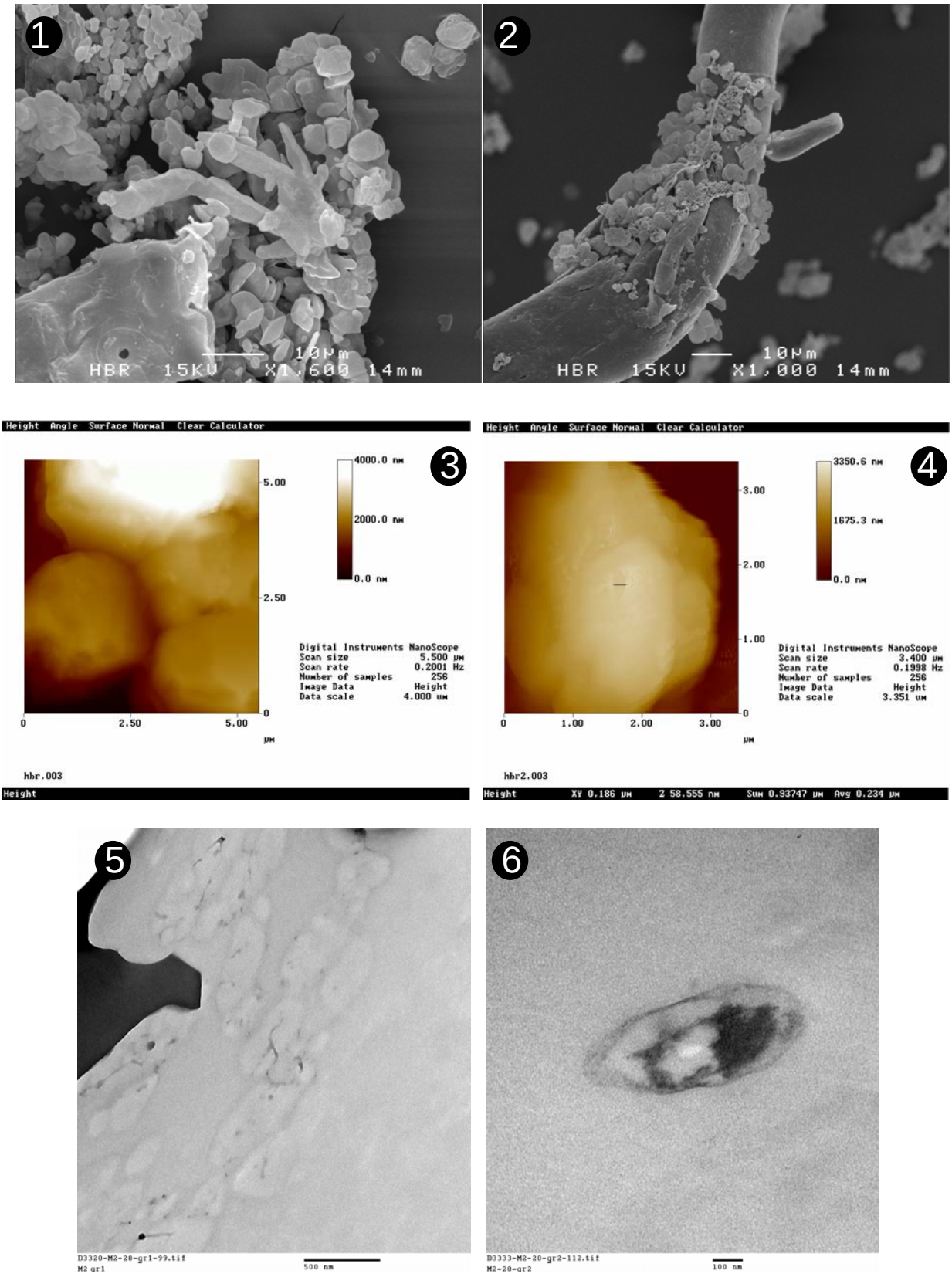

Plate 7c: sulfuroxidizing bacteria after acid treatment (EPS)

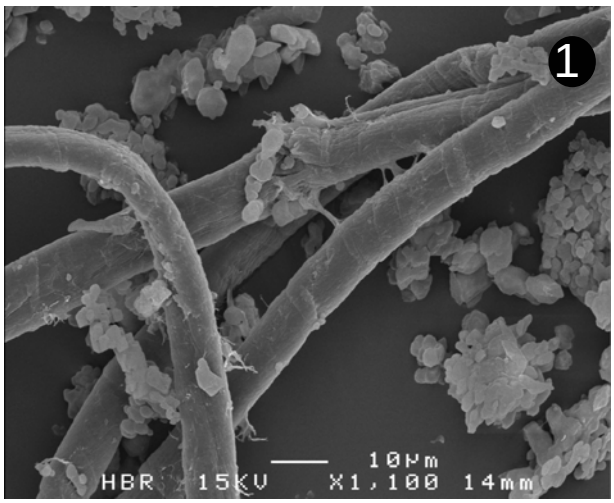

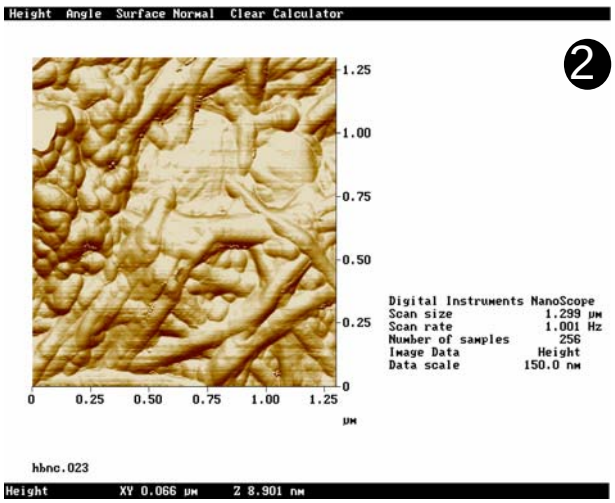

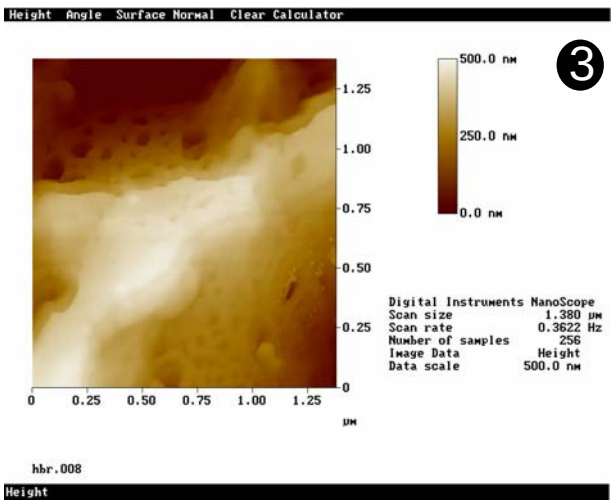

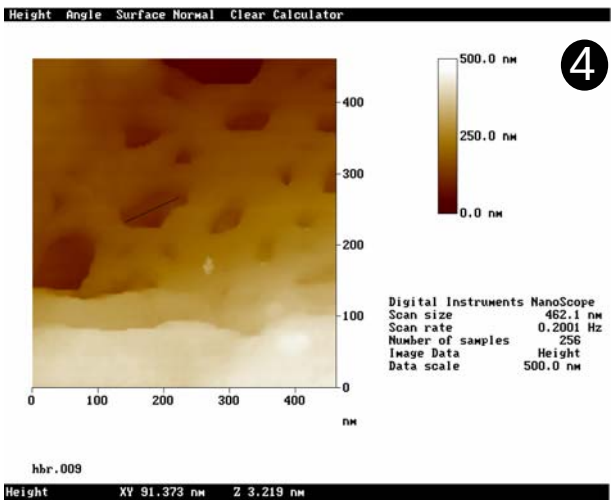

Plate 7d: cyanobacterial biofilm after acid treatment

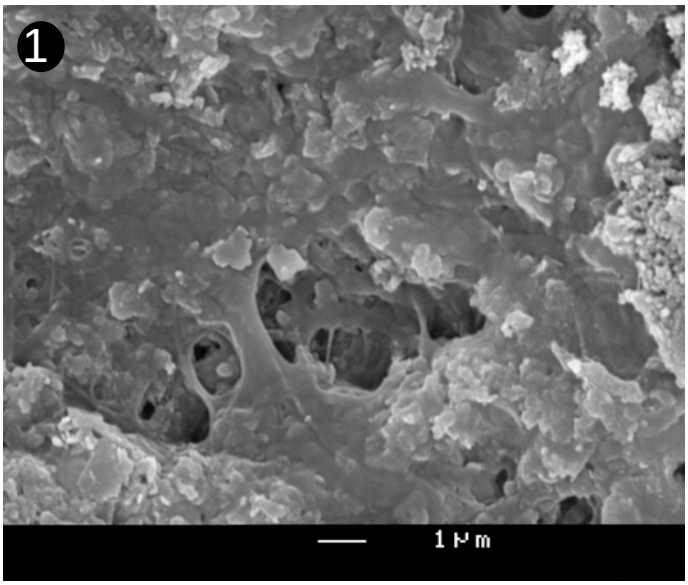

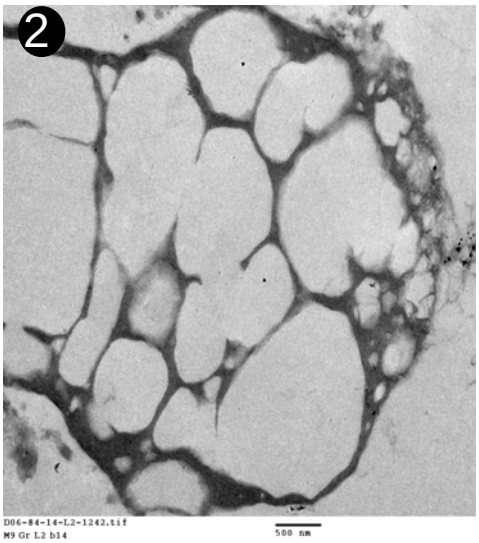

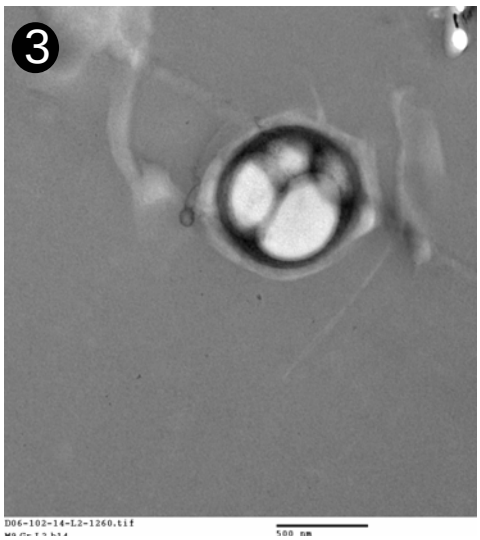

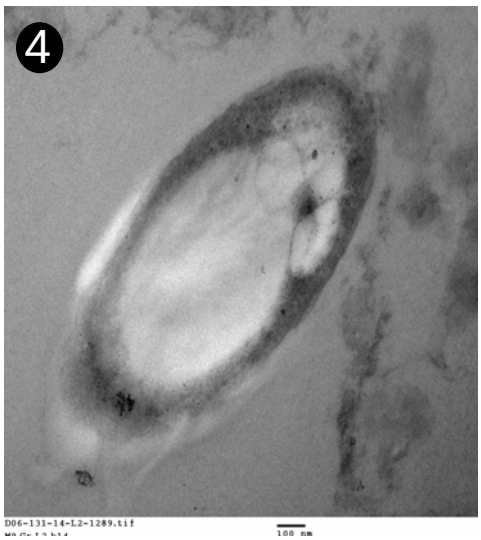

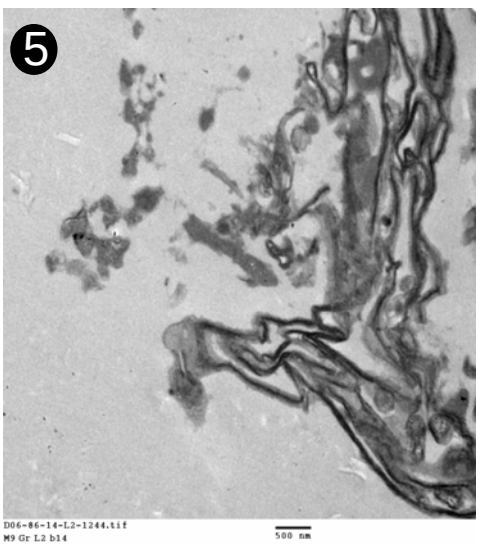

Plate 7e: algal mat & continental sediments after acid treatment

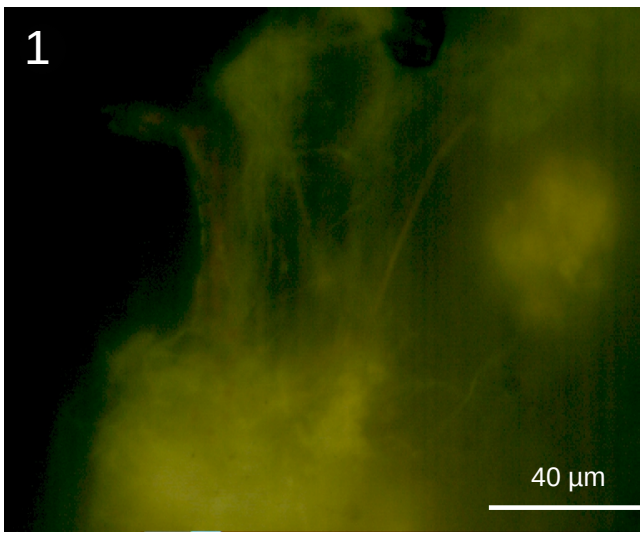

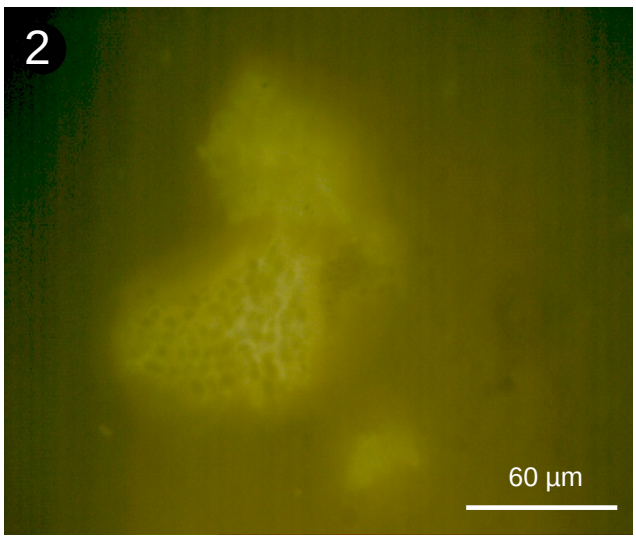

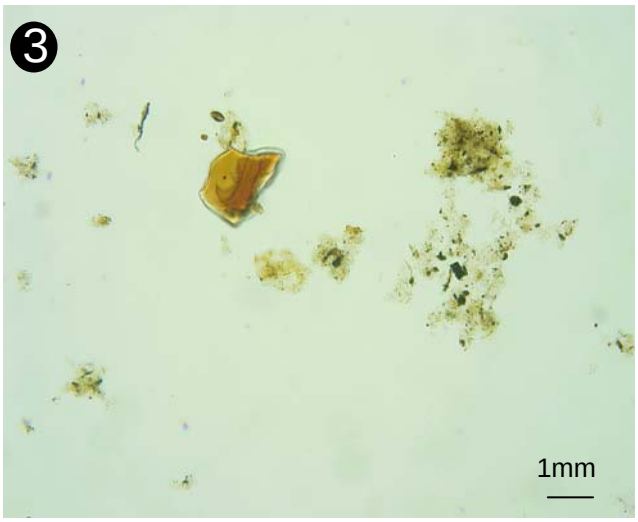

Plate 8a: the Monterey Formation N35 (bulk rock)

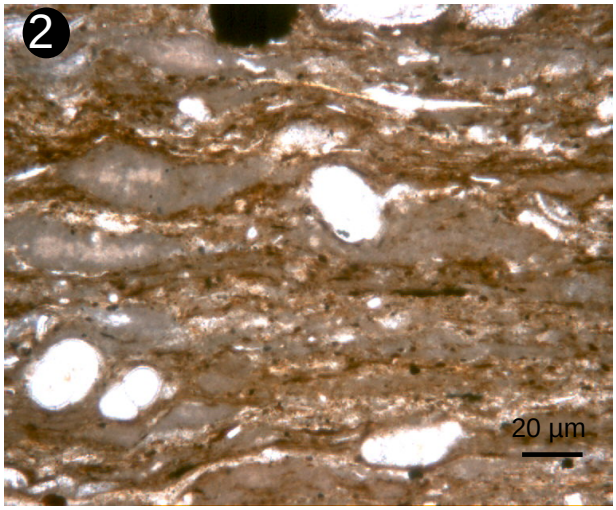

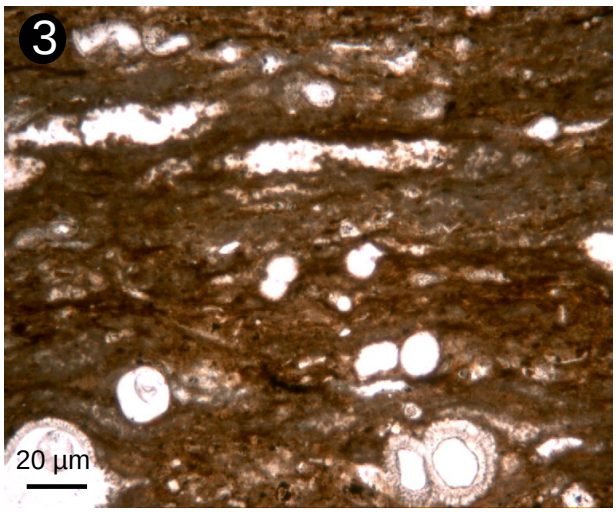

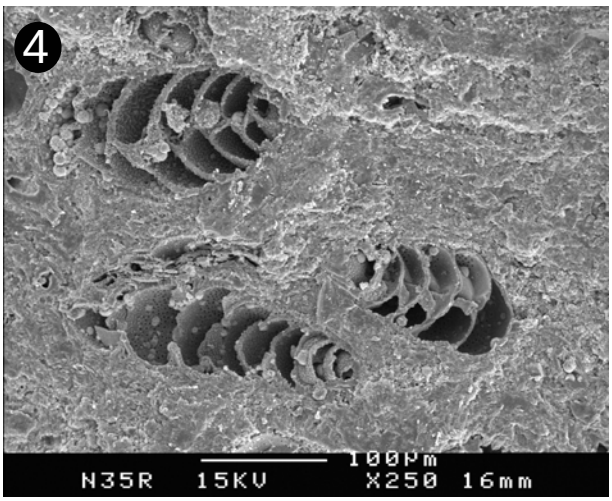

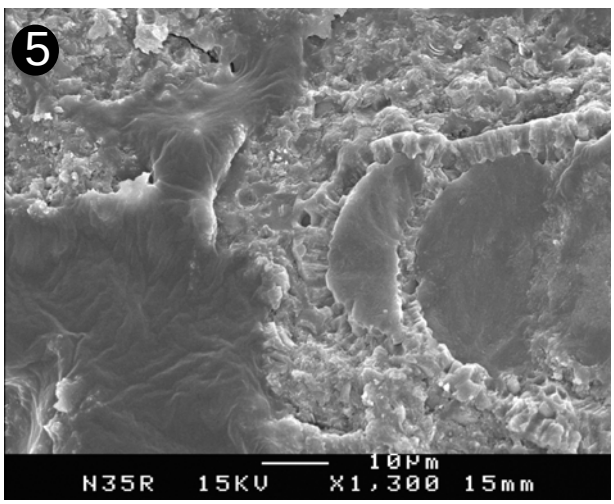

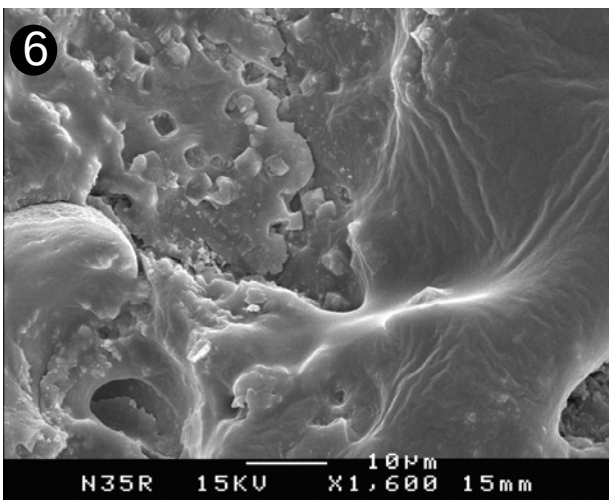

Plate 8b: the Monterey Formation N35 (kerogen)

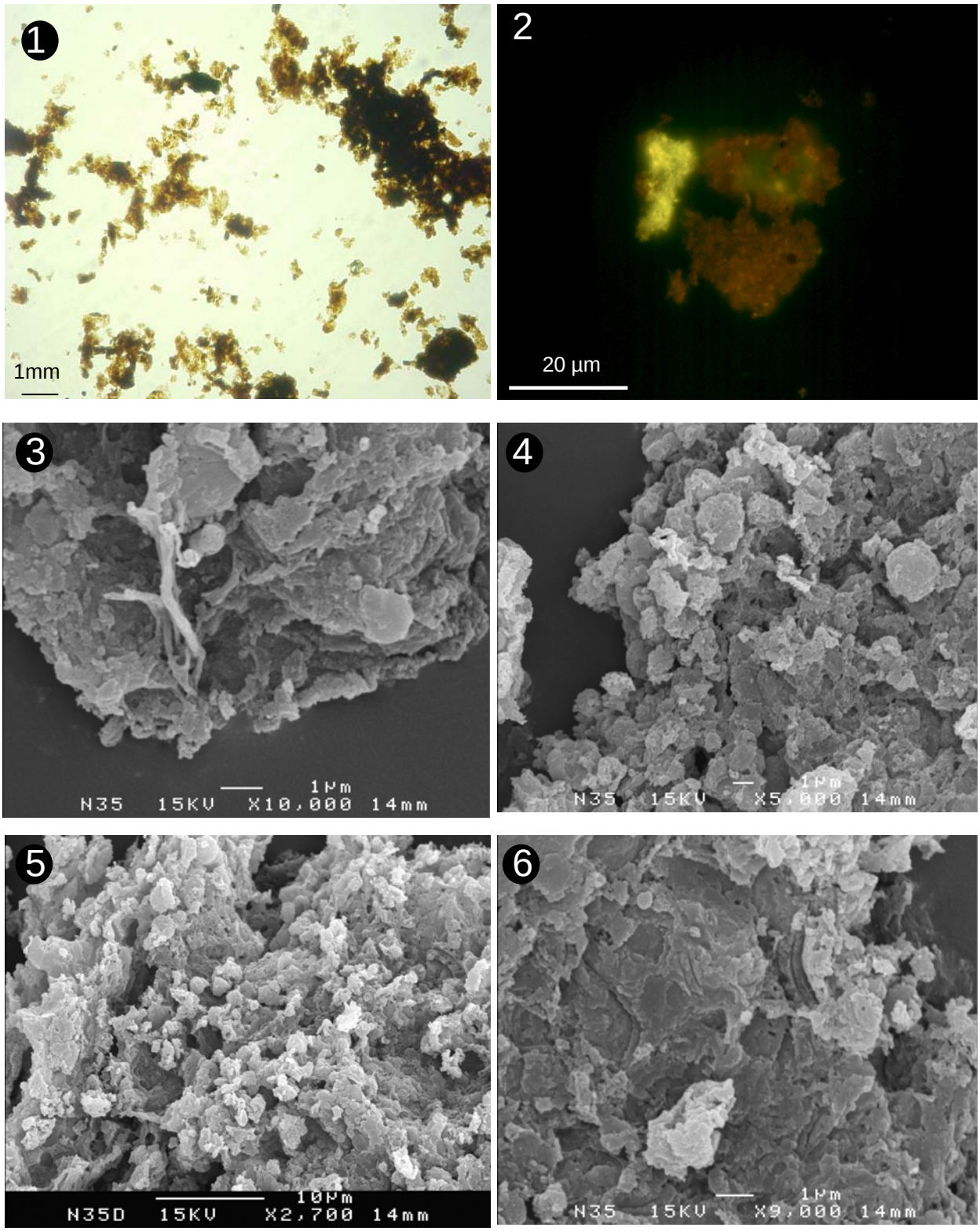

Plate 8c: the Monterey Formation N35 (kerogen) in AFM

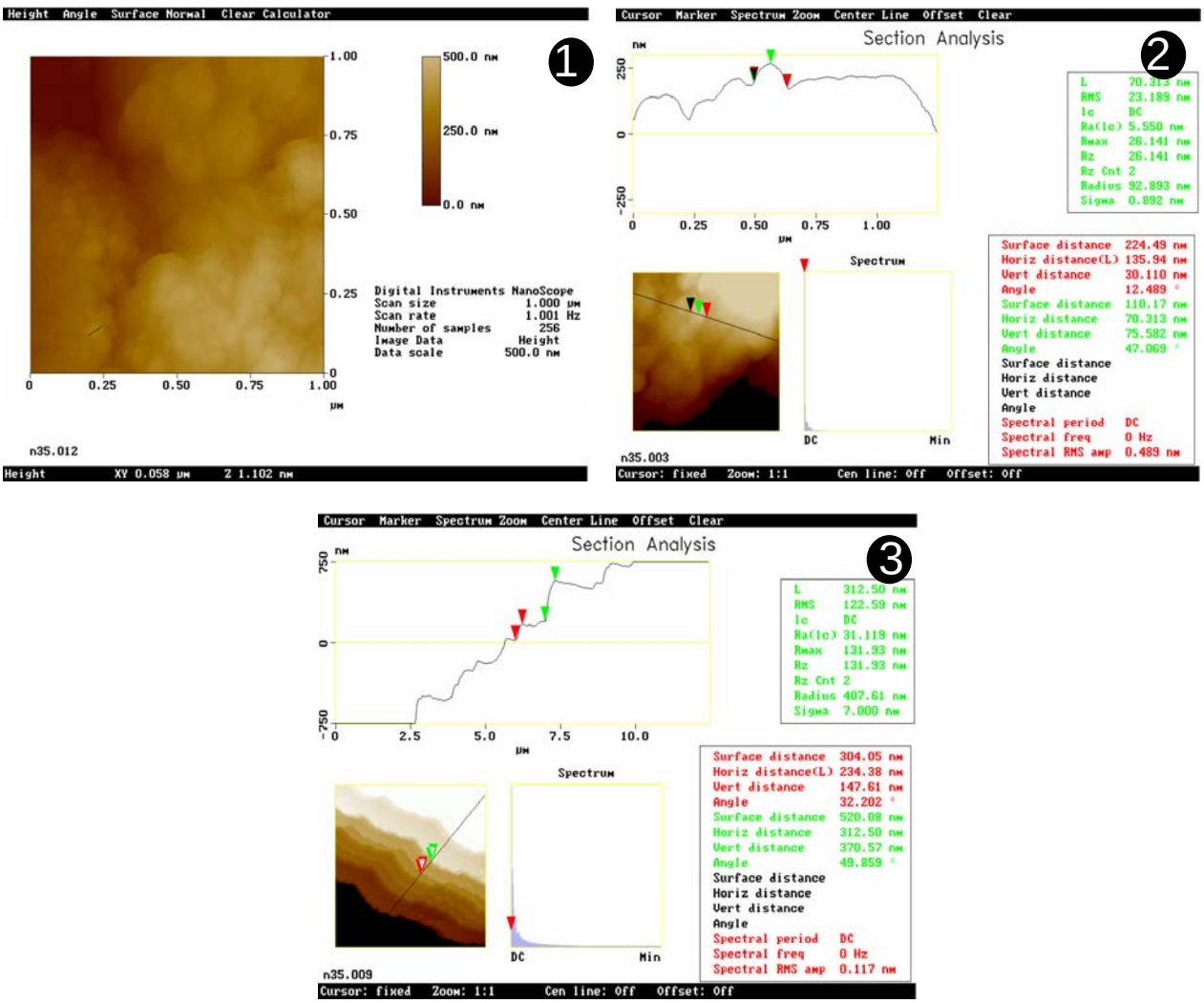

Plate 8d: the Monterey Formation N35 (kerogen) in TEM

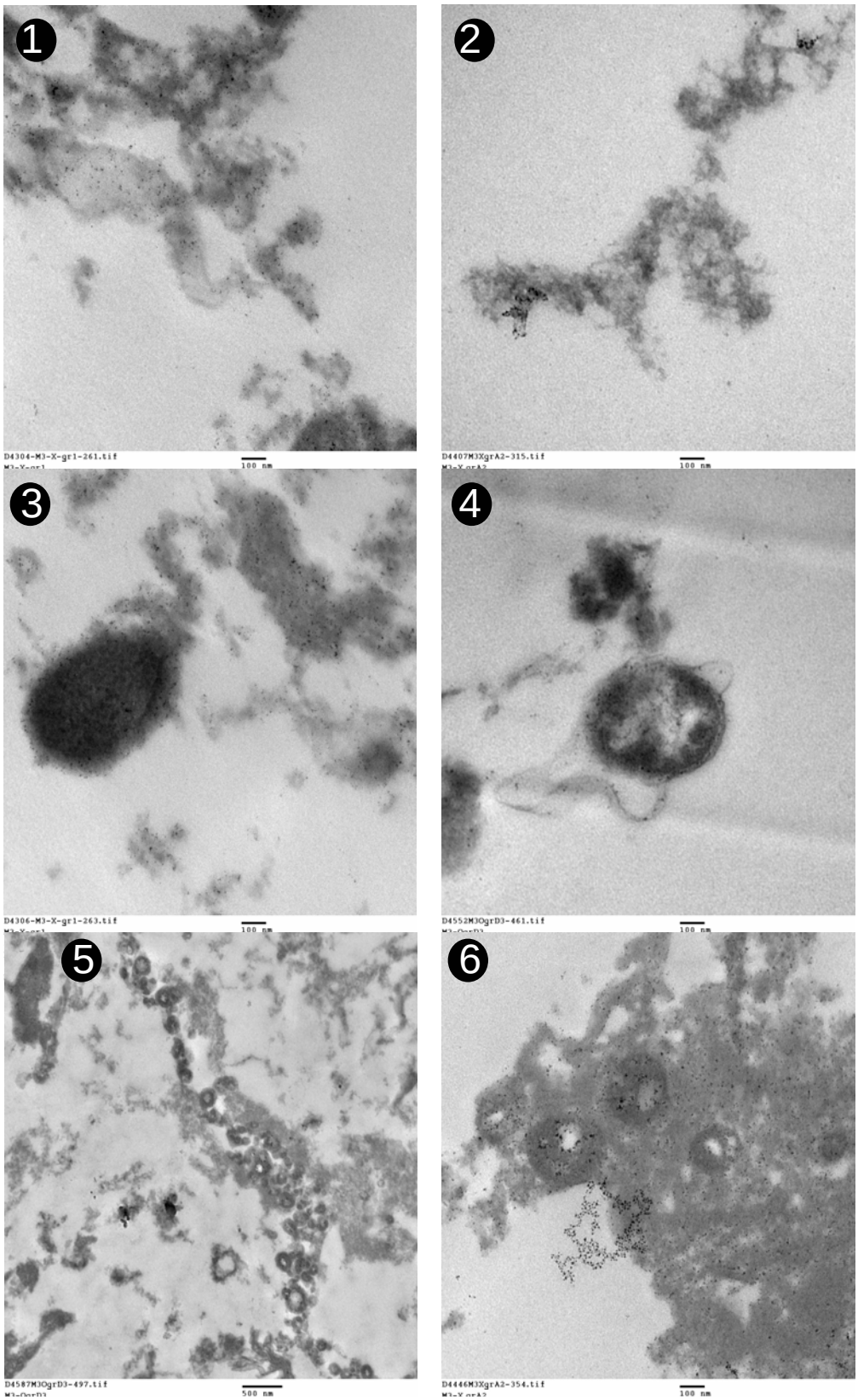

Plate 9: the Monterey Formation N12 (kerogen)

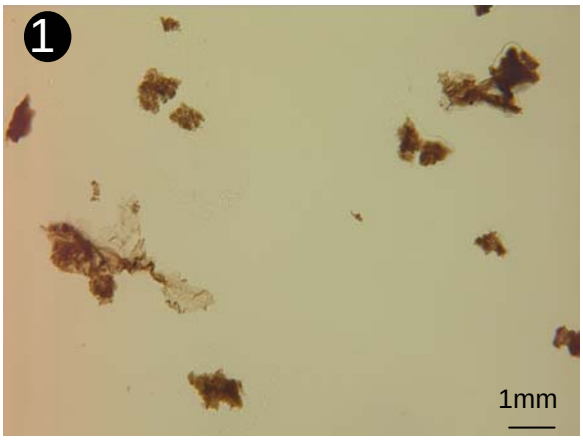

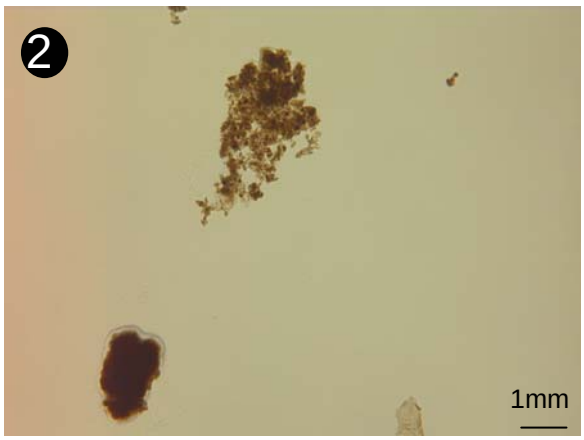

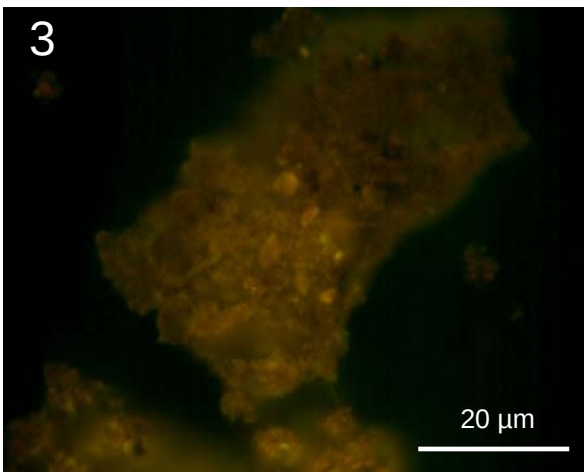

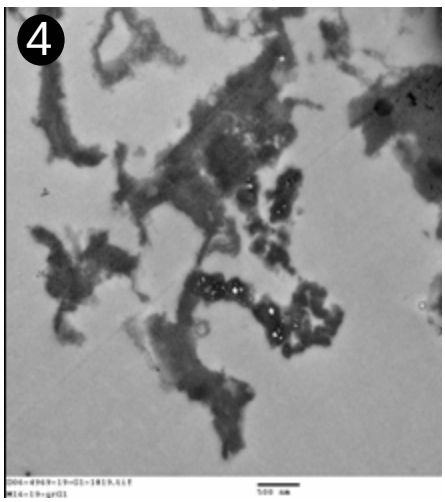

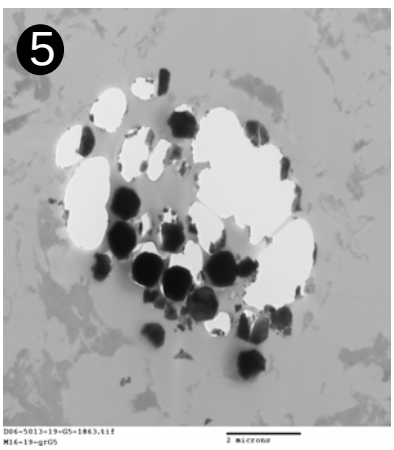

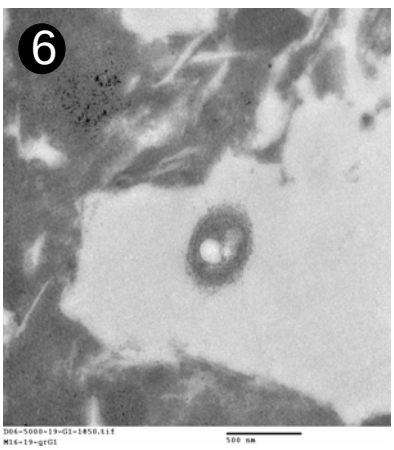

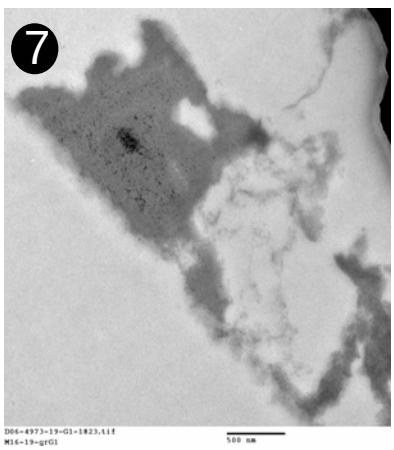

Plate 10: the Monterey Formation N23 (kerogen)

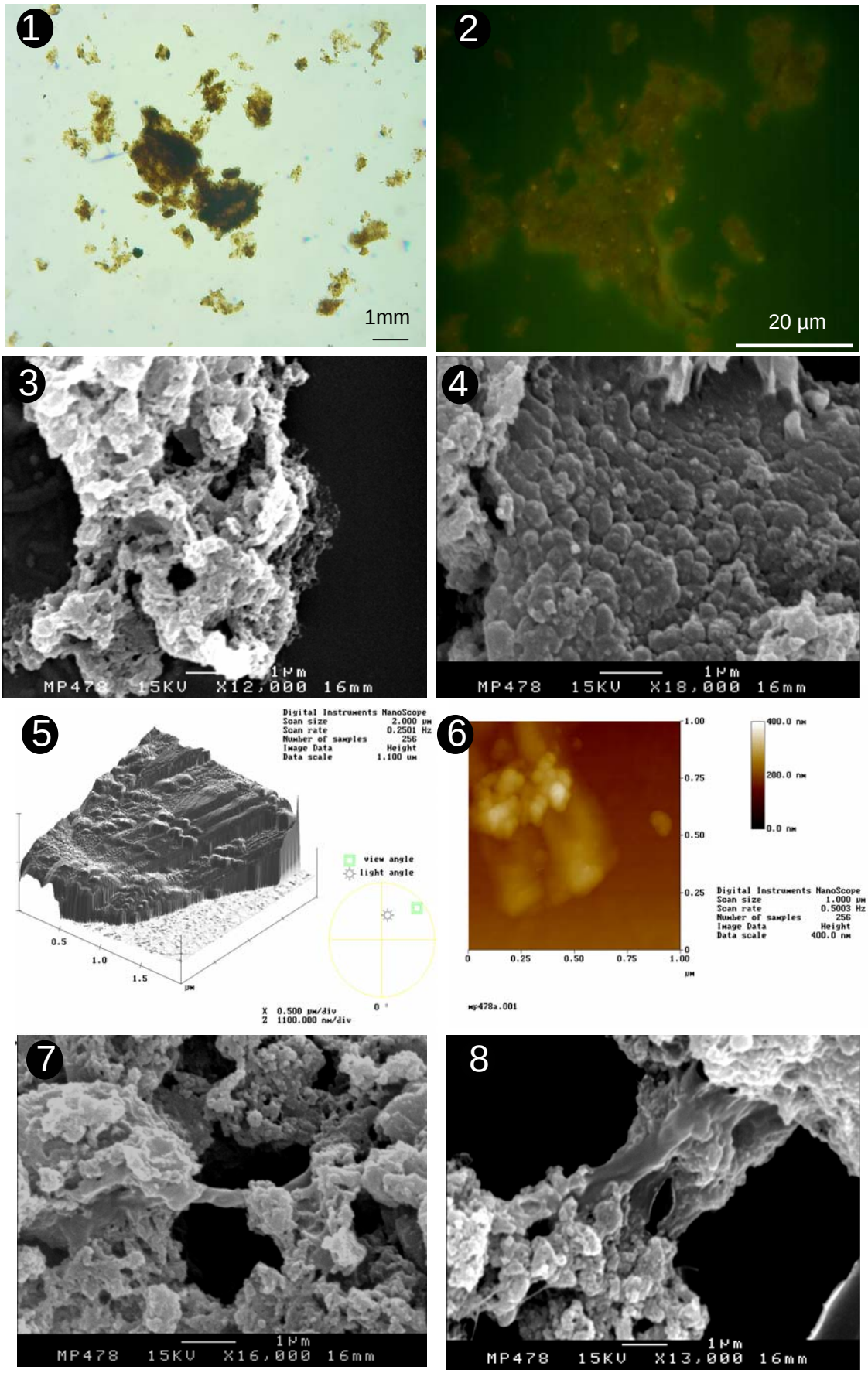

Plate 11a: Kimmeridgian laminites

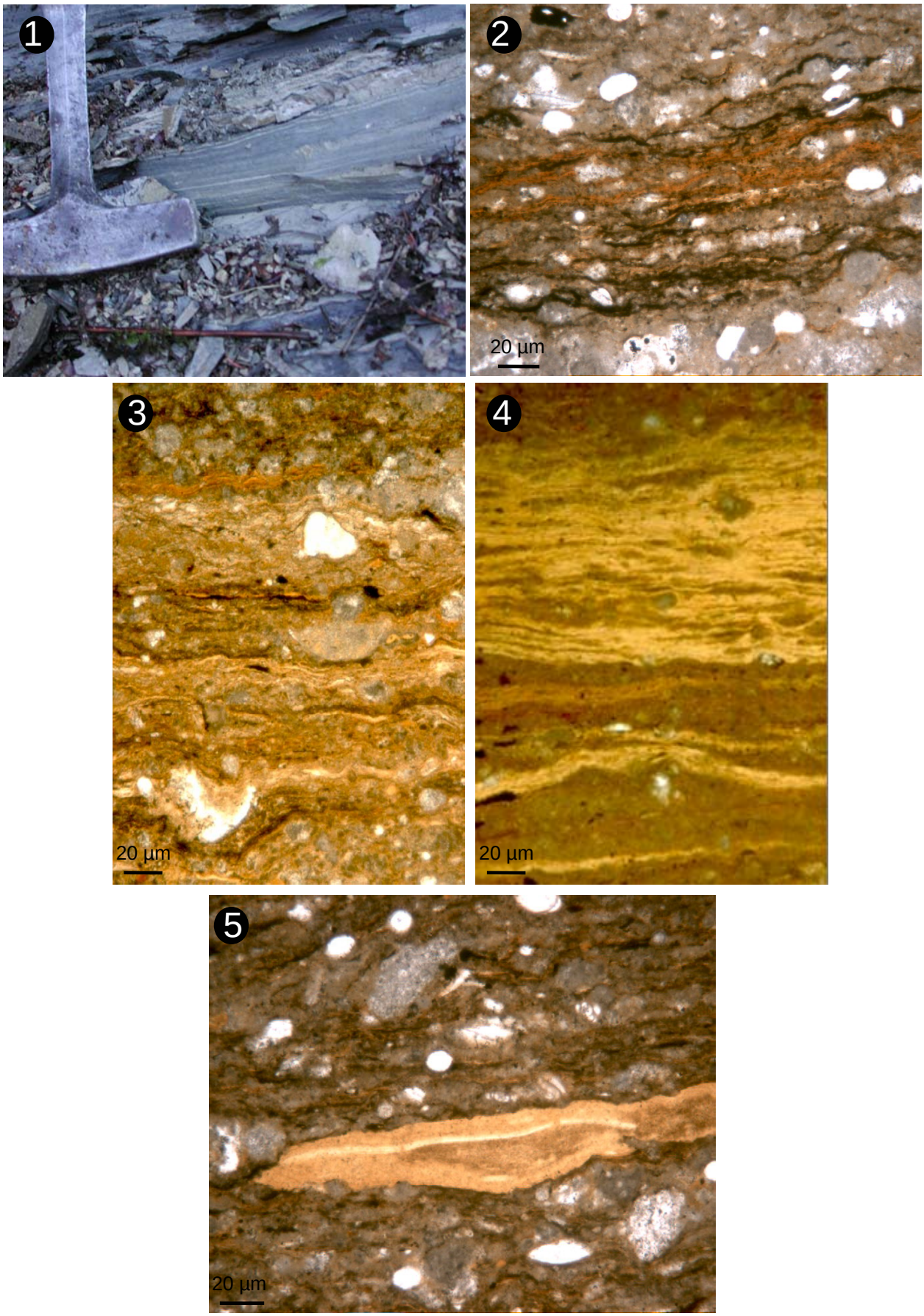

Plate 11b: Kimmeridgian laminites

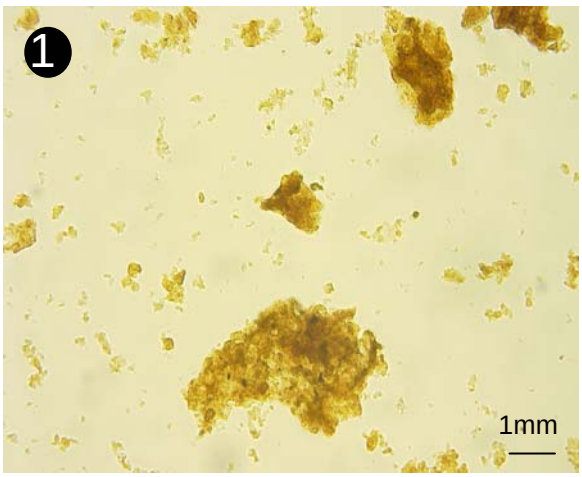

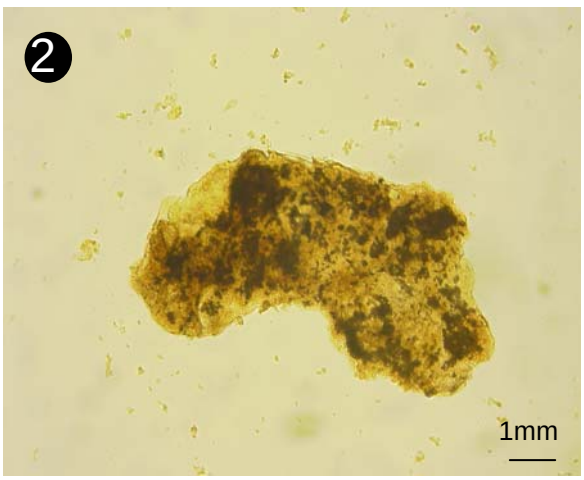

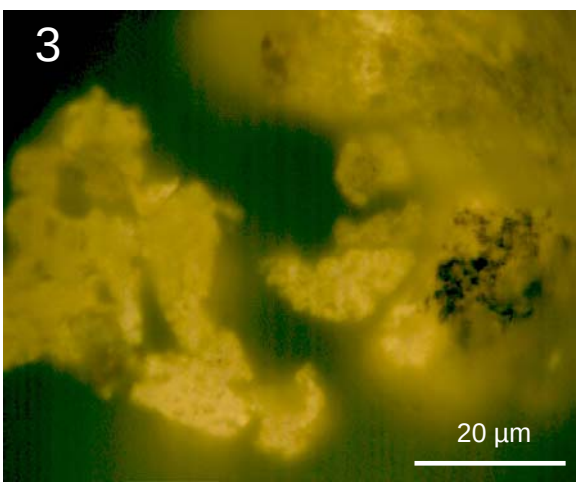

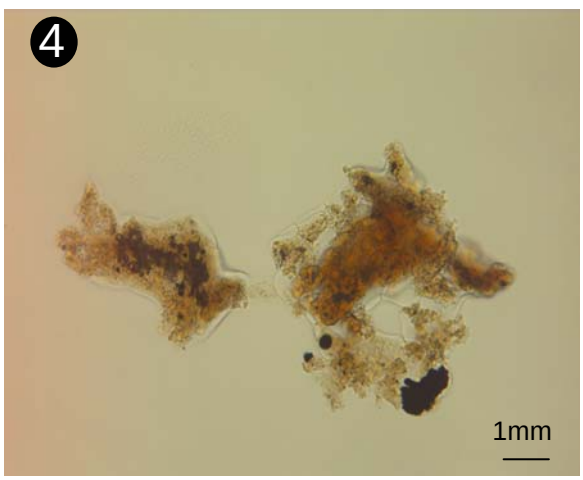

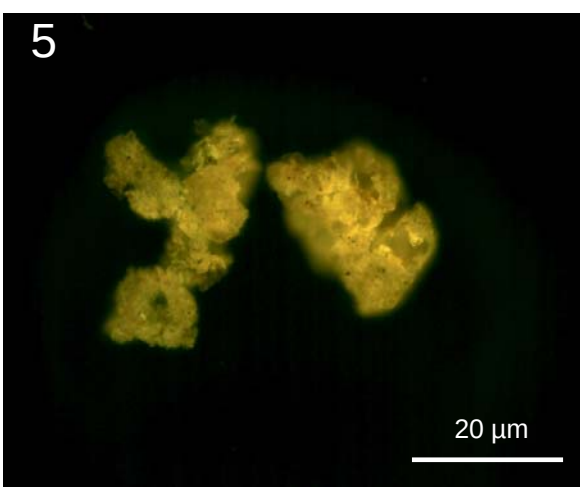

Plate 11c: Kimmeridgian laminites MP5

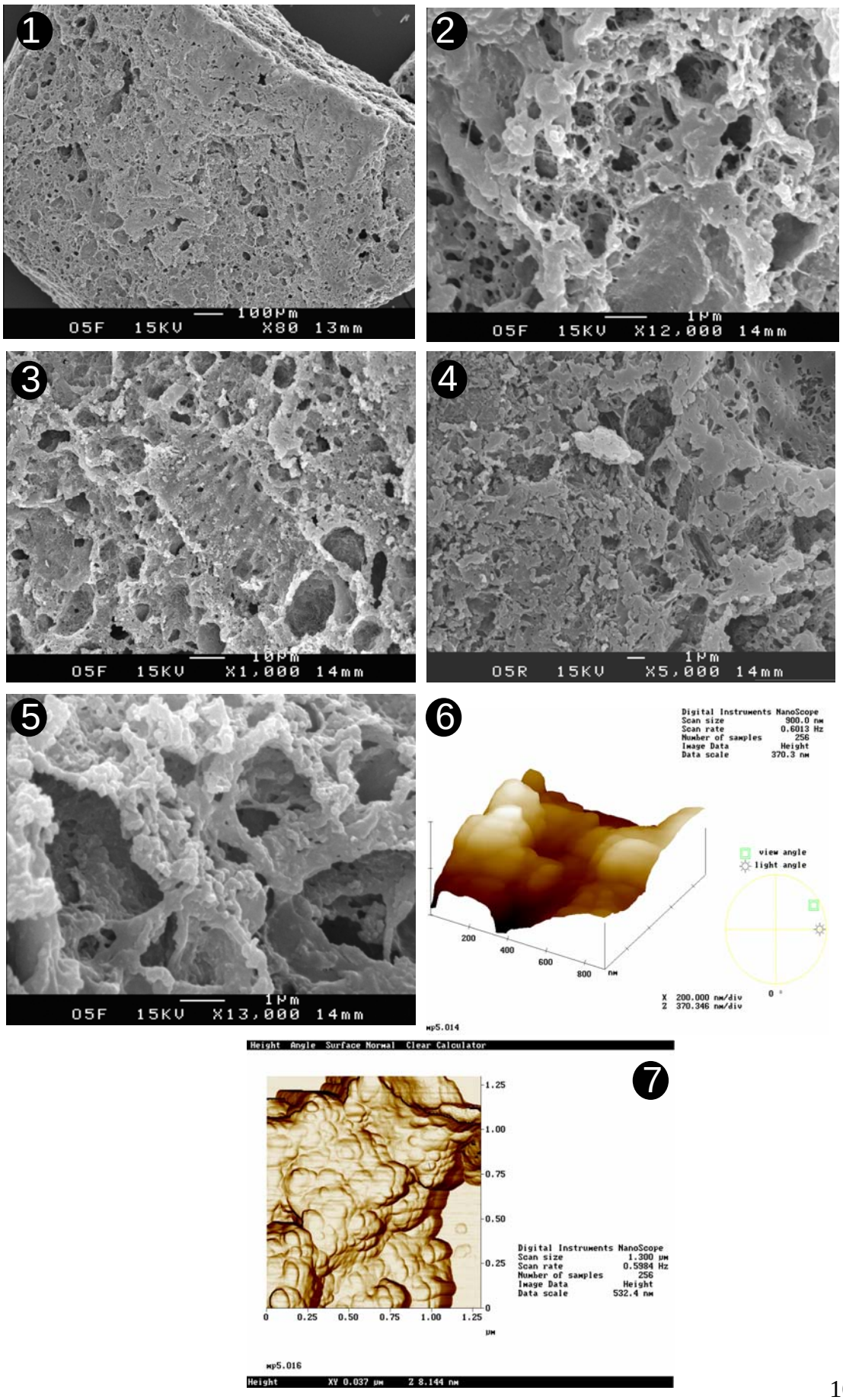

Plate 11d: Kimmeridgian laminites MP5

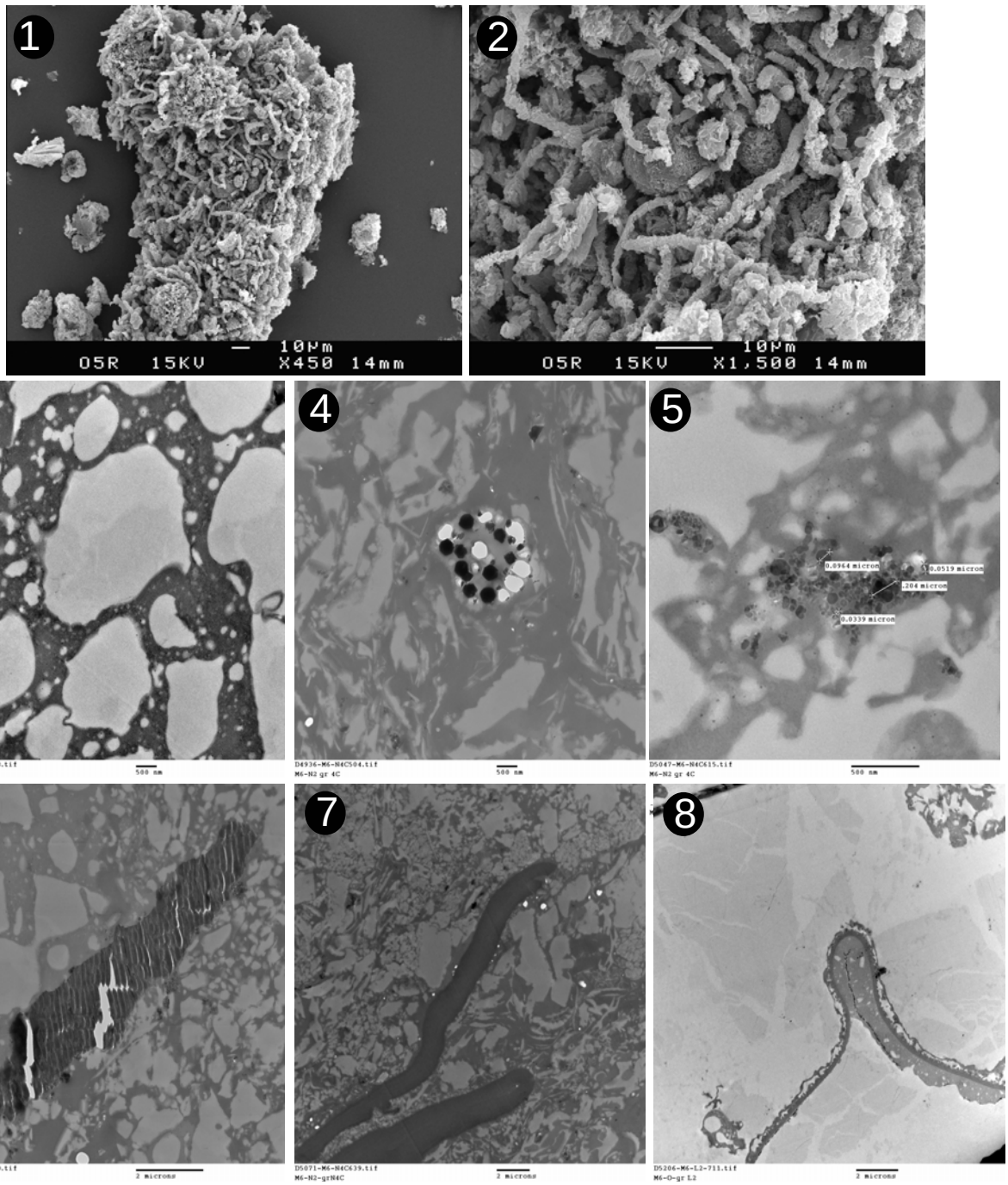

Plate 12a: Kimmeridgian laminites MP19

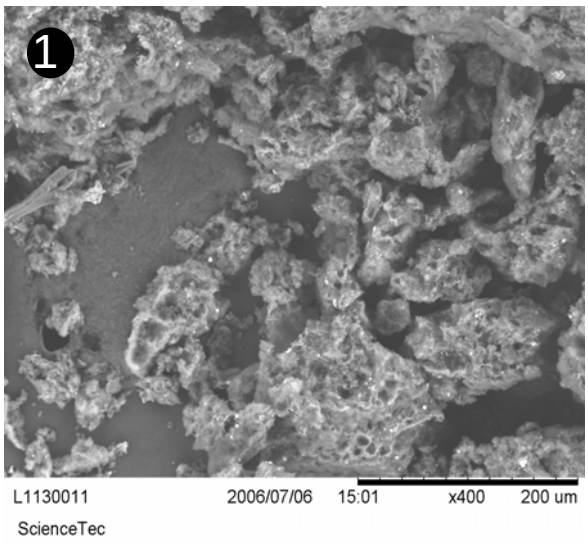

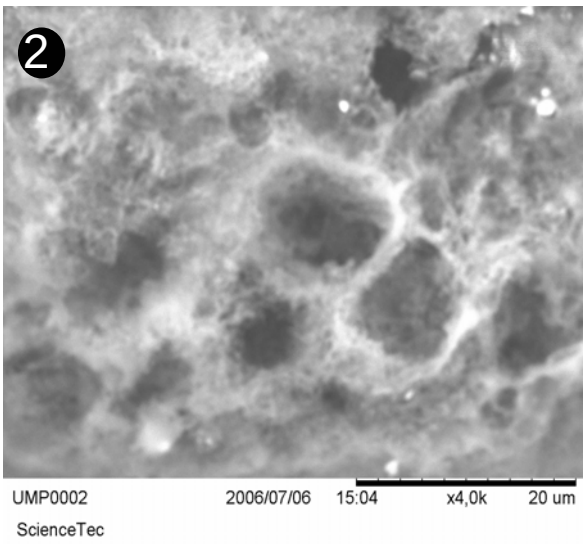

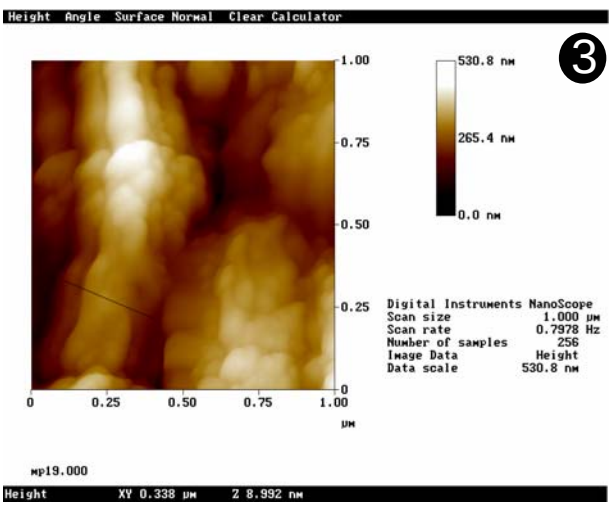

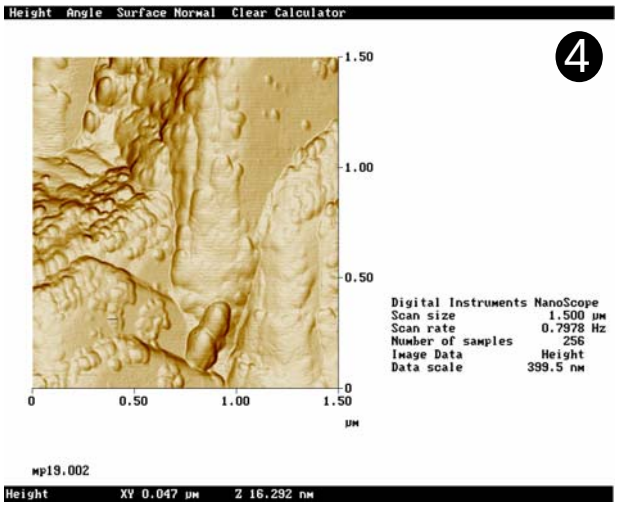

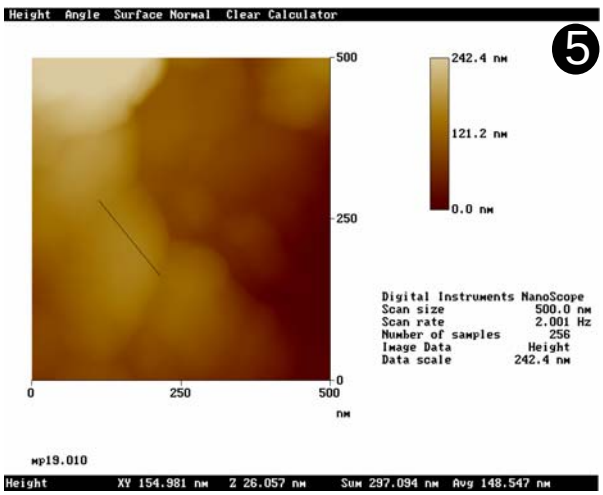

Plate 12b: Kimmeridgian laminites MP19 in TEM

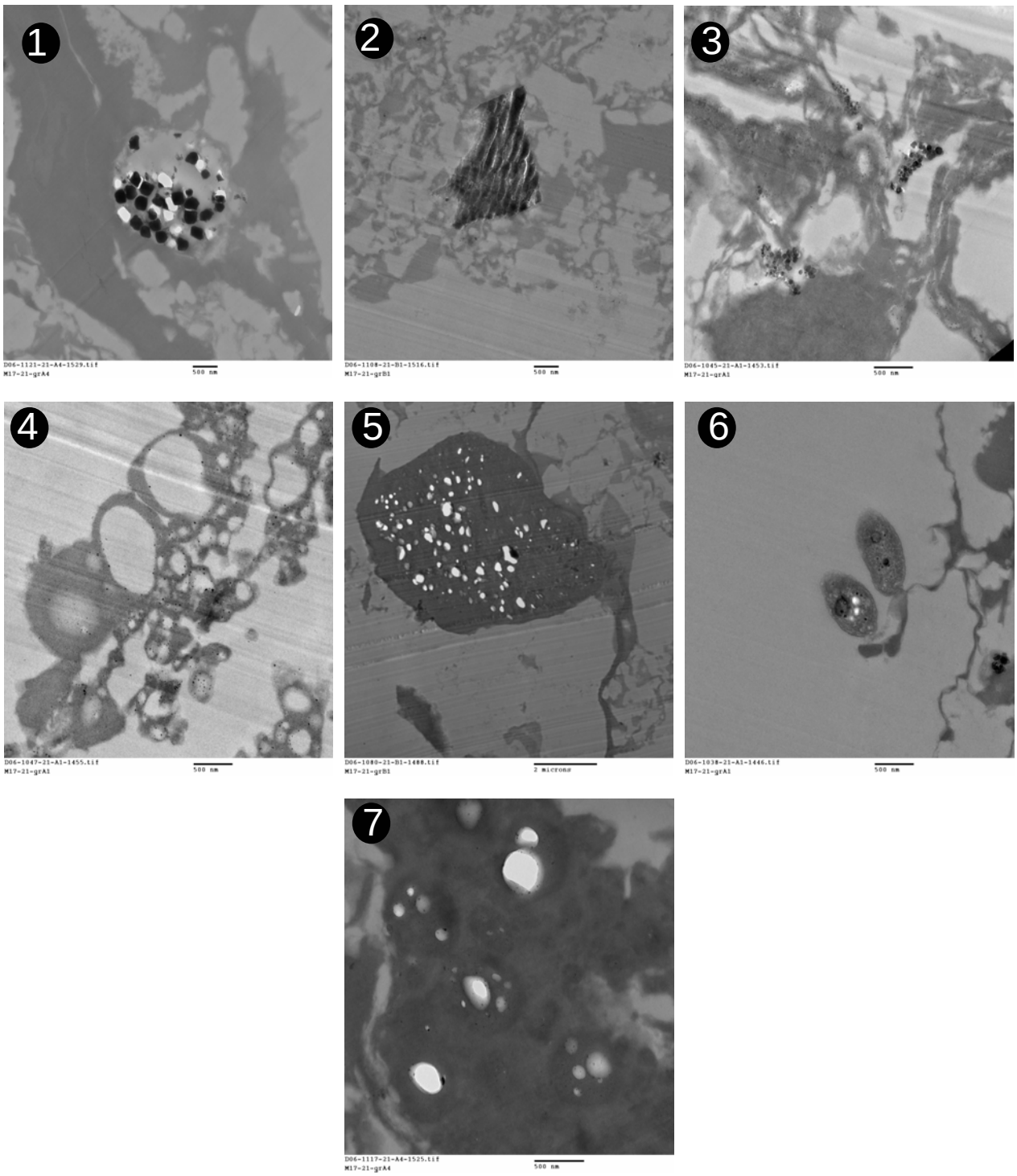

Plate 13a: Selli level (OAE1a)

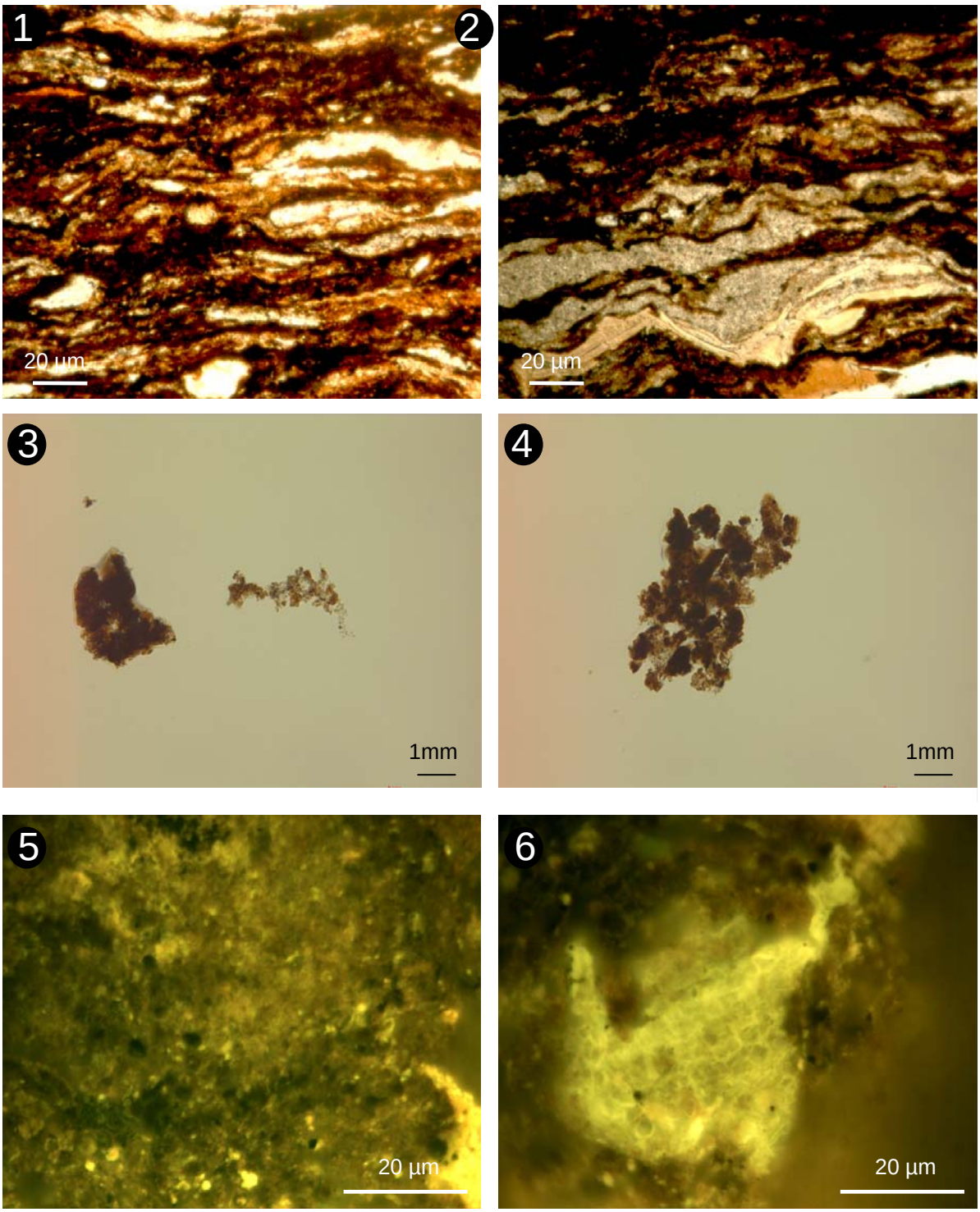

Plate 13b: Selli level (OAE1a) S20

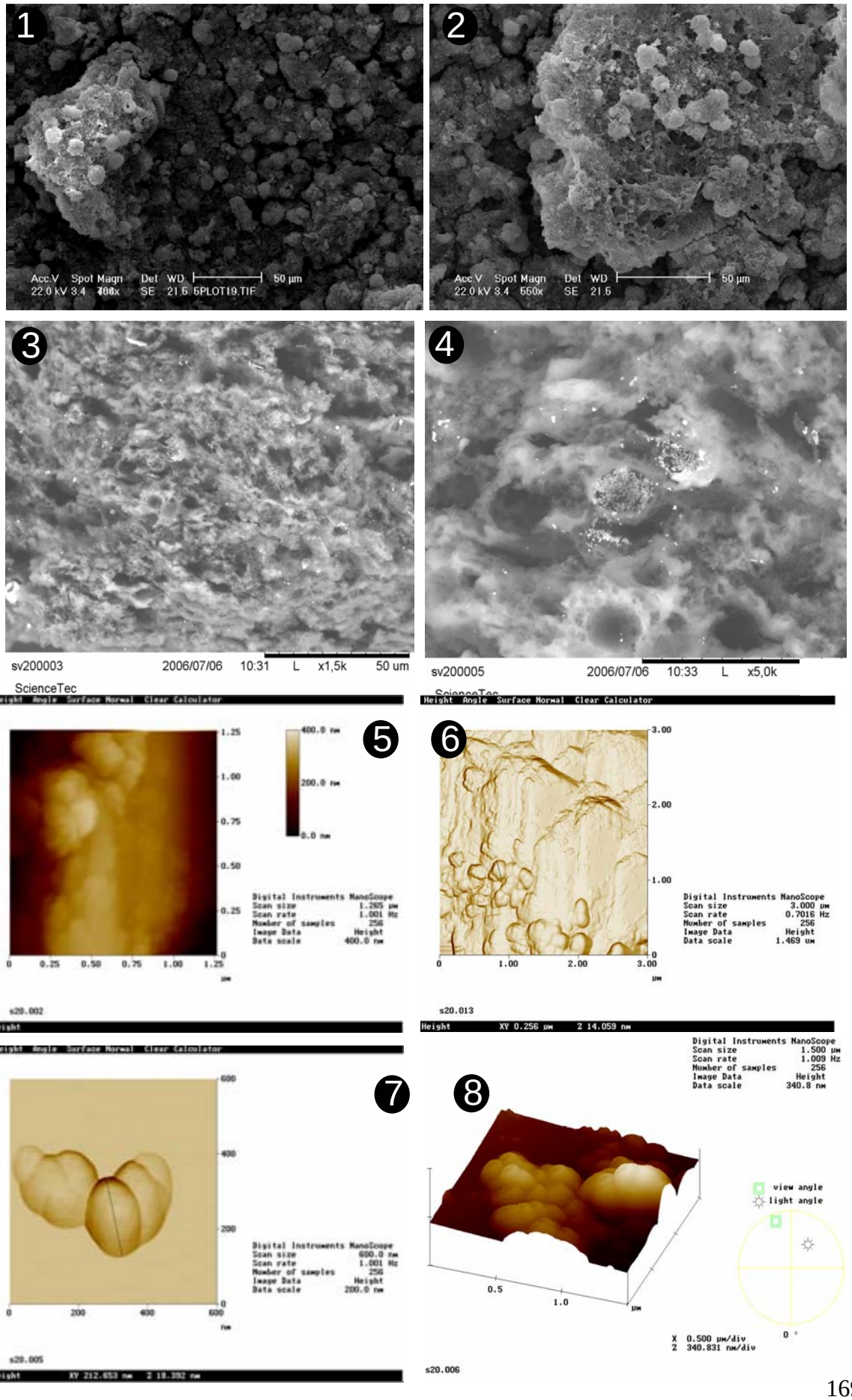

Plate 13c: Selli level (OAE1a) S20 in TEM

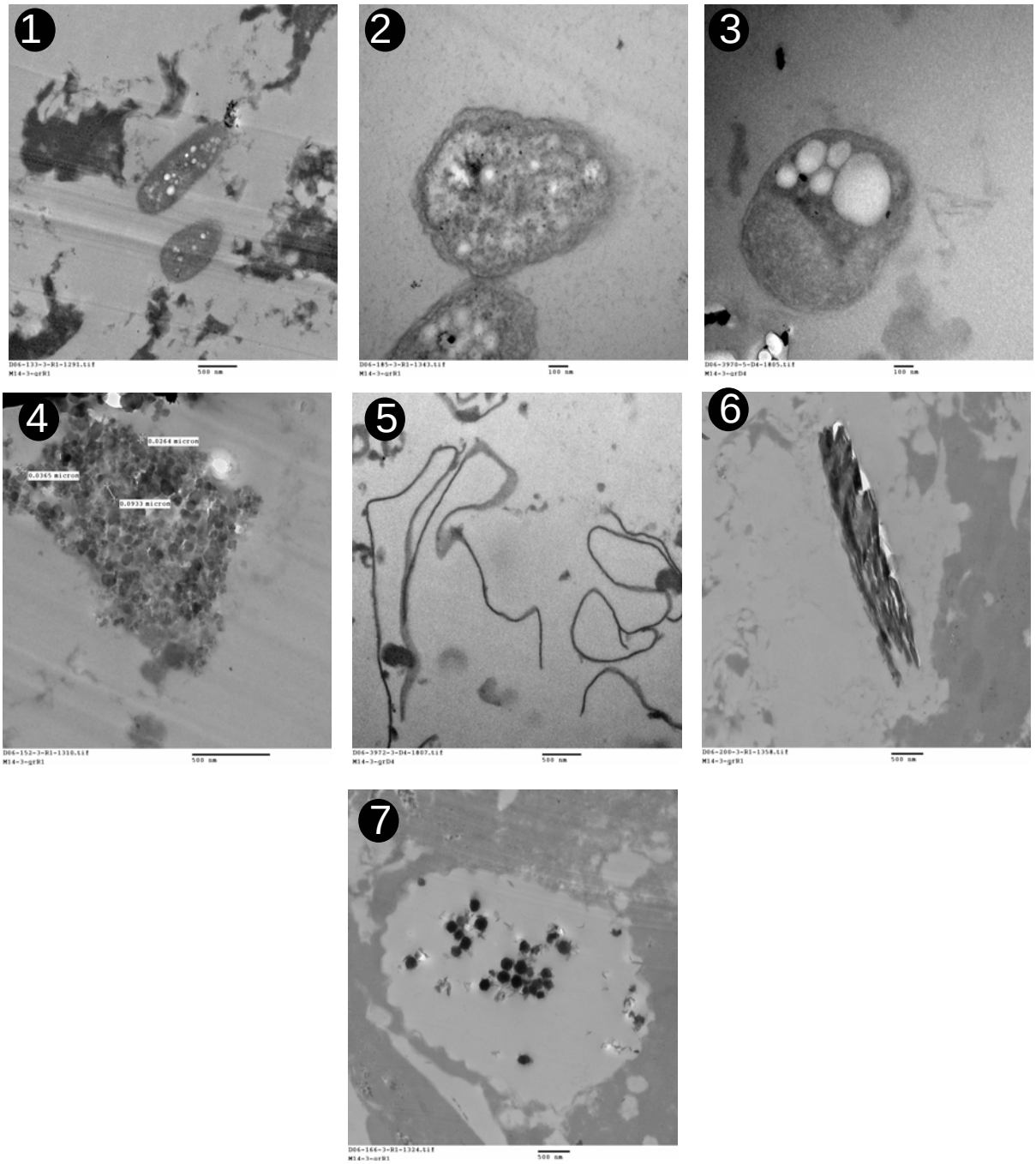

Plate 14a: Selli level (OAE1a) S27

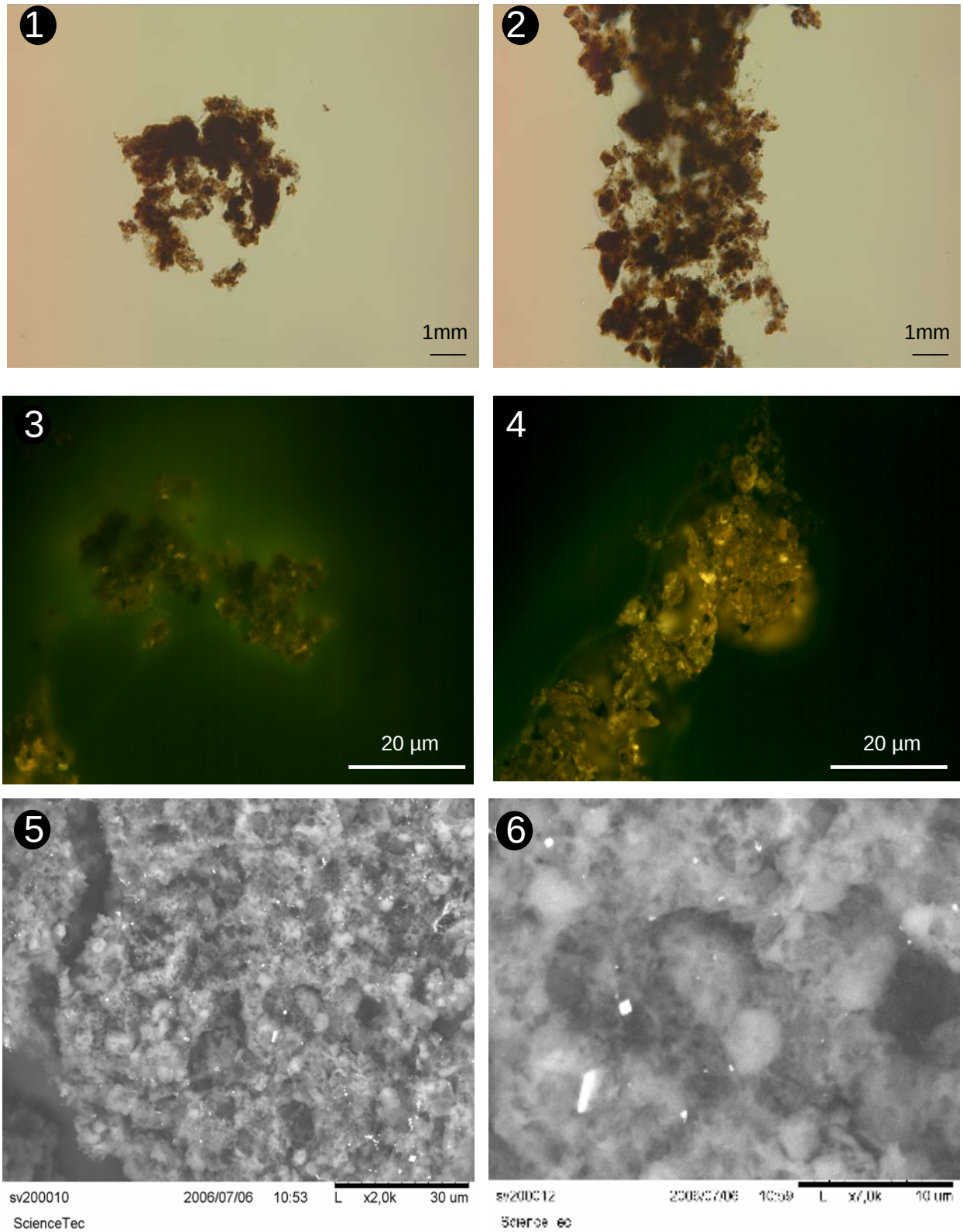

Plate 14b: Selli level (OAE1a) S27

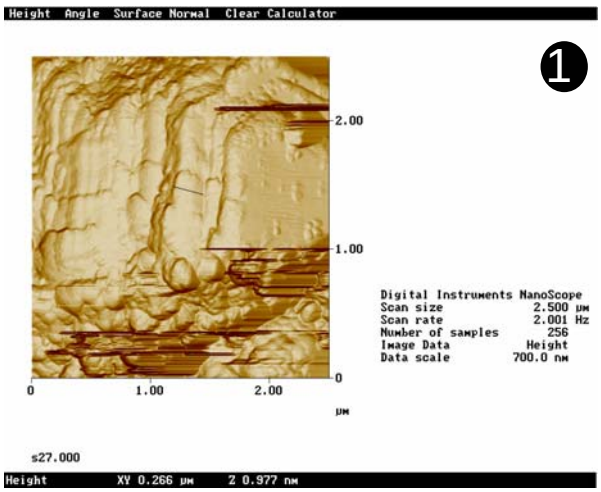

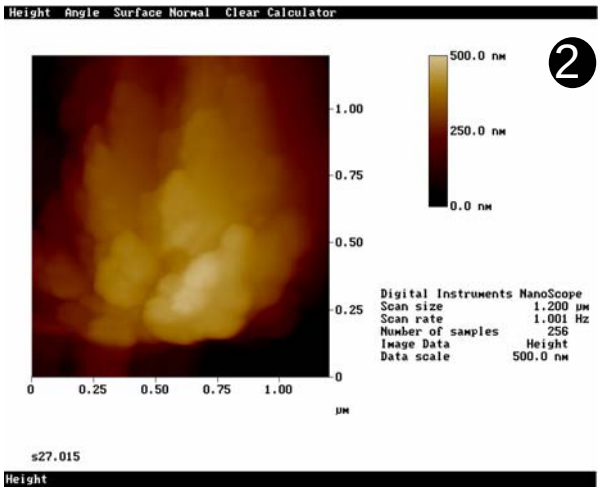

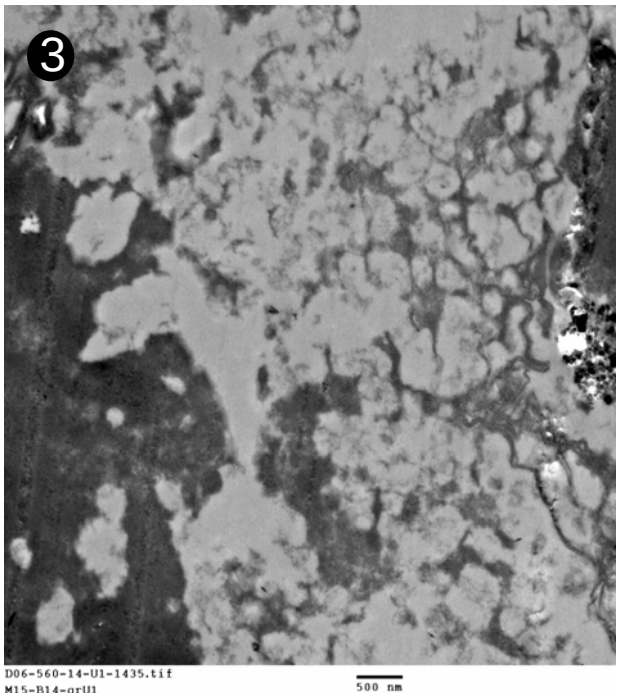

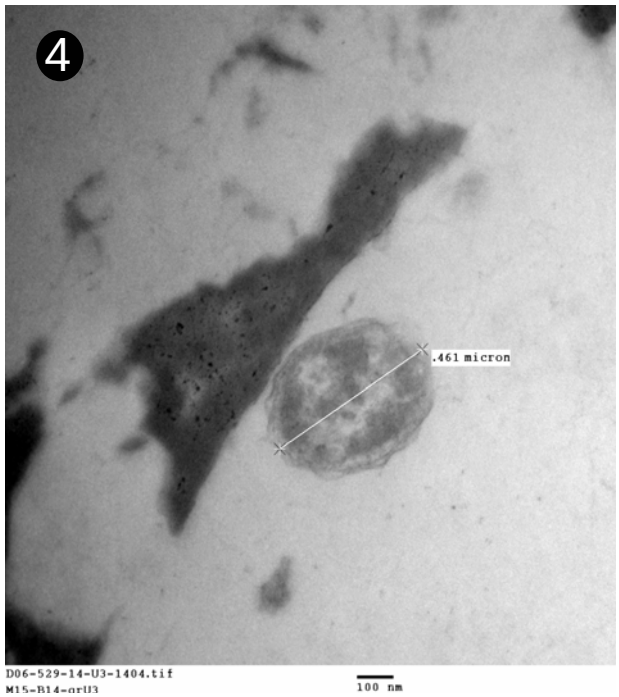

Plate 14c: Selli level (OAE1a) S27 in TEM

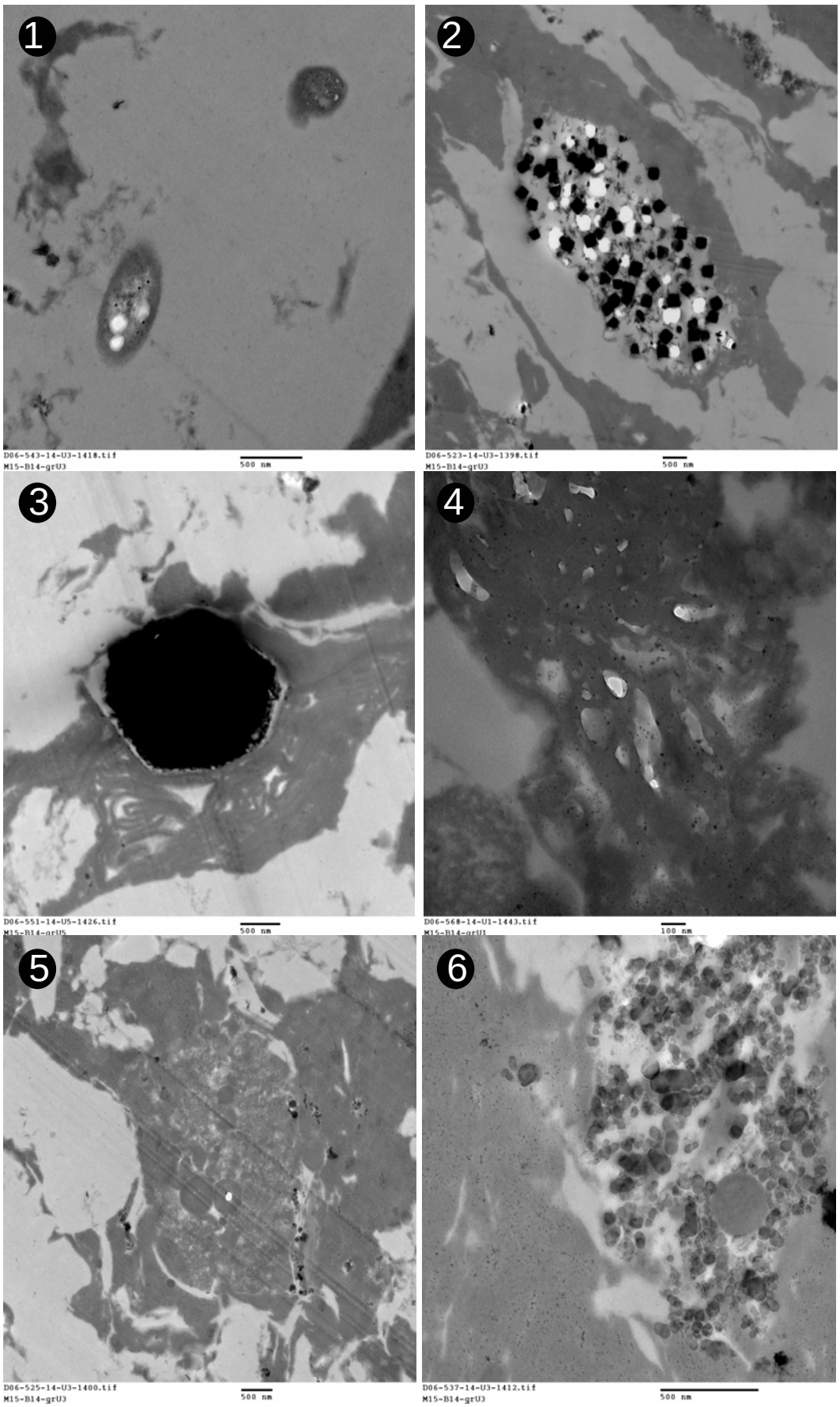

Plate 15a: Urbino level (OAE1b)

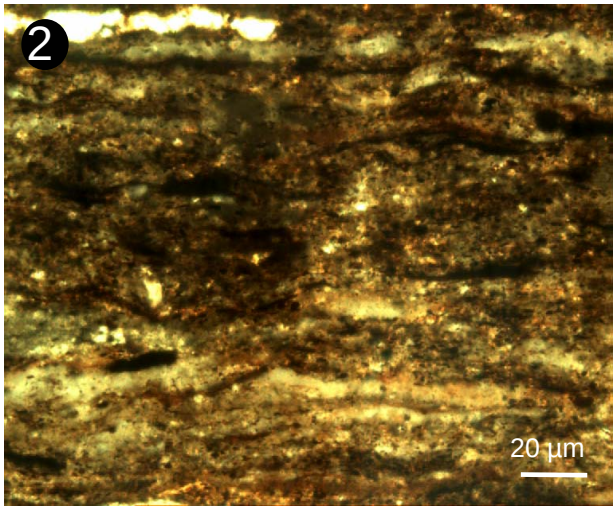

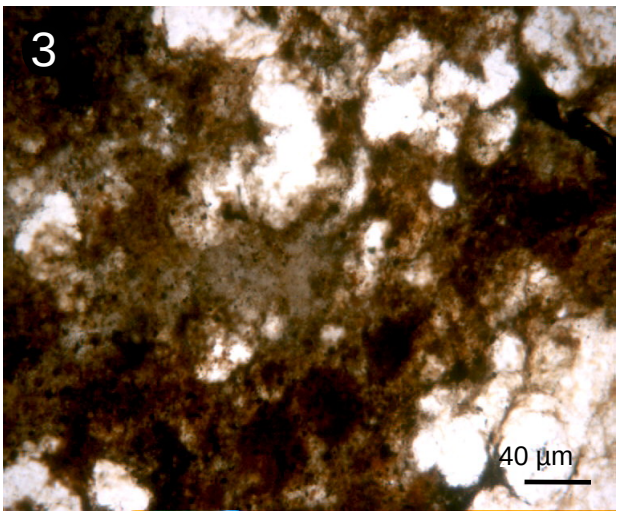

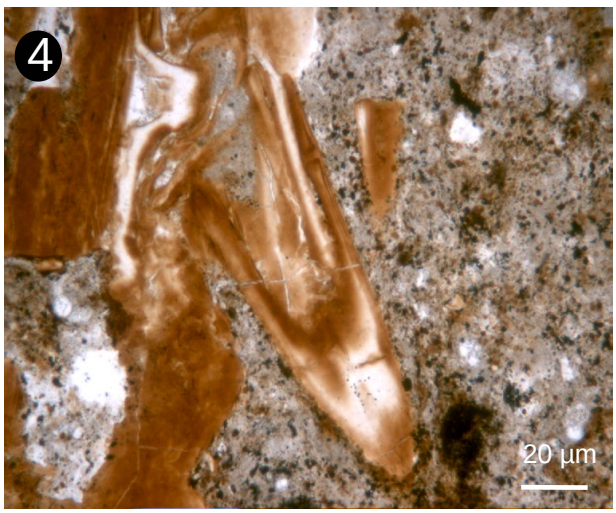

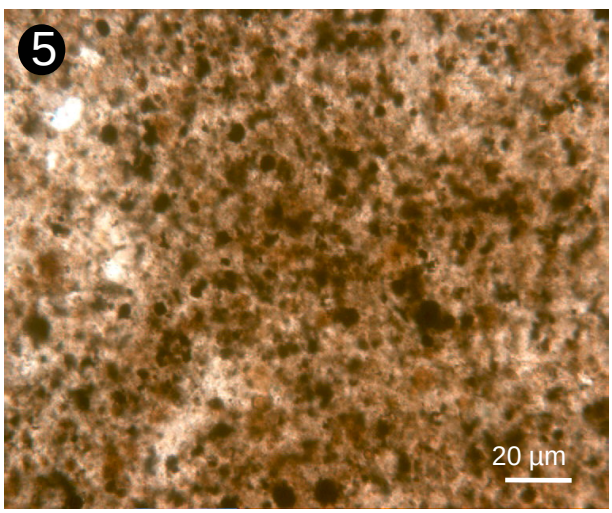

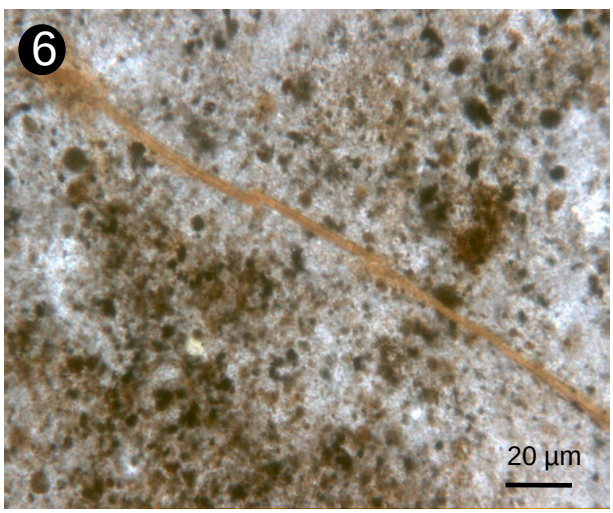

Plate 15b: Urbino level (OAE1b) Ump

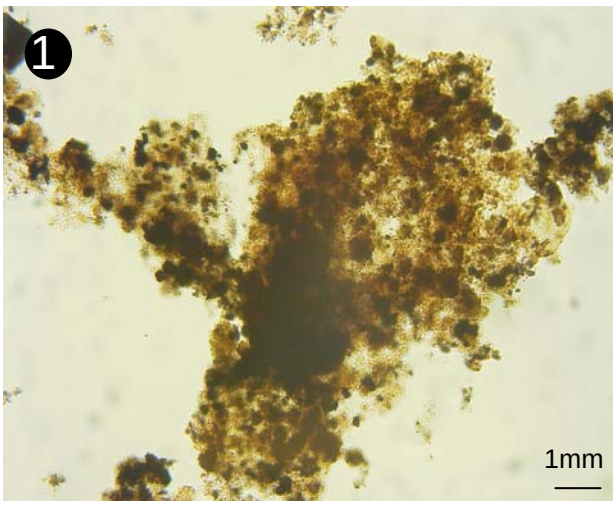

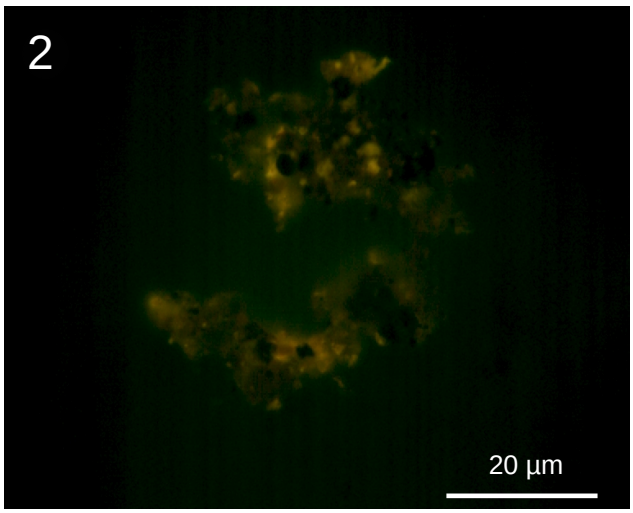

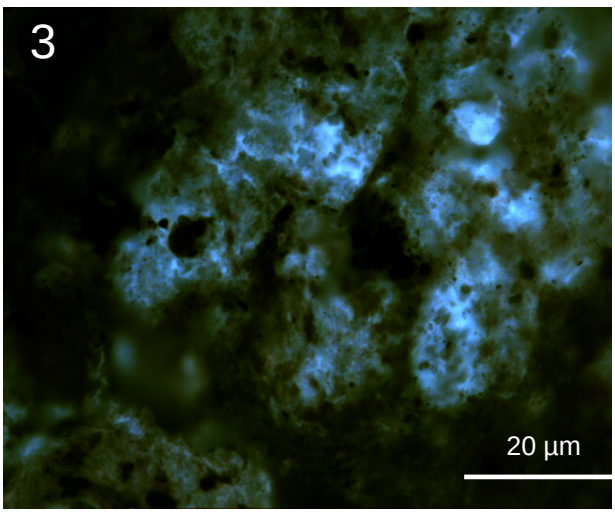

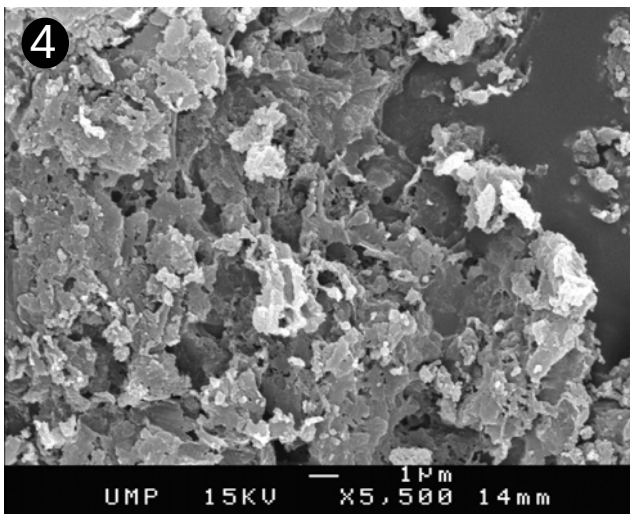

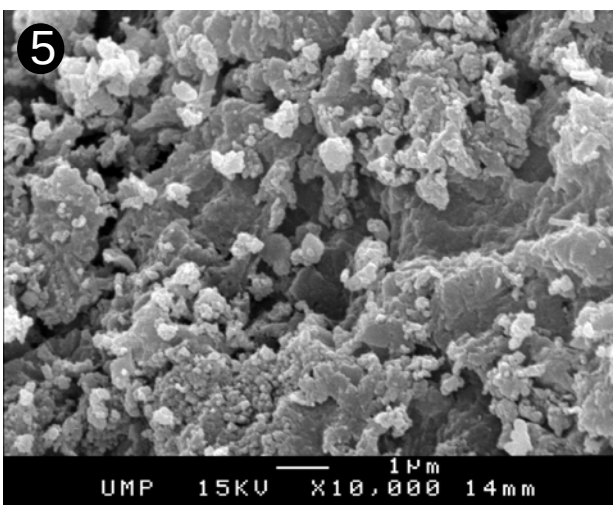

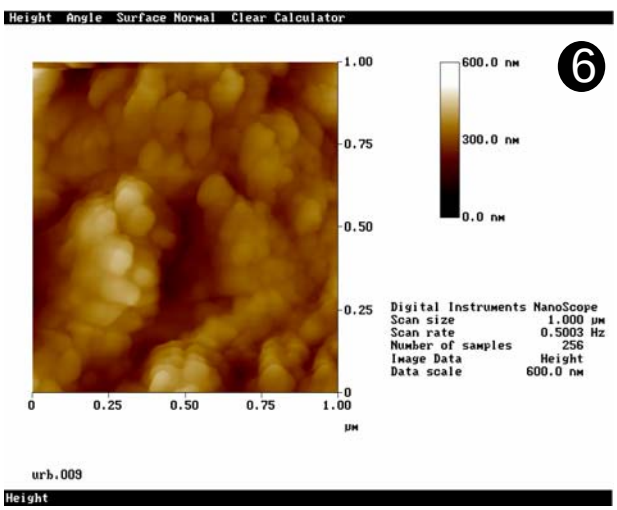

Plate 15c: Urbino level (OAE1b) Ump

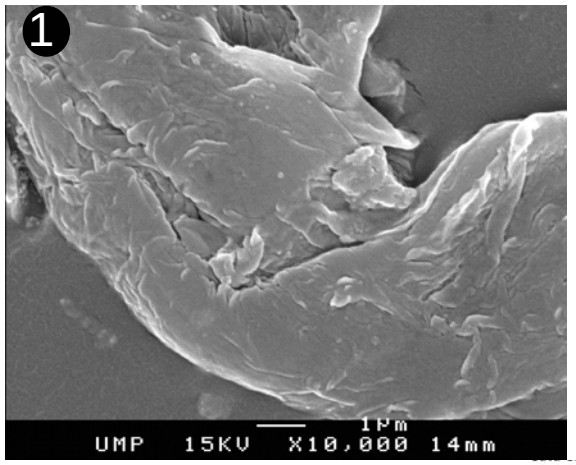

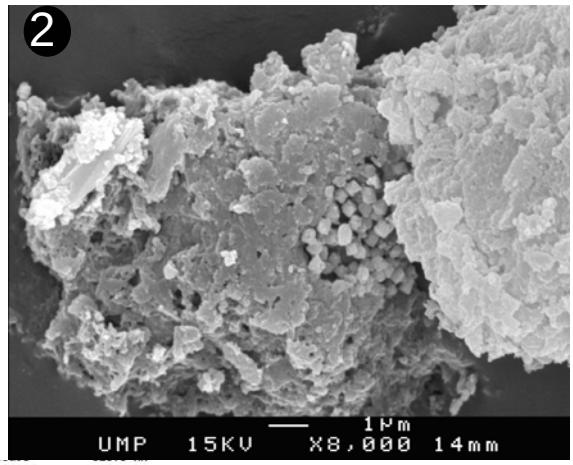

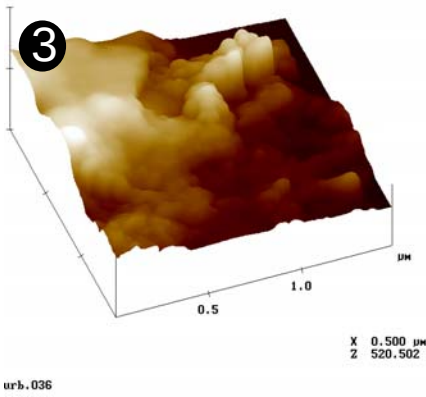

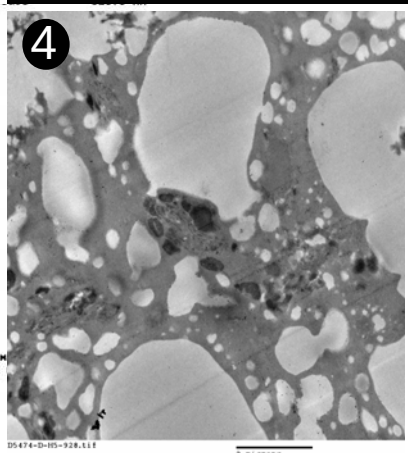

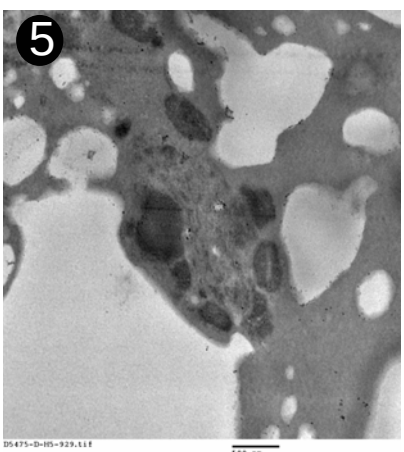

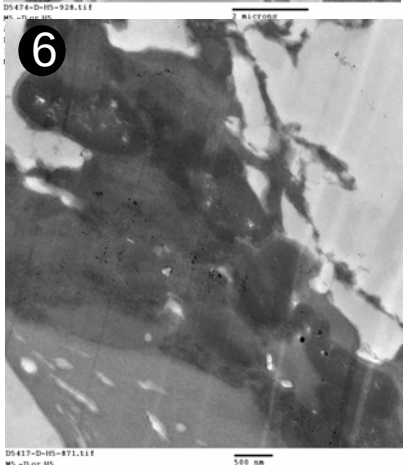

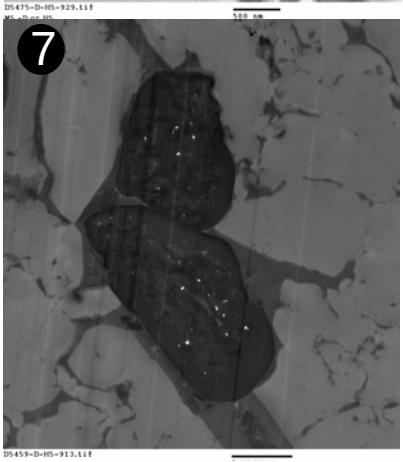

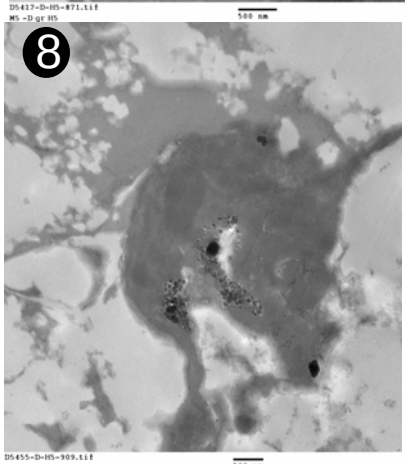

Plate 16a: Urbino level (OAE1b) Uk

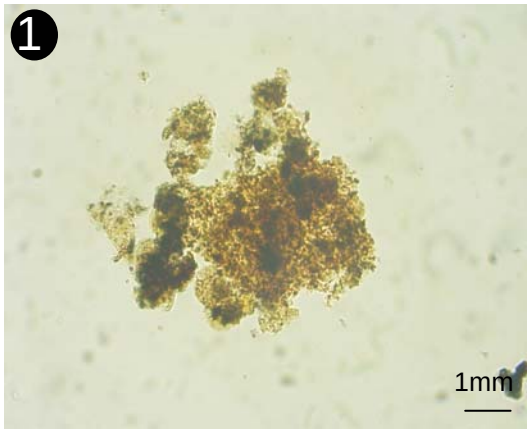

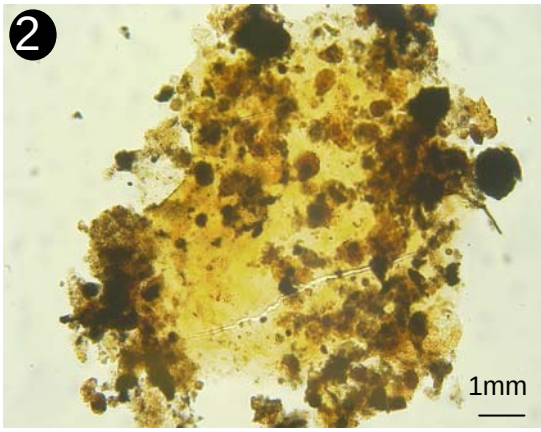

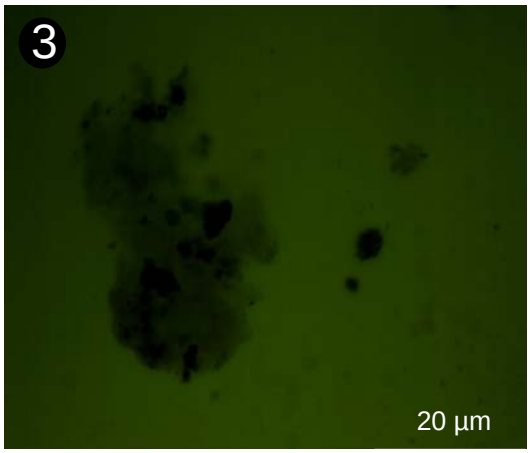

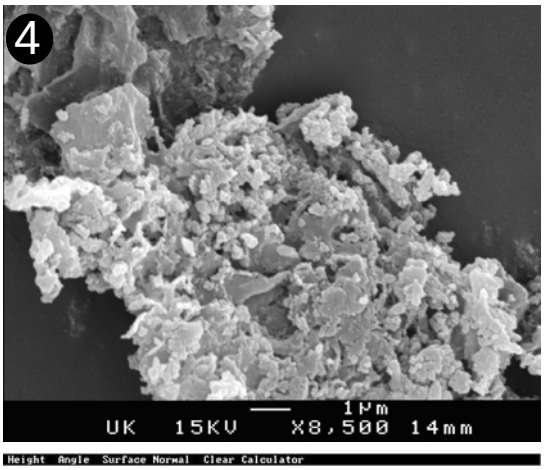

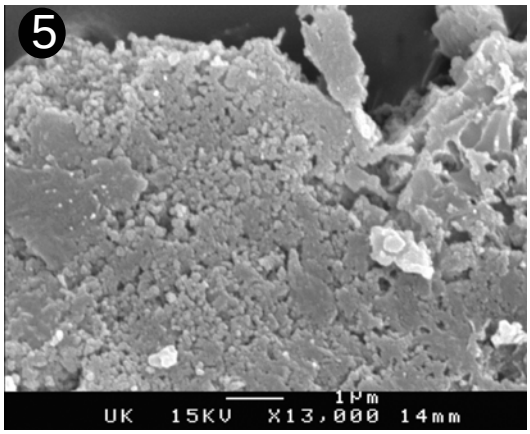

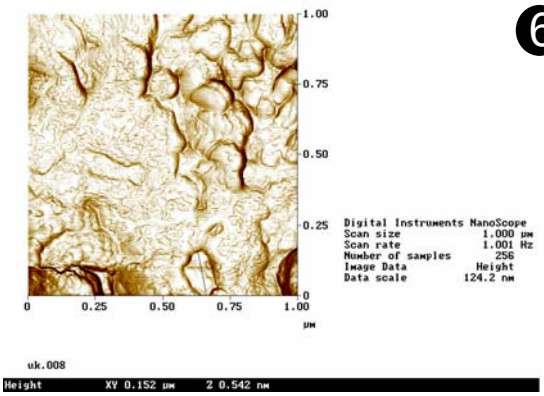

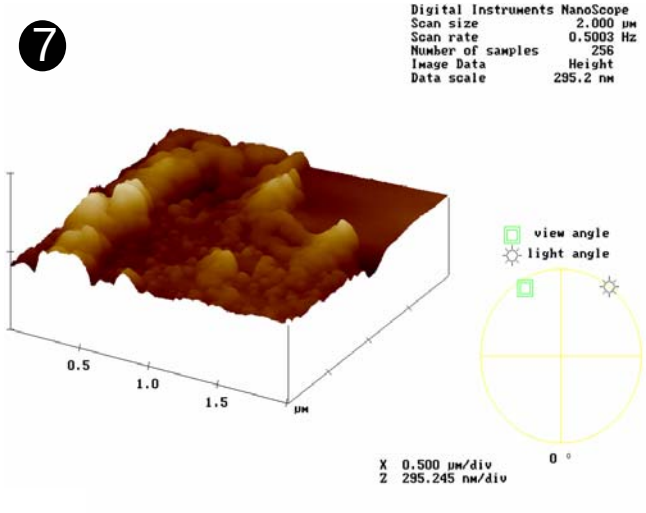

Plate 16b: Urbino level (OAE1b) Uk in TEM

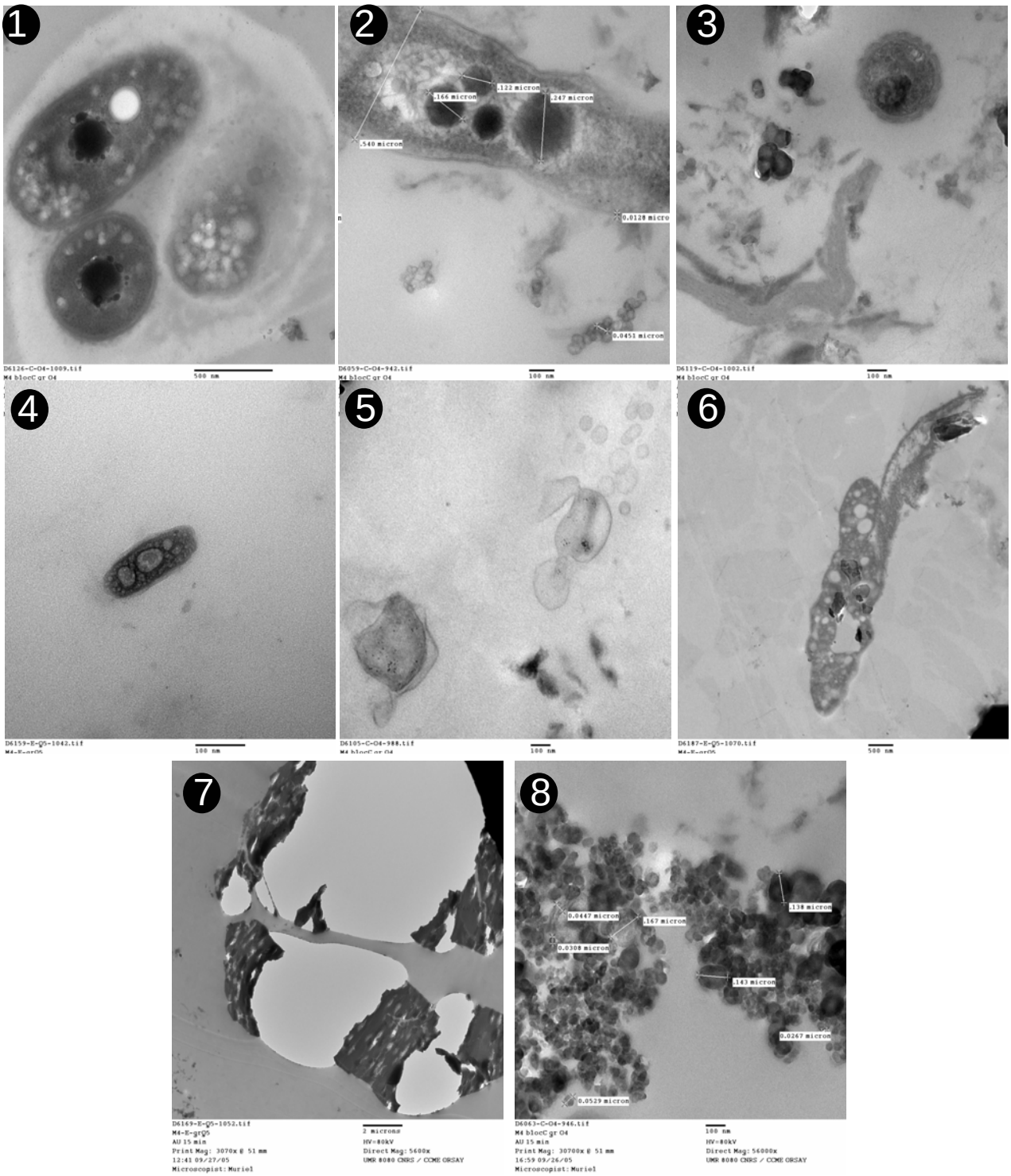

Plate 17a: 113 level (OAE1b)

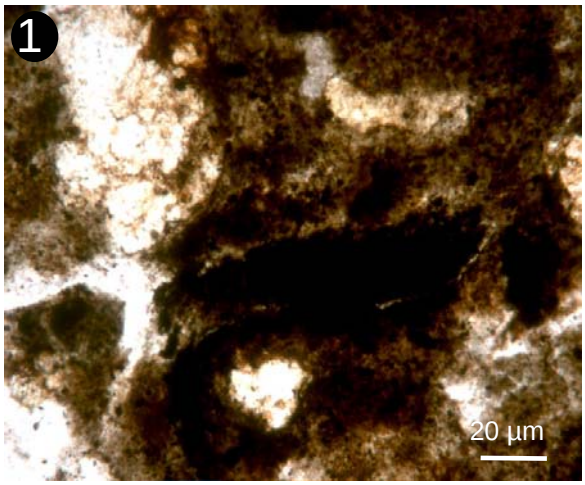

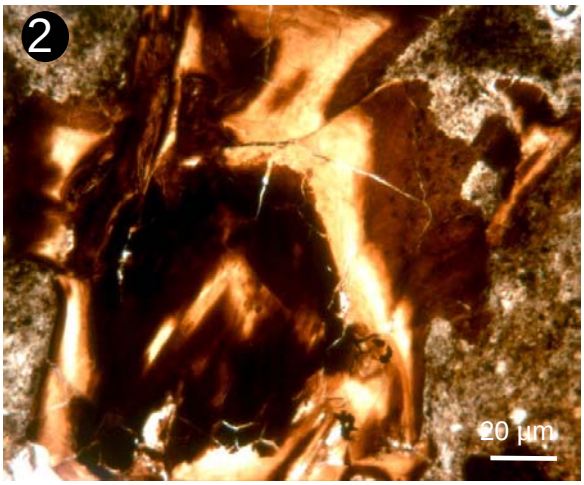

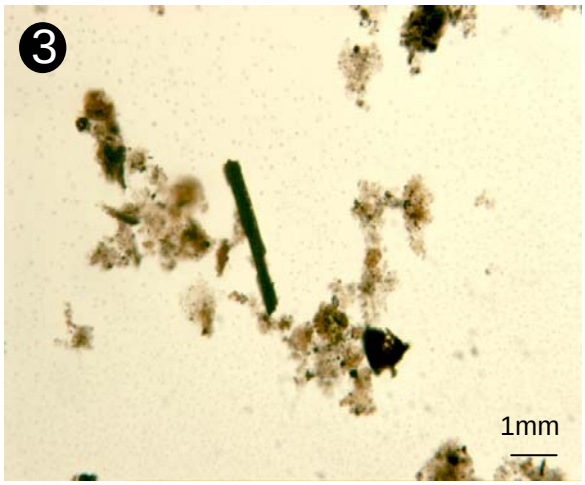

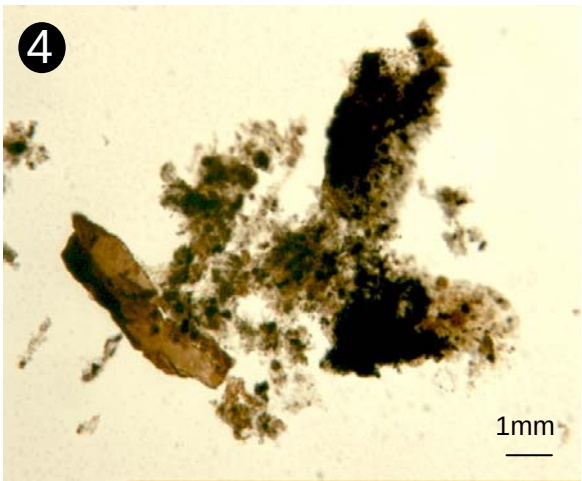

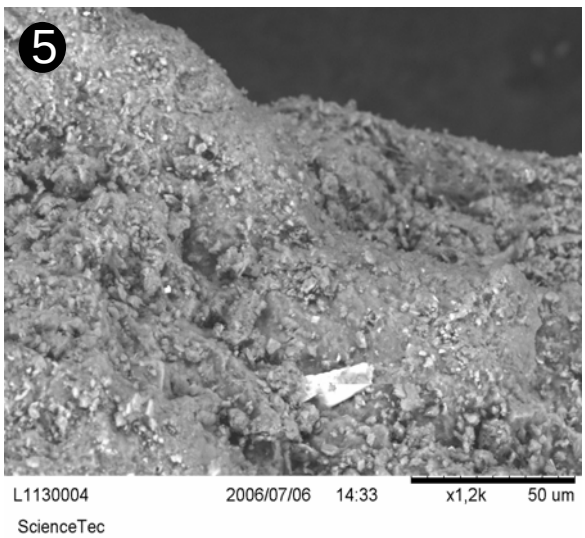

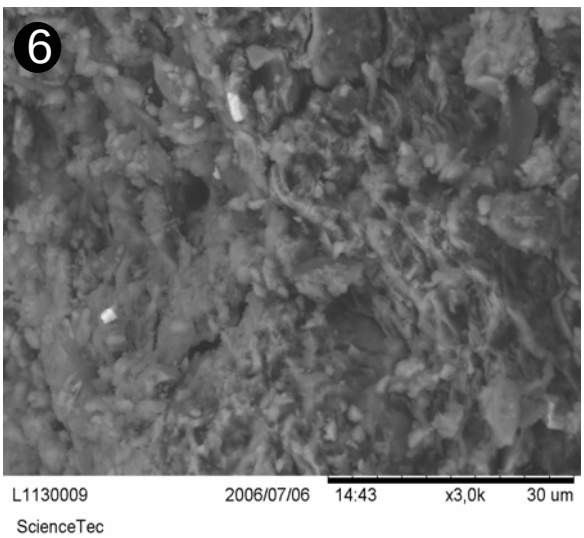

Plate 17b: 113 level (OAE1b)

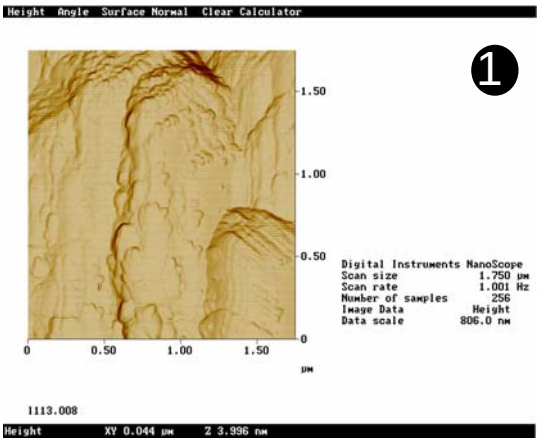

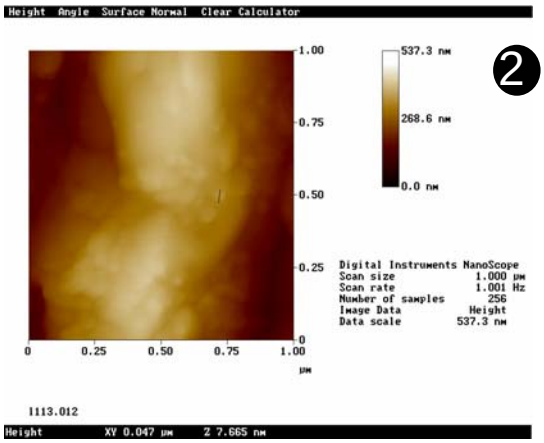

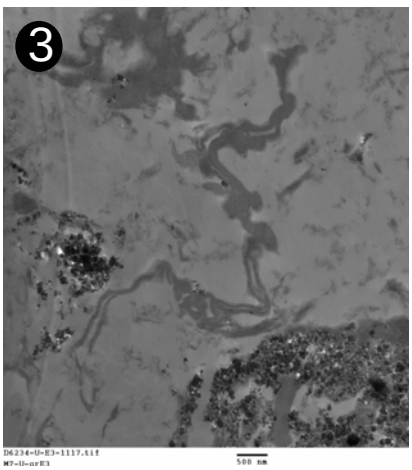

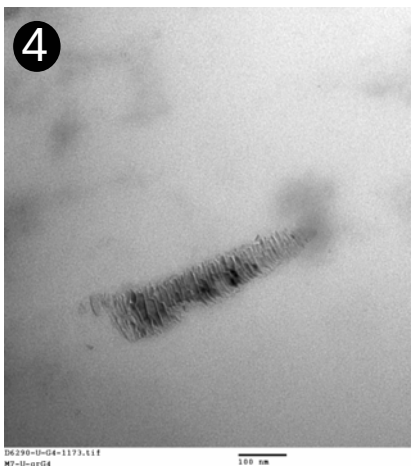

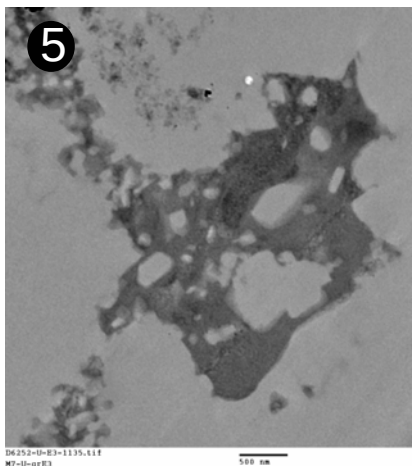

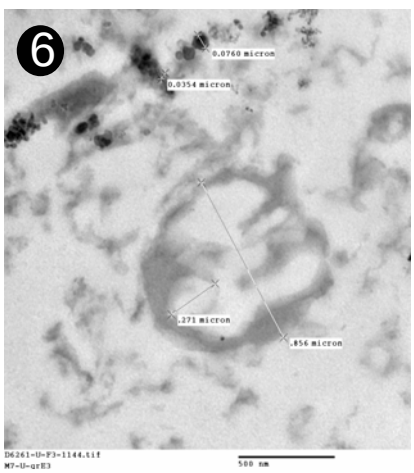

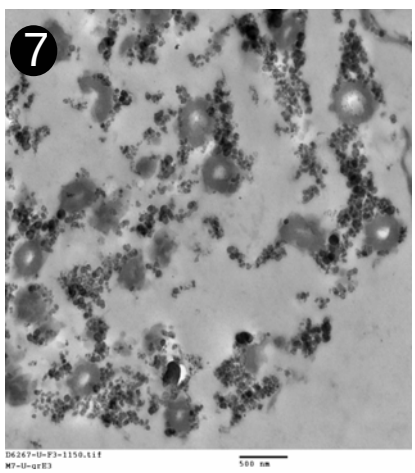

Plate 18: ultralaminae as recent algal cell walls in TEM

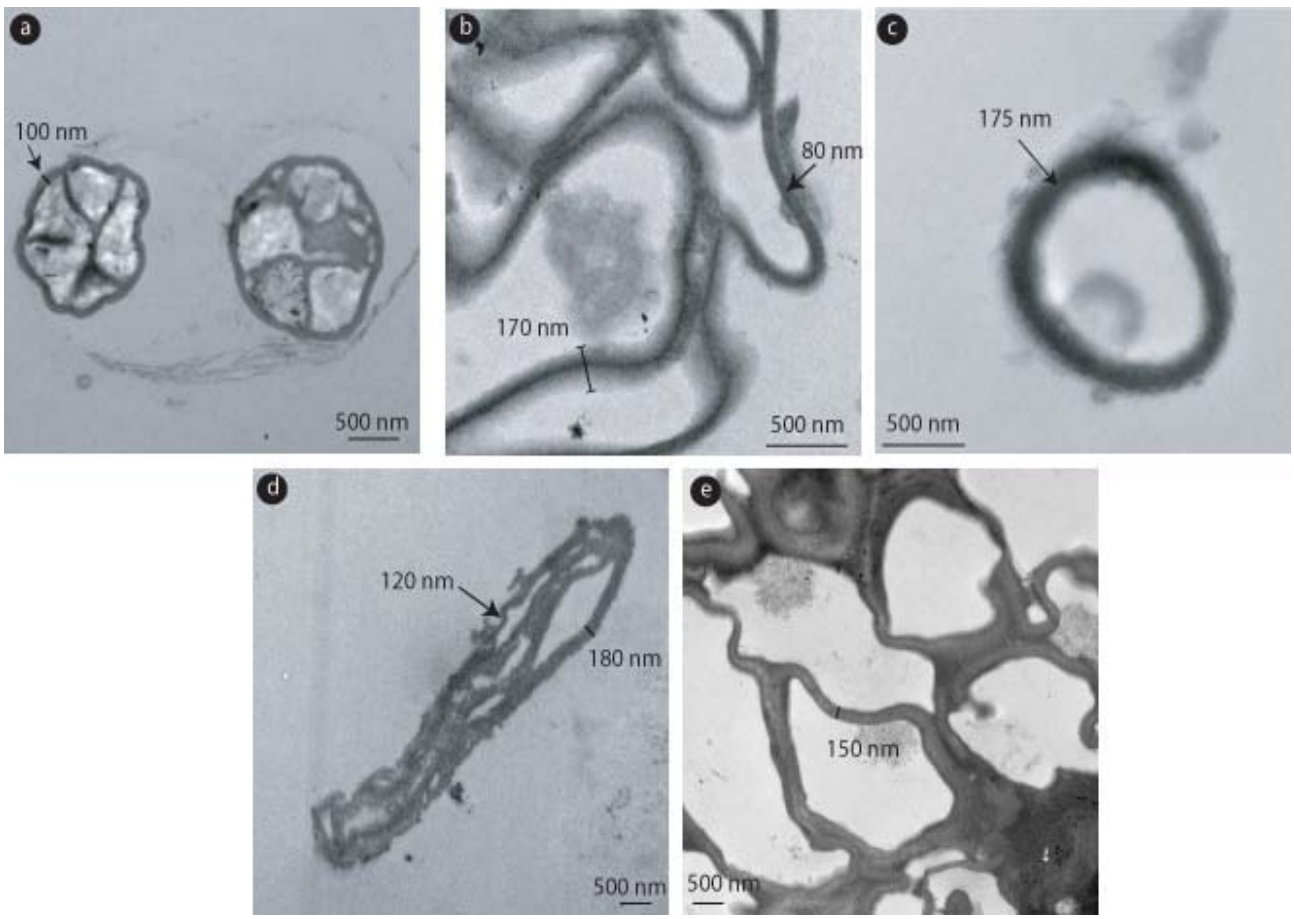

Plate 19: ultralaminae as fossil algal cell walls in TEM

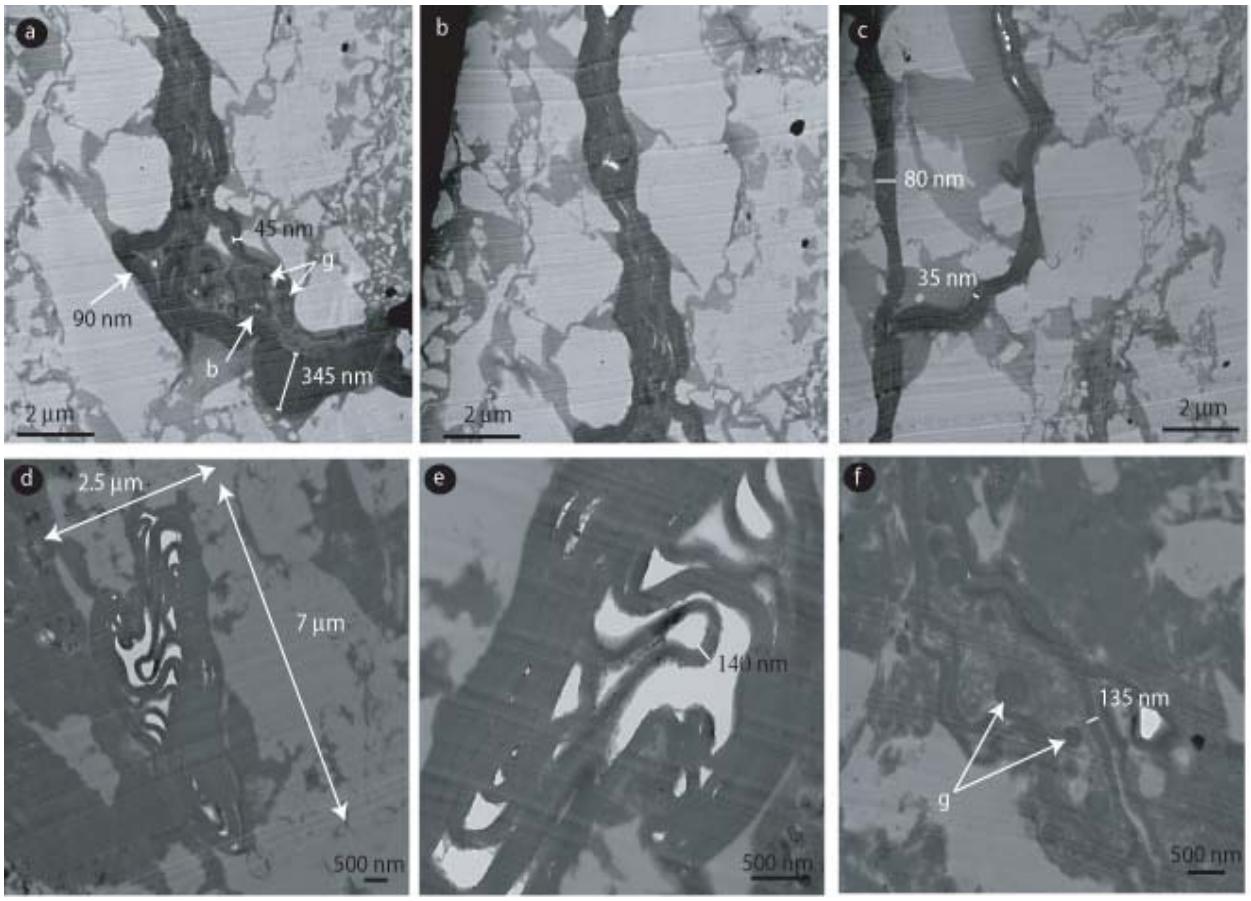

Plate 20: ultralaminae as fossil algal cell walls in TEM

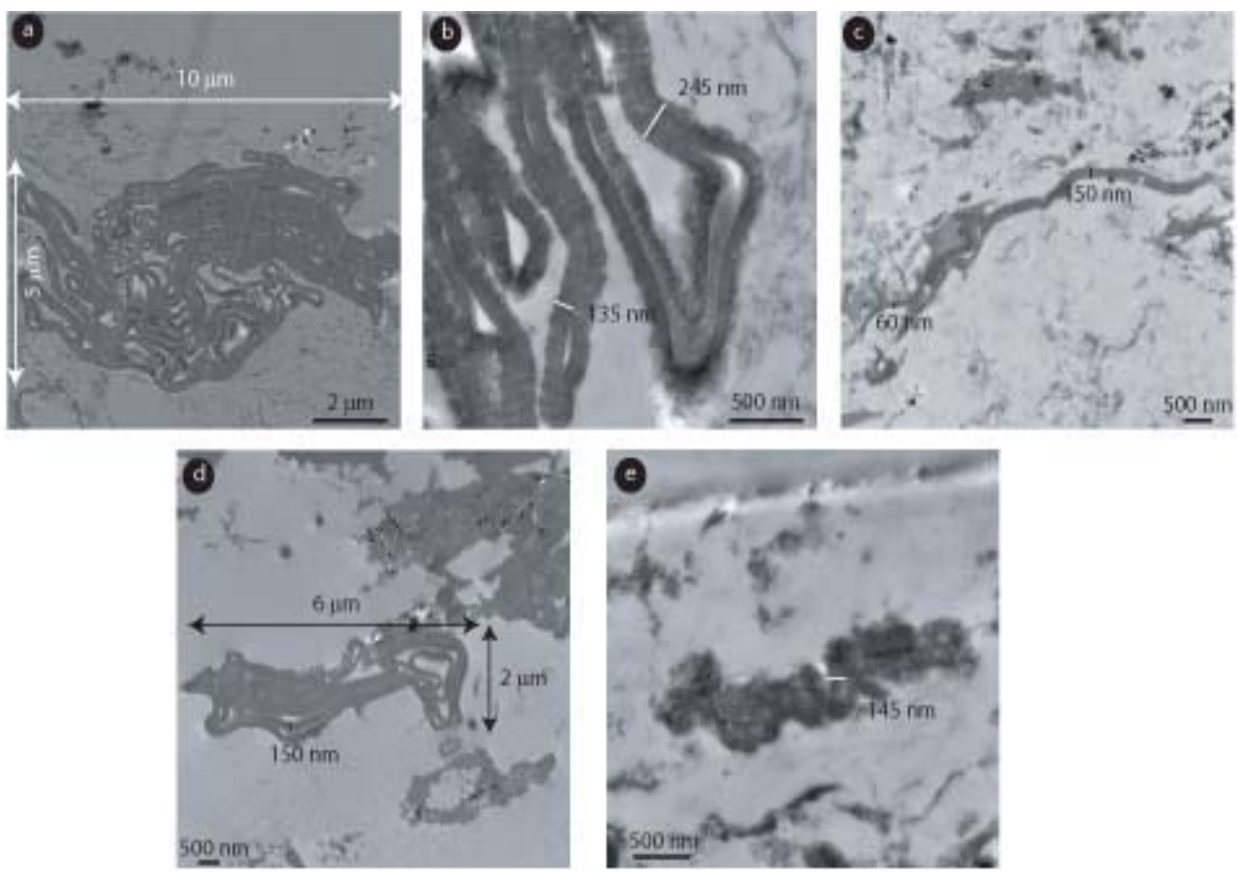

Plate 21: ultralaminae as recent bacterial cell walls in TEM

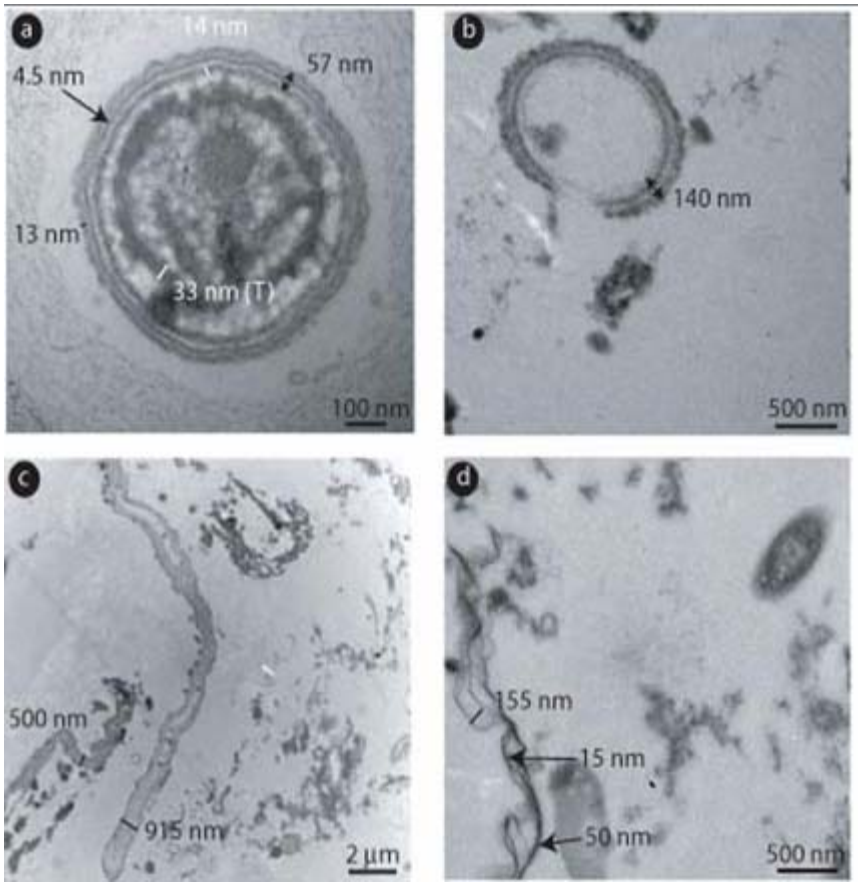

Plate 22: ultralaminae as fossil bacterial cell walls in TEM

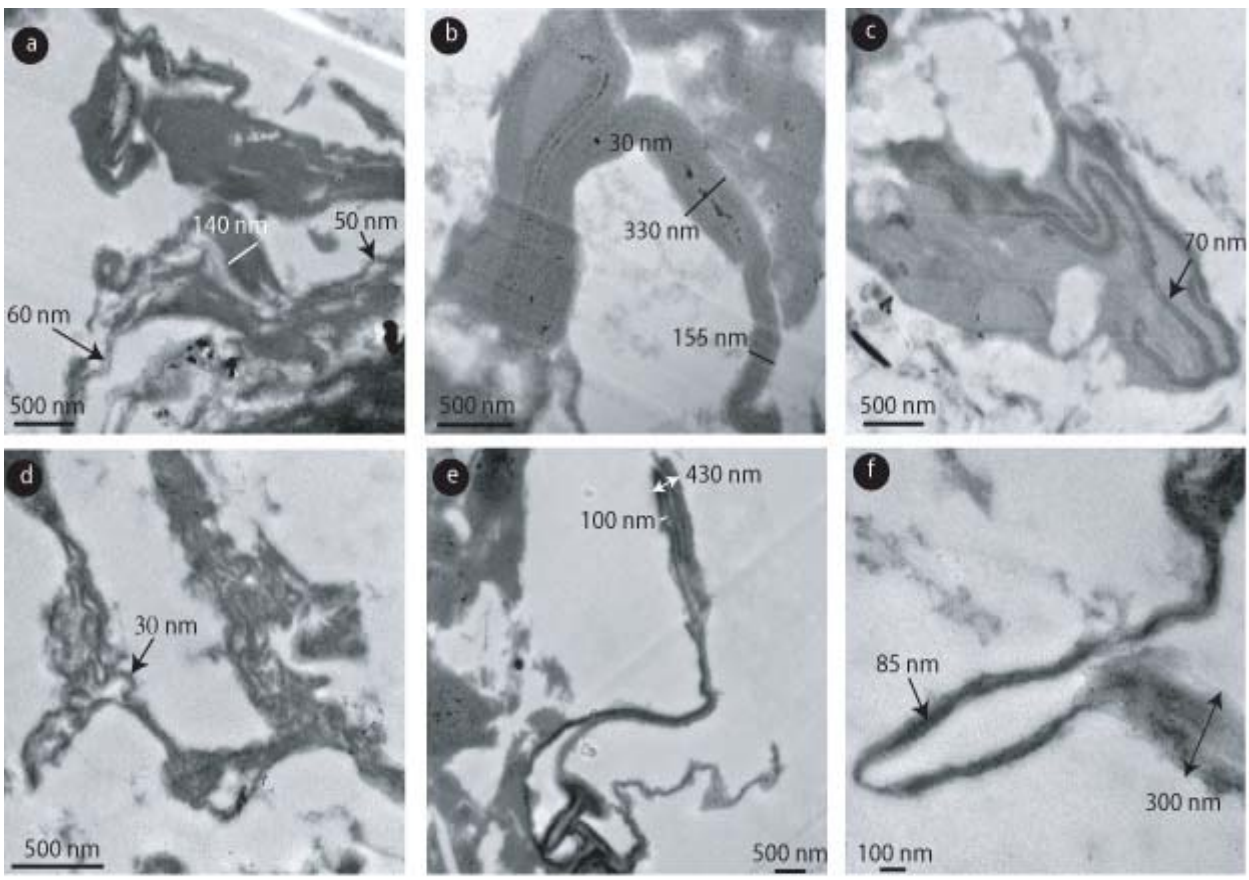

Plate 23: ultralaminae as recent thylakoid membranes in TEM

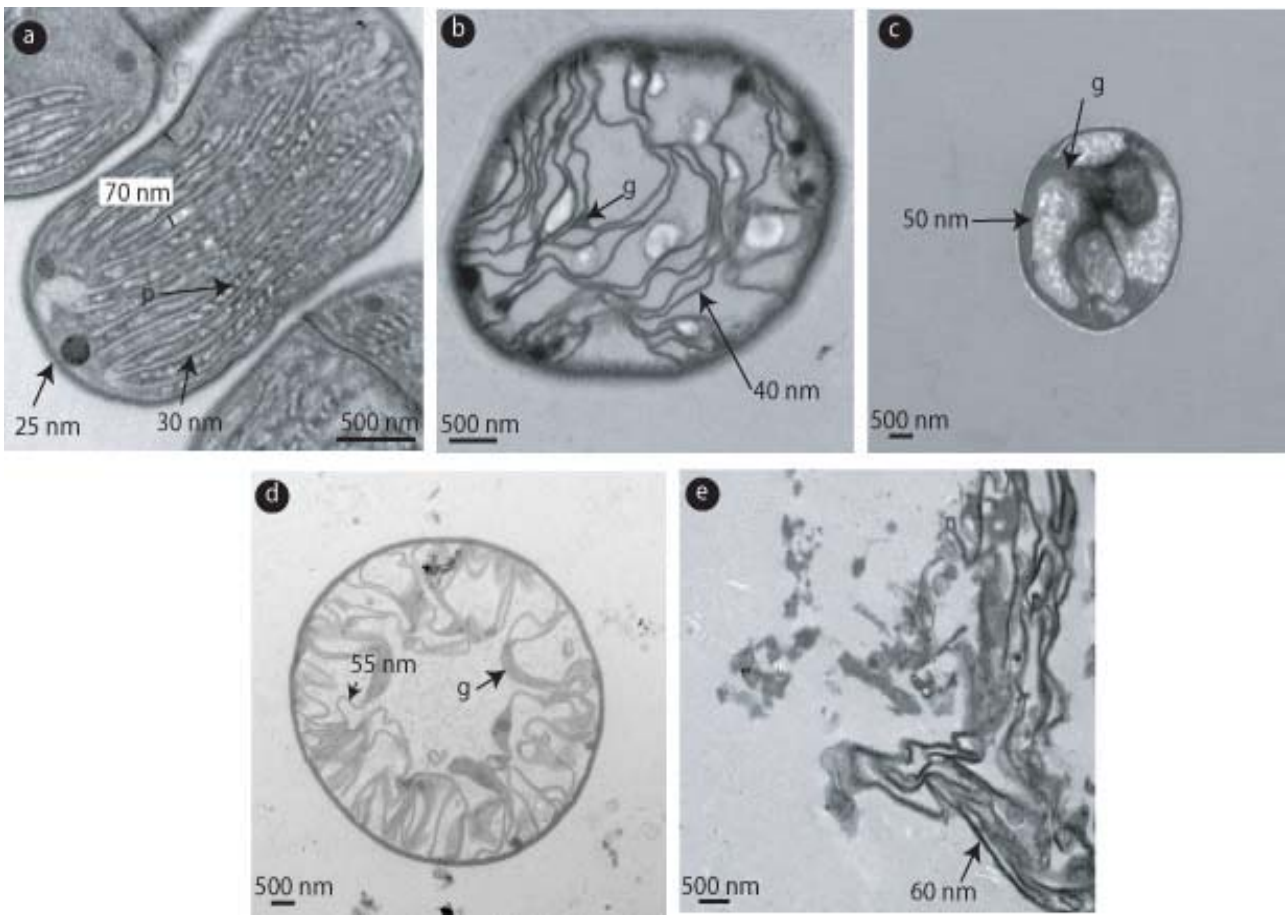

Plate 24: ultralaminae as fossil thylakoid membranes in TEM

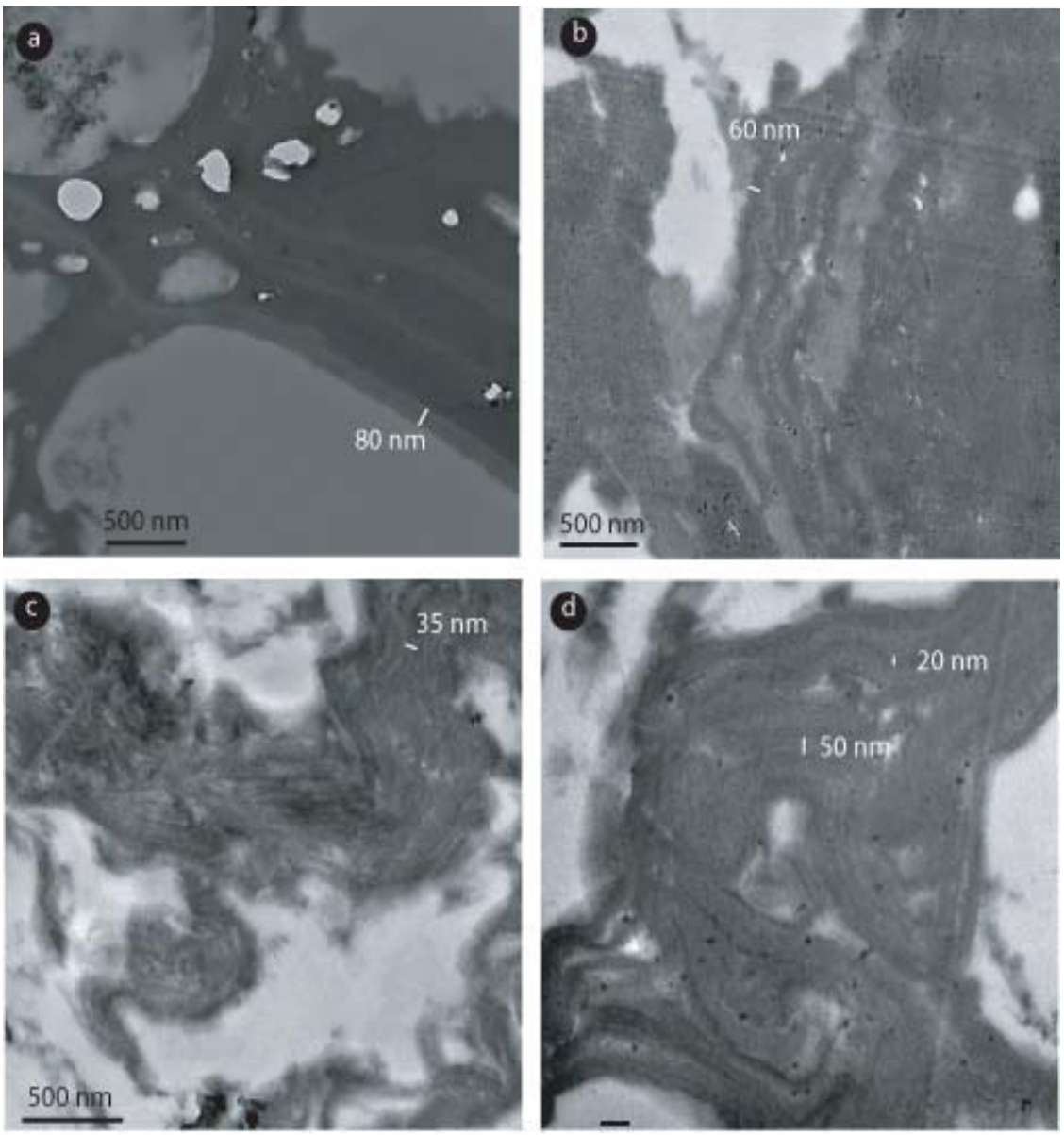

Plate 25: ultralaminae as organisms and cuticles in TEM